INTEGRATION OF TRANSPORT PATHWAYS IN YEAST

by

Gabriel A. Alfaro

B. Sc, University of British Columbia, 2004

THESIS
SUBMITTED IN PARTIAL FULFILLMENT OF
THE REQUIREMENTS FOR THE DEGREE OF

DOCTOR OF PHILOSOPHY

In the
Department of Molecular Biology and Biochemistry

© Gabriel A. Alfaro 2012

SIMON FRASER UNIVERSITY

Spring 2012

Approval

Name: **Gabriel A. Alfaro**

Degree: **Doctor in Philosophy**

Title of Thesis: **Integration of transport pathways in yeast.**

Examining Committee:

Chair: **Dr. Bruce Brandhorst**

Professor and Chair – Dept. MBB - SFU

_____

Dr. Christopher Beh
Senior Supervisor
Associate professor -SFU– Dept. MBB - SFU

_____

Dr. Nicholas Harden
Ph.D. Supervisory Committee Member
Professor – SFU– Dept. MBB - SFU

_____

Dr. Lynne Quarmby
Ph.D. Supervisory Committee Member
Professor - SFU– Dept. MBB - SFU

_____

Dr. Barry Honda

Internal Examiner
Professor – SFU– Dept. MBB - SFU

_____

Dr. David Goldfarb

External Examiner
Professor – Dept. Biology

University of Rochester

Date Defended/Approved:
23 April 2012
_____

Abstract

Cell polarity is maintained via a balance of exocytosis and endocytosis; the protein machinery that mediates these transport processes must be co-ordinated with membrane lipid signals. This lipid signalling is, in part, dependent on the establishment of membrane domains through lipid transport. Cholesterol is transported via a poorly defined route that is independent of vesicle-mediated secretory protein transport. This "non-vesicular" sterol transport is postulated to involve the conserved family of Oxysterol binding protein (OSBP) Related Proteins (ORPs), which are proposed to be sterol lipid transport proteins (LTPs). To test if ORPs primarily act as sterol LTPs or alternatively as sterol-responsive signalling proteins, the function of *Saccharomyces cerevisiae* OSBP Homologues (*OSH1-OSH7)* were analyzed. Depletion of all Osh proteins in yeast cells inhibited growth, and defects in endocytosis, polarized exocytosis, and sterol homeostasis, were observed. Consistent with a direct role in exocytosis, Osh-depletion disrupted the polarized localization of vesicle transport regulators (Rho- and Rab-GTPases, and exocyst complex subunits) and the Osh protein Osh4p was observed to travel on exocytic vesicles to sites of polarized growth. Osh4p also formed complexes *in vivo* with specific Rho- and Rab-GTPases, and exocyst complex subunits. Contrary to the postulated role of ORPs as LTPs, a designed mutation in Osh4p that disrupts its ability to bind and thereby transport sterols, did not inactivate the protein but caused a gain-of-function phenotype affecting exocytosis. Our experiments suggested that ORPs are not sterol LTPs and implied that sterols act as signalling ligands that repress Osh4p, and potentially other ORPs. To understand how Osh proteins might simultaneously affect both exocytosis and endocytosis, I tested whether the regulation of the exocytic and endocytic machinery are directly coupled. I found that the Rab GTPase Sec4p, which is an integral component of exocytosis, directly interacted with specific endocytic proteins at actin patches. *SEC4* was required for proper endocytic site assembly and actin patch polarization, indicating that Sec4p links exocytosis and endocytosis to maintain cell polarization. Because these novel mechanisms involving sterol signalling and cell polarization are likely to be conserved, I propose these studies have broader medical implications applicable to cancer cell growth and metastasis.

Dedication

For my family.

Acknowledgements

To all those who have helped me and supported me over the years…thank you.

Table of Contents

1: **General introduction**

The wealth of polarized cell types is dependent on the establishment and maintenance of a subcellular protein and lipid asymmetry. The molecular basis for cell polarization is mediated by generally conserved steps (Johnston and Ahringer, 2010): identification of symmetry breakage, asymmetric redistribution of the cytoskeleton, recruitment of highly conserved protein and lipid transport regulators, and integration of cargo transport with the polarity information. In eukaryotes, a conserved family of Oxysterol Binding Protein (OSBP) Related Proteins (ORPs) is implicated in both cell polarity and lipid homeostasis (Beh and Rine, 2004). Ultrastructural analysis of ORP depleted budding yeast identified defects in bud formation and defects in both vesicular and sterol transport to the plasma membrane (PM) (Beh and Rine, 2004). Since ORPs are implicated in sterol transport *in vivo* (Beh and Rine, 2004), and promote sterol transport between liposomes *in vitro* (Raychaudhuri et al., 2006), ORPs are proposed to act as sterol Lipid Transport Proteins (LTPs) that directly shuttle sterol lipids between membranes (Shulz et al., 2009). The data presented in this thesis will test and ultimately challenge the ORP sterol LTP model by establishing ORPs as sterol dependent regulatory proteins. Moreover, this thesis will show that yeast ORPs use sterol signalling to integrate lipid and protein transport. Ultimately, this thesis will identify cells can establish and maintain cell polarity through the integration of protein and lipid transport to and from the cell surface.

1.1 Establishing and maintaining cell polarity through lipid and protein regulators: a process conserved across Eukarya

The protein regulators that mediate cell polarity are highly conserved across eukaryotes. In the budding yeast *Saccharomyces cerevisiae*, cell polarization is directly coupled to its life cycle. During vegetative growth, the yeast mother cell will establish a bud, or daughter cell, at one site on its cell surface, in part, through the activity of conserved GTPases. Mutants of the Rho-GTPase *CDC42* result in the loss of both actin polarization and vesicular transport to the daughter bud (Adamo et al., 2001), which implicates Cdc42p as a regulator of yeast polarity. In the *Caenorhabditis elegans* embryo, the partitioning defective (PAR) proteins, which are a family of proteins that establish cell polarity, are maintained polarized to the apical membrane through Cdc42-dependent endocytic recycling (Balklava et al., 2007). In 2D cultured Madin-Darby Canine Kidney (MDCK) cells, Cdc42 promotes the polarized transport of cargo to the basolateral membrane (Kroschewski et al., 1999). Together these results emphasize that polarity regulators, such as the Rho-GTPase Cdc42p, maintain conserved functions across eukaryotes. Interestingly, when MDCK cells are cultured in 3D, Cdc42 now promotes the apical targeting of both the PAR complex and vesicles (Martin-Belmonte et al., 2007), instead of their basolateral targeting (Kroschewski et al., 1999). This change in Cdc42 activity is due to the re-distribution of the phosphatidylinositol phospholipid (PIP) PI(4,5)P to the apical membrane (Martin-Belmonte et al., 2007). PI(4,5)P will recruit Cdc42 to the apical membrane through the PI(4,5)P binding protein Annexin 2 (Martin-Belmonte et al., 2007). In yeast, the maintenance of Cdc42p at polarized sites is dependent, in part, on the flipping of phosphoethanolamine to the cytosolic leaflet of the

PM (Das et al. 2012). This increase in neutral lipid weakens the interaction between charged residues of Cdc42p and the PM, which then permits the extraction of Cdc42p from the PM by the Rho GDP dissociation inhibitor Rdi1p (Das et al., 2012). Membrane extraction maintains Cdc42p polarity, since any Cdc42p diffusing away from polarized sites is removed from the PM (Das et al., 2012). Taken together, well-studied protein regulators of polarity have conserved functions across eukaryotes and are regulated, in part, through lipid activity.

Underlying the protein dependent regulation of cell polarity is lipid homeostasis. In mammalian cells, the broad spectra of headgroups and aliphatic side chains results in over 1000 different species of lipids existing at any one time (Prinz, 2010). Although some lipids, such as PIPs, act as signalling ligands by direct association with proteins (Antonietta De Matteis and Godi, 2004), others utilize their biophysical properties to form functional ordered domains within membranes. For example, sphingolipids have long saturated acyl side-chains that naturally form hydrophobic interactions with cholesterol. As a result, sphingolipids and cholesterol will coalesce in membranes forming tightly packed membrane micro-domains called lipid rafts (Rajendran and Simons, 2005). Proteins with affinity for these lipid domains, such as the Hedgehog signaling protein (Karpen et al., 2001), can then be clustered within the membrane resulting in localized protein signalling. During yeast mating, two haploids, of opposite mating types, will form polarized mating projections or "schmoos" towards the other cell. The schmoo is enriched in lipid rafts allowing for the polarized localization of the yeast Mitogen Activated Protein Kinase (MAPK) Fus1p (Proszynski et al., 2006). In yeast cells defective in sterol production or treated with cyclodextrin, which extracts sterols from

membranes, these polarized lipid rafts will not form, preventing schmoo formation and Fus1p activation (Proszynski et al., 2006). Interestingly, the activity of the human Extracellular signal-related kinase (ERK) MAPK is also affected by cholesterol, since the ERK phosphatases can form a cholesterol-dependent regulatory complex with OSBP, resulting in ERK dephosphorylation and inactivation (Wang et al., 2005b). These results demonstrate that sterol lipids play both a structural role through lipid rafts and a direct signalling role to modulate cell signalling and polarity. Therefore, the regulators of these signalling lipids, such as the ORP family, could couple lipid homeostasis with the protein regulators of cell polarity.

1.2 ORPs: a conserved and essential protein family that mediates lipid homeostasis and cell polarity

To identify the function or functions for the ORP family, forward genetic approaches have been widely used (Beh et al., 2001; Laitinen et al., 2002; Johansson et al., 2003; Lehto et al., 2004). However, ORPs are always found as a multi-gene family, with both mice and humans having 12 ORPs in their haploid genome (Yan and Olkkonen, 2008). Although animal and human tissue culture models are utilized in ORP studies, identifying conserved functions for the entire ORP gene family, through forward genetic approaches, is almost impossible in these systems. This technical feat would require a mouse model with 23 ORP loci disrupted and the final canonical OSBP locus under the control of a regulated promoter. The regulated OSBP is required since the homozygous deletion of OSBP results in murine embryonic lethality (Beh et al., 2001; Im et al., 2005). As a result of these technical limitations and also due to its simplified, yet conserved,

polarity and lipid regulatory processes, studies utilizing the budding yeast *S. cerevisiae* have been critical in elucidating the function of the entire ORP family.

S. cerevisiae have seven OSBP homologues (*OSH*s), *OSH1/SWH1*, *OSH2*, and *OSH3*, *OSH4/KES1, OSH5/HES1, OSH6*, and *OSH7*, (Figure 1.5.1) that together perform at least one essential function (Beh et al., 2001). Depleting a cell of all seven Osh proteins results in cell growth arrest and defects in both sterol homeostasis and cell polarization (Beh and Rine, 2004). These sterol defects are manifested as an accumulation of free and stored sterols within the cell, while the loss of cell polarity is a consequence of polarized vesicle accumulation and a block in endocytosis (Beh and Rine, 2004). Interestingly, the expression of any single *OSH* gene can rescue these phenotypes demonstrating that the *OSH* family members perform an essential but overlapping function (Beh et al., 2001) linked to both sterol homeostasis and polarized vesicular transport (Beh and Rine, 2004). However, the mechanism and the protein partners used to mediate these essential polarity and sterol regulatory functions are unclear.

The entire ORP family is defined by an OSBP-Related ligand binding Domain (ORD) (Lehto and Olkkonen, 2003) that binds lipid ligands, such as cholesterol, ergosterol, and oxysterols (Im et al., 2005). Since the ORD motif is highly conserved across Eukarya (Lehto and Olkkonen, 2003), it suggests that the protein and lipid interactions mediated by it are also conserved. In general, ORPs are found either as short proteins comprised almost entirely of the ORD motif or as long proteins with an N-terminal extension and a C-terminal ORD motif. This N-terminal extension contains protein-binding domains, such as ankyrin repeats, and lipid interaction domains, such as pleckstrin homology domains that bind PIPs (Figure 1.5.1). Since the short ORPs can

complement the *OSH* essential function (Beh et al., 2001), it demonstrates that the short ORPs define the minimum ORP requirement. Therefore, studies focusing on the short ORPs, such as Osh4p, can identify the conserved sterol homeostasis and cell polarity function mediated by the entire ORP family.

1.2.1 Models for sterol transport: Possible mechanisms for a putative ORP sterol transport activity

The regulation of free sterols in yeast is mediated, in part, by its transport between membranes and its storage as sterol-esters in lipid droplet organelles (Model for Lipid droplet formation outlined in Figure 1.5.2). In Osh protein depleted cells, the levels of free sterols decrease at the PM, while sterol levels increase in internal membranes (Beh and Rine, 2004), implicating ORPs in the maintenance of normal sterol distribution. In addition, there is an increase in the number of lipid droplet organelles (Beh and Rine, 2004). Since the sterol storage machinery is still active in an Osh protein depleted cell, it suggests that the primary role for Osh proteins, in sterol homeostasis, is the regulation of sterol lipid transport.

In both human fibroblasts (Lange et al., 1989) and yeast cells (Maxfield and Menon, 2006), up to 90% of the cells total cholesterol accumulates in the PM. This suggests that a vectoral cholesterol transport mechanism exists between the ER (the site of synthesis) and the PM. Although ORPs are implicated in sterol transport (Beh and Rine, 2004), no proteins have been identified that directly mediate sterol transport *in vivo* (Beh et al., 2012). To try to address this issue, several non-mutually exclusive cholesterol transport models have been proposed (Figure 1.5.3). One model postulates that the transport of cholesterol between membranes can utilize a non-vesicular/vesicle-

6

independent mechanism, such as passive diffusion or a lipid carrier protein. Another model suggests that cholesterol primarily utilizes the ER to Golgi to PM secretory vesicle transport route. By addressing these models we can identify the role for Osh proteins in sterol transport.

The original model for cholesterol transport implicated the _secretory vesicle transport machinery_. This model was supported by the observed increase in cholesterol concentration along the ER to PM secretory transport route (DeGrella and Simoni, 1982) and by the ability to block both vesicular and cholesterol transport upon culturing mammalian cells at 15°C (Kaplan and Simoni, 1985). However, subsequent studies showed that blocking of vesicular transport, by Golgi disruption through the treatment of mammalian cells with monensin (Kaplan and Simoni, 1985) and Brefeldin A (Urbani and Simoni, 1990), did not disrupt sterol transport from the ER to the PM. Moreover, blocking of yeast vesicular transport through the use of _SEC18/_N-ethylmaleimide Sensitive Factor (NSF) conditional mutants did not result in a change in sterol transport between the ER and the PM (Baumann et al., 2005; Li and Prinz, 2004). Overall, these results demonstrate that cholesterol can utilize a "non-vesicular" transport process independent of the classical Sec18p/NSF dependent vesicle trafficking pathway. However, the relative contribution of this "non-vesicular" pathway to cholesterol transport, when vesicular transport is still functional, is unclear.

Interestingly, a Golgi independent ER to PM protein transport process has been identified. The transport of the cystic fibrosis transmembrane receptor (CFTR) protein to the PM, in Chinese hamster ovary (CHO) cells, is unaffected by Golgi

7

disruption through Brefeldin A treatment (Yoo et al., 2002). Importantly, the transport of CFTR is dependent on the COPII carriers from the ER (Yoo et al., 2002), demonstrating that vesicles are still used in this Golgi independent transport process. These observations suggest that "non-vesicular" sterol transport could still utilize a vesicle intermediate. Nevertheless, the preferred non-vesicular transport models (detailed below) postulate that sterol transport is a vesicle independent process.

A *passive diffusion non-vesicular transport mechanism* (Figure 1.5.3) is supported by the observation that cholesterol can spontaneously transfer, albeit slowly, between two artificial vesicles *in vitro* (McLean and Phillips, 1981). Decreasing the distance between the donor and recipient membranes can increase the rate of spontaneous transport, due to the increasing "collision" frequency of the two membranes (Jones and Thompson, 1989). However, the measured *in vitro* transport rates are over 100,000 fold slower than the *in vivo* rate of cholesterol transport to the PM (Sullivan et al., 2006). Thus, although a spontaneous diffusion mechanism could play a role in cholesterol transport, it is not likely to be the proposed Osh protein dependent sterol transport process.

Since a diffusion based non-vesicular cholesterol transport process is insufficient to mediate cholesterol transport *in vivo*, a *conserved protein dependent non-vesicular lipid transport mechanism* is likely involved. Although proteins could stimulate spontaneous cholesterol transport by promoting membrane curvature (Figure 1.5.3) (Nichols and Pagano, 1983), proteins could also act as lipid transport proteins (LTPs) to physically transport cholesterol between cellular membranes (Figure 1.5.3). This latter model has gained wide acceptance (Liscum and Munn, 1999) despite being controversial (Lehto and

8

Olkkonen, 2003; Olkkonen et al., 2006). LTPs for other lipids have been identified and the best studied are the START (Steroidogenic Acute Regulatory protein related lipid Transfer) domain containing proteins. These START proteins have been implicated in the non-vesicular transport of ceramide (Hanada et al., 2003) and of cholesterol (Kallen et al., 1998). However, no START domain proteins are found in yeast, demonstrating that START proteins cannot be the non-vesicular cholesterol transport proteins conserved across eukaryotes. Therefore, another conserved group of proteins, such as the ORPs, must mediate non-vesicular sterol transport.

1.2.2 Are ORPs sterol transporters or lipid dependent regulators?

The conserved ORP family is the preferred candidate protein family to mediate sterol LTP function (Schulz et al., 2009; Raychaudhuri and Prinz, 2010). In support of this sterol LTP model, the Osh4p crystal structure was solved with and without its sterol ligand bound within a hydrophobic core (Figure 1.5.4) (Im et al., 2005). Osh4p also has a α-helical lid that covers the sterol-binding pocket, which is proposed to protect the sterol from the aqueous environment during sterol lipid transport (Im et al., 2005). In further support of the sterol LTP model, specific Osh4p sterol binding mutants are non-functional and cannot suppress the *OSH* essential function (Im et al., 2005). However, structural features also challenge this ORP sterol LTP model. Firstly, the Osh4p hydrophobic pocket actually contains 15 water molecules, which is surprisingly "watery", and the sterol molecule is maintained through hydrogen binding between its 3`-OH to a water molecule (Im et al., 2005). Moreover, an Osh4p with its lid removed has the same affinity for sterols, even though the sterol molecule is now exposed to the aqueous environment (Im et al., 2005). Lastly, PI4P competes for binding within the Osh4p sterol

binding pocket (de Saint-Jean et al., 2011) demonstrating that an exclusive sterol LTP function is improbable.

Alternate models for ORP activity postulate that ORPs are not sterol transporters but rather utilize sterols as regulatory ligands (Wang et al., 2005b; Olkkonen et al., 2006). The canonical OSBP, when bound to oxysterols, will translocate to the Golgi where it then promotes CERT mediated ceramide production (Perry and Ridgway, 2006). Moreover, OSBP, when bound to cholesterol, will form a complex with the phosphatases of ERK resulting in ERK dephophorylation and inactivation (Wang et al., 2005b). However, when OSBP is bound to oxysterols this regulatory complex does not form and ERK activation is maintained (Wang et al., 2005b). Therefore, OSBP can use sterol binding as a regulatory ligand to modulate the activity of different proteins. ORPs can also utilize sterol binding to modulate polarized organelle transport. The mammalian ORP1L promotes Rab7-GTPase mediated trafficking of the late endosome (LE) (Johansson et al., 2005; Johansson et al., 2007). ORP1L, upon cholesterol binding (Vihervaara et al., 2010), will form a complex with Rab7 and RILP, a Rab7 effector protein, at the LE (Vihervaara et al., 2010; Johansson et al. 2007). This complex will recruit the Dynein motor, through interactions with the Dynactin complex, which allows for the transport and peri-nuclear clustering of LEs (Johansson et al. 2007). This demonstrates that ORPs utilize sterol binding to directly regulate polarized transport. In Osh protein depleted yeast cells, polarized vesicles, which are transported by the Rab-GTPase Sec4p, accumulate in the daughter bud (Beh and Rine, 2004). Therefore, in a manner analogous to ORP1L, Osh proteins, in response to sterol binding, could affect

yeast cell polarity by directly regulating the protein machinery that controls polarized vesicle transport.

1.3 Mechanism for polarity establishment and polarized vesicular transport: lipid and protein targets for ORP polarity activity

Yeast cells depleted of Osh proteins often have multiple buds (Beh and Rine., 2004), demonstrating that Osh proteins affect the bud formation machinery. The formation of a yeast daughter bud (Figure 1.5.5) begins by establishing an incipient bud-site on the cell cortex. This breakage of cell symmetry is mediated by the bud site selection complex, which recruits the Rho-GTPase Cdc42p to the incipient bud-site (Zheng et al., 1995). The recruitment of Cdc42p results in the polarized activation of both the formin proteins and the Arp2/3 complex, which are both actin nucleators (Schott et al., 2002). These proteins will promote actin polymerization at the incipient bud-site resulting in a polarized redistribution of actin filaments and actin patches (Figure 1.5.5) (Schott et al., 2002). Subsequently, the vesicle associated Rab-GTPase Sec4p, through its binding of the type-V myosin motor Myo2p, will facilitate the transport of vesicles along the now polarized actin filaments (Figure 1.5.6)(Schott et al., 1999). Once the vesicle reaches the plasma membrane, a conserved octameric protein complex called the exocyst complex (Figure 1.5.6), mediates vesicle docking (Munson and Novick, 2006; Novick et al., 2006).

The exocyst complex is separated into two parts. Two exocyst subunits, Sec3p and Exo70p, are localized to the PM through interactions with the Rho-GTPases Rho1p (Guo et al., 2001), Rho3p (He et al., 2007b), and Cdc42p (Zhang et al., 2008). The remaining six exocyst subunits associate with Sec4p to transit with the secretory vesicle

to the PM (Boyd et al., 2004; Guo et al., 1999). Once the vesicle reaches the target membrane, the two halves of the exocyst assemble, which docks the vesicle (Munson and Novick, 2006). Although the PM targeting of the exocyst complex is facilitated by Rho-GTPase binding (Guo et al., 2001; He et al., 2007b), direct interactions with PI(4,5)P also promotes Sec3p and Exo70p recruitment to the PM (He et al., 2007b; Zhang et al., 2008). In contrast to the positive role PIPs play in Sec3p and Exo70p recruitment, the vesicle recruitment of the exocyst protein Sec15p, by Sec2p,(Zajac et al., 2005) is inhibited by PI(4)P (Mizuno-Yamasaki et al., 2010). Overall, PIPs and GTPases work in concert to mediate polarized vesicular transport. Since cells depleted of Osh proteins accumulate vesicles in the daughter bud (Beh and Rine, 2004), the exocyst complex along with the lipids and GTPases that regulate polarized vesicular transport are possible targets for Osh protein function in cell polarity.

GTPase activity not only promotes the polarized targeting and delivery of secretory vesicles, but it also mediates vesicle biogenesis from the trans Golgi network (TGN). The Rab-GTPase Ypt31p binds Myo2p to facilitate the transport of the newly formed vesicle from the TGN (Mizuno-Yamasaki et al., 2010). The recruitment of Ypt31p to the TGN is dependent on its binding to PI(4)P; once at the TGN, Ypt31p recruits the Sec4p GEF, Sec2p (Mizuno-Yamasaki et al., 2010). The importance of TGN PI(4)P levels on vesicle biogenesis is further highlighted by the essential gene *SEC14,* which is a yeast phosphatidylinositol transfer protein (Bankaitis et al., 1989; Fang et al., 1996). Loss of Sec14p function results in an increase in Golgi phosphatidylcholine levels and a decrease in PI(4)P levels, suggesting that Sec14p establishes the membrane environment necessary for

vesicle budding (Bankaitis et al., 1989; Fang et al., 1996). Interestingly, the deletion of *SAC1*, which is a Golgi PI(4)P phosphatase, bypasses a *sec14-1* loss of function temperature sensitive mutation (Cleves et al., 1989). *PIK1* over-expression, which is the primary PI-4-kinase, suppresses the *sec14-1* mutation (Hama et al 1999), presumably due to the resulting increase in PI(4)P levels. Taken together, the regulation of vesicle budding from the TGN is not only dependent on Rab-GTPase protein function but also on PI(4)P regulatory signalling. Importantly, *OSH4* is also a by-pass suppressor of *SEC14* mutations (Fang et al., 1996; Li et al., 2002) and Osh4p promotes Sac1p mediated PI(4)P dephosphorylation *in vitro* (Stefan et al., 2011). This suggests that Osh4p can negatively regulate vesicle budding at the TGN by decreasing Golgi PI(4)P levels through Sac1p activation. However, Osh protein depleted cells accumulate vesicles in the bud, suggesting that Osh proteins also play a later role in vesicle docking.

Altogether a model for PIP mediated regulation of GTPase dependent vesicular transport can be proposed (Figure 1.5.7). Sec2p will associate with vesicles as they are released from the Golgi, due to the presence of PI(4)P and Ypt31p. Although the cause is unknown, vesicle PI(4)P levels reduce as they transit from TGN to the PM (Mizuno-Yamasaki et al., 2010). As vesicle PI(4)P levels lower, Sec2p can then bind Sec15p and activate Sec4p resulting in the recruitment of the other vesicle associated exocyst components (Figure 1.5.7) (Mizuno-Yamasaki et al., 2010). Lastly, the association of Sec3p and Exo70p with both PI(4,5)P (He et al., 2007b; Zhang et al., 2008) and Rho-GTPases (Guo et al., 2001; He et al., 2007b) allows for the proper targeting and docking of vesicles to the PM. Since yeast ORPs affect PIP homeostasis at the Golgi (Fang et al.,

1996), and are required for the late stages of polarized vesicular transport (Beh and Rine, 2004), ORPs could play an active, but yet to be defined, role in cell polarity by integrating lipid signalling with polarized vesicular transport.

1.4 Maintaining cell polarity: A balance between polarized exocytosis, passive diffusion, and endocytosis

The formation of the polarized yeast daughter bud requires both the establishment and *maintenance* of subcellular protein and lipid asymmetry. In epithelial cells, tight junctions act as diffusion barriers that maintain the polarized apical and basal membrane domains separate (Matter and Mellman, 1994). In *S. cerevisiae,* the multimeric septin protein complex acts as a diffusion barrier at the yeast bud neck (Schmidt and Nichols, 2004; Takizawa et al., 2000), maintaining the polarized localization of exocytic cargo in the daughter bud. Although a diffusion barrier is important in maintaining cell polarity, yeast also utilize a balance between polarized exocytosis and endocytosis to recycle all polarized material before it can diffuse to equilibrium with the mother call (Bretscher and Thomson, 1983). During the establishment of yeast cell polarity by Cdc42p, actin-mediated endocytic recycling maintains Cdc42p polarization by compensating for the diffusion of Cdc42p away from the incipient bud-site (Slaughter et al., 2009). During daughter bud growth, the v-SNARE Snc1p is enriched in the daughter bud PM. However, in endocytosis mutants, Snc1p is depolarized and reaches equilibrium with the mother cell (Valdez-Taubas and Pelham, 2003). Mathematical models postulate that polarized exocytosis, endocytosis, and a diffusion barrier must act in concert to maintain yeast cell polarity (Marco et al., 2007). Therefore, cell polarity is maintained by balancing

polarized exocytosis, endocytosis and diffusion; however, the mechanism by which they are integrated is unclear.

Late *SEC* mutants involved in Golgi to PM transport block endocytosis, suggesting that late Sec proteins could integrate exocytosis with endocytosis (Riezman, 1985). In yeast and mammalian cells, clathrin mediated endocytosis occurs at the actin patches that form on the PM (Kaksonen et al., 2003; Kaksonen et al., 2005), which suggests that late Sec proteins could mediate their endocytic activity through actin patches. The formation of the actin patch occurs in a temporal manner. Initially, several long-lived, slow-moving proteins arrive at the incipient endocytic site followed by the recruitment of shorter-lived, highly motile proteins that promote actin nucleation and endocytic vesicle formation (detailed in Figure 1.5.8) (Kaksonen et al., 2005). Although much is known with respect to the assembly of actin patches, it is unclear what promotes the transition from the early stage to the subsequent active coat assembly stage. Recent data suggests that the recruitment of cargo to the endocytic site promotes this transition (Carroll et al. 2012). This cargo-driven endocytosis is dependent on *SEC18*/NSF mediated endocytic recycling, implicating Sec proteins at this step in the endocytic process (Carroll et al. 2012). In addition to the role for Sec proteins in endocytosis, mutants in the ergosterol biosynthesis gene *ERG2/END11* also fail to internalize endocytic vesicles from the PM (Munn et al., 1999; Munn and Riezman, 1994). In support of a role for sterols in endocytosis, over-expression of ORP2, in both HeLa and CHO cells, resulted in increased cholesterol transport to the PM and increased endocytosis of transferrin (Hynynen et al., 2005). Yeast ORPs are also required for both sterol homeostasis and endocytosis (Beh and Rine., 2004), demonstrating that integrating these processes could be a conserved

ORP function. Taken together, yeast could link exocytosis, endocytosis and sterol regulation to maintain protein polarization to the daughter bud.

1.4.1 Models for the coupling of exocytosis to endocytosis: Possible mechanisms for a homologous process in yeast

Although links between yeast exocytosis and endocytosis have been identified, such as the endocytosis defects of late *SEC* mutants (Riezman, 1985), the mechanism linking the two processes is unknown. In higher eukaryotes, it has been shown that a "compensatory endocytosis" mechanism integrates exocytosis with endocytosis. Compensatory endocytosis is used by several cell types, such as neuronal cells (Jarousse and Kelly, 2001), secretory cells (Schneider et al., 1997), and *Xenopus* oocytes (Jarousse and Kelly, 2001; Sokac et al., 2003), to "compensate" for rapid bursts of exocytosis by coupling it with an endocytic event. For example, the rapid release of neurotransmitter at the synapse by exocytosis requires an efficient and rapid endocytic response to maintain PM composition (Jarousse and Kelly, 2001). In the case of a neuronal cell, this process is commonly called the Synaptic Vesicle cycle. Although endocytosis and exocytosis are independently well studied in yeast, no similar compensatory endocytosis mechanism has been established. In metazoans, three models for compensatory endocytosis have been defined (Figure 1.5.9):

a)   **Full Fusion compensatory endocytosis:** This model is the traditional view of the exocytosis and endocytosis relationship. In this model, an exocytic vesicle will fuse completely with the target membrane resulting in complete vesicle membrane insertion to the PM. In addition to membrane insertion, this exocytic vesicle could deposit a specific

cargo, such as a membrane bound protein, that then triggers an endocytic event to occur. Although this endocytic event will compensate for the earlier exocytic event, this endocytic vesicle will not be directly coupled to the exocytic vesicle. Moreover, the time between the vesicle fusion and endocytosis event is not necessarily constant.

b) **Kiss and Run compensatory endocytosis:** In this model of compensatory endocytosis, an exocytic vesicle will dock with the PM and a small 1 to 5nm fusion pore will form between the PM and vesicle membranes. This fusion pore will allow for the short-lived release of exocytic cargo resulting in the rapid dissociation of the exocytic vesicle from the PM. There are several studies that support this model of endocytosis. It was observed that the exocytic vesicle in some cell types does not fuse completely with the PM and the resulting fusion pore has the conductivity of a small ion channel (Lollike et al., 1995). Subsequent studies demonstrated that during dopamine release at the chemical synapse of neurones, the synaptic vesicle fusion pore would flicker open and closed releasing only around 25% of the dopamine cargo at a time (Staal et al., 2004). This rapidly forming and then disassembling fusion pore suggests that these dopamine-secreting cells utilize a "kiss-and-run" mechanism that quickly reuses vesicles to regulate neurotransmitter release. However, although kiss-and-run has been observed, there are some observations that cannot be explained by this mechanism.

c)   **Kiss-and-Coat compensatory endocytosis:** In some cell types, the fusion pore between the vesicle and PM dilates more than the 5nm seen in Kiss-and-Run. Also the vesicles remain fused for a much longer period of time due to formation of an actin patch around this fused exocytic vesicle. For example, granule vesicles in *Xenopus* oocytes will rapidly fuse with the PM upon fertilization to release its cargo resulting in PM expansion (Sokac et al., 2003). However, these partially fused vesicles will remain associated with the PM for up to one minute (Sokac et al., 2003). In pancreatic acinar cells, the granular vesicles can remain fused with the PM for over 15 minutes (Thorn et al., 2004). These vesicles associate with the PM for a longer period of time since they are secreting much larger and/or hydrophobic proteins (Dietl and Haller, 2005; Wessel et al., 2001) that require more time to secrete. It is noteworthy that the actin polymerization around this docked secretory vesicle can stabilize the vesicle and also provide the force for the subsequent internalization of the vesicle (Sokac et al., 2003). This Kiss-and-Coat mechanism will couples an exocytic vesicle directly with the formation of an actin patch..

1.4.2 Hypothesis: ORPs integrate sterol signalling with a novel yeast compensatory endocytosis mechanism

Compensatory endocytosis is utilized to internalize excess membrane during times of rapid exocytosis (Jarousse and Kelly, 2001; Sokac et al., 2003). The coupling of exocytosis and endocytosis also maintains cell polarity by preventing the

equilibration of polarized components (Bretscher and Thomson, 1983; Valdez-Taubas and Pelham, 2003; Slaughter et al., 2009). Although a yeast compensatory endocytosis mechanism has not been defined, two models were proposed to explain the functional connection between yeast late *SEC* genes and endocytosis (Figure 1.5.10) (Riezman, 1985). Firstly, it was proposed that the late *SEC* proteins have multiple functions, one of which will affect exocytosis and another that will affect endocytosis. This situation is similar to the full fusion model of compensatory endocytosis where exocytosis deposits a protein, after full fusion with the PM, which will then stimulate a compensatory endocytic event to occur (Figure 1.5.9). The second model postulated that an exocytic vesicle, and its associated Sec proteins, would directly associate with an endocytic site and as a result directly couple endocytosis with exocytosis. The latter model is supported by the morphological data that shows exocytic vesicles are adjacent to sites of endocytosis (Adams and Pringle, 1984; Kilmartin and Adams, 1984). Interestingly, *OSH* depleted cells have both an endocytic defect and a late secretory defect (Beh and Rine, 2004), demonstrating that Osh proteins could affect the Sec proteins implicated in endocytosis and exocytosis integration. Moreover, Osh protein activity is linked to sterol and PIP homeostasis, which are lipid regulators of both endocytosis and exocytosis. Therefore, Osh proteins could affect a putative *SEC* dependent compensatory endocytosis mechanism by coupling it to lipid signalling.

Overall, the research presented in this thesis will address how ORP activity links seemingly disparate transport pathways. Previous studies defined ORPs as exclusive non-vesicular sterol LTPs (Im et al., 2005), while other studies implicate ORPs as sterol dependent regulatory proteins (Wang et al., 2005b). To address these ORP models, we

demonstrate, in Chapter 2, that *OSHs* affect a specific polarized secretion pathway through conserved exocytosis regulatory proteins. In Chapter 4, we establish a direct role for Osh proteins in vesicular transport and identify that an Osh4p sterol-binding mutant is a gain-of-function mutant. Through this work, we establish ORPs as lipid dependent regulatory proteins and not exclusive sterol LTPs. During the study of Osh proteins in secretion, a novel link between exocytosis and endocytosis is identified. Osh and late *SEC* proteins are known to affect both endocytosis and exocytosis, yet a mechanism coupling these transport pathways is unknown. In Chapter 5, we show that the Rab-GTPase Sec4p co-localizes with and physically interacts with actin patch proteins identifying Sec4p as a bonafide actin patch component. Since a coupled exocytosis and endocytosis process is utilized by other eukaryotes, this novel endocytic role for the highly conserved Rab-GTPases could apply to other systems. On the whole, this thesis will provide novel mechanistic insight to not only the field of ORP research, but also to the study of transport pathways that control cell polarization.

1.5 Figures

Figure 1.5.1: Domain structure of the *OSH* gene family
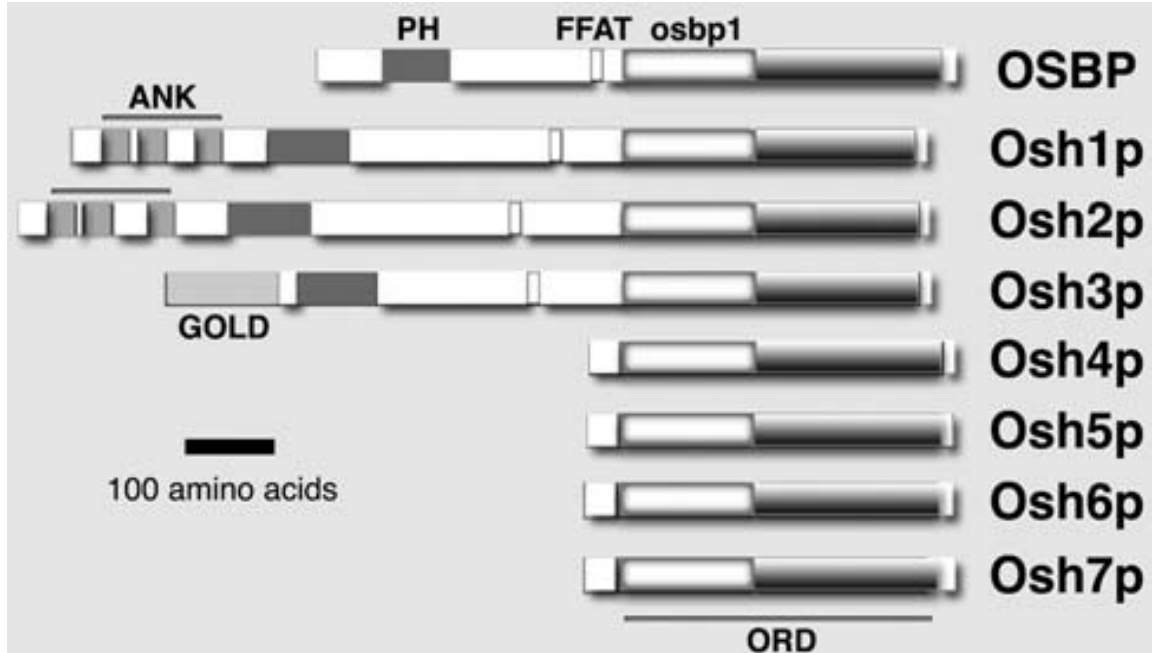
Figure 1.5.1: <u>**The domain structure of the OSH family relative to canonical OSBP**</u>. The entire ORP superfamily is defined by an OSBP related domain (ORD) within which resides a ~150 amino acid OSBP1 region that contains the highest sequence identity across the entire superfamily. The ORPs can be divided into two forms: long and short proteins. Long ORPs (OSBP, *OSH1*, *OSH2* and *OSH3*) contain an N-terminal extension with a phosphoinositide lipid interacting domain (PH-domain) and protein interaction domains (Ankyrin repeats, GOLD domains, and FFAT motifs). Short ORPs (*OSH4*, *OSH5*, *OSH6*, and *OSH7*) are composed almost entirely of the ORD motif and lack these domains yet have shown an affinity for phosphoinositide lipids and protein-

protein interactions possibly through a C-terminal coiled-coil domain. From Beh et al.,(2009).

Figure 1.5.2: Model for lipid droplet formation in yeast
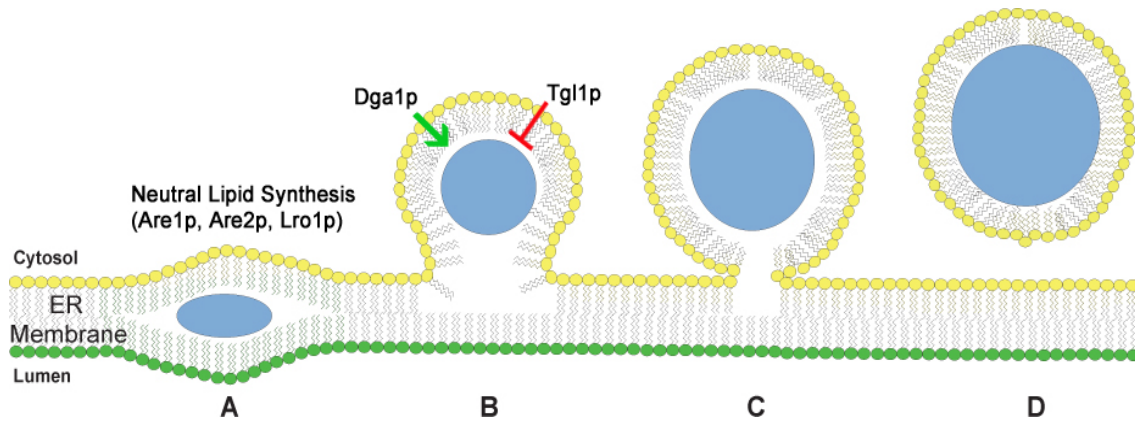
Figure 1.5.2: In yeast, the lipid droplet organelle is composed of a phospholipid monolayer (yellow) surrounding a core of neutral lipids (blue). (a) ER resident acyltransferases such as Are1p, Are2p, and Lro1p generate neutral lipids within the lumen of the ER membrane. (b) As neutral lipid synthesis progresses, the lipid droplet organelle forms from the ER membrane. The neutral lipid core in lipid droplets is modified by the activity of lipid droplet resident lipases such as the sterol ester hydrolase Tglp1 and acyltransferases such as Dga1p. (c) Continued lipid droplet organelle expansion will allow it to reach a critical size (d) and release from the ER membrane into the cytoplasm through an energy dependent but yet to be defined mechanism.

Figure 1.5.3: Models for non-vesicular lipid transport
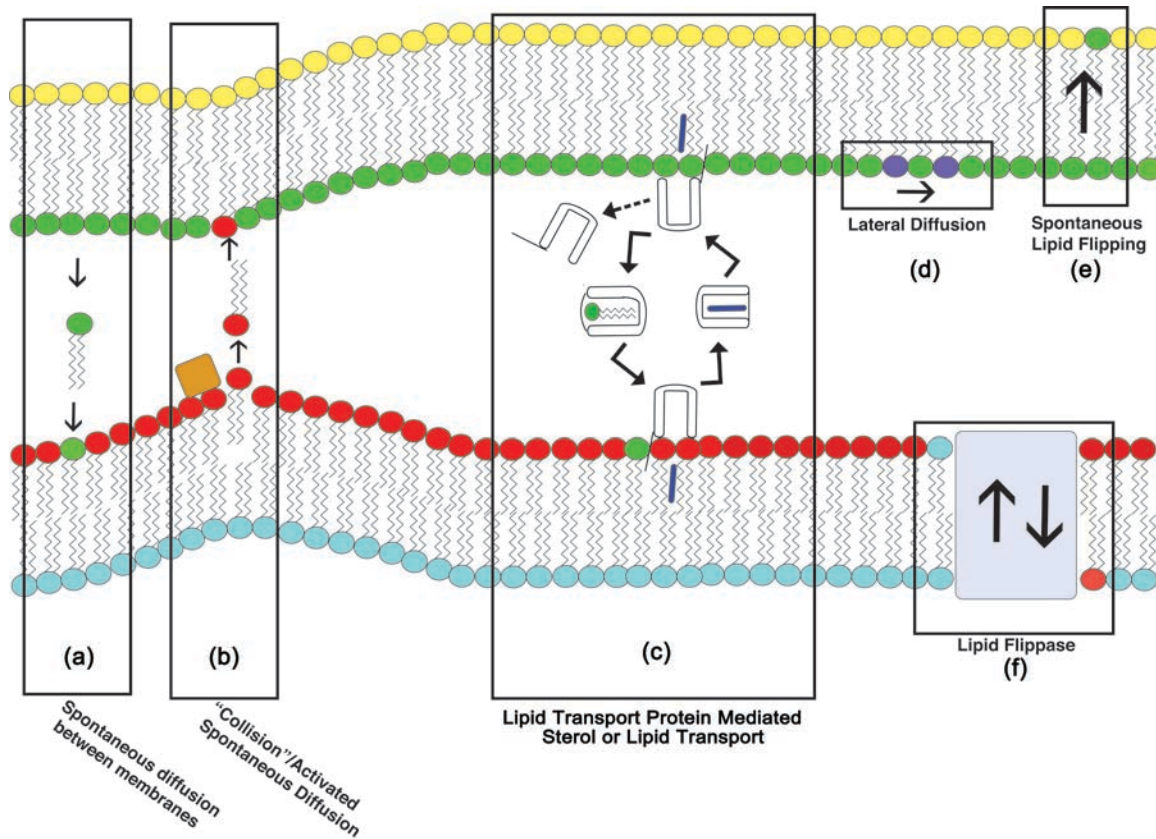
Figure 1.5.3: Models for the spontaneous movement of lipids between or within membranes. (a) Lipids can spontaneously diffuse between membranes even though lipids are poorly soluble. This spontaneous transfer can increase if membranes are closely juxtaposed. (b) Membrane curvature through protein binding (orange box) or membrane composition can "activate" a lipid, which facilitates its spontaneous transport to a closely juxtaposed membrane. The increased proximity between membranes can also increase the "collision" between membranes facilitating lipid transfer. (c) A soluble lipid transport protein (LTP) has a hydrophobic lipid binding domain, which protects the bound lipid from the aqueous environment. This LTP takes a lipid or sterol from a donor membrane (red) and transports it to the recipient membrane (green). After depositing the lipid, this

24

LTP can either dissociate from the membrane (dashed arrow) or take another lipid (green) for a subsequent transport event. (d) Lipids can move laterally within a leaflet of a membrane by diffusion, which is important in establishing membrane lipid domains. (e) Although movement of the charged lipid headgroup across a membrane bilayer is unfavourable, a lipid can spontaneously flip from one leaflet to another. (f) A lipid flippase can utilize ATP to move a lipid between membrane leaflets, overcoming the impediment of the charged lipid headgroup.

Figure 1.5.4: Structure of Osh4p bound to cholesterol
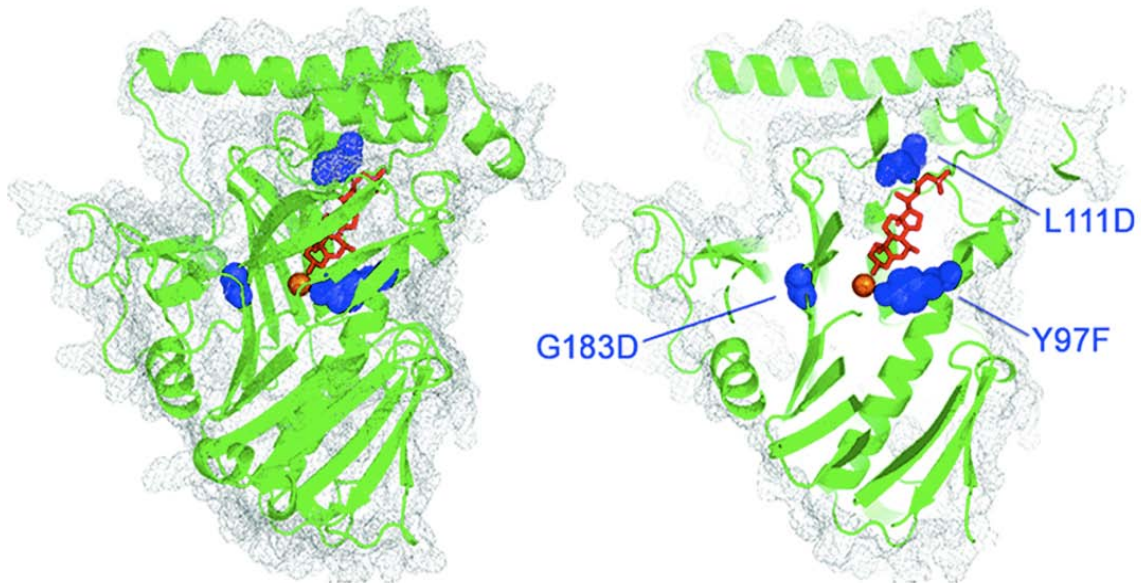
Figure 1.5.4: Ribbon diagram of full-length Osh4p (left) crystal structure and cutaway view of Osh4p (right). Cholesterol (red) is stabilized in the lipid-binding domain through hydrogen bonding with a water molecule (orange). The cutaway view of Osh4p details further cholesterol binding within the lipid-binding domain. The mutations noted result in different loss of function phenotypes. L111D adds a charged residue to the lid preventing membrane association and sterol extraction while Y97F prevents stabilization of the water molecule; both mutations result in loss of sterol binding. G183D results in the temperature sensitive loss of function *osh4-1* mutant allele. From Alfaro et al. (2011).

Figure 1.5.5: The Rho-GTPase Cdc42p regulates actin organization and polarized vesicular transport during yeast daughter bud formation
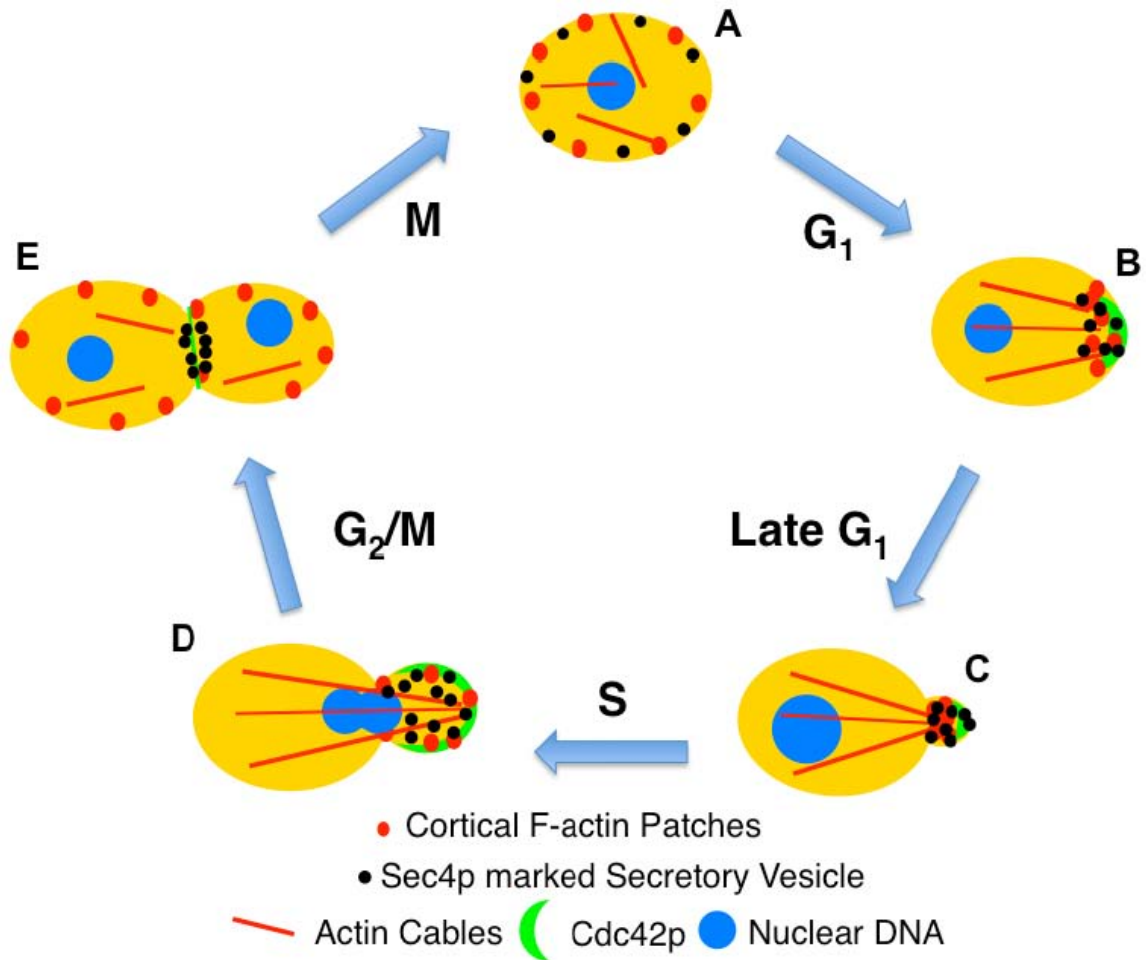
Figure 1.5.5: (a) Isotropic growth results in random vesicle and actin localization. (b) The bud-site selection complex (not shown) recruits Cdc42p to the PM, which polarizes the actin machinery to this site by actin nucleation. The polarized actin allows for the polarized delivery of vesicles to this site. (c) Polarized vesicular transport to this incipient site allows for polarized membrane insertion and small bud formation. (d) Cdc42p localization broadens around the daughter bud membrane allowing for isotropic daughter bud growth. The actin patches around the daughter bud maintain polarization through polarized endocytic recycling. (e) Cdc42p localization switches from the

daughter bud membrane to the budneck to allow for membrane insertion and septum formation, which ultimately generates two separate cells.

Figure 1.5.6: Vesicle docking during yeast polarized vesicular transport mediated by the exocyst complex, Rho-, and Rab-GTPases
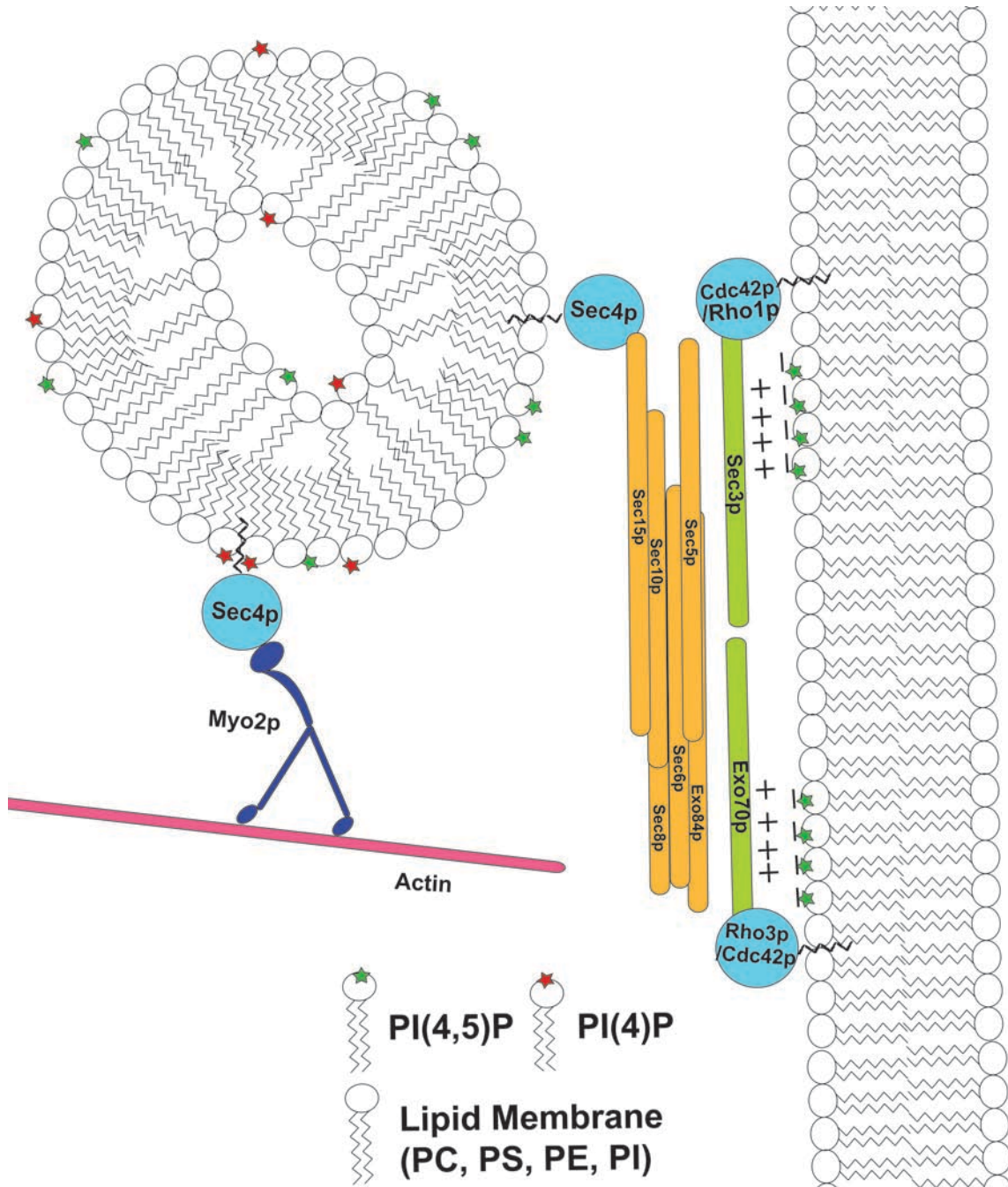
Figure 1.5.6: Vesicles are transported to the PM along actin cables by the binding of the Type V myosin motor Myo2p to the Rab-GTPase Sec4p. This association is

promoted by PI(4)P. Sec4p also associates with the octameric exocyst protein complex through direct binding to Sec15p. At the PM, Sec3p and Exo70p will bind PM-associated Rho-GTPases, providing a spatial and temporal landmark for vesicle docking. Sec3p and Exo70p also are recruited to the PM through interactions between charged residues and PI(4,5)P, which is made at the PM by the PI(4)P-kinase Mss4p. As the vesicle reaches the target membrane, the vesicle and PM-associated exocyst proteins assemble, resulting in vesicle docking to the PM.

Figure 1.5.7: Controlling Sec4p activation through Sec2p and PIP regulation
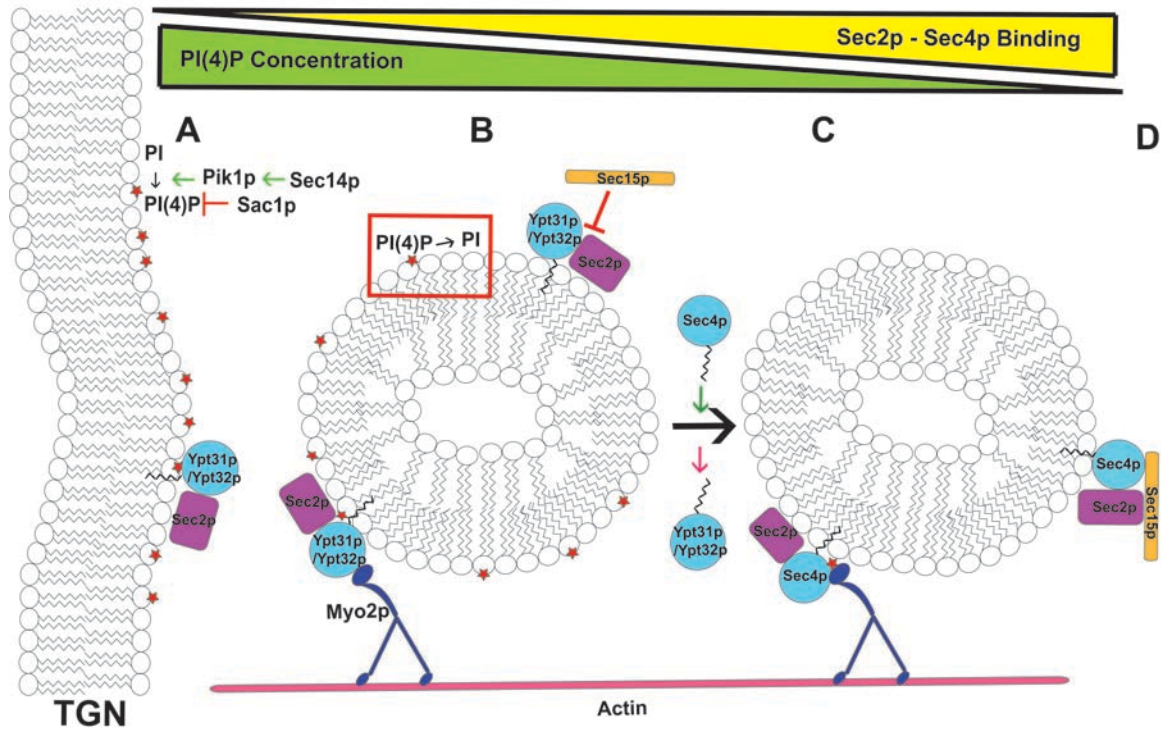
Figure 1.5.7: (a) Sec14p promotes the synthesis of PI(4)P at the TGN by activating the PI-4-Kinase, Pik1p. The formation of PI(4)P is antagonized by the PI(4)P phosphatase, Sac1p. During vesicle release from the TGN, Ypt31p/32p will associate to the developing vesicle along with PI4P and Sec2p. (b) Ypt31p associates with the Myo2p motor allowing for vesicle transport. During vesicle transport, PI(4)P levels are reduced by an unclear mechanism. With the reduction in vesicle PI(4)P levels, Sec15p can displace Ypt31p/32p from Sec2p allowing for Ypt31p/32p vesicle dissociation. (c) Sec15p associated with Sec2p promotes Sec4p recruitment and activation on the vesicle membrane, allowing for vesicle transport through Sec4p binding to Myo2p. (d) The assembly of Sec4p, Sec2p, and Sec15p into a protein complex allows for the eventual

association with the entire exocyst complex (not shown), which ultimately leads to vesicle docking at the PM.

Figure 1.5.8: The ordered assembly of Actin patches in yeast
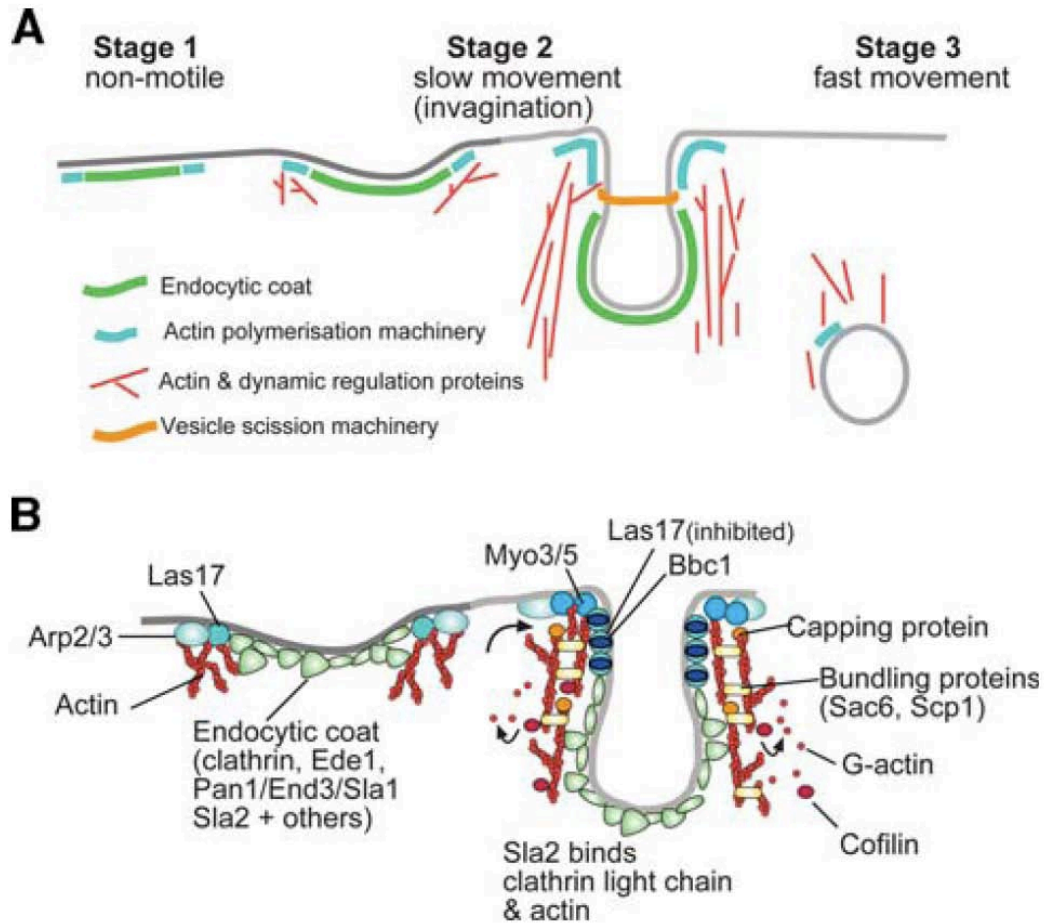
Figure 1.5.8: a) <u>**Actin patch formation is an ordered step-wise process.**</u> The non-motile long-lived stage 1 is marked by the recruitment of the endocytic coat proteins and actin polymerization machinery. During the slow movement stage 2, actin polymerization pushes against the endocytic coat, providing the force to generate the endocytic invagination. During the fast moving stage 3, actin polymerization continues to rapidly extend the endocytic invagination. The recruitment of the amphiphysin proteins to the endocytic invagination mediates vesicle scission and the released endocytic vesicle is rapidly internalized. **b)** <u>**Depiction of key protein regulators of endocytic vesicle**</u>

formation. In Stage 2, actin polymerization, mediated by the WASp/Las17p activated Arp2p/3p complex, is coupled to the endocytic coat through the adapter protein Sla2p. This actin polymerization provides the force to push the endocytic vesicle into the cell. Subsequently, the type-I myosin motors Myo3p/5p are recruited to spatially restrict actin polymerization and lateral movement. The recruitment of amphyphysin Rvs161p/167p results in the scission of the endocytic vesicle from the PM and subsequent endocytosis. From Robertson et al., (2009).

Figure 1.5.9: Models of Compensatory Endocytosis
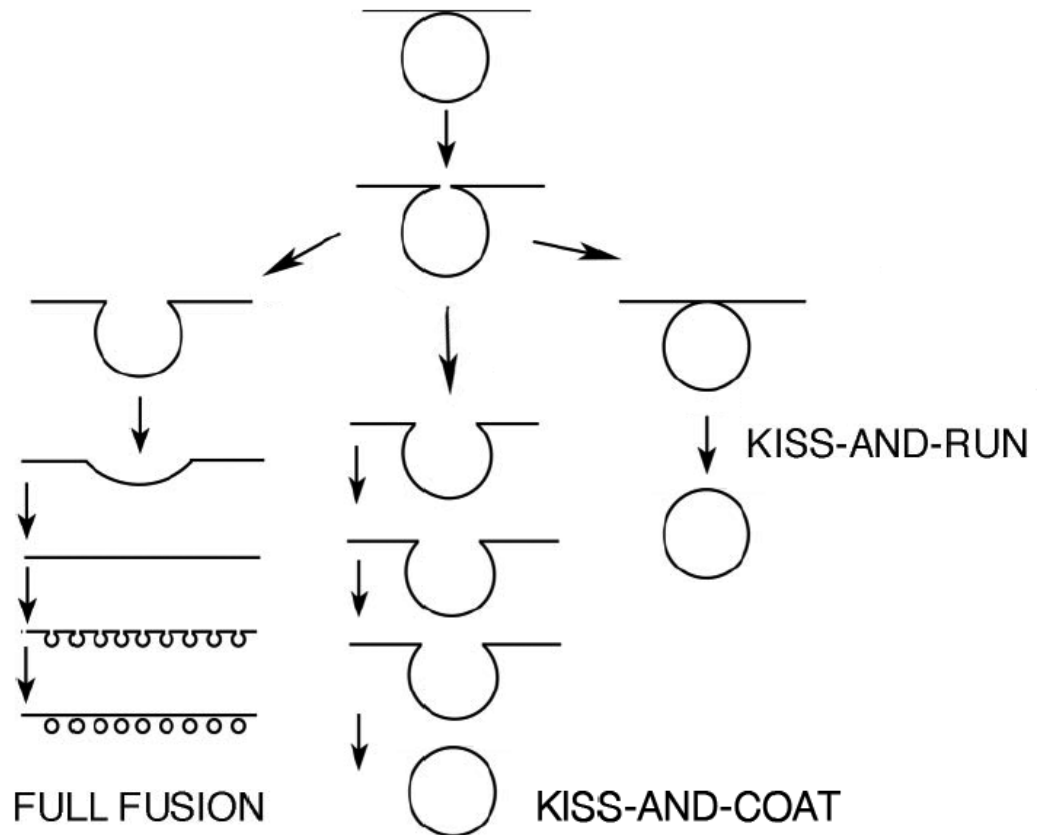
Figure 1.5.9: In the full fusion model (left) an exocytic vesicle fuses with the PM and the deposited material re-internalizes by subsequent endocytic events. In the Kiss-and Coat" model (middle), an exocytic vesicle partially fuses with the PM, leaving an open pore that is stabilized for an extended period of time by an actin patch that forms around this partially fused vesicle. After cargo release the vesicle is re-internalized compensating for the membrane expansion caused by vesicle fusion. In the "Kiss-and-Run" model (right), an exocytic vesicle briefly docks at the PM, and opens a small fusion pore to

release cargo, and then quickly dissociates and internalizes. All three models allow for an

endocytic event to be coupled to an exocytic event. From Sokac and Bement, (2006).

Figure 1.5.10 Models proposed by H. Riezman for coupling late Sec protein activity with endocytosis in yeast
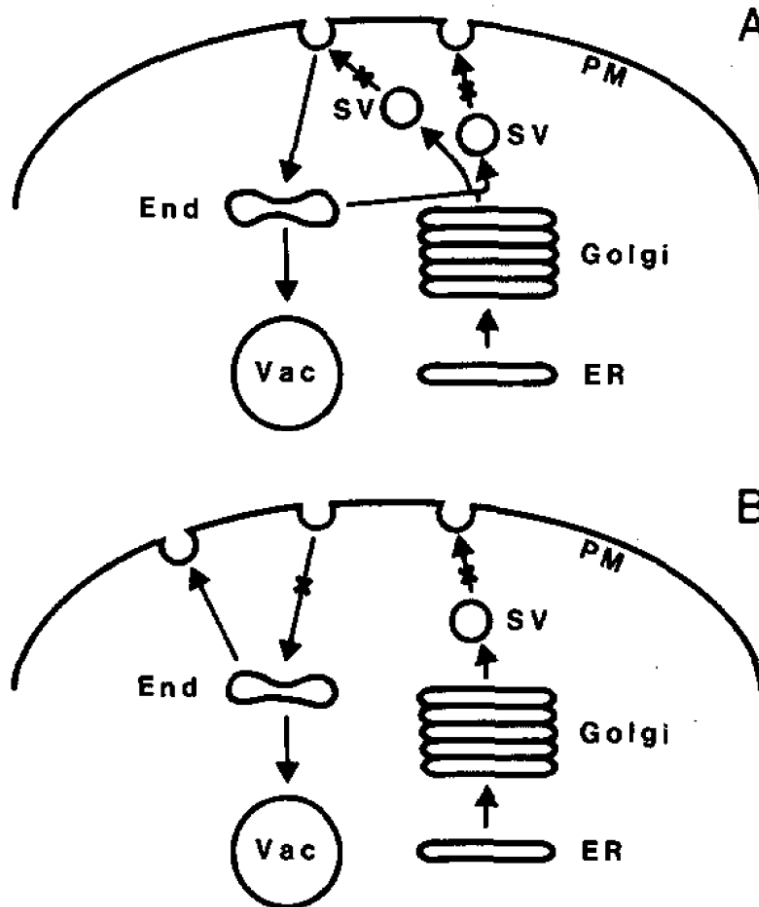
Figure 1.5.10: a) In this model, late Sec proteins (arrow with double hash mark) directly contribute to an endocytic event while associated with a secretory vesicle or while associated with a recycling vesicle. These are not mutually exclusive activties. b) In this model, late Sec proteins play an active but independent role in both endocytosis and exocytosis. In this model the secretory vesicles and endocytic pathway are maintained separate and the only link are the shared late Sec protein components. Overall, both

models provide an explanation for how late Sec proteins can affect both endocytosis and

exocytosis. From Riezman, (1985).

1.6 Reference List

Adams, A.E., and Pringle, J.R. (1984). Relationship of actin and tubulin distribution to bud growth in wild-type and morphogenetic-mutant Saccharomyces cerevisiae. J Cell Biol *98*, 934-945.

Alder-Baerens, N., Lisman, Q., Luong, L., Pomorski, T., and Holthuis, J.C. (2006). Loss of P4 ATPases Drs2p and Dnf3p disrupts aminophospholipid transport and asymmetry in yeast post-Golgi secretory vesicles. Mol Biol Cell *17*, 1632-1642.

Alfaro, G., Johansen, J., Dighe, S.A., Duamel, G., Kozminski, K.G., and Beh, C.T. (2011). The sterol-binding protein Kes1/Osh4p is a regulator of polarized exocytosis. Traffic *12*, 1521-1536.

Alphey, L., Jimenez, J., and Glover, D. (1998). A Drosophila homologue of oxysterol binding protein (OSBP)--implications for the role of OSBP. Biochim Biophys Acta *1395*, 159-164.

Anantharaman, V., and Aravind, L. (2002). The GOLD domain, a novel protein module involved in Golgi function and secretion. Genome Biol *3*, research0023.

Balklava, Z., Pant, S., Fares, H., and Grant, B.D. (2007). Genome-wide analysis identifies a general requirement for polarity proteins in endocytic traffic. Nat Cell Biol *9*, 1066-1073.

Bankaitis, V.A., Malehorn, D.E., Emr, S.D., and Greene, R. (1989). The Saccharomyces cerevisiae SEC14 gene encodes a cytosolic factor that is required for transport of secretory proteins from the yeast Golgi complex. J Cell Biol *108*, 1271-1281.

Baumann, N.A., Sullivan, D.P., Ohvo-Rekila, H., Simonot, C., Pottekat, A., Klaassen, Z., Beh, C.T., and Menon, A.K. (2005). Transport of newly synthesized sterol to the sterol-enriched plasma membrane occurs via nonvesicular equilibration. Biochemistry *44*, 5816-5826.

Beh, C.T., Alfaro, G., Duamel, G., Sullivan, D.P., Kersting, M.C., Dighe, S., Kozminski, K.G., and Menon, A.K. (2009). Yeast oxysterol-binding proteins: sterol transporters or regulators of cell polarization? Mol Cell Biochem *326*, 9-13.

Beh, C.T., Cool, L., Phillips, J., and Rine, J. (2001). Overlapping functions of the yeast oxysterol-binding protein homologues. Genetics *157*, 1117-1140.

Beh, C.T., and Rine, J. (2004). A role for yeast oxysterol-binding protein homologs in endocytosis and in the maintenance of intracellular sterol-lipid distribution. J Cell Sci *117*, 2983-2996.

Boyd, C., Hughes, T., Pypaert, M., and Novick, P. (2004). Vesicles carry most exocyst subunits to exocytic sites marked by the remaining two subunits, Sec3p and Exo70p. J Cell Biol *167*, 889-901.

Bretscher, M.S., and Thomson, J.N. (1983). Distribution of ferritin receptors and coated pits on giant HeLa cells. EMBO J *2*, 599-603.

Brown, A.J., Sun, L., Feramisco, J.D., Brown, M.S., and Goldstein, J.L. (2002). Cholesterol addition to ER membranes alters conformation of SCAP, the SREBP escort protein that regulates cholesterol metabolism. Mol Cell *10*, 237-245.

Cermelli, S., Guo, Y., Gross, S.P., and Welte, M.A. (2006). The lipid-droplet proteome reveals that droplets are a protein-storage depot. Curr Biol *16*, 1783-1795.

Cherezov, V., Rosenbaum, D.M., Hanson, M.A., Rasmussen, S.G., Thian, F.S., Kobilka, T.S., Choi, H.J., Kuhn, P., Weis, W.I., Kobilka, B.K.*, et al.* (2007). High-resolution crystal structure of an engineered human beta2-adrenergic G protein-coupled receptor. Science *318*, 1258-1265.

Cleves, A.E., Novick, P.J., and Bankaitis, V.A. (1989). Mutations in the SAC1 gene suppress defects in yeast Golgi and yeast actin function. J Cell Biol *109*, 2939-2950.

Consortium, C.e.S. (1998). Genome sequence of the nematode C. elegans: a platform for investigating biology. Science *282*, 2012-2018.

Cushman, S.W. (1970). Structure-function relationships in the adipose cell. I. Ultrastructure of the isolated adipose cell. J Cell Biol *46*, 326-341.

Dawson, P.A., Van der Westhuyzen, D.R., Goldstein, J.L., and Brown, M.S. (1989). Purification of oxysterol binding protein from hamster liver cytosol. J Biol Chem *264*, 9046-9052.

de Graaf, P., Zwart, W.T., van Dijken, R.A., Deneka, M., Schulz, T.K., Geijsen, N., Coffer, P.J., Gadella, B.M., Verkleij, A.J., van der Sluijs, P.*, et al.* (2004). Phosphatidylinositol 4-kinasebeta is critical for functional association of rab11 with the Golgi complex. Mol Biol Cell *15*, 2038-2047.

de Saint-Jean, M., Delfosse, V., Douguet, D., Chicanne, G., Payrastre, B., Bourguet, W., Antonny, B., and Drin, G. (2011). Osh4p exchanges sterols for phosphatidylinositol 4-phosphate between lipid bilayers. J Cell Biol *195*, 965-978.

DeGrella, R.F., and Simoni, R.D. (1982). Intracellular transport of cholesterol to the plasma membrane. J Biol Chem *257*, 14256-14262.

Demmel, L., Gravert, M., Ercan, E., Habermann, B., Muller-Reichert, T., Kukhtina, V., Haucke, V., Baust, T., Sohrmann, M., Kalaidzidis, Y.*, et al.* (2008). The clathrin adaptor Gga2p is a phosphatidylinositol 4-phosphate effector at the Golgi exit. Mol Biol Cell *19*, 1991-2002.

Dietl, P., and Haller, T. (2005). Exocytosis of lung surfactant: from the secretory vesicle to the air-liquid interface. Annu Rev Physiol *67*, 595-621.

Dong, Y., Pruyne, D., and Bretscher, A. (2003). Formin-dependent actin assembly is regulated by distinct modes of Rho signaling in yeast. J Cell Biol *161*, 1081-1092.

Engqvist-Goldstein, A.E., Kessels, M.M., Chopra, V.S., Hayden, M.R., and Drubin, D.G. (1999). An actin-binding protein of the Sla2/Huntingtin interacting protein 1 family is a novel component of clathrin-coated pits and vesicles. J Cell Biol *147*, 1503-1518.

Etienne-Manneville, S., and Hall, A. (2002). Rho GTPases in cell biology. Nature *420*, 629-635.

Evangelista, M., Blundell, K., Longtine, M.S., Chow, C.J., Adames, N., Pringle, J.R., Peter, M., and Boone, C. (1997). Bni1p, a yeast formin linking cdc42p and the actin cytoskeleton during polarized morphogenesis. Science *276*, 118-122.

Fadok, V.A., Bratton, D.L., Rose, D.M., Pearson, A., Ezekewitz, R.A., and Henson, P.M. (2000). A receptor for phosphatidylserine-specific clearance of apoptotic cells. Nature *405*, 85-90.

Fang, M., Kearns, B.G., Gedvilaite, A., Kagiwada, S., Kearns, M., Fung, M.K., and Bankaitis, V.A. (1996). Kes1p shares homology with human oxysterol binding protein and participates in a novel regulatory pathway for yeast Golgi-derived transport vesicle biogenesis. EMBO J *15*, 6447-6459.

Fukuzawa, M., and Williams, J.G. (2002). OSBPa, a predicted oxysterol binding protein of Dictyostelium, is required for regulated entry into culmination. FEBS Lett *527*, 37-42.

Georgiev, A.G., Sullivan, D.P., Kersting, M.C., Dittman, J.S., Beh, C.T., and Menon, A.K. (2011). Osh proteins regulate membrane sterol organization but are not required for sterol movement between the ER and PM. Traffic *12*, 1341-1355.

Goud, B., Salminen, A., Walworth, N.C., and Novick, P.J. (1988). A GTP-binding protein required for secretion rapidly associates with secretory vesicles and the plasma membrane in yeast. Cell *53*, 753-768.

Grillitsch, K., Connerth, M., Kofeler, H., Arrey, T.N., Rietschel, B., Wagner, B., Karas, M., and Daum, G. (2011). Lipid particles/droplets of the yeast Saccharomyces cerevisiae revisited: Lipidome meets Proteome. Biochim Biophys Acta.

Guo, W., Roth, D., Walch-Solimena, C., and Novick, P. (1999). The exocyst is an effector for Sec4p, targeting secretory vesicles to sites of exocytosis. EMBO J *18*, 1071-1080.

Guo, W., Tamanoi, F., and Novick, P. (2001). Spatial regulation of the exocyst complex by Rho1 GTPase. Nat Cell Biol *3*, 353-360.

Hanada, K., Kumagai, K., Yasuda, S., Miura, Y., Kawano, M., Fukasawa, M., and Nishijima, M. (2003). Molecular machinery for non-vesicular trafficking of ceramide. Nature *426*, 803-809.

Harsay, E., and Bretscher, A. (1995). Parallel secretory pathways to the cell surface in yeast. J Cell Biol *131*, 297-310.

He, B., Xi, F., Zhang, J., TerBush, D., Zhang, X., and Guo, W. (2007a). Exo70p mediates the secretion of specific exocytic vesicles at early stages of the cell cycle for polarized cell growth. J Cell Biol *176*, 771-777.

He, B., Xi, F., Zhang, X., Zhang, J., and Guo, W. (2007b). Exo70 interacts with phospholipids and mediates the targeting of the exocyst to the plasma membrane. EMBO J *26*, 4053-4065.

Higgs, H.N., and Pollard, T.D. (2000). Activation by Cdc42 and PIP(2) of Wiskott-Aldrich syndrome protein (WASp) stimulates actin nucleation by Arp2/3 complex. J Cell Biol *150*, 1311-1320.

Holthuis, J.C., and Levine, T.P. (2005). Lipid traffic: floppy drives and a superhighway. Nat Rev Mol Cell Biol *6*, 209-220.

Howard, J.P., Hutton, J.L., Olson, J.M., and Payne, G.S. (2002). Sla1p serves as the targeting signal recognition factor for NPFX(1,2)D-mediated endocytosis. J Cell Biol *157*, 315-326.

Im, Y.J., Raychaudhuri, S., Prinz, W.A., and Hurley, J.H. (2005). Structural mechanism for sterol sensing and transport by OSBP-related proteins. Nature *437*, 154-158.

Jacobson, K., Sheets, E.D., and Simson, R. (1995). Revisiting the fluid mosaic model of membranes. Science *268*, 1441-1442.

Jarousse, N., and Kelly, R.B. (2001). Endocytotic mechanisms in synapses. Curr Opin Cell Biol *13*, 461-469.

Jiang, B., Brown, J.L., Sheraton, J., Fortin, N., and Bussey, H. (1994). A new family of yeast genes implicated in ergosterol synthesis is related to the human oxysterol binding protein. Yeast *10*, 341-353.

Johansson, M., Lehto, M., Tanhuanpaa, K., Cover, T.L., and Olkkonen, V.M. (2005). The oxysterol-binding protein homologue ORP1L interacts with Rab7 and alters functional properties of late endocytic compartments. Mol Biol Cell *16*, 5480-5492.

Johansson, M., Rocha, N., Zwart, W., Jordens, I., Janssen, L., Kuijl, C., Olkkonen, V.M., and Neefjes, J. (2007). Activation of endosomal dynein motors by stepwise assembly of

Rab7-RILP-p150Glued, ORP1L, and the receptor betaIII spectrin. J Cell Biol *176*, 459-471.

Jones, J.D., and Thompson, T.E. (1989). Spontaneous phosphatidylcholine transfer by collision between vesicles at high lipid concentration. Biochemistry *28*, 129-134.

Kaksonen, M., Sun, Y., and Drubin, D.G. (2003). A pathway for association of receptors, adaptors, and actin during endocytic internalization. Cell *115*, 475-487.

Kaksonen, M., Toret, C.P., and Drubin, D.G. (2005). A modular design for the clathrin- and actin-mediated endocytosis machinery. Cell *123*, 305-320.

Kallen, C.B., Billheimer, J.T., Summers, S.A., Stayrook, S.E., Lewis, M., and Strauss, J.F., 3rd (1998). Steroidogenic acute regulatory protein (StAR) is a sterol transfer protein. J Biol Chem *273*, 26285-26288.

Kandutsch, A.A., Chen, H.W., and Shown, E.P. (1977). Binding of 25-hydroxycholesterol and cholesterol to different cytoplasmic proteins. Proc Natl Acad Sci U S A *74*, 2500-2503.

Kandutsch, A.A., and Thompson, E.B. (1980). Cytosolic proteins that bind oxygenated sterols. Cellular distribution, specificity, and some properties. J Biol Chem *255*, 10813-10821.

Kaplan, M.R., and Simoni, R.D. (1985). Transport of cholesterol from the endoplasmic reticulum to the plasma membrane. J Cell Biol *101*, 446-453.

Keller, P., and Simons, K. (1998). Cholesterol is required for surface transport of influenza virus hemagglutinin. J Cell Biol *140*, 1357-1367.

Kilmartin, J.V., and Adams, A.E. (1984). Structural rearrangements of tubulin and actin during the cell cycle of the yeast Saccharomyces. J Cell Biol *98*, 922-933.

Kroschewski, R., Hall, A., and Mellman, I. (1999). Cdc42 controls secretory and endocytic transport to the basolateral plasma membrane of MDCK cells. Nat Cell Biol *1*, 8-13.

Krut, L.H. (1982). Solubility of cholesterol in vitro promoted by oxidation products of cholesterol. Atherosclerosis *43*, 95-104.

Kvam, E., and Goldfarb, D.S. (2004). Nvj1p is the outer-nuclear-membrane receptor for oxysterol-binding protein homolog Osh1p in Saccharomyces cerevisiae. J Cell Sci *117*, 4959-4968.

Lange, Y. (1991). Disposition of intracellular cholesterol in human fibroblasts. J Lipid Res *32*, 329-339.

Lehto, M., and Olkkonen, V.M. (2003). The OSBP-related proteins: a novel protein family involved in vesicle transport, cellular lipid metabolism, and cell signalling. Biochim Biophys Acta *1631*, 1-11.

Levanon, D., Hsieh, C.L., Francke, U., Dawson, P.A., Ridgway, N.D., Brown, M.S., and Goldstein, J.L. (1990). cDNA cloning of human oxysterol-binding protein and localization of the gene to human chromosome 11 and mouse chromosome 19. Genomics *7*, 65-74.

Levine, T., and Loewen, C. (2006). Inter-organelle membrane contact sites: through a glass, darkly. Curr Opin Cell Biol *18*, 371-378.

Levine, T.P., and Munro, S. (2001). Dual targeting of Osh1p, a yeast homologue of oxysterol-binding protein, to both the Golgi and the nucleus-vacuole junction. Mol Biol Cell *12*, 1633-1644.

Li, X., Rivas, M.P., Fang, M., Marchena, J., Mehrotra, B., Chaudhary, A., Feng, L., Prestwich, G.D., and Bankaitis, V.A. (2002). Analysis of oxysterol binding protein homologue Kes1p function in regulation of Sec14p-dependent protein transport from the yeast Golgi complex. J Cell Biol *157*, 63-77.

Li, Y., and Prinz, W.A. (2004). ATP-binding cassette (ABC) transporters mediate nonvesicular, raft-modulated sterol movement from the plasma membrane to the endoplasmic reticulum. J Biol Chem *279*, 45226-45234.

Link, E., Edelmann, L., Chou, J.H., Binz, T., Yamasaki, S., Eisel, U., Baumert, M., Sudhof, T.C., Niemann, H., and Jahn, R. (1992). Tetanus toxin action: inhibition of neurotransmitter release linked to synaptobrevin proteolysis. Biochem Biophys Res Commun *189*, 1017-1023.

Liscum, L., and Munn, N.J. (1999). Intracellular cholesterol transport. Biochim Biophys Acta *1438*, 19-37.

Lodish, H.B., A., Zipursky, S.L., Matsudaira, P., Baltimore, D., and Darnell, J. (2000). Biomembranes: Structural organization and basic functions, 4th Edition edn (New York, W. H. Freeman and company).

Loewen, C.J., Roy, A., and Levine, T.P. (2003). A conserved ER targeting motif in three families of lipid binding proteins and in Opi1p binds VAP. EMBO J *22*, 2025-2035.

Lollike, K., Borregaard, N., and Lindau, M. (1995). The exocytotic fusion pore of small granules has a conductance similar to an ion channel. J Cell Biol *129*, 99-104.

Marco, E., Wedlich-Soldner, R., Li, R., Altschuler, S.J., and Wu, L.F. (2007). Endocytosis optimizes the dynamic localization of membrane proteins that regulate cortical polarity. Cell *129*, 411-422.

Matter, K., and Mellman, I. (1994). Mechanisms of cell polarity: sorting and transport in epithelial cells. Curr Opin Cell Biol *6*, 545-554.

McLean, L.R., and Phillips, M.C. (1981). Mechanism of cholesterol and phosphatidylcholine exchange or transfer between unilamellar vesicles. Biochemistry *20*, 2893-2900.

Mizuno-Yamasaki, E., Medkova, M., Coleman, J., and Novick, P. (2010). Phosphatidylinositol 4-phosphate controls both membrane recruitment and a regulatory switch of the Rab GEF Sec2p. Dev Cell *18*, 828-840.

Munson, M., and Novick, P. (2006). The exocyst defrocked, a framework of rods revealed. Nat Struct Mol Biol *13*, 577-581.

Murphy, D.J. (2001). The biogenesis and functions of lipid bodies in animals, plants and microorganisms. Prog Lipid Res *40*, 325-438.

Murphy, D.J., and Vance, J. (1999). Mechanisms of lipid-body formation. Trends Biochem Sci *24*, 109-115.

Muthusamy, B.P., Raychaudhuri, S., Natarajan, P., Abe, F., Liu, K., Prinz, W.A., and Graham, T.R. (2009). Control of protein and sterol trafficking by antagonistic activities of a type IV P-type ATPase and oxysterol binding protein homologue. Mol Biol Cell *20*, 2920-2931.

Nakada, C., Ritchie, K., Oba, Y., Nakamura, M., Hotta, Y., Iino, R., Kasai, R.S., Yamaguchi, K., Fujiwara, T., and Kusumi, A. (2003). Accumulation of anchored proteins forms membrane diffusion barriers during neuronal polarization. Nat Cell Biol *5*, 626-632.

Ngo, M.H., Colbourne, T.R., and Ridgway, N.D. (2010). Functional implications of sterol transport by the oxysterol-binding protein gene family. Biochem J *429*, 13-24.

Nichols, J.W., and Pagano, R.E. (1983). Resonance energy transfer assay of protein-mediated lipid transfer between vesicles. J Biol Chem *258*, 5368-5371.

Novick, P., Field, C., and Schekman, R. (1980). Identification of 23 complementation groups required for post-translational events in the yeast secretory pathway. Cell *21*, 205-215.

Novick, P., Medkova, M., Dong, G., Hutagalung, A., Reinisch, K., and Grosshans, B. (2006). Interactions between Rabs, tethers, SNAREs and their regulators in exocytosis. Biochem Soc Trans *34*, 683-686.

Novick, P., and Schekman, R. (1983). Export of major cell surface proteins is blocked in yeast secretory mutants. J Cell Biol *96*, 541-547.

Ohsaki, Y., Cheng, J., Fujita, A., Tokumoto, T., and Fujimoto, T. (2006). Cytoplasmic lipid droplets are sites of convergence of proteasomal and autophagic degradation of apolipoprotein B. Mol Biol Cell *17*, 2674-2683.

Olkkonen, V.M., Johansson, M., Suchanek, M., Yan, D., Hynynen, R., Ehnholm, C., Jauhiainen, M., Thiele, C., and Lehto, M. (2006). The OSBP-related proteins (ORPs): global sterol sensors for co-ordination of cellular lipid metabolism, membrane trafficking and signalling processes? Biochem Soc Trans *34*, 389-391.

Park, H.O., Sanson, A., and Herskowitz, I. (1999). Localization of Bud2p, a GTPase-activating protein necessary for programming cell polarity in yeast to the presumptive bud site. Genes Dev *13*, 1912-1917.

Peake, K.B., and Vance, J.E. (2010). Defective cholesterol trafficking in Niemann-Pick C-deficient cells. FEBS Lett *584*, 2731-2739.

Perry, R.J., and Ridgway, N.D. (2006). Oxysterol-binding protein and vesicle-associated membrane protein-associated protein are required for sterol-dependent activation of the ceramide transport protein. Mol Biol Cell *17*, 2604-2616.

Pol, A., Martin, S., Fernandez, M.A., Ferguson, C., Carozzi, A., Luetterforst, R., Enrich, C., and Parton, R.G. (2004). Dynamic and regulated association of caveolin with lipid bodies: modulation of lipid body motility and function by a dominant negative mutant. Mol Biol Cell *15*, 99-110.

Pomorski, T., Hrafnsdottir, S., Devaux, P.F., and van Meer, G. (2001). Lipid distribution and transport across cellular membranes. Semin Cell Dev Biol *12*, 139-148.

Pomorski, T., Lombardi, R., Riezman, H., Devaux, P.F., van Meer, G., and Holthuis, J.C. (2003). Drs2p-related P-type ATPases Dnf1p and Dnf2p are required for phospholipid translocation across the yeast plasma membrane and serve a role in endocytosis. Mol Biol Cell *14*, 1240-1254.

Prinz, W.A. (2007). Non-vesicular sterol transport in cells. Prog Lipid Res *46*, 297-314.

Puertollano, R., Randazzo, P.A., Presley, J.F., Hartnell, L.M., and Bonifacino, J.S. (2001). The GGAs promote ARF-dependent recruitment of clathrin to the TGN. Cell *105*, 93-102.

Radhakrishnan, A., Ikeda, Y., Kwon, H.J., Brown, M.S., and Goldstein, J.L. (2007). Sterol-regulated transport of SREBPs from endoplasmic reticulum to Golgi: oxysterols block transport by binding to Insig. Proc Natl Acad Sci U S A *104*, 6511-6518.

Raychaudhuri, S., Im, Y.J., Hurley, J.H., and Prinz, W.A. (2006). Nonvesicular sterol movement from plasma membrane to ER requires oxysterol-binding protein-related proteins and phosphoinositides. J Cell Biol *173*, 107-119.

Ridgway, N.D., Dawson, P.A., Ho, Y.K., Brown, M.S., and Goldstein, J.L. (1992). Translocation of oxysterol binding protein to Golgi apparatus triggered by ligand binding. J Cell Biol *116*, 307-319.

Riezman, H. (1985). Endocytosis in yeast: several of the yeast secretory mutants are defective in endocytosis. Cell *40*, 1001-1009.

Robertson, A.S., Smythe, E., and Ayscough, K.R. (2009). Functions of actin in endocytosis. Cell Mol Life Sci *66*, 2049-2065.

Roy, A., and Levine, T.P. (2004). Multiple pools of phosphatidylinositol 4-phosphate detected using the pleckstrin homology domain of Osh2p. J Biol Chem *279*, 44683-44689.

Sandager, L., Gustavsson, M.H., Stahl, U., Dahlqvist, A., Wiberg, E., Banas, A., Lenman, M., Ronne, H., and Stymne, S. (2002). Storage lipid synthesis is non-essential in yeast. J Biol Chem *277*, 6478-6482.

Schmidt, K., and Nichols, B.J. (2004). A barrier to lateral diffusion in the cleavage furrow of dividing mammalian cells. Curr Biol *14*, 1002-1006.

Schneider, S.W., Sritharan, K.C., Geibel, J.P., Oberleithner, H., and Jena, B.P. (1997). Surface dynamics in living acinar cells imaged by atomic force microscopy: identification of plasma membrane structures involved in exocytosis. Proc Natl Acad Sci U S A *94*, 316-321.

Schott, D., Ho, J., Pruyne, D., and Bretscher, A. (1999). The COOH-terminal domain of Myo2p, a yeast myosin V, has a direct role in secretory vesicle targeting. J Cell Biol *147*, 791-808.

Schott, D., Huffaker, T., and Bretscher, A. (2002). Microfilaments and microtubules: the news from yeast. Curr Opin Microbiol *5*, 564-574.

Singer, S.J., and Nicolson, G.L. (1972). The fluid mosaic model of the structure of cell membranes. Science *175*, 720-731.

Skirpan, A.L., Dowd, P.E., Sijacic, P., Jaworski, C.J., Gilroy, S., and Kao, T.H. (2006). Identification and characterization of PiORP1, a Petunia oxysterol-binding-protein related protein involved in receptor-kinase mediated signaling in pollen, and analysis of the ORP gene family in Arabidopsis. Plant Mol Biol *61*, 553-565.

Sokac, A.M., and Bement, W.M. (2006). Kiss-and-coat and compartment mixing: coupling exocytosis to signal generation and local actin assembly. Mol Biol Cell *17*, 1495-1502.

Sokac, A.M., Co, C., Taunton, J., and Bement, W. (2003). Cdc42-dependent actin polymerization during compensatory endocytosis in Xenopus eggs. Nat Cell Biol *5*, 727-732.

Soulard, A., Friant, S., Fitterer, C., Orange, C., Kaneva, G., Mirey, G., and Winsor, B. (2005). The WASP/Las17p-interacting protein Bzz1p functions with Myo5p in an early stage of endocytosis. Protoplasma *226*, 89-101.

Staal, R.G., Mosharov, E.V., and Sulzer, D. (2004). Dopamine neurons release transmitter via a flickering fusion pore. Nat Neurosci *7*, 341-346.

Stearns, T., Willingham, M.C., Botstein, D., and Kahn, R.A. (1990). ADP-ribosylation factor is functionally and physically associated with the Golgi complex. Proc Natl Acad Sci U S A *87*, 1238-1242.

Stefan, C.J., Manford, A.G., Baird, D., Yamada-Hanff, J., Mao, Y., and Emr, S.D. (2011). Osh proteins regulate phosphoinositide metabolism at ER-plasma membrane contact sites. Cell *144*, 389-401.

Storey, M.K., Byers, D.M., Cook, H.W., and Ridgway, N.D. (1998). Cholesterol regulates oxysterol binding protein (OSBP) phosphorylation and Golgi localization in Chinese hamster ovary cells: correlation with stimulation of sphingomyelin synthesis by 25-hydroxycholesterol. Biochem J *336 (Pt 1)*, 247-256.

Sturley, S.L. (2000). Conservation of eukaryotic sterol homeostasis: new insights from studies in budding yeast. Biochim Biophys Acta *1529*, 155-163.

Sullivan, D.P., Georgiev, A., and Menon, A.K. (2009). Tritium suicide selection identifies proteins involved in the uptake and intracellular transport of sterols in Saccharomyces cerevisiae. Eukaryot Cell *8*, 161-169.

Sullivan, D.P., Ohvo-Rekila, H., Baumann, N.A., Beh, C.T., and Menon, A.K. (2006). Sterol trafficking between the endoplasmic reticulum and plasma membrane in yeast. Biochem Soc Trans *34*, 356-358.

Takizawa, P.A., DeRisi, J.L., Wilhelm, J.E., and Vale, R.D. (2000). Plasma membrane compartmentalization in yeast by messenger RNA transport and a septin diffusion barrier. Science *290*, 341-344.

Tauchi-Sato, K., Ozeki, S., Houjou, T., Taguchi, R., and Fujimoto, T. (2002). The surface of lipid droplets is a phospholipid monolayer with a unique Fatty Acid composition. J Biol Chem *277*, 44507-44512.

Taylor, F.R., and Kandutsch, A.A. (1985). Oxysterol binding protein. Chem Phys Lipids *38*, 187-194.

Taylor, F.R., Saucier, S.E., Shown, E.P., Parish, E.J., and Kandutsch, A.A. (1984). Correlation between oxysterol binding to a cytosolic binding protein and potency in the repression of hydroxymethylglutaryl coenzyme A reductase. J Biol Chem *259*, 12382-12387.

Taylor, F.R., Shown, E.P., Thompson, E.B., and Kandutsch, A.A. (1989). Purification, subunit structure, and DNA binding properties of the mouse oxysterol receptor. J Biol Chem *264*, 18433-18439.

Thorn, P., Fogarty, K.E., and Parker, I. (2004). Zymogen granule exocytosis is characterized by long fusion pore openings and preservation of vesicle lipid identity. Proc Natl Acad Sci U S A *101*, 6774-6779.

Tinkelenberg, A.H., Liu, Y., Alcantara, F., Khan, S., Guo, Z., Bard, M., and Sturley, S.L. (2000). Mutations in yeast ARV1 alter intracellular sterol distribution and are complemented by human ARV1. J Biol Chem *275*, 40667-40670.

Tolliday, N., VerPlank, L., and Li, R. (2002). Rho1 directs formin-mediated actin ring assembly during budding yeast cytokinesis. Curr Biol *12*, 1864-1870.

Urbani, L., and Simoni, R.D. (1990). Cholesterol and vesicular stomatitis virus G protein take separate routes from the endoplasmic reticulum to the plasma membrane. J Biol Chem *265*, 1919-1923.

Valdez-Taubas, J., and Pelham, H.R. (2003). Slow diffusion of proteins in the yeast plasma membrane allows polarity to be maintained by endocytic cycling. Curr Biol *13*, 1636-1640.

van Meer, G., and de Kroon, A.I. (2011). Lipid map of the mammalian cell. J Cell Sci *124*, 5-8.

Walch-Solimena, C., Collins, R.N., and Novick, P.J. (1997). Sec2p mediates nucleotide exchange on Sec4p and is involved in polarized delivery of post-Golgi vesicles. J Cell Biol *137*, 1495-1509.

Wang, P.Y., Weng, J., and Anderson, R.G. (2005). OSBP is a cholesterol-regulated scaffolding protein in control of ERK 1/2 activation. Science *307*, 1472-1476.

Wessel, G.M., Brooks, J.M., Green, E., Haley, S., Voronina, E., Wong, J., Zaydfudim, V., and Conner, S. (2001). The biology of cortical granules. Int Rev Cytol *209*, 117-206.

Wilcox, L.J., Balderes, D.A., Wharton, B., Tinkelenberg, A.H., Rao, G., and Sturley, S.L. (2002). Transcriptional profiling identifies two members of the ATP-binding cassette transporter superfamily required for sterol uptake in yeast. J Biol Chem *277*, 32466-32472.

Wong, T.A., Fairn, G.D., Poon, P.P., Shmulevitz, M., McMaster, C.R., Singer, R.A., and Johnston, G.C. (2005). Membrane metabolism mediated by Sec14 family members influences Arf GTPase activating protein activity for transport from the trans-Golgi. Proc Natl Acad Sci U S A *102*, 12777-12782.

Wu, B., Chien, E.Y., Mol, C.D., Fenalti, G., Liu, W., Katritch, V., Abagyan, R., Brooun, A., Wells, P., Bi, F.C.*, et al.* (2010). Structures of the CXCR4 chemokine GPCR with small-molecule and cyclic peptide antagonists. Science *330*, 1066-1071.

Yan, D., and Olkkonen, V.M. (2008). Characteristics of oxysterol binding proteins. Int Rev Cytol *265*, 253-285.

Yang, T., Espenshade, P.J., Wright, M.E., Yabe, D., Gong, Y., Aebersold, R., Goldstein, J.L., and Brown, M.S. (2002). Crucial step in cholesterol homeostasis: sterols promote binding of SCAP to INSIG-1, a membrane protein that facilitates retention of SREBPs in ER. Cell *110*, 489-500.

Yeagle, P.L. (1985). Cholesterol and the cell membrane. Biochim Biophys Acta *822*, 267-287.

Zajac, A., Sun, X., Zhang, J., and Guo, W. (2005). Cyclical regulation of the exocyst and cell polarity determinants for polarized cell growth. Mol Biol Cell *16*, 1500-1512.

Zhang, X., Orlando, K., He, B., Xi, F., Zhang, J., Zajac, A., and Guo, W. (2008). Membrane association and functional regulation of Sec3 by phospholipids and Cdc42. J Cell Biol *180*, 145-158.

2: **Homologues of Oxysterol-Binding Proteins Affect Cdc42p- and Rho1p-Mediated Cell Polarization in** *Saccharomyces cerevisiae*

Author list: Keith G. Kozminski, **Gabriel Alfaro**, Shubha Dighe, and Christopher T. Beh.

Author contribution: The initial suppressor screen for *cdc42* conditional alleles, the localization of Cdc42p, and the distribution of actin generating Figure 2.5.1, 2.5.2, and 2.5.5 was performed by K.G.K and S.D. Figure 2.5.6 performed by C.T.B. The text was written by K.G.K and C.T.B. I contributed to materials and methods and figure legends. I performed all aspects of the experiments to generate Figures 2.5.3, 2.5.4, 2.5.7, 2.5.9, 2.5.10, 2.5.11, and 2.5.12.

Abstract

Polarized cell growth requires the establishment of an axis of growth along which secretion can be targeted to a specific site on the cell cortex. How polarity establishment and secretion are choreographed is not fully understood, though Rho GTPase-and Rab GTPase-mediated signaling is required. Superimposed on this regulation are the functions of specific lipids and their cognate binding proteins. In a screen for *Saccharomyces cerevisiae* genes that interact with Rho family *CDC42* to promote polarity establishment, we identified *KES1*/*OSH4*, which encodes a homologue of mammalian oxysterol-binding protein (OSBP). Other yeast OSH genes (OSBP homologues) had comparable genetic interactions with *CDC42*, implicating *OSH* genes in the regulation of *CDC42*-dependent polarity establishment. We found that the *OSH* gene family (*OSH1−OSH7*) promotes cell

polarization by maintaining the proper localization of septins, the Rho GTPases Cdc42p and Rho1p, and the Rab GTPase Sec4p. Disruption of all *OSH* gene function caused specific defects in polarized exocytosis, indicating that the Osh proteins are collectively required for a secretory pathway implicated in the maintenance of polarized growth.

2.1 Introduction

An asymmetric organization of the cytoskeleton and secretory apparatus supports polarized cell growth. This organization is effected, in part, by the interaction of Ras, Rho and Rab family small GTPases (and/or their associated regulatory proteins) with cortical proteins that mark an axis for cell growth (Drubin and Nelson, 1996; Etienne-Manneville and Hall, 2002; Gulli and Peter, 2001; Hsu et al., 2004; Pruyne et al., 2004b; Van Aelst and Symons, 2002). The activities of these GTPases depend on their nucleotide state and are regulated by associated GTPase-activating proteins (GAPs) and GTP exchange factors (GEFs) (Wennerberg et al., 2005). When bound to GTP, these small GTPases bind target proteins that promote cytoskeletal assembly (e.g. formins, p21-activated kinases [PAK] and Wiskott-Aldrich Syndrome protein [WASP] family) or permit exocytosis (e.g. Sec3p and Sec15p homologues) at specific sites on the cell cortex (Dong et al., 2003; Guo et al., 1999; Higgs and Pollard, 2001; Hofmann et al., 2004; Kadota et al., 2004; Versele and Thorner, 2004; Zhang et al., 2008). Although many effectors of small GTPase signaling have been identified, less is known about how the small GTPases themselves are recruited to and retained at sites of polarized growth. Moreover, it is poorly understood how a cell coordinates this chorus of small GTPases such that the asymmetric reorganization of the cytoskeleton and secretory apparatus occurs as an

orderly progression of events.

Bud formation in the yeast *Saccharomyces cerevisiae* illustrates the choreography of small GTPase signaling required for polarized cell growth. In the earliest events of this process, in late G1 of the cell cycle, the Rho family GTPase Cdc42p (Adams et al., 1990) in conjunction with the Ras family GTPase Rsr1p (Kozminski et al., 2003) establishes an axis of polarity that directs *RHO1*-dependent secretion towards a specific area of the yeast cell cortex (Guo et al., 2001; Zhang, 2001), where the bud will emerge. Through this process, new membrane and cell wall material is brought to the cell surface to accommodate bud growth (Novick and Schekman, 1983; Ramirez et al., 1983). Mutations that uncouple secretion from the upstream events that establish cell polarity result in the misdirected deposition of new membrane and can cause bud morphology defects or isotropic growth of the mother cell (Mondesert et al., 1997; Ozaki-Kuroda et al., 2001).

Superimposed upon the regulation of cell polarity by small GTPases is the functional contribution of specific lipids. In diverse species, phosphoinositides have been defined as second messengers essential for polarized cell growth (Desrivieres et al., 1998; Merlot and Firtel, 2003; Servant et al., 2000; Weiner et al., 2002; Wild et al., 2004). In contrast, sterol lipids such as cholesterol have not generally been considered to be second messengers associated with the signaling cascades that initiate polarized cell growth. Nonetheless, sterols have essential roles in cell polarization (Carland et al., 2002; Diederich et al., 2001; Pierini et al., 2003; Willemsen et al., 2003). Both sterol-dependent increases in membrane viscosity (Valdez-Taubas and Pelham, 2003; Vasanji et al., 2004) and the formation of sterol-enriched membrane domains [i.e. lipid rafts (Bagnat and Simons, 2002; Gomez-Mouton et al., 2001; Guan, 2004; Manes et al., 1999; Martin and

Konopka, 2004; Wachtler et al., 2003)] have a role in establishing or maintaining an axis of polarized growth. For example, in response to cell adhesion to the extracellular matrix, integrins utilize sterol-enriched lipid rafts to target small GTPases of the Rho family to specific plasma membrane domains and couple them to PAK effectors (del Pozo et al., 2000; Palazzo et al., 2004). Sterols have additional roles as signaling molecules in growth control. For instance, in response to cholesterol binding, the mammalian oxysterol-binding protein (OSBP) assembles an oligomeric phosphatase complex that dephosphorylates extracellular signal-regulated kinase (ERK) (Wang et al., 2005b). Thus, Oxysterol-binding proteins represent a large ubiquitous family of eukaryotic lipid-binding proteins. They are soluble intracellular receptors, some of which bind cholesterol and oxysterols (Im et al., 2005; Kandutsch and Shown, 1981), the latter being potent feedback regulators of cholesterol synthesis. It is unclear whether all OSBP homologues bind cholesterol or oxysterols, but most OSBP homologues appear to contain at least one lipid-binding motif (Fang et al., 1996; Olkkonen and Levine, 2004; Taylor and Kandutsch, 1985). Studies with budding yeast have implicated OSBP homologues in the regulation of secretory transport, nonvesicular lipid transport and membrane dynamics (Beh et al., 2001; Beh and Rine, 2004; Fang et al., 1996; Im et al., 2005; Kvam and Goldfarb, 2004; Levine and Munro, 2001; Li et al., 2002). *Saccharomyces cerevisiae* has seven genes that encode OSBP homologues, *OSH1− OSH7* (Beh et al., 2001; Jiang et al., 1994; Schmalix and Bandlow, 1994). Each individual *OSH* gene in *S. cerevisiae* is dispensable for growth, but deletion of all seven *OSH* genes is lethal, indicating that these genes perform at least one overlapping essential function (Beh et al., 2001). Depletion of all Osh proteins from yeast cells results in an intracellular accumulation of the cholesterol-like

lipid ergosterol, which otherwise resides in the plasma membrane (Beh and Rine, 2004).

Individual *OSH* genes are also implicated in specific transport processes. For example,

Osh1p is recruited to contact sites between the nuclear envelope and the vacuole, where

components of the nuclear envelope are directly transferred to the vacuole (Beh and Rine,

2004; Kvam and Goldfarb, 2004; Levine and Munro, 2001; Loewen et al., 2003). In

contrast, Osh4p is a negative regulator of Sec14p-dependent vesicle formation from the

Golgi apparatus (Fang et al., 1996). Prima facie, these trafficking events appear dissimilar

but are controlled in both cases by lipids interacting directly with an OSBP (Li et al.,

2002; Wyles et al., 2002). Although there is some overlap in the various cellular locations

occupied by each localization (Levine and Munro, 2001; Li et al., 2002; Wang et al.,

2005a). In this regard, the vectoral translocation of Osh proteins in yeast between various

membrane compartments, or the canonical OSBP in mammalian cells, appears to be

triggered by binding specific lipids (Li et al., 2002; Ridgway et al., 1992). In addition to

transport and membrane dynamics, there is suggestive evidence that OSBPs affect cell

cycle regulation and development. In *Caenorhabditis elegans*, for example, an OSBP

homologue has been implicated in transforming growth factor-b signaling (Sugawara et

al., 2001), and a *Drosophila* OSBP homologue expressed in fission yeast suppresses the

mitotic checkpoint arrest caused by Wee1p overexpression (Alphey et al., 1998).

In budding yeast, we examined OSBP function in relation to the role of small

GTPases in polarized cell growth during bud formation. We report that *S. cerevisiae OSH*

genes interact with *CDC42* to promote cell polarity establishment and, in a coordinated

but distinct manner, with *RHO1* to affect polarized cell growth. After the bud site is

established, *OSH* genes are required for the proper localization of small GTPases that

regulate polarized secretion. Consistent with this result, we also found that the *OSH* genes were collectively required for a specific secretory pathway associated with polarized exocytosis. Thus, the *OSH* genes maintain cell polarization by their effect on vesicular transport to sites of membrane growth.

2.2 Results

2.2.1 *CDC42–OSH* gene family interactions

To identify genes that interact with *CDC42* during the establishment of cell polarity in late G1, we screened for multicopy dosage suppressors of *cdc42-118*^{D76A} [(Kozminski et al., 2003); see also Materials and Methods), a temperature-conditional *CDC42* allele specifically defective in polarity establishment (Kozminski et al., 2000). At restrictive temperatures, *cdc42-118* cells are unable to establish an axis of polarized growth and arrest as large, unbudded, multinucleated cells with a depolarized actin cytoskeleton. Among the suppressors identified was *KES1/OSH4* (hereafter *OSH4*). At 36°C, the temperature-sensitive growth defect of *cdc42-118* cells was rescued by *OSH4* whether expressed from its own promoter on a high-copy vector (Figure 2.5.1A), or on low-copy *CEN* plasmid, or if expressed from the *GAL10* promoter on multi-copy plasmid (not shown). In comparison, the growth defect of *cdc42-118* cells at 36°C was not suppressed in transformants containing a vector control (Figure 2.5.1A). These findings revealed an interaction between *OSH4* and *CDC42* and suggested that Osh4p is involved in Cdc42p-dependent signaling during budding.

Several lines of evidence indicated that *OSH4* interacts specifically with *CDC42*

to affect cell polarization prior to bud emergence. First, dosage suppression by *OSH4* was specific to *CDC42*. We tested whether multicopy *OSH4* suppressed a temperature-sensitive allele of *RHO1*, which encodes another Rho family small GTPase required for polarized bud growth (Yamochi et al., 1994). Although *OSH4* overexpression did have an effect on *RHO1* signaling, multicopy *OSH4* failed to suppress the *rho1-104*^{ts} growth defect at any temperature tested (see below). This result indicated that *OSH4* does not suppress all mutations in Rho family GTPases. Second, suppression by multicopy *OSH4* was observed only with specific *CDC42* separation-of-function alleles (Figure 2.5.1A). When multicopy *OSH4* was transformed into *cdc42-129*, which is not defective in establishing an axis of polarized growth (Kozminski et al., 2000), or *cdc42-123*, which disrupts a different aspect of polarized growth apart from polarity establishment (Kozminski et al., 2000), neither allele was suppressed compared with the vector control transformants (Figure 2.5.1 A). In fact, multicopy *OSH4* worsened the growth defect of *cdc42-129* cells. However, multicopy *OSH4* weakly suppressed the *cdc42-101* temperature-sensitive growth defect (Figure 2.5.1A). At 36°C, *cdc42-101* cells exhibit a polarity establishment defect similar to that observed in *cdc42-118* cells at restrictive temperatures (Kozminski et al., 2000). Therefore, of all the *cdc42* alleles examined, multicopy *OSH4* suppressed only those alleles with a defined cell polarization defect.

OSH4 suppression of *cdc42* polarization defects appears to be *CDC42* dependent; that is, it does not circumvent the normal polarization of Cdc42p required for polarity establishment. In wild-type and *cdc42-118* cells grown at 25°C, Cdc42p localized to the presumptive bud site in unbudded cells and to the apical cortex of small- and medium-budded cells [data not shown; see also (Kozminski et al., 2000)]. In wild-type cells

shifted to 36°C, the distribution of Cdc42p detected by immunofluorescence microscopy was unchanged (Figure 2.5.1B). However, when *cdc42-118* cultures were shifted to 36°C, cell growth was arrested and unbudded cells (many large) accumulated. In these cells, the distribution of Cdc42p was diffuse or absent from the presumptive bud site (Figure 2.5.1B). If *OSH4* suppressed *cdc42* polarization defects in a Cdc42p-dependent manner, then multicopy *OSH4* should restore proper Cdc42p polarization in unbudded *cdc42-118* cells grown at the restrictive temperature. This outcome was in fact observed (Figure 2.5.1 B). To analyze Cdc42p distribution in *cdc42-118* and wild-type cells that contained an *OSH4* multicopy plasmid or a vector control, log-phase cultures in minimal medium were shifted from 25 to 36°C for 9 h. Under these culture conditions, >90% of *cdc42-118* cells transformed with the vector alone accumulated as unbudded cells. In contrast, Cdc42p was properly polarized at the presumptive bud site in a greater percentage of unbudded *cdc42-118* cells that contained multicopy *OSH4* plasmid (Figure 2.5.1B and graph) than with the vector control (Figure 2.5.1B and graph). Moreover, in *cdc42-118* cells transformed with multicopy *OSH4*, Cdc42p was properly polarized in approximately the same percentage of unbudded cells as observed in wild-type cells with the control vector (Figure 2.5.1B and graph). These results indicated that multicopy *OSH4* rescued the *cdc42-118* polarization defect and that this effect was due, at least in part, to the restoration of the polarized localization of Cdc42p. Thus, suppression by *OSH4* does not appear to be due to the activation of a *CDC42*-independent pathway.

Three additional observations provided further evidence that multicopy *OSH4* promotes Cdc42p polarization. First, multicopy *OSH4* promoted Cdc42p polarization in multinucleated *cdc42-118* cells in which mutant Cdc42p is rarely polarized. At 36°C, we

observed a six-fold increase in large, multinucleated, unbudded cells with polarized Cdc42p in cultures of *cdc42-118* transformants with multicopy *OSH4*, as compared with those with the vector control (Figure 2.5.1B, graph). Polarized multinucleated cells accumulated in the presence of multicopy *OSH4*, indicating that whereas *OSH4* suppressed defects in Cdc42p localization it did not restore proper coupling of cell and nuclear division in all cells. Second, at 36°C, wild-type Cdc42p was detected at the presumptive bud site more often in unbudded wild-type cells transformed with multicopy *OSH4* than those with the control vector (Figure 2.5.1B, graph). This observation indicated that multicopy *OSH4* augments wild-type Cdc42p polarization as well as the mutant protein encoded by *cdc42-118*. Third, in both mutant and wild-type cells at 36°C, Cdc42p staining was more intense in unbudded cells that contained multicopy OSH4 than in those containing the vector control (Figure 2.5.1B). This observation strongly suggested that more Cdc42p is present at the bud site when *OSH4* is present at multiple copies. Together, these findings suggested that *OSH4* helps establish Cdc42p polarity or maintain its polarized localization at the presumptive bud site once polarity is established.

Because the *OSH* genes have overlapping functions (Beh et al., 2001), we expanded our initial suppression analysis to include the entire *OSH* gene family. Similar to *OSH4*, several of the other *OSH* genes proved to be suppressors of cdc42 conditional growth defects. In multicopy plasmid constructs, *OSH1*, *OSH2* or *OSH6* expressed from their own promoters (Figure 2.5.1C) suppressed *cdc42-101* and *cdc42-118* temperature-conditional growth defects. *OSH3* only suppressed *cdc42-118*. Multicopy *OSH5* and *OSH7* did not suppress the growth defects of either *cdc42-101* or *cdc42-118* cells grown at 36°C. In contrast, only multicopy *OSH6* suppressed the temperature-sensitive growth

defect of *cdc42-129* cells in addition to the other mutants tested (Figure 2.5.1B). These results suggested that specific *OSH* genes interact with *CDC42* to promote the establishment of cell polarity, but, as shown below, the *OSH* gene family was collectively required for polarized cell growth. Because of the complexity inherent in analyzing all seven *OSH* genes (Beh et al., 2001), we limited our analyses to *OSH2* and *OSH4* in many of the investigations described below. These two genes were chosen because they strongly suppressed *cdc42*^{ts} alleles with polarized growth defects (Figure 2.5.1). Because *OSH2* and *OSH4* are representative of different *OSH* gene subfamilies and all *OSH* genes have shared function(s) (Beh et al., 2001), the activities of these two *OSH* genes are likely to approximate the others. As such, the analysis of *OSH2* and *OSH4* expedited our analyses of how the entire *OSH* gene family affects polarized cell growth.

2.2.2 *OSH* genes maintain cell polarization

Because multicopy *OSH* genes suppressed *cdc42* polarization defects, we tested the converse to establish whether the loss of *OSH* gene function resulted in the loss of cell polarization. In this regard, we used the organization of the actin cytoskeleton as a read-out for cell polarization. In unbudded wild-type cells during late G1 of the cell cycle, cortical actin patches are found predominantly at the presumptive bud site and actin cables run approximately parallel to the mother-bud axis. In S and G2 phases, actin polarization persists but patches are predominantly found within the bud. Deletion of any single *OSH* gene did not result in a loss of actin cytoskeleton polarization, nor did the combined deletion of *OSH* genes that suppress *cdc42* cell polarity defects (i.e. *osh1Δ– osh4Δ osh6Δ*) (data not shown).

To investigate whether a complete loss of *OSH* gene function affects the polarization of the actin cytoskeleton, we examined actin organization in a yeast strain lacking six of the seven *OSH* genes, with the remaining *OSH* gene, *OSH2*, under the regulatory control of a *MET3* promoter [*oshΔ* P*MET3*-*OSH2* (*oshΔ* refers to the deletion of all *OSH* genes other than those indicated)]. In the absence of methionine in the culture medium, *OSH2* is expressed in *oshΔ* P*MET3*-*OSH2* cells, permitting growth. In these cells, actin patches are polarized to the bud site in unbudded cells and towards the bud tip in small-budded cells (Figure 2A,B) as observed in wild-type strains (not shown). However, in the presence of added methionine, *OSH2* expression is repressed, resulting in a gradual growth arrest (Beh et al., 2001; Beh and Rine, 2004). After culturing in the presence of methionine, *oshΔ* P*MET3*-*OSH2* cells displayed distinct morphological defects. Cells became larger and rounder, having wider mother/bud necks and/or reiterative buds [Figure 2.5.2C–F(Beh et al., 2001; Beh and Rine, 2004)]. Also observed was a decrease (~45%) in the number of cells with a polarized actin cytoskeleton, as compared with the same strain cultured in medium lacking methionine (Figure 2, graph). Actin patch polarization was lost in these methionine-repressed *oshΔ* P*MET3*-*OSH2* cells (Figure 2.5.2C–F) and actin cables were disorganized (Figure 2.5.2C, E), no longer running parallel to the mother-bud axis (compare with Figure 2A,B). The lower baseline of actin polarization observed in unbudded cells versus budded cells is normal and reflects the portion of the unbudded cell population in early G1 when the bud site is not yet established. These data indicated that *OSH* gene function is required for proper cell polarization and contributes to the polarized organization of the actin cytoskeleton.

2.2.3 Polarization of actin-assembly-promoting protein complexes is unaffected in *osh∆ osh4-1*[ts] cells

Loss of cell polarization in the absence of *OSH* gene function might reflect defects in either actin assembly or in the localization of protein complex(es) required for the spatial organization of the actin cytoskeleton. To address the former possibility, we tested whether multicopy *OSH4* affected *ACT1* mutations defective in actin assembly. Multicopy *OSH4* plasmids had no observable effect on the growth of either a wild-type strain or several actin assembly mutants [e.g. *act1-157*, *act1-158*, *act1-159*; data not shown (Belmont and Drubin, 1998; Belmont et al., 1999)]. This observation suggested that *OSH* gene function does not directly affect actin assembly, but it did not rule out the possibility that *OSH* genes regulate the localization of proteins that spatially organize actin.

To determine how *OSH* genes affect Cdc42p signaling and cytoskeletal polarity, we examined in *OSH* mutants the localization of green fluorescent protein (GFP) fusion proteins that associate with polarity-promoting protein complexes. In addition to using the *osh∆* P*MET3*-*OSH2* strain described above, we incorporated into our study a temperature-sensitive *OSH* mutant strain, *osh∆ osh4-1* (CBY926). This strain lacks all chromosomal copies of the *OSH* genes but carries a plasmid containing the *osh4-1*[ts] allele, which is rapidly inactivated at 37°C (Beh and Rine, 2004). When shifted to the restrictive temperature (37°C), *osh∆ osh4-1* cells arrest growth within the period of one cell cycle, but the arrest is reversed if the strain is then returned to grow at 23°C (Beh and Rine, 2004). In this mutant, we analyzed the localization of the polarisome, a 12S protein complex that contributes to the spatial organization of the actin cytoskeleton (Amberg et

al., 1997; Evangelista et al., 1997; Sheu et al., 1998). Polarisome proteins facilitate the localization of the formin Bni1p, which nucleates actin cable assembly at the bud site and apical bud tip (Evangelista et al., 2002; Fujiwara et al., 1998; Jaquenoud and Peter, 2000; Ozaki-Kuroda et al., 2001; Pruyne et al., 2004a; Sagot et al., 2002). The two yeast formins, encoded by *BNI1* and its paralogue *BNR1*, share some functional overlap (Imamura et al., 1997). Elimination of *OSH* function did not significantly affect Bni1p localization to the bud (Figure 2.5.3) or the Bnr1p localization to the bud neck (data not shown).

A plasmid expressing GFP-HA-Bni1p was transformed into *osh*Δ *osh4-1*, *osh*Δ *OSH4* and wild-type cells. After 4 h at 37°C (one to two cell cycles), there was no detectable difference in GFP-HA-Bni1p localization in any of these strains (Figure 2.5.3). In all the strains examined, including the wild-type control, GFP-HA-Bni1p was sometimes detected at the opposite pole of the cell, consistent with previous studies (Matheos et al., 2004; Pruyne et al., 2004b). Compared with wild type, GFP-Bnr1p was also properly localized in *osh*Δ *osh4-1* cells at 37°C (data not shown). These results were consistent with our finding that neither *OSH2* nor *OSH4* on a multicopy plasmid suppressed the temperature-sensitive growth defect of *bnr1*Δ *bni1-11*^{ts} or *bnr1*Δ *bni1-12*^{ts} mutants [data not shown (Evangelista et al., 2002)]. GFP fusions of two other polarisome proteins, Bud6p and Spa2p (Sheu et al., 1998), were also examined in *osh*Δ *osh4-1* and wild-type cells at 37°C. Both GFP-Spa2p and GFP-Bud6p properly localized to the bud site and bud tip in these mutant cells (Figures 2.5.3 and 2.5.9), albeit more GFP-Bud6p aggregates were observed in the *OSH* mutant cells than in wild type. These results indicated that *OSH* genes have little, if any, effect on formin or polarisome localization.

We also monitored the localization of Arc15p, a subunit of the Arp2/3 complex (Winter et al., 1997) that together with its associated proteins has a direct role in nucleating the assembly of cortical actin patches (Nicholson-Dykstra et al., 2005; Rodal et al., 2005; Welch and Mullins, 2002). As such, in wild-type cells, Arc15p localization resembles that of actin patches [described above (Kaksonen et al., 2003)]. As shown in Figure 2.5.3, GFP-Arc15p localization was unaffected by the inactivation of *OSH* function. This finding suggested that the spatial distribution of the Arp2/3 complex as a whole was unaffected by inactivation of the *OSH* genes. Together with the actin, formin and polarisome data described above, these results suggested that Osh proteins promote cell polarization by a mechanism that is not directed towards the actin cytoskeleton per se.

2.2.4 *OSH* genes maintain proper septin polarization and septin ring assembly

Our observation that multicopy *OSH4* rescued *cdc42*[ts] cell polarity defects by restoring the polarized localization of mutant Cdc42p (Figure 2.5.1B) strongly suggested that *OSH* gene function is necessary prior to or during bud site establishment. As an additional read-out for early cell polarization events, we examined how *OSH* gene function impacted septin localization. Although formins, the Arp2/3 complex and polarisome were properly polarized in *oshΔ osh4-1* cells at restrictive temperature, we found defects in septin localization and assembly. The mitotic septin ring complex [Cdc3p, Cdc10p, Cdc11p, Cdc12p and Shs1p/ Sep7p (Longtine and Bi, 2003)] assembles at the bud site in a Cdc42p dependent (Caviston et al., 2003; Gladfelter et al., 2002) but actin-independent manner (Ayscough et al., 1997; Ford and Pringle, 1991). As shown in

Figure 2.5.4,when *oshΔ osh4-1* cells were incubated at 23°C, a ring of GFP-Cdc3p was observed at the presumptive bud site and the mother-bud neck, in the same manner as either wild-type or *oshΔ OSH4* control strains cultured under the same conditions at 23 or 37°C. In contrast, GFP-Cdc3p was not fully polarized or properly assembled in *oshΔ osh4-1* cells grown at 37°C for 4 h (Figure 2.5.4). These defects were most apparent in *oshΔ osh4-1* large-budded cells and less evident in unbudded and small-budded cells (Figure 2.5.10), suggesting that *OSH*s affect septin localization only at later times during bud growth. In the majority of *oshΔ osh4-1* cells with large buds (67%) grown at 37°C for 4 h, GFP-Cdc3p was not polarized to the extent observed in control cells, and randomly arranged GFP-Cdc3p dots accumulated on the cell cortex. In addition, a significant number of oshΔ osh4-1 large-budded cells (76%) were observed with defects in ring assembly. Similar ring defects were also observed in *oshΔ osh4-1* cells expressing either GFP-Cdc10p or GFP-Cdc12p, or in *OSH2*-repressed *oshΔ* P^{MET3}-*OSH2* cells expressing GFP-Cdc3p (data not shown). Thus, the *OSH* genes appear unnecessary for the initial polarization and assembly of septins/septin rings, but *OSH*s do appear necessary for maintaining septin polarization and septin ring integrity.

2.2.5 *OSH* genes affect Cdc42p localization

Polarisome assembly is dependent on the prior localization of Cdc42p to the incipient bud site (Jaquenoud and Peter, 2000), but *OSH* mutants had little effect on polarisome localization. These findings suggested that Osh proteins maintain Cdc42p polarization after the initial polarization of Cdc42p to the incipient bud site. To test directly whether Osh function is necessary for proper Cdc42p localization to the bud

cortex, we examined Cdc42p polarization by indirect immunofluorescence microscopy in wild-type, *oshΔ OSH4* and *oshΔ osh4-1*[ts] cells. Cdc42p was found in wild-type and *oshΔ OSH4* control cells at one pole in unbudded cells and at the apical bud cortex in small- and medium-budded cells, regardless of temperature (Figure 2.5.5A). After shifting from 23 to 37°C, however, Cdc42p localization was significantly perturbed in *oshΔ osh4-1*[ts] cells (Figure 2.5.5A). When compared with control cells, Cdc42p staining was detected in fewer unbudded *oshΔ osh4-1*[ts] cells (Figure 2.5.5B). In unbudded *oshΔ osh4-1*[ts] cells in which staining was evident, Cdc42p was mislocalized and appeared as a thin crescent at the cell cortex [Figure 2.5.5A (rightmost panel, top insert) and B]. The most apparent difference, however, was observed in small-and medium-budded cells. Cdc42p was observed in fewer small-and medium-budded *oshΔ osh4-1*[ts] cells than in control strains (Figure 2.5.5A,B). When detected, Cdc42p was often mislocalized to the side of the bud (Figure 2.5.5A,B). In a few *oshΔ osh4-1*[ts] cells, Cdc42p was mislocalized at the mother side of the bud neck (Figure 2.5.5A [rightmost panel, bottom inset]). Loss or mislocalization of Cdc42p in *oshΔ osh4-1*[ts] cells was not due to a decrease in the total amount of Cdc42p. Mutant and control cells contained equivalent amounts of Cdc42p whether grown at 23 or 37°C (Figure 2.5.5C). In *OSH*-repressed *oshΔ* P[MET3]-*OSH2* cells, Cdc42p was also expressed at normal levels and a similar loss of Cdc42p localization was also observed (data not shown). These results indicated that Osh proteins promote Cdc42p polarization in both unbudded and budded cells and suggested that Osh proteins manifest their effects through the maintenance of Cdc42p polarization.

2.2.6 *OSH* genes affect polarized secretion; Bgl2p secretion is blocked in *oshΔ*

** *osh4-1*^{ts} cells**

Because our data indicated a role for Osh proteins in maintaining Cdc42p-dependent cell polarity, we investigated whether the *OSH* genes affect polarized secretion. Both Cdc42p and Rho1p are required (Guo et al., 2001; Zajac et al., 2005; Zhang, 2001) for the polarized localization of proteins that comprise the exocyst, a protein complex that spatially restricts secretory vesicle docking to the bud site and to bud tips undergoing polar growth (Hsu et al., 2004). Consistent with a role for Osh proteins in the regulation of polarized secretion, we found that several *OSH* genes interacted with both *CDC42* (Figure 2.5.1A) and *RHO1* (Figure 2.5.6A). Remarkably, *OSH* genes on multicopy plasmids had the opposite effect on *RHO1* as compared with *CDC42* mutants. When multicopy plasmids containing the *OSH2* or *OSH4* gene were introduced into *rho1-104*^{ts} strains, these transformants could only survive at drastically reduced temperatures compared with vector-alone control transformants (multicopy *OSH1*, *OSH5*, *OSH6* and *OSH7* also exacerbated *rho1-104*^{ts} defects; Figure 2.5.6A). These findings indicated that the *OSH*s not only affect Rho family GTPases in a gene-specific manner but that Osh proteins might modulate opposing interactions between Cdc42p and Rho1p.

The antagonistic effect of *OSH* gene overexpression was not restricted to *rho1-104* but was also observed with other mutations that confer defects in polarized secretion. Multicopy *OSH2* or *OSH4* exacerbated the growth defects of the conditional *sec3-2*^{ts} and *sec5-24*^{ts} mutants, even at temperatures that permit growth (Figure 2.5.6B). At restrictive

temperatures, *sec3-2*[ts] and *sec5-24*[ts] mutations disrupt the function of the exocyst complex, which is otherwise the target for vesicle docking and fusion at the plasma membrane (Novick et al., 1980; TerBush et al., 1996). Vesicle targeting is mediated by the Sec4p Rab GTPase, which is present on post-Golgi secretory vesicles and is required for their docking with the exocyst (Guo et al., 1999). Multicopy *OSH2* and *OSH4* also exacerbated the defects of the *sec4-2*[ts] mutant (Figure 2.5.6B) at 30°C, which is otherwise an acceptable temperature for the growth of this mutant strain. Multicopy *OSH2* or *OSH4* had no effect on the growth of a *sec18*[ts] strain, which is defective in SNARE complex disassembly (Ungermann et al., 1998) and is blocked in multiple secretory transport pathways (Graham and Emr, 1991). These findings suggested that *OSH2* and *OSH4* regulate specific events during polarized secretion.

Although our results indicated a role for *OSH2* and *OSH4* in polarized secretion, it was previously shown in *OSH* mutant cells that the transport of proteins that mark different secretory pathways was unaffected (Beh and Rine, 2004; Fang et al., 1996; Kvam and Goldfarb, 2004). To reconcile these results, we assayed the secretory transport of a protein specifically targeted to sites of polarized growth. In yeast strains grown at 23 or 37°C, we assayed the exocytosis of b-1,3-glucanase (Bgl2p), which is normally secreted to the plasma membrane by a population of late secretory vesicles distinct from those which transport invertase (Harsay and Bretscher, 1995). When shifted from 23 to 37°C for 90 min, Bgl2p accumulated within *oshΔ osh4-1*[ts] cells and was not transported to the plasma membrane. This defect in Bgl2p exocytosis was comparable to that in a *sec6-4*[ts] strain (Figure 2.5.6C), which is a well-characterized late secretory mutant that also blocks the pathway for Bgl2p transport (Harsay and Bretscher, 1995). Bgl2p

accumulation was not observed in the control *oshΔ OSH4* (Figure 2.5.6C) or wild-type cells (data not shown) grown under the same conditions. This result revealed a previously unknown secretory defect in *oshΔ osh4-1*[ts] cells and indicated that the *OSH* genes are necessary for a specific pathway of vesicular transport.

2.2.7 *OSH* genes are required for Rho1p and Sec4p localization to the bud tip

To better understand how the *OSH* gene family regulates polarized secretion, we tested whether *OSH* genes are required for the localization of several proteins that regulate polarized secretion. We found that *OSH* genes are necessary for the proper localization of Rho1p and GFP-Sec4p but not GFP-Sec3p. Regardless of temperature, in wild-type and *oshΔ OSH4* control cells, Rho1p was observed at one pole in unbudded cells and at the apical bud tip in small-and medium-budded cells (Figure 2.5.7A). In some cells, Rho1p staining also localized to the mitotic spindle and spindle pole bodies, though independent identification of these structures was not made. After shifting from 23 to 37°C for 4 h, Rho1p polarization was perturbed in *oshΔ osh4-1*[ts] cells, whether budded or unbudded (Figure 2.5.7A; also Figure 2.5.11). When compared with the controls, Rho1p staining at the cortex was less intense and more diffuse in the mutant cells. Similar results were obtained with a GFP-Rho1p fusion protein as well (data not shown). The decreased intensity of Rho1p fluorescence in cells was not a result of lower Rho1p levels. As detected by immunoblot, Rho1p levels were equivalent in wild-type, *oshΔ OSH4* and *oshΔ osh4-1*[ts] cells regardless of temperature (Figure 2.5.7B). Thus, *OSH* function is necessary for proper Rho1p polarization in both budded and unbudded cells.

To examine the localization of Sec3p and Sec4p by fluorescence microscopy,

GFP fusion proteins were expressed from plasmids transformed into wild-type, *oshΔ OSH4* and *oshΔ osh4-1* cells. When *oshΔ osh4-1* cells were incubated at 23 or 37°C, GFP-Sec3p localization to bud tips and bud necks was comparable to that seen in the wild-type or *oshΔ OSH4* controls (Figure 2.5.7A). GFP-Sec4p localization, however, was aberrant in the large proportion (46%) of *oshΔ osh4-1* cells grown at 37°C for 4 h. In wild-type cells, GFP-Sec4p fluorescence was detected primarily at the bud tip immediately adjacent to the plasma membrane [(Goud et al., 1988); Figure 2.5.7A]. Although GFP-Sec4p was observed in the bud in *oshΔ osh4-1* cells, a dramatic increase in fluorescence was detected, not at the bud tip, but generally dispersed within the bud (Figure 2.5.7A). This increase in fluorescence was consistent with an increase in GFP-Sec4p levels detected by immunoblot in *oshΔ osh4-1* cells at 37°C (Figure 2.5.7C). These findings suggested that secretory vesicles carrying GFP-Sec4p accumulated in the bud in the absence of *OSH* function, which is consistent with the observation by electron microscopy that *OSH* inactivation causes vesicle accumulation in some cells (Beh and Rine, 2004). This also implied that *OSH* genes promote vesicle docking at the bud tip and affect the Sec4p-dependent interaction between transport vesicles and the exocyst. Thus, *OSH* genes impact polarized secretion through Rho1p polarization and Sec4p-dependent vesicular transport.

2.2.8 Perturbing the balance in dosage between *OSH* genes and *MSB* genes inhibited growth

MSB3 and *MSB4* encode negative regulators (GAPs) of the Sec4p Rab GTPase (Gao et al., 2003). Consistent with our observation that the *OSH* genes antagonize *sec4*[ts]

69

mutations and polarized secretion, we found that multicopy *OSH4* (and, to a lesser degree, multicopy *OSH2*) exacerbated the otherwise minor growth defects of a *msb3Δ msb4Δ* strain (Figure 2.5.8A). Wild-type cells were unaffected by *OSH2* or *OSH4* overexpression (Figure 2.5.8A), as were transformants with either *MSB3* or *MSB4* deleted alone (data not shown). The reciprocal experiment in which OSH mutants were transformed with a high-expression -*MSB3* plasmid also inhibited cell growth. On galactose-containing medium, the induction of P^{GAL}-*MSB3* expression did not rescue the temperature-sensitive growth defect of *oshΔ osh4-1*^{ts} cells, rather it caused lethality at temperatures that otherwise permit growth as shown by the vector-alone control (Figure 2.5.8B). P^{GAL}-*MSB3* expression in wild-type or *oshΔ OSH4* cells caused only a modest growth inhibition at 37°C (Figure 2.5.8B). These results indicated that increased *MSB3* expression antagonizes loss of *OSH* function, and in the reciprocal experiment, increased *OSH2* or *OSH4* expression antagonized the loss of *MSB* function. Taken together, these findings suggested that yeast growth requires a balance in expression of *OSH* and *MSB* genes and that these genes are mutually antagonistic.

To investigate further how *MSB3* affects *OSH* gene function, P^{GAL}-*MSB3 oshΔ osh4-1* cells were cultured in galactose-containing medium and ensuing cellular defects were analyzed by microscopy. Galactose-induced P^{GAL}-*MSB3* overexpression in *oshΔ osh4-1* transformants caused growth arrest and an amassing of unbudded cells (71% of cells) at 30°C, as compared to either the P^{GAL}-*MSB3 oshΔ OSH4* (40% of unbudded cells) or P^{GAL}-*MSB3* wild-type controls (39% of unbudded cells) (Figure 2.5.12). These results indicated that *MSB3* overexpression exacerbates budding defects observed in mutants that

compromise the collective function of the *OSH* gene family. In the reciprocal experiment, *msb3Δ msb4Δ* cells transformed with multicopy *OSH4* also accumulated 53% of unbudded cells when cultured at 30°C, whereas in the vector-alone control, only 39% of the cells were unbudded (Figure 2.5.12). A similar cell arrest was not observed in *msb3Δ msb4Δ* cells transformed with multicopy *OSH2* (Figure 2.5.12). Taken together, these results affirmed a functional link between the *OSH* and *MSB* gene families.

2.3 Discussion

A genetic screen for genes important for *CDC42*-dependent polarity establishment identified *KES1*/*OSH4*, which encodes a yeast homologue of mammalian OSBP. We found that several other OSBP homologues in budding yeast had comparable genetic interactions with *CDC42*, linking the *OSH* gene family to the regulation of *CDC42*-dependent polarity establishment. Previous work implicated the *OSH* genes in bud formation and cell polarization (Beh and Rine, 2004). In this study, we showed that the *OSH* genes are collectively required to maintain cell polarity and secretion. Our data indicated that *OSH* genes reinforce *CDC42*-dependent polarity by maintaining Cdc42p localization at the apical bud tip after its initial polarization at the incipient bud site. *OSH* genes were also important for the polarized localization of Rho1p and were required for both Sec4p vesicle docking at sites of membrane growth and the transport of Bgl2p, a secreted protein that marks a pathway for polarized exocytosis. These findings strongly suggested that the *OSH* gene family is collectively required for a secretory pathway involved in the maintenance of Cdc42p-and Rho1p-dependent polarized growth.

2.3.1 *OSH* genes promote polarized growth

Several lines of evidence indicated that *OSH* family genes have an important role in polarized bud growth. First, certain OSH genes are dosage suppressors of *cdc42*ts polarity establishment defects. The mechanism of this suppression involves, in part, Cdc42p localization at cortical sites as increased *OSH4* dosage partially restored polarized localization to mutant forms of Cdc42p, and in the absence of *OSH* function, Cdc42p was mislocalized. Second, in the absence of *OSH* function, cytoplasmic structures (i.e. cortical actin patches and septin rings) necessary for proper bud growth were depolarized. Third, GTPases required for polarized secretion (Cdc42p, Rho1p and Sec4p) were mislocalized in the absence of *OSH* function. However, the localization of other proteins involved in actin and secretory polarization (e.g. formins, Arp2/3 complex, polarisome and Sec3p) was unaffected by *OSH* gene inactivation. The result that these proteins were properly localized seems, at first glance, to be at odds with the findings that Rho1p and Cdc42p are mislocalized upon *OSH* inactivation. After all, the polarized localization of the polarisome, Arp2/3 complex and Sec3p are dependent on Rho1p and/or Cdc42p (Jaquenoud and Peter, 2000; Munn and Riezman, 1994; Zhang, 2001). In *oshΔ osh4-1* cells at 37°C, it is possible that an undetectable but sufficient amount of Cdc42p and Rho1p remains properly polarized at the bud site or bud tip to ensure the proper localization of these proteins and proper budding. It is known in hypomorphic *cdc42-1* cells, for example, that Cdc42p levels are barely detectable by immunoblotting and immunofluorescence microscopy; yet, the cells appear morphologically wild type at permissive temperatures (Kozminski et al., 2000), implying proper localization of actin-organizing proteins. Last of all, the polarized exocytosis of Bgl2p, but not other secreted

proteins (Beh and Rine, 2004), was defective in response to *OSH* inactivation. Thus, *OSH* function is necessary for specific events required for cell polarization.

Our data indicated that many *OSH* family genes interact with *CDC42*, but *OSH2* and *OSH4* were the most effective suppressors of *cdc42*^{ts} cell polarity defects. Because defects in cell polarization were only observed with the loss of all *OSH* gene function, it appears that the *OSH* genes share at least one common function necessary for this process. Although the mechanism for this common function is not yet known, it may involve the OSBP-related domain (ORD) that is common to all Osh proteins and OSBP homologues (Olkkonen and Levine, 2004). Why some *OSH* genes were less effective dosage suppressors compared with others might relate to differences in localization of individual Osh proteins. In response to lipid binding, the canonical OSBP and many of its homologues translocate between membrane compartments (Li et al., 2002; Ridgway et al., 1992). Thus, the transport dynamics of individual Osh proteins might modulate their respective ability to promote Cdc42p-dependent cell polarization. Increased expression might result in ectopic expression, providing more Osh protein to sites where it can better facilitate Cdc42p function. Alternatively, increased dosage of certain *OSH* genes might lead to a gain-of-function that bypasses the requirement for *CDC42* during cell polarization. This possibility, however, is unlikely because our data indicated that *OSH4* is not a bypass suppressor of *cdc42*^{ts} polarity defects and that suppression occurs even with low-copy *OSH* expression. Thus, the *OSH* genes promote cell polarization, not in place of *CDC42* but in concert with *CDC42*.

Could the observed depolarization of yeast cell in the absence of *OSH* function be due to a general defect in endocytosis? In short, the answer is no. It is true that defects in

endocytosis can lead to depolarization of the cortical actin cytoskeleton (Gao et al., 2003), and Osh proteins promote endocytosis by affecting membrane sterol levels (Beh and Rine, 2004). However, this type of defect might account for depolarization of the cortical actin cytoskeleton, but it is inconsistent with septin mislocalization and assembly defects when *OSH* function is absent. There is no evidence to our knowledge that indicates that septin organization is dependent on endocytosis. If a causal link exists between *OSH*s/membrane sterols/endocytosis and cytoskeletal polarity, then defects in endocytosis resulting from perturbation in sterol distribution would also be predicted to cause polarity defects. *ERG2*, which encodes a sterol biosynthetic enzyme, was independently identified as the endocytosis gene *END11* (Munn et al., 1999; Munn and Riezman, 1994). Similar to *OSH* mutants, the deletion of *ERG2/END11* affects membrane sterols and blocks endocytosis (Beh and Rine, 2004). Unlike *OSH* mutants, however, defects in cell polarity are not apparent in *erg2/end11Δ* cells (unpublished observation). This is likewise true of *arv1Δ* cells, in which the normal cellular distribution of sterols is defective (Tinkelenberg et al., 2000) but cell polarization is not (unpublished observation). These results suggest that endocytic defects caused by perturbations in sterol trafficking do not cause cellular depolarization per se. Thus, the loss of *OSH* function does not affect polarized cell growth through sterol-related defects in endocytosis. Rather, consistent with our findings, the *OSH* gene family directly affects cell polarization through its role in polarized exocytosis.

2.3.2 *OSH* genes mediate opposing interactions between *CDC42* and *RHO1* during polarized growth

In contrast to how the *OSH* genes maintain *CDC42*-dependent cell polarization, *OSH* genes have the opposite effect on *RHO1* and other genes that mediate polarized secretion. On multicopy plasmids, most of the *OSH* genes exacerbated the growth defects of conditional mutants that disrupt polarized secretion. When transformed with multicopy *OSH* constructs, permissive temperatures for growth were reduced for temperature-sensitive *SEC3*, *SEC4*, *SEC5* and *RHO1* mutants. In the absence of *OSH* function, however, Sec4p localization was disrupted and undocked Sec4p-associated vesicles appeared to accumulate throughout the bud but not at the bud tip. This mislocalization did not appear to result from a depolarization of Bni1p, Bud6p or Spa2p, which contribute to the proper localization of Sec4p (Sheu et al., 2000). Under the same conditions, the localization of the exocyst component, Sec3p, was unaffected. This observation suggested that *OSH* genes facilitate vesicle docking at the bud tip but that *OSH* genes have no direct impact on exocyst structure or localization. *OSH*-dependent vesicle docking also appears independent of the functional interaction between *OSH4* and *SEC14*-dependent transport from the Golgi apparatus (Li et al., 2002). The deletion of *OSH4*, but none of the other *OSH* genes, bypasses the essential requirement for Sec14p, a phosphatidylcholine/phosphatidylinositol transfer protein necessary for vesicle budding from the Golgi apparatus (Fang et al., 1996). In this regard, the accumulation of Sec4p-associated vesicles in the absence of *OSH* function represents a late secretory event independent of Sec14p-mediated Golgi vesicularization. Thus, the *OSH* gene family exerts its effects on polarized secretion via vesicle delivery to the bud tip but not through

vesicle budding from the Golgi apparatus, nor maintenance of the vesicle-receiving exocyst complex. The opposing effects of *OSH* genes on polarity establishment and polarized secretion suggests a model in which two different small GTPase-mediated processes are regulated relative to each other to orchestrate an orderly progression of polarization events. This proposed coordination of events is similar to the proposed function of Pxl1p, a yeast paxillin homologue (Gao et al., 2004). Yeast *PXL1* has an effect on signalling reminiscent of mammalian paxillin (Brown et al., 1996; Gao et al., 2004; Mackin et al., 2004), which integrates signalling events at focal adhesions (Brown et al., 1996; Turner, 2000). Similar to the *OSH*s, *PXL1* overexpression suppresses *cdc42* mutations but inhibits growth of *rho1* mutants, suggesting that *PXL1* coordinates the Cdc42p and Rho1p functions during budding (Gao et al., 2004). However, it is unlikely that *PXL1* and *OSH* genes affect the same stages of yeast budding and polarization. Multicopy *OSH* genes suppressed *cdc42*^{ts} mutations that disrupt polarity establishment, whereas *PXL1* overexpression suppressed *cdc42*^{ts} alleles that disrupt later events in budding (Gao et al., 2004). In both cases, however, these findings imply that transitions between Cdc42p and Rho1p signalling advance the progress of cell polarization. Possibly, each event in cell polarization is licensed by a different set of regulators; *OSH* genes permit polarized secretion once polarity is established, and *PXL1* controls a later transition.

The link between *OSH* genes and *RHO1*/*CDC42* signalling during polarized growth might reflect a direct physical interaction between Osh proteins and these small GTPases or with their regulators. As of yet, however, we have been unable to detect such an interaction or identify relevant binding partners by standard techniques. In this regard,

the dynamic nature of OSBPs, and their requisite lipid binding for complex formation (Wang et al., 2005a), might contribute to the technical difficulty of isolating stable Osh protein complexes. For specific subsets of Osh proteins, proteomic interaction screens have identified specific protein interactions (Gavin et al., 2002; Hazbun et al., 2003; Ho et al., 2002; Uetz et al., 2000). In particular, Osh1p and Osh2p interact with Scs2p, the yeast homologue of VAMP-associated protein (Gavin et al., 2002; Loewen et al., 2003). However, the interaction with Scs2p is restricted to only Osh1p and Osh2p, and no link between *SCS2* and cell polarization has yet been established. It should be noted that a human OSBP homologue, ORP1L, physically interacts with the small GTPase Rab7 (Johansson et al., 2005), which is closely related to yeast Sec4p. This is consistent with our findings that *OSH* function is necessary for normal Sec4p localization and that *SEC4* function is sensitive to *OSH4* dosage effects.

The Osh proteins might maintain polarization by either regulating Cdc42p transport to the plasma membrane and the bud site/bud tip (Irazoqui et al., 2005) or by trafficking a key regulator required for maintaining Cdc42p at sites of polarization. This model is consistent with the genetic interactions between *OSH* genes and regulators of polarized secretion and the accumulation of GFP-Sec4p vesicles in *oshΔ osh4-1*[ts] cells. Vesicle accumulation was also observed by electron microscopy in Osh-depleted cells, but no corresponding defects in general protein exocytosis were detected (Beh and Rine, 2004). However, as shown by the intracellular accumulation of the exoglucanase Bgl2p in *oshΔ osh4-1*[ts] cells, Osh proteins promote a specialized transport pathway (Goud et al., 1988) that mediates secretory exocytosis to sites of polarized growth (Adamo et al., 2001). In this regard, *OSH* genes might maintain Cdc42p polarized localization by

controlling trafficking events that transport Cdc42p (or a Cdc42p regulator) to sites of polarization. Based on the fact that Rho1p is also depolarized in the absence of *OSH* function, *OSH* genes likely regulate Rho1p polarized transport as well.

Msb3/4p represent a regulatory interface between Cdc42p and Rho1p signalling pathways. *MSB3* and *MSB4* encode negative regulators (i.e. GAPs) of the Sec4p Rab GTPase and Rho1p-dependent polarized secretion (Gao et al., 2003), but *MSB3* overexpression also suppresses a *cdc42*[ts] allele defective in polarity establishment (Bi et al., 2000). Furthermore, *msb3Δ msb4Δ* cells internally accumulate Bgl2p, with little effect on the exocytosis of invertase (Gao et al., 2003). We found that multi-copy *OSH2* or *OSH4* exacerbated the otherwise minor growth defects of a msb3Δ msb4Δ strain, and in the reciprocal experiment, *MSB3* overexpression in *oshΔ osh4-1*[ts] cells caused lethality at temperatures that otherwise permit *OSH* mutant growth. These results suggested that cell growth requires a balance between Osh and Msb protein activities and implied a possible mechanism for *OSH* coordinated regulation of Cdc42p and Rho1p signalling. As perturbations in the functional balance between Osh and Msb proteins causes an accumulation of unbudded cells, it is an attractive possibility that Osh proteins exert their effects on polarity establishment in concert with Msb3/4p.

The recent structural determination of Osh4p led to the conclusion that the OSBP family of proteins is involved in the nonvesicular transport of sterols (Im et al., 2005; Levine, 2005). This is supported by recent in vitro results that Osh4p transfers sterols between liposomes (Raychaudhuri et al., 2006). However, previous in vivo analyses, as well as the data presented herein, suggest a direct role for Osh proteins in vesicular transport. The *OSH4* mutants bypass the essential requirement for *SEC14*, which is

necessary for vesicle budding from the Golgi apparatus (Fang et al., 1996). This bypass suppression is abolished in the absence of *GCS1*, which encodes a GAP for the small GTPase ADP ribosylation factor 1 (Arf1p) (Li et al., 2002). This finding establishes another link between a yeast Osh protein and a GAP, in addition to the connection with Msb3/4p. This observation suggests that *OSH* genes might regulate either GAP function or small GTPase function directly in several signalling pathways. In this regard, the PH domain of human OSBP has affinity for the small GTPase, ARF (Godi et al., 2004). What is clear from these studies, and the finding that OSBP affects ERK1/2 phosphorylation and signalling in mammalian cells (Wang et al., 2005b), is that a general function of OSBP homologues is to integrate lipid trafficking, cell signalling, and secretory transport.

2.4   Materials and Methods

2.4.1 Strains, microbial and genetic techniques

Strains and plasmids used in this study are listed in Tables 2.6.1 and 2.6.2, respectively. Saccharomyces cerevisiae strains were cultured as described in Kozminski et al. (Kozminski et al., 2003). All transformations were performed according to Schiestl and Gietz (Schiestl and Gietz, 1989). To select for the kanMX gene (Wach et al., 1994), yeast were grown on rich medium containing 200 mg/mL G418 (GIBCO-Invitrogen Inc., Carlsbad, CA, USA). For repression of the *MET3* promoter in yeast strain JRY6326 (Beh et al., 2001), log-phase cultures in minimal medium were supplemented with 100 mg/mL methionine. To induce expression of *GAL10* promoter fusions, 2% galactose (final concentration) was added to log-phase cultures grown in minimal medium containing 2% raffinose

2.4.2 Identification of *KES1*/*OSH4* as a dosage suppressor of *cdc42-118*

The screen for *cdc42-118* dosage suppressors is described in Kozminski et al. (Kozminski et al., 2003). One YEp24 library plasmid identified in this screen, pKK1825, contained a genomic fragment of chromosome XVI (base pairs 275701-281371) that includes *KES1*/*OSH4*. To determine that *OSH4* was indeed the suppressor on pKK1825, isogenic *cdc42* strains were transformed with a2-m plasmid with (pKK1821) or without (YEplac195) an *OSH4* insert. Transformants were streaked onto solid selective synthetic medium and scored for growth after incubation at 25 and 36°C for 5 days.

2.4.3 Plasmid constructs

To construct pKK1821, *OSH4* was amplified from pKK1825 by polymerase chain reaction (PCR) using primers (BamHI sites underlined) *kes1*-forward (AAGCTC<u>GGATCC</u>GTTCTGTCTTGAGCTGTG) and *kes1*-reverse (TGTCGA<u>GGATCC</u>CATATCCTTTCCTGTCACA) and cloned into the BamHI site of YCplac33, forming pKK1062. The coding sequence of *OSH4* in pKK1062 was sequenced and found error free, relative to the Saccharomyces Genome Database (www.yeastgenome.org). An *OSH4*-containing SphI–KpnI fragment from pKK1062 was then subcloned into the SphI and KpnI sites of YEplac195, forming pKK1821. To construct pKK1826, *ARC15*-GFP:HIS3MX6 was PCR amplified from DDY2752, using primers oKK212 (AGCT<u>GCATGC</u>CTCTGCTACTTGTTGTCTATG; SphI site underlined) and oKK213 (TATAGGATCCGTTTATGCGTACTTGTTTTGTG). Digestion of the PCR product with SphI and BglII produced an *ARC15*-GFP-containing fragment that was cloned into the SphI and BamHI sites of YCplac33. To construct

pCB368, *MSB3* was amplified from SEY6210, using primers CBP242 (<u>GGTACC</u>ATGCAGAACGATCAACAGAG; KpnI site underlined) and CBP243 (<u>CTCGAG</u>GTTAGTCACCCTTGTCTTTTTC; XhoI site underlined) and cloned into pGEM-T-Easy (Promega, Madison, WI, USA). From the resulting plasmid, digestion with KpnI and XhoI produced a 1.9-kb *MSB3* fragment that was subcloned in-frame into the KpnI and XhoI sites of pKT10-*GAL*-HA. To construct pCB494, *SPA2*-GFP was excised from pRS416Spa2GFP with PvuI and subcloned into the PvuI sites of pRS426.

Constructs containing OSH genes on 2-m plasmids (pCB236-242) were isolated from a YEp24 genomic library (Carlson and Botstein, 1982) in screens for genes that in high copy suppressed the defects of *osh∆ osh4-1* (CBY926) and/or *osh∆* P^{MET3} -*OSH2* under restrictive conditions. Genetic interactions described in this article using the YEp24 *OSH* plasmids were confirmed with independently isolated P^{GAL} -*OSH* cDNAs and, in the case of *OSH2* and *OSH4*, with amplified sequences that do not contain flanking gene sequences.

2.4.4 Fluorescence microscopy

Indirect immunofluorescence microscopy for Cdc42p and actin was performed as described in Kozminski et al. (Kozminski et al., 2000) and for Rho1p as described in Ayscough et al. (Ayscough et al., 1999), except that cells were cultured in minimal medium, and sodium dodecyl sulfate (US Biological, Swampscott, ME, USA) was used at 0.2% for Cdc42p and actin and at 0.3% for Rho1p. Affinity-purified rabbit anti-yeast Cdc42p peptide antibody (Kozminski et al., 2000), guinea-pig anti-yeast actin antibody (Palmgren et al., 2002) and affinity-purified rabbit anti-yeast Rho1p peptide antibody

were diluted 1:625, 1:500, 1:100 in PBS containing 1 mg/mL BSA, respectively. Secondary antibodies (Jackson ImmunoResearch Laboratories, West Grove, PA, USA) were diluted 1:100 in the same buffer. For visualization of epitope-tagged hemagglutinin (HA)-Bni1p-GFP by indirect immunofluorescence, cells were fixed in 10% formalin for 30 min and incubated with a 1:1000 dilution of anti-HA antibody (Covance Research Products, Denver, PA, USA) followed by a 1:1000 dilution of an Alexa 488-conjugated anti-mouse secondary antibody (Invitrogen − Molecular Probes). Fixed cells stained for immunofluorescence, and cells expressing GFP fusions, were observed with epifluorescence with either a Nikon E800 microscope equipped with a x100/1.3 Plan-Neofluar objective or a Leica DMXRA2 microscope equipped with a x100/1.40 Plan-Apo objective. Images were captured with an Orca100ER or AG digital cameras (Hamamatsu Photonics, Hamamatsu-City, Japan) and Openlab software (Improvision Inc., Lexington, MA, USA). Unless otherwise noted, exposure times and contrast enhancement were constant for a given series of images.

In experiments that only examined cell morphology and nuclear staining, mid-log phase cells were pelleted and resuspended in 1 mL 3:1 (v/v) methanol/acetic acid. After 30 min at room temperature, cells were pelleted and resuspended in 1 mL PBS. Following an additional wash with 1 mL PBS, the final pellet was resuspended in mounting medium containing 1 mg/mL 4',6-diamidino-2-phenylindole (DAPI; Accurate Chemicals and Scientific Corp., Westbury, NY, USA) to stain nuclei.

2.4.5 Immunoblots

Immunoblotting for Cdc42p and Rho1p was performed as described in Kozminski et al. (Kozminski et al., 2000) and Ayscough et al. (Ayscough et al., 1999), respectively. Immunoblots to detect GFP-Sec4p used a polyclonal anti-GFP antibody (Molecular Probes Inc., Eugene, OR, USA) at a titre of 1:1000 with a 1:5000 titre of goat horseradish peroxidase (HRP)-conjugated anti-rabbit immunoglobulin G secondary antibody (Promega, Madison, WI, USA). Tubulin served as a loading control and was detected with AA2, a mouse monoclonal antibody raised against amino acids 412–430 of bovine brain b-tubulin (the kind gift of Dr Tony Frankfurter, University of Virginia). AA2 was diluted to 130 ng/mL with Tris-buffered saline (TBS) containing 0.1% Tween-20 (Fisher Scientific) and incubated with blots overnight at room temperature.

2.4.6 Assay for Bgl2p secretion

The secretion of Bgl2p was assayed following the method of Harsay and Schekman (manuscript in preparation). Yeast cells were grown overnight at 25°C in YPD to mid-log phase (~0.3 OD600 units/mL). Each culture was then split equally and 3.75 OD600 units were transferred to each of two new flasks. One culture was incubated at 25°C and the other culture was shifted to 37°C for 90 min. Cells from both cultures were then harvested by centrifugation at 900x g for 5 min. Cell pellets were resuspended in 1 mL ice-cold 10 mM NaN3,10 mM KF solution, followed by a 10-min incubation on ice. The suspension was transferred to microfuge tubes and microfuged at 10 000x g for 1 min. Cell pellets were resuspended in fresh prespheroplasting buffer (100 mM Tris–H2SO4,pH 9.4;50 mM ß-mercaptoethanol; 10 mM NaN3;10mM KF) and incubated on

ice for 15 min. Cells were pelleted as before, washed with 0.5 mL spheroplast buffer (50 mM KH2PO4–KOH, pH 7; 1.4 M sorbitol; 10 mM NaN3) and pelleted. After resuspension in 1 mL spheroplast buffer containing 167 mg/mL zymolyase 100T (Seikagaku Corporation, Tokyo, Japan), cells were incubated with gentle agitation for 30 min at 30°C. Spheroplasts were then pelleted at 5000x g for 10 min before their preparation for SDS–PAGE in 100 mL 2x SDS–PAGE sample buffer. About 5 mL of each sample was loaded per lane on a 13% SDS– PAGE gel. Detection of Bgl2p was made by immunoblotting, using a rabbit polyclonal antibody against Bgl2p (the kind gift of Dr Randy Schekman University of California at Berkeley) that was preabsorbed against SEY2102, a bgl2Δ strain (Klebl and Tanner, 1989), following the method of Roberts et al. (Roberts et al., 1991).

2.5 Figures and Tables

Figure 2.5.1: Suppression of *cdc42*[ts] growth defects by multicopy *OSH* genes.
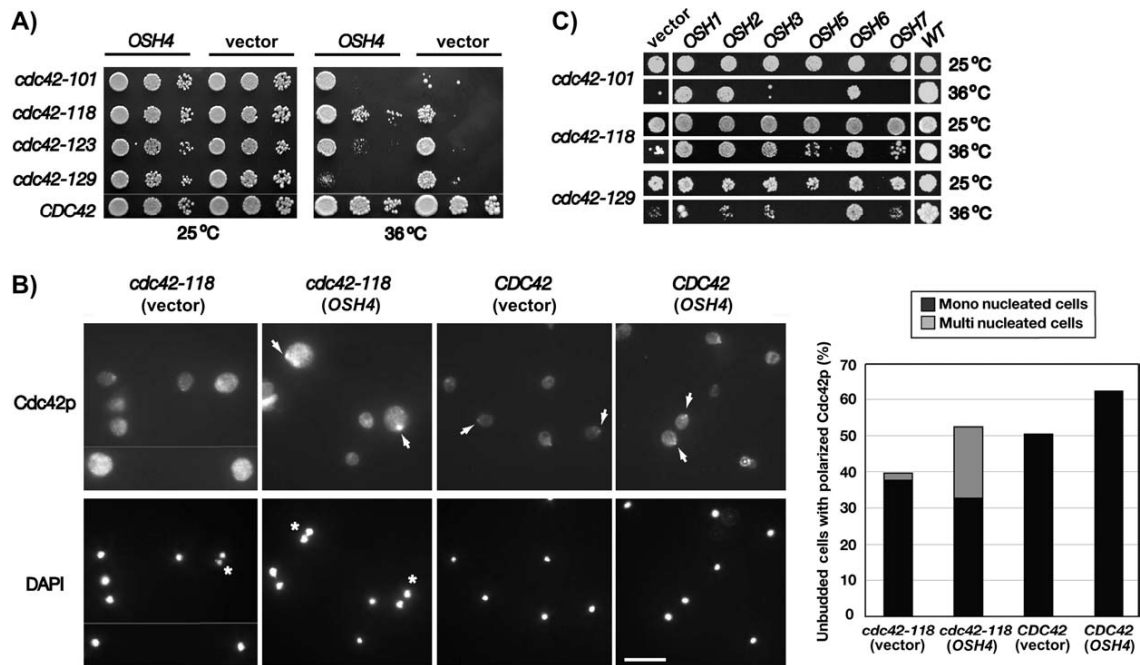
Figure 2.5.1: A) *OSH4* suppressed the temperature-conditional growth defect of *cdc42*[ts] cells defective in polarity establishment. Ten-fold serial dilutions (left to right) of cultures were spotted onto selective minimal medium and growth was compared at 25 and 36°C (5 days) for wild-type and mutant yeast transformed with a multicopy plasmid containing *OSH4* (pKK1821) or vector only (YEplac195). The strains transformed were *CDC42* (DDY1300), *cdc42-101* (DDY1304), *cdc42-118* (DDY1326), *cdc42-123* (DDY1336) and *cdc42-129* (DDY1344). B) Multicopy *OSH4* promoted Cdc42p polarization in *cdc42-118* and wild-type strains. The strains shown are the same described in (A). After a shift from 25°C, strains were incubated for 9 h at 36°C in minimal selective medium. Cdc42p was visualized by indirect immunofluorescence microscopy

and nuclei were visualized with DAPI. Arrows highlight examples of polarized Cdc42p, and asterisks identify multinucleated cells. Although some cultures contained cells distributed throughout the cell cycle, unbudded cells are selectively shown because they were the focus of comparison. The scale bar is 10 mm. Measurement of Cdc42p polarization in both unbudded mononucleated and multinucleated cells is presented in the graph. Cells were scored as polarized when Cdc42p was visualized as a distinct spot at one pole of a cell (n > 200 unbudded cells scored for each strain). C) Additional *OSH* family genes suppressed specific *cdc42*^ts^ growth defects. Equivalent dilutions on selective synthetic medium compared growth at 25 and 36°C (5 days) of *cdc42-101* (DDY1304), *cdc42-118* (DDY1326) and *cdc42-129* (DDY1344) strains transformed with a multicopy (YEplac195) vector (left column) or a multicopy genomic library clone (pCB236-240, 242) containing the *OSH* family gene indicated. A wild-type (WT) control strain (DDY1300) transformed with vector (YEplac195) is shown in the rightmost column. All strains in each row were grown on the same plate. ***This work was performed by K.G.K.**

Figure 2.5.2: Osh-protein-depleted cells exhibited a depolarization of the actin cytoskeleton
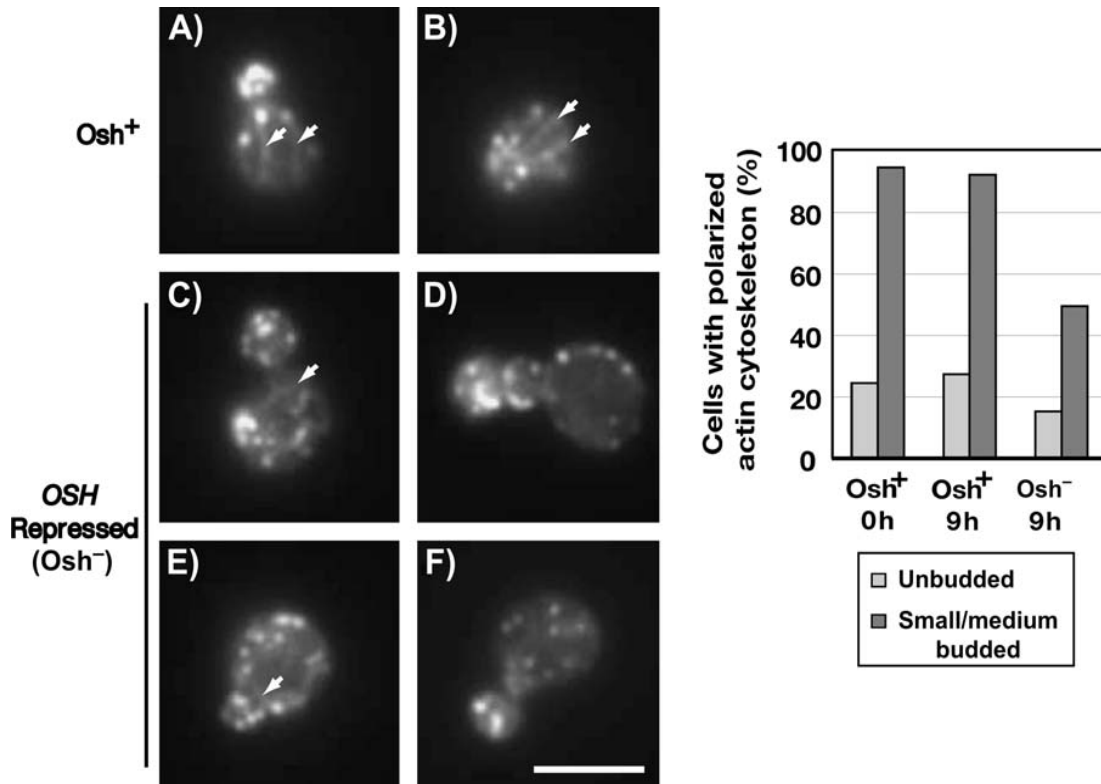
Figure 2.5.2: Indirect immunofluorescence micrographs of *osh*Δ P*MET*-*OSH2* (JRY6326) cells cultured in minimal medium at 25°C for 9 h in the absence (A,B) or presence (C–F) of methionine and probed with an antibody against actin. Actin cables (arrowheads) were present but more difficult to visualize in Osh-depleted cells (C–F) than in Osh-containing cells (A,B). Scale bar is 5 mm. Measurement of actin polarization in the aforementioned cells is summarized in the graph. The actin cytoskeleton was scored as polarized when cortical actin patches were distributed toward one pole of the cell. All cells counted had a single nucleus as visualized with DAPI (n > 300 cells scored for each morphological class of each strain). ***This work was performed by K.G.K.**

Figure 2.5.3: Proteins that promote actin assembly and/or organization exhibited proper polarization in cells defective for *OSH* function
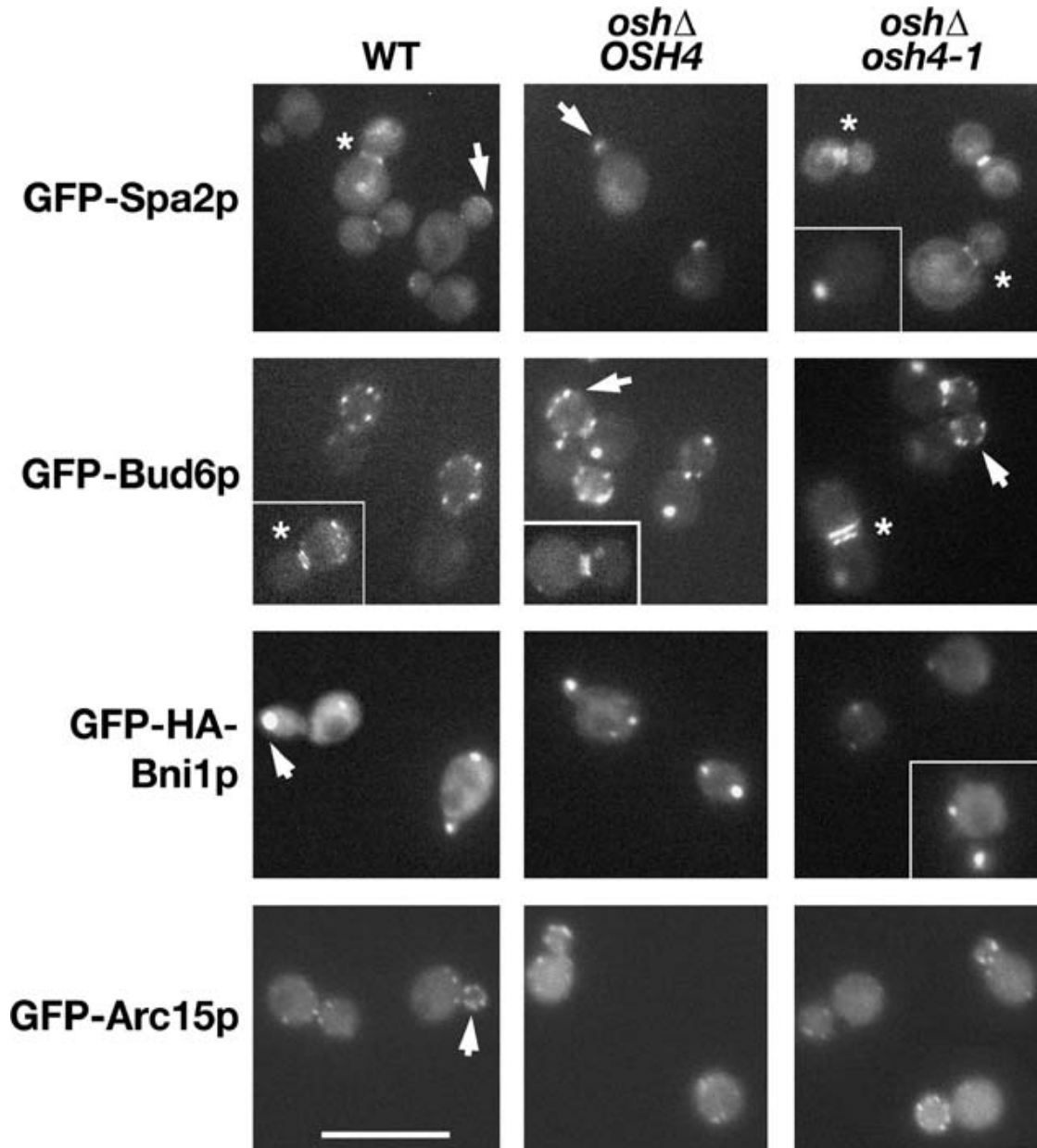
Figure 2.5.3: Spatial distribution of polarity-promoting proteins in wild-type (WT; SEY6210), *osh*Δ *OSH4* (CBY924) and *osh*Δ *osh4-1* (CBY926) cells after log-phase cultures were shifted from 23°C to 37°C for 4 h. GFP-Spa2p and GFP-Bud6p were expressed from pCB494 and pRB2190, respectively. GFP-Arc15p, which was used to localize the Arp2/3 complex, was expressed from pKK1826. Indirect

immunofluorescence using an anti-HA epitope antibody was used to detect GFP-HA-Bni1p expressed from p1955, 4 h after galactose induction. Scale bar for all panels is 10 mm. Arrows indicate examples of proper bud or bud tip polarization, and asterisks indicate examples of proper bud neck localization. Cells were scored for proper fusion protein localization, which is presented in Figure 2.5.9. At 23°C, the spatial distribution of GFP-HA-Bni1p, GFP-Spa2p, GFP-Bud6p and GFP-Arc15p was found to be indistinguishable among wild-type, *osh*Δ *OSH4* and *osh*Δ *osh4-1* cells (not shown). ***This work was performed by Gabriel Alfaro.**

Figure 2.5.4: Septin defects in *oshΔ osh4-1* cells
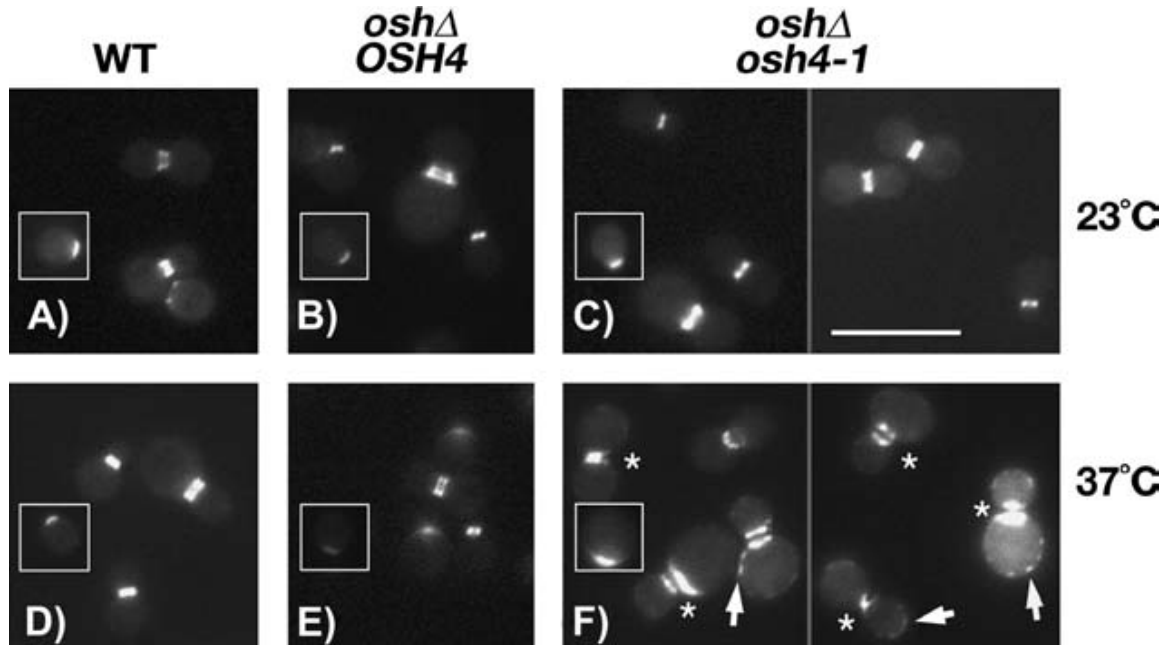
Figure 2.5.4: GFP-Cdc3p localization (expressed from pRS316-*CDC3*-GFP) as observed by fluorescence microscopy shown for wild-type (SEY6210) cells (A,D), *oshΔ OSH4* (CBY924) cells (B,E) and *oshΔ osh4-1* (CBY926) cells (C,F). Each panel shows representative large-budded cells. Unbudded cells do not show septin defects; representative unbudded cells for each strain are shown in the insets. After log-phase cultures were shifted from 23 to 37°C for 4 h, GFP-Cdc3p was partially depolarized (indicated by arrows) and the assembly of septin rings was defective (indicated by asterisks) but only in *oshΔ osh4-1* cells. Scale bar for all panels is 10 mm. Septin/GFP-Cdc3p assembly and polarization were scored in each strain and the data are presented in Figure 2.5.10. ***This work was performed by Gabriel Alfaro.**

Figure 2.5.5: Cdc42p was mislocalized in *osh∆ osh4-1* cells at restrictive temperature

A)

B) Localization pattern of Cdc42p in

Strain	Temperature	Unbudded cells			Small- and medium-budded cells				
		None (%)	Polarized (%)	n	None (%)	Polarized (%)	Polarized off-axis (%)	Polarized in mother (%)	n
Wild type	37°C	48.1	51.9	(349)	6.2	93.8	0.0	0.0	273
osh∆ OSH4	37°C	46.4	53.6	(425)	8.1	90.9	1.0	0.0	296
osh∆ osh4-1	37°C	63.1	36.9	(515)	23.3	41.4	31.2	4.2	215

C)
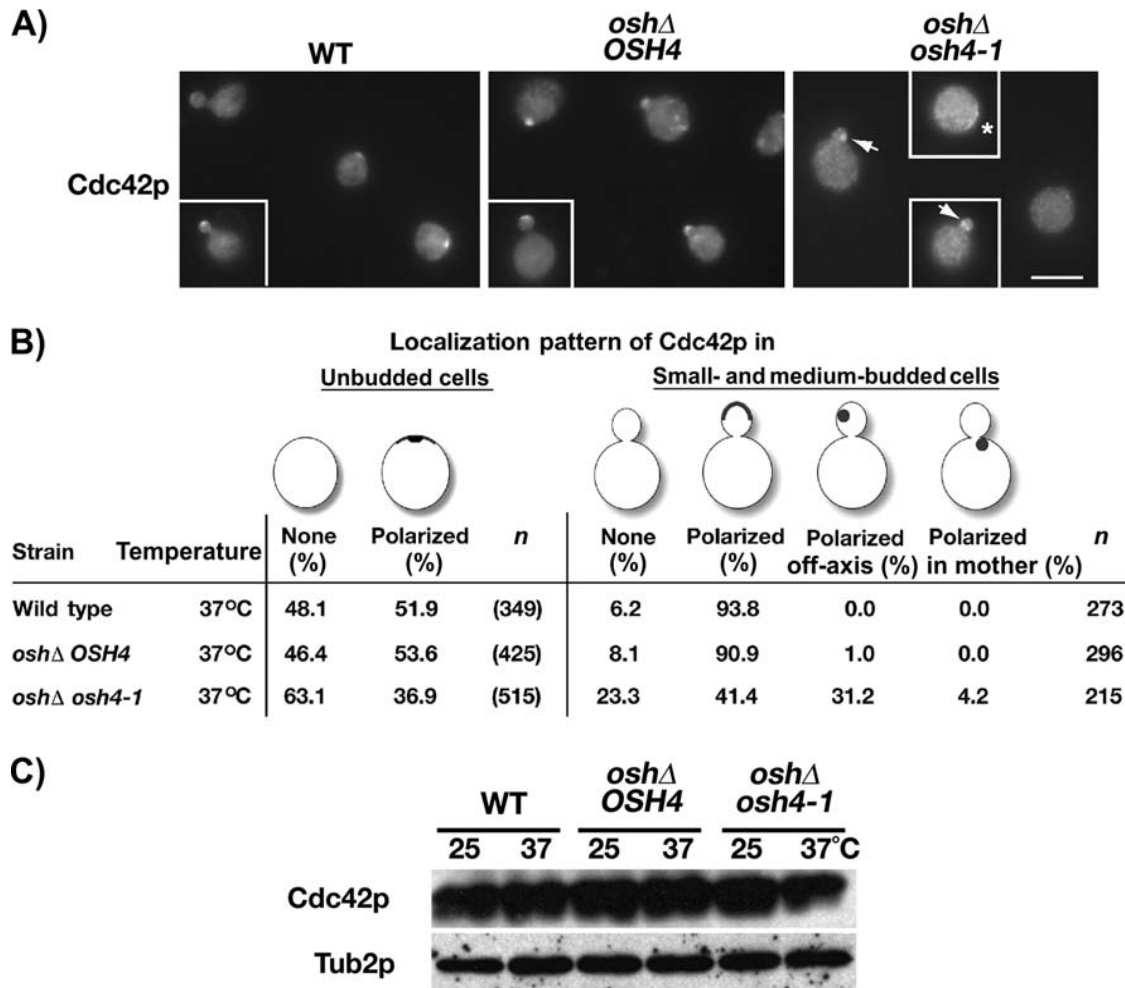
Figure 2.5.5: A) Cdc42p was visualized by indirect immunofluorescence microscopy in wild-type (WT; SEY6210), *osh∆ OSH4* (CBY924) and *osh∆ osh4-1* (CBY926) cells after log-phase cultures grown in minimal medium were shifted from 23 to 37°C for 4 h. Arrows indicate examples of polarized Cdc42p that is 'off-axis'; that is, not at the apical bud tip but rather to the flank or base of the bud. The asterisk indicates an example of an unbudded cell in which Cdc42p is otherwise polarized but distributed as a crescent on the cell cortex rather than a distinct spot. The scale bar is 5 mm. B) Quantification of the distribution patterns of Cdc42p in the cells shown in (A). C) As

shown by an anti-Cdc42p immunoblot, Cdc42p levels remain constant in wild-type (WT;

SEY6210), *oshΔ OSH4* (CBY924) and *oshΔ osh4-1* (CBY926) cells whether grown at

23°C or shifted to 37°C for 4 h. To demonstrate equivalent loading, the same blot was

probed with an antibody against b-tubulin that detects yeast Tub2p. ***This work was

performed by K.G.K.**

Figure 2.5.6: Exacerbation of growth defects in polarized secretion mutants by multicopy *OSH* genes
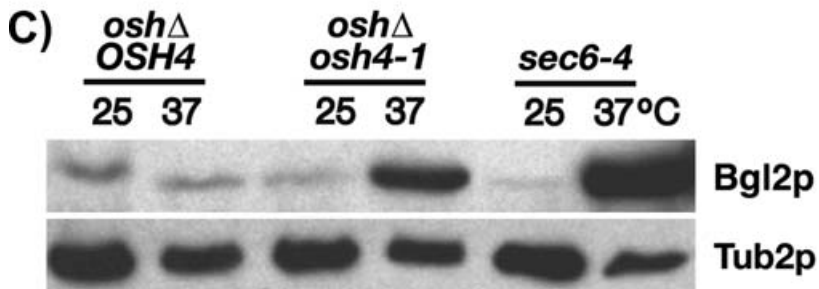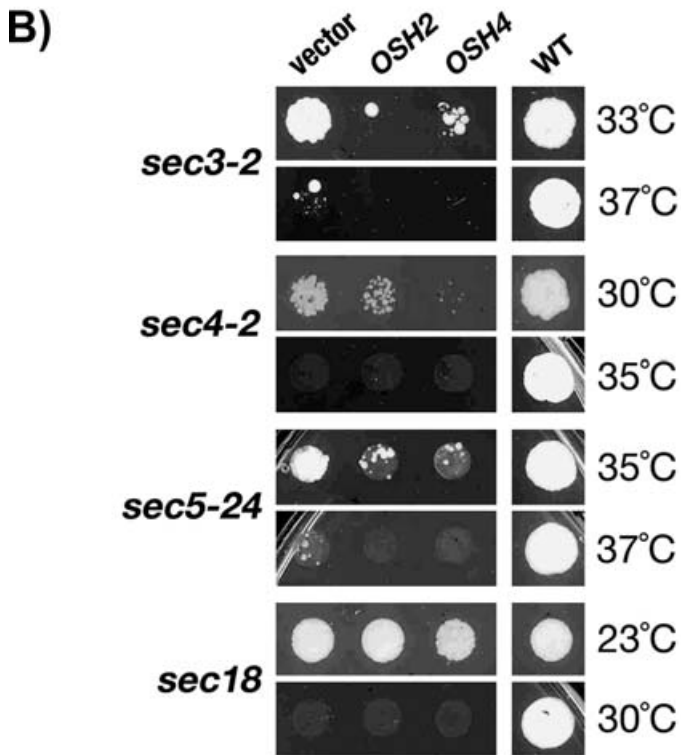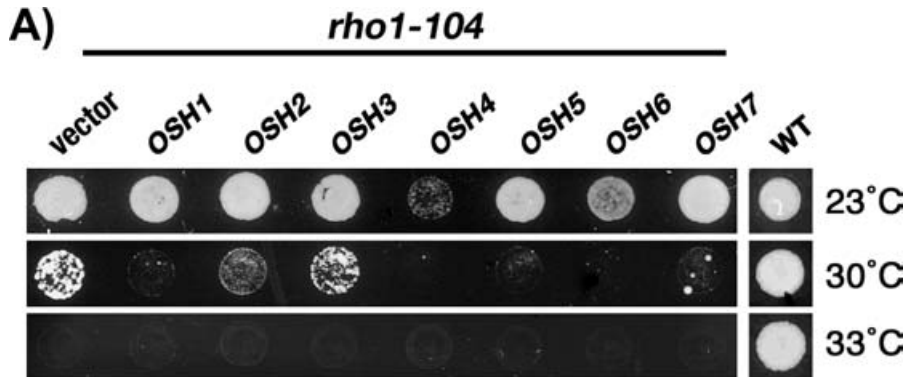
Figure 2.5.6: A) Equivalent culture dilutions spotted onto selective synthetic medium to compare growth of *rho1-104*^ts (KKY37) cells transformed with multicopy plasmids containing the indicated *OSH* genes (pCB236-242) or a vector-alone control (pRS426). Transformed strains were incubated at 23°C (permissive growth temperature for *rho1-104*^ts), 30°C (semipermissive growth temperature) and 33°C (restrictive growth temperature). A wild-type control strain (DDY1300) transformed with vector (pRS426) is shown in the rightmost column. Note that the effect of multicopy *OSH* genes on *RHO1* was the opposite of that observed on *CDC42*.B) *OSH* family genes exacerbated growth defects of specific polarized secretion mutants. Equivalent dilutions on selective synthetic medium compared growth at permissive (top panels) and restrictive temperatures (bottom panels) for each mutant, respectively. The *sec3-2*^ts (CBY1345), *sec4-2*^ts (CBY1480), *sec5-24*^ts (CBY1474) and *sec18*^ts (JRY4130) strains were transformed with a multicopy plasmid containing *OSH2* (pCB239), *OSH4* (pCB241) or a vector (pRS426) control. A wild-type control strain (RSY255) transformed with vector (pRS426) is shown in the rightmost column. C) Immunoblots showing internal Bgl2p levels accumulating within *oshΔ OSH4* (CBY924), *oshΔ osh4-1* (CBY926) and *sec6-4* cells (NY17) whether grown at 25°C or shifted to 37°C and cultured for 90 min. To demonstrate equivalent loading, the same blot was probed with an antibody against b-tubulin that detects yeast Tub2p.

*Panels A and B performed by C.T.B and panel C performed by K.G.K.

Figure 2.5.7: Disruption of Rho1p and Sec4p localization in *OSH* mutants
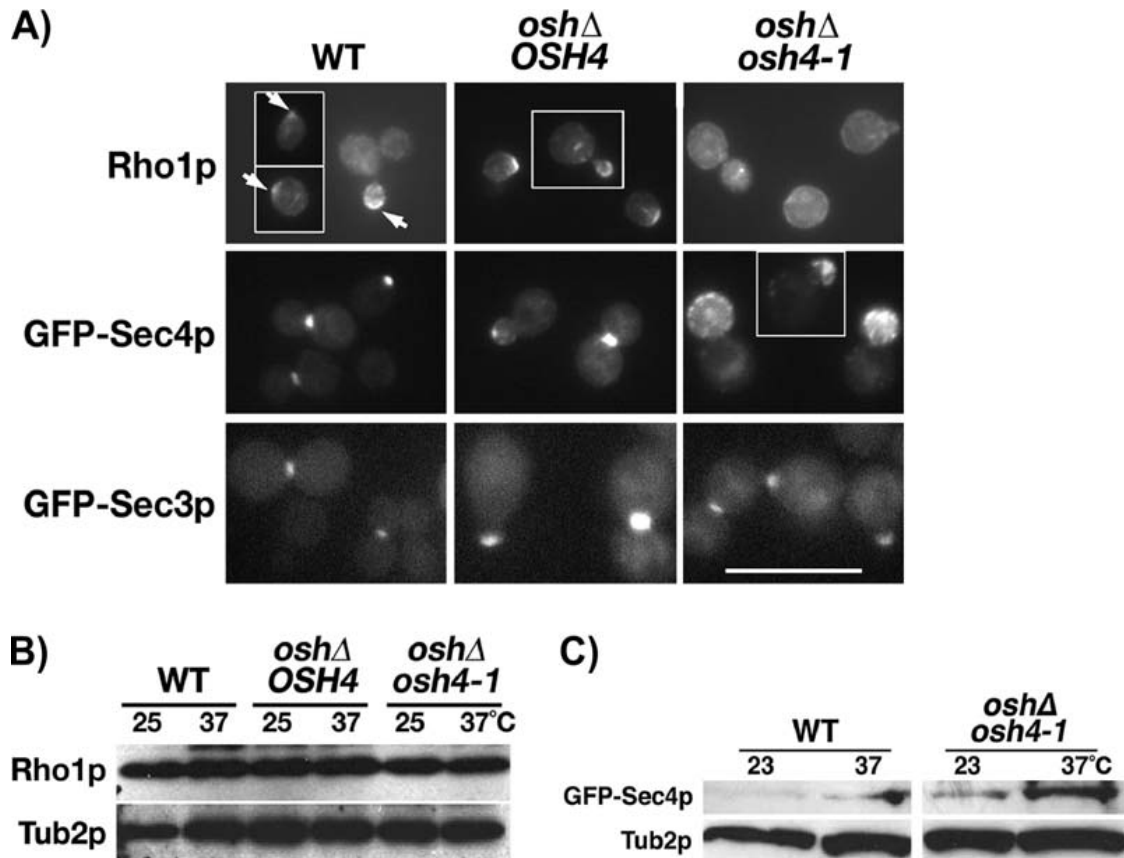
Figure 2.5.7: A) After log-phase cultures were shifted from 23 to 37°C for 4 h, indirect immunofluorescence microscopy revealed the spatial distribution of Rho1p, and fluorescence microscopy revealed the spatial distribution of GFP-Sec4p (expressed from pRC2098) and GFP-Sec3p (expressed from pNB810) in *oshΔ osh4-1* (CBY926), *oshΔ OSH4* (CBY924) and wild-type cells (SEY6210). Arrows indicate examples of sites of Rho1p polarization. Note that because of the intensity of GFP-Sec4p fluorescence in *oshΔ osh4-1* cells, the corresponding image represents an exposure time that is one fourth of that shown for the other transformed strains. The insert in the GFP-Sec4p *oshΔ osh4-1* panel shows Sec4p mislocalization in a small-budded cell. Scale bar for all panels is 10

mm. Among these strains at 23°C, no significant differences in Rho1p, GFP-Sec4p or GFP-Sec3p localization were apparent (not shown). Cells were scored for proper protein localization, which is presented in Figure 2.5.11. B) Immunoblots that show Rho1p levels in wild-type (WT; SEY6210), *oshΔ OSH4* (CBY924) and/or *oshΔ osh4-1* (CBY926) cells whether grown at 23°C or shifted to 37°C for 4 h. To demonstrate equivalent loading, the same blot was probed with an antibody against b-tubulin (Tub2p). C) As compared to the wild-type strain (SEY6210), GFP-Sec4p levels are markedly increased in *oshΔ osh4-1* (CBY926) cells grown at 23°C and shifted to 37°C for 4 h, which is consistent with the fluorescence microscopy results in (A). At 23°C, GFP-Sec4p levels were equivalent in both strains tested. To show equal loading, the same blot was probed with an anti-b-tubulin antibody that detects yeast Tub2p. ***This work was performed by Gabriel Alfaro except immunofluorescence and immunoblot of Rho1p which was performed by K.G.K. Please note I generated similar results with GFP-Rho1p (not shown) but there was irregular GFP fluorescence in the vacuole, which was not seen by immunofluorescence.**

Figure 2.5.8: Mutual antagonism of *OSH* and *MSB* function
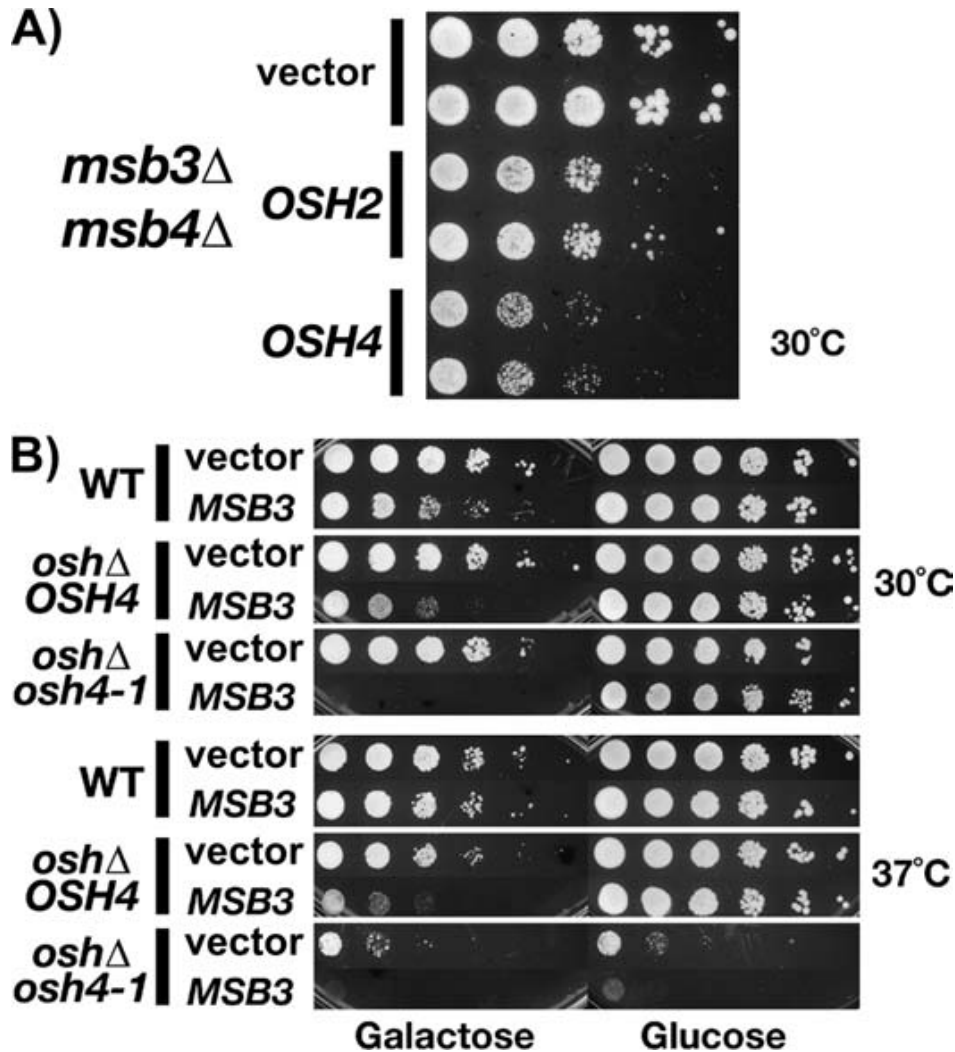
Figure 2.5.8: A) Ten-fold serial dilutions (left to right) of cultures were spotted onto synthetic selective medium and grown at 30°C (4 days) for *msb3Δ msb4Δ* mutant yeast transformed with a multicopy plasmid containing *OSH2* (pCB239), *OSH4* (pCB241) or the vector alone (pRS426). Duplicate independent transformants are shown. Wild-type, *msb3Δ* or *msb4Δ*congenic strains were unaffected by multicopy *OSH2* or *OSH4* plasmids (not shown). B) Ten-fold serial dilutions (left to right) of cultures were spotted onto synthetic selective medium containing either 2% glucose or 2% galactose and incubated at 30 or 37°C. Growth of wild-type (SEY6210), *oshΔ osh4-1* (CBY926)

and *oshΔ OSH4* (CBY924) cells was compared when transformed with a P^{GAL}-*MSB3* (pCB368) or vector control plasmid (pKT10-*GAL*-HA). ***This work was performed by Gabriel Alfaro.**

Figure 2.5.9: Quantitative analysis of *OSH*-dependent polarization of proteins involved in actin organization and/or assembly (complementary to 2.5.3)
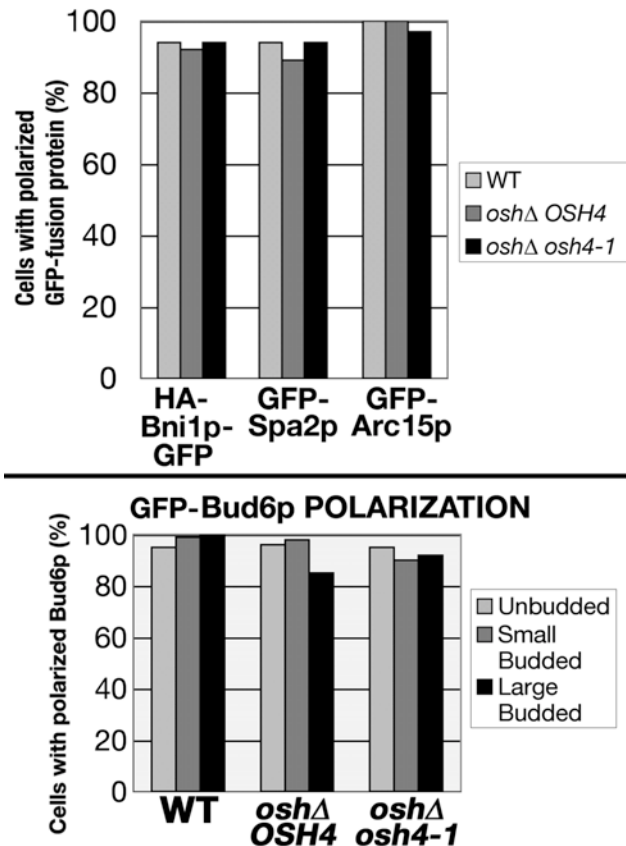
Figure 2.5.9: Top) Polarized localization of GFP-HA-Bni1p, GFP-Spa2p and GFP-Arc15p to either the presumptive bud site in unbudded cells, the bud or bud tip in small-budded cells or the bud neck in large-budded cells was determined in wild-type (SEY6210), *osh∆ OSH4* (CBY924) and *osh∆ osh4-1* (CBY926) cells at 37°C. The number of cells counted for each strain ranged from 85 to 126 for the GFP-HA-Bni1p localization, from 62 to 132 for the GFP-Spa2p localization and from 220 to 429 for the GFP-Arc15p localization. Bottom) Polarized localization of GFP-Bud6p in unbudded,

small-and large-budded cells at 37°C (n > 72 for each morphological class counted).

*This work was performed by Gabriel Alfaro.

Figure 2.5.10: Quantitative analysis of septin polarization and assembly in *OSH* mutants (complementary to 2.5.4)
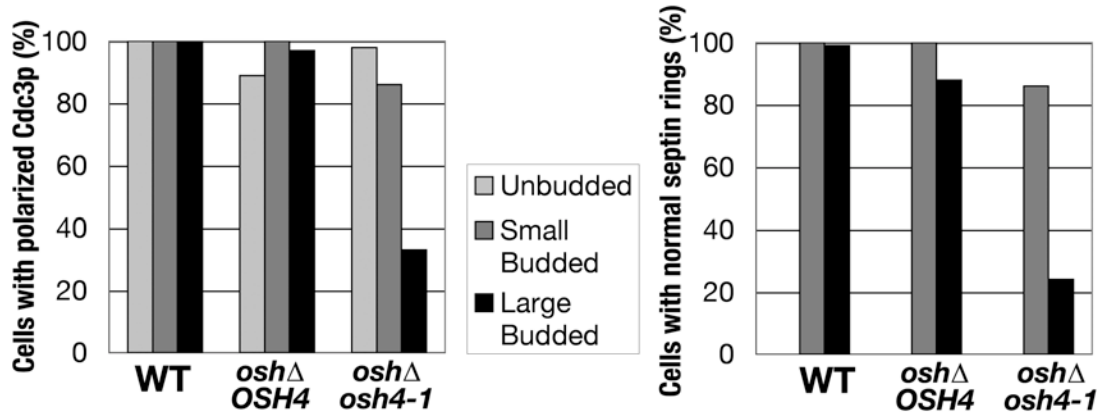
Figure 2.5.10: Left) Septin (GFP-Cdc3p) polarization exclusively to the presumptive bud site was scored in unbudded cells and to the bud neck in small-and large-budded cells in wild-type (SEY6210), *osh*Δ *OSH4* (CBY924) and *osh*Δ *osh4-1* (CBY926) cells at 37°C. The appearance of cortical septin patches at locations other than those observed in wild-type cells was defined as unpolarized. Right) Septin ring assembly in wild-type, *osh*Δ *OSH4* and *osh*Δ *osh4-1* budded cells at 37°C. Defective septin rings included those with fragmented morphology, asymmetric localization around the bud neck and/or irregular accumulations of septins within the rings. Cells counted for both analyses ranged from 260 to 300. ***This work was performed by Gabriel Alfaro.**

Figure 2.5.11: Quantitative analysis of Rho1p, GFP-Sec3p and GFP-Sec4p polarized localization in *OSH* mutants in wild-type (SEY6210), *oshΔ OSH4* (CBY925) and *oshΔ osh4-1* (CBY926) cells (complementary to Figure 2.5.7 A)
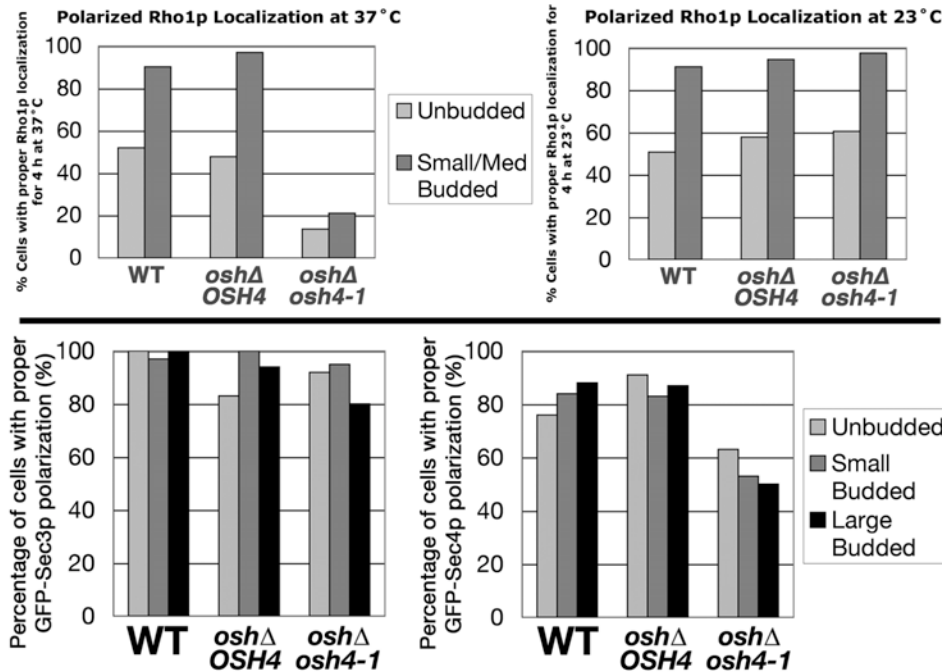
Figure 2.5.11: Rho1p polarized localization to the presumptive bud site in unbudded cells, to sites of polarized growth in small-and medium-budded cells and to the bud neck in large-budded cells after a shift from 23 to 37°C for 4 h (top right) or growth at 23°C (top left). GFP-Sec3p (bottom left) and GFP-Sec4p (bottom right) polarized localization to the presumptive bud site in unbudded cells, to the bud tip in small-budded cells and to the bud neck in large-budded cells, after a shift from 23 to 37°C for 4 h. The number of cells counted for each morphological class ranged from 200 to 308 for the Rho1p localization, from 86 to 137 for the GFP-Sec3p localization and from 178 to 635 for the GFP-Sec4p. For GFP-Sec4p, a cell in which localization was observed in the bud but not restricted to bud tip was not counted as polarized. ***This work was performed by Gabriel Alfaro except the Rho1p counts which are by K.G.K.**

Figure 2.5.12: Cellular defects resulting from perturbations in *OSH* and *MSB* gene dosage.
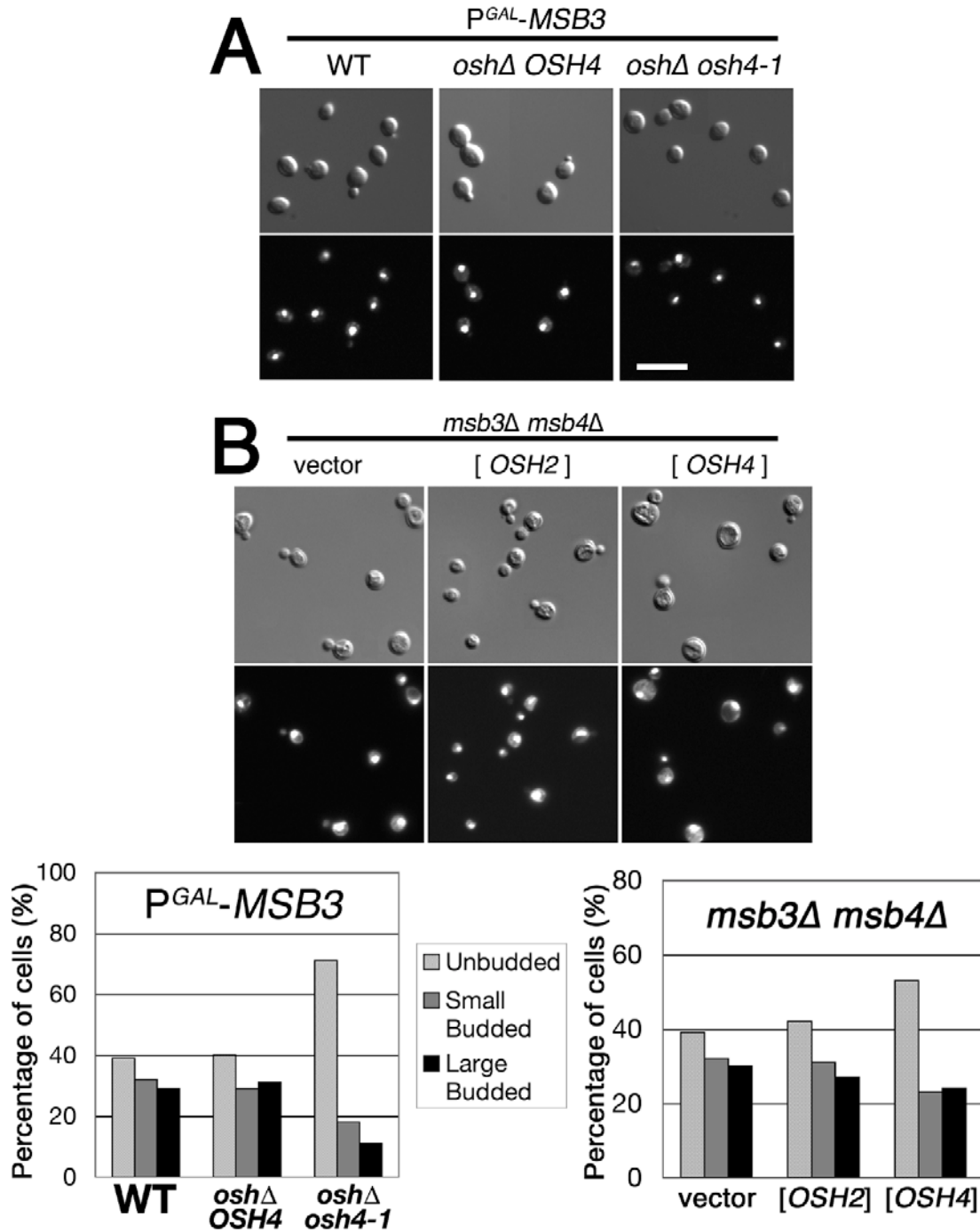
Figure 2.5.12: A) Unbudded cells accumulated in *oshΔ osh4-1* transformants expressing P^{GAL}-*MSB3*. Differential-interference contrast microscopy images (top panels) and corresponding DAPI-stained nuclei (bottom panels) of wild-type (SEY6210), *oshΔ*

osh4-1 (CBY926) and *oshΔ OSH4* (CBY924) cells transformed with the P^{GAL}-*MSB3* (pCB368) plasmid after log-phase cultures were transferred from 2% raffinose-to 2% galactose-containing medium at 30°C for 4 h. The corresponding percentages of unbudded, small-budded and large-budded cells are presented in the left graph. Cells counted for each strain in this analysis ranged from 348 to 755. B) Unbudded cell accumulation in *msb3Δ msb4Δ* cells transformed with multicopy *OSH4*. Differential-interference contrast microscopy (top panels) and corresponding DAPI staining (bottom panels) for *msb3Δ msb4Δ* (CBY1981) log-phase cells transformed with either multicopy *OSH2* (pCB239), *OSH4* (pCB241) or the vector control (pRS426) after growth in synthetic medium at 30°C. Scale bar for all panels is 10 mm. The corresponding percentages of budded and unbudded cells are presented in the right graph. Cells counted for each strain ranged from 189 to 243. In wild-type (BY4742) cells transformed with the multicopy *OSH2*, *OSH4* or the vector alone, no significant differences in the proportion of unbudded and budded were observed (data not shown). ***This work was performed by Gabriel Alfaro.**

Tables

Saccharomyces cerevisiae **strains used table**

Strain	Genotype	Source
BY4742	MATα *his3Δ1 leu2Δ0 lys2Δ0 ura3Δ0*	(Winzeler et al., 1999a)
CBY924	SEY6210 *osh1Δ::kanMX4 osh2Δ::kanMX4 osh3Δ::LYS2 osh4Δ::HIS3 osh5Δ::LEU2 osh6Δ::LEU2 osh7Δ::HIS3* [pCB254]	(Beh and Rine, 2004)
CBY926	SEY6210 *osh1Δ::kanMX4 osh2Δ::kanMX4 osh3Δ::LYS2 osh4Δ::HIS3 osh5Δ::LEU2 osh6Δ::LEU2 osh7Δ::HIS3* [pCB255]	(Beh and Rine, 2004)
CBY1345	MATα *his4-619 lys2-801 ura3 sec3-2*	
CBY1474	MATα *his4-619 lys2-801 ura3 sec5-24*	
CBY1480	*MATa ura3 sec4-2*	
CBY1981	*BY4742 LYS2 msb3Δ::kanMX4 msb4Δ::kanMX4*	
DDY1300	*MATa ura3-52 leu2-3,112 his3Δ200 lys2-801 CDC42:LEU2*	(Kozminski et al., 2000)
DDY1326	*MATa ura3-52 leu2-3,112 his3Δ200 lys2-801 cdc42-118:LEU2*	(Kozminski et al., 2000)
DDY1336	*MATa ura3-52 leu2-3,112 his3Δ200 lys2-801 cdc42-123:LEU2*	(Kozminski et al., 2000)
DDY1344	*MATa ura3-52 leu2-3,112 his3Δ200 lys2-801 cdc42-129:LEU2*	(Kozminski et al., 2000)
DDY1493	*MATa act1-159:HIS3 tub2-201 his3Δ200 leu2-3,112 ura3-52 can1Δ*	(Belmont and Drubin., 1998)
DDY1495	*MATa ACT1:HIS3 tub2-201 his3Δ200 leu2-3,112 ura3-52 can1Δ*	(Belmont and Drubin., 1998)
DDY1544	*MATa act1-157:HIS3 tub2-201 his3Δ200 leu2-3,112 ura3-52 can1Δ*	(Belmont et al., 1999)
DDY1545	*MATa act1-158:HIS3 tub2-201 his3Δ200 leu2-3,112 ura3-52 can1Δ*	(Belmont et al., 1999)
DDY2752	*MATα ura3-52 his3Δ200 lys2-801am leu2-3,112 ARC15-GFP::HIS3*	(Kaksonen et al., 2003)
HAB821	SEY6210 *kes1/osh4Δ::HIS3*	(Jiang et al., 1994)
HAB835	SEY6210 *swh1/osh1Δ::URA3*	(Jiang et al., 1994)
JRY4130	*MATα his4-619 ura3052 sec18*	(Beh and Rine, 2004)
JRY6200	SEY6210 *osh7Δ::HIS3*	(Beh et al., 2001)
JRY6201	SEY6210 *osh6Δ::LEU2*	(Beh et al., 2001)
JRY6202	SEY6210 *osh3Δ::LYS2*	(Beh et al., 2001)
JRY6203	SEY6210 *osh2Δ::URA3*	(Beh et al., 2001)
JRY6206	SEY6210 *osh5Δ::LEU2*	(Beh et al., 2001)
JRY6313	SEY6210 *osh1Δ::kanMX4*	(Beh et al., 2001)
JRY6326	SEY6210 *TRP1::P^{MET3}-OSH2 osh1Δ::kanMX4 osh2Δ::URA3 osh3Δ::LYS2 osh4Δ::HIS3 osh5Δ::LEU2 osh6Δ::LEU2 osh7Δ::HIS3*	(Beh et al., 2001)

KKY37	*MAT*a *rho1-104ᵗˢ leu2-3, 112 ura3-52 lys2-801am*	(Kozminski et al., 2003)
NY17	*MAT*a *sec6-4ᵗˢ ura3-52*	(Novick et al., 1980)
RSY255	*MATα ura3-52 leu2-3,112*	(Novick and Schekman, 1979)
SEY2102	*MATα his4-519 leu2-3,112 ura3-52 bgl2::URA3*	(Klebl and Tanner, 1989)
SEY6210	*MATα ura3-52 his3Δ200 lys2-801am leu2-3,112 trp1Δ901 suc2Δ9*	(Robinson et al., 1988)
Y1240	MAT*α his3Δ leu2Δ lys2Δ ura3Δ*	(Evangelista et al., 2002)
Y4133	MAT*α his3Δ leu2Δ lys2Δ ura3Δ bnr1Δ::kanMX6 bni1-11:URA3*	(Evangelista et al., 2002)
Y4135	MAT*α his3Δ leu2Δ lys2Δ ura3Δ bnr1Δ::kanMX6 bni1-12:URA3*	(Evangelista et al., 2002)

All strains were created as part of this study unless referenced otherwise

Plasmids used Table

Plasmid	Description	Source
P1955	P^{GAL}-HA-*BNI1*-GFP *CEN URA3*	C. Boone (University of Toronto, Toronto, Canada)
pAGX1-BNR1	P^{ACT1}-*BNR1*-GFP *CEN URA3*	C. Tanaka (University of Hokkaido, Sapporo, Japan)
pCB236	*OSH7 2μ URA3*	
pCB237	*OSH6 2μ URA3*	
pCB238	*OSH3 2μ URA3*	
pCB239	*OSH2 2μ URA3*	
pCB240	*OSH1 2μ URA3*	
pCB241	*OSH4 2μ URA3*	
pCB242	*OSH5 2μ URA3*	
pCB254	*OSH4 CEN TRP1*	(Beh and Rine, 2004)
pCB255	*osh4-1 CEN TRP1*	(Beh and Rine, 2004)
pCB368	P^{GAL}-HA-*MSB3 2μ URA3*	
pCB494	*SPA2*GFP *2μ URA3*	
pGFP-RHO1	GFP-*RHO1 CEN URA3*	(Marelli et al., 2004)
pKK1062	*OSH4 CEN URA3*	
pKK1821	*OSH4 2μ URA3*	
pKK1825	*OSH4 2μ URA3*	(Kozminski et al., 2003)
pKK1826	*ARC15*-GFP *CEN URA3*	
pKT10-GAL-HA	P^{GAL}-HA *2μ URA3*	(Misu et al., 2003)
pM-2	*CDC10*-GFP *CEN URA3*	(Iwase and Toh-e. 2001)
pM-4	*CDC12*-GFP *CEN URA3*	(Iwase and Toh-e. 2001)
pNB810	*SEC3*-GFP *CEN URA3*	(Finger et al., 1998)
pRB2190	P^{ACT1}-*BUD6*-GFP *CEN URA3*	(Amberg et al., 1997)
pRC2098	GFP-*SEC4 CEN URA3*	(Calero et al., 2003)
pRS316-CDC3-GFP	*CDC3*-GFP *CEN URA3*	(Caviston et al. 2003)
pRS416Spa2GFP	*SPA2*-GFP *CEN URA3*	(Arkowitz and Lowe. 1997)
pRS426	*2μ URA3*	(Sikorski and Hieter. 1989)
YCplac33	*CEN URA3*	(Gietz and Sugino. 1988)
YEplac195	*2μ URA3*	(Gietz and Sugino. 1988)

Unless otherwise referenced, all plasmids were created as part of this study.

2.6 Reference List

Adamo, J.E., Moskow, J.J., Gladfelter, A.S., Viterbo, D., Lew, D.J., and Brennwald, P.J. (2001). Yeast Cdc42 functions at a late step in exocytosis, specifically during polarized growth of the emerging bud. J Cell Biol *155*, 581-592.

Adams, A.E., Johnson, D.I., Longnecker, R.M., Sloat, B.F., and Pringle, J.R. (1990). CDC42 and CDC43, two additional genes involved in budding and the establishment of cell polarity in the yeast Saccharomyces cerevisiae. J Cell Biol *111*, 131-142.

Alphey, L., Jimenez, J., and Glover, D. (1998). A Drosophila homologue of oxysterol binding protein (OSBP)--implications for the role of OSBP. Biochim Biophys Acta *1395*, 159-164.

Amberg, D.C., Zahner, J.E., Mulholland, J.W., Pringle, J.R., and Botstein, D. (1997). Aip3p/Bud6p, a yeast actin-interacting protein that is involved in morphogenesis and the selection of bipolar budding sites. Mol Biol Cell *8*, 729-753.

Arkowitz, R.A., and Lowe, N. (1997). A small conserved domain in the yeast Spa2p is necessary and sufficient for its polarized localization. J Cell Biol *138*, 17-36.

Ayscough, K.R., Eby, J.J., Lila, T., Dewar, H., Kozminski, K.G., and Drubin, D.G. (1999). Sla1p is a functionally modular component of the yeast cortical actin cytoskeleton required for correct localization of both Rho1p-GTPase and Sla2p, a protein with talin homology. Mol Biol Cell *10*, 1061-1075.

Ayscough, K.R., Stryker, J., Pokala, N., Sanders, M., Crews, P., and Drubin, D.G. (1997). High rates of actin filament turnover in budding yeast and roles for actin in establishment and maintenance of cell polarity revealed using the actin inhibitor latrunculin-A. J Cell Biol *137*, 399-416.

Bagnat, M., and Simons, K. (2002). Cell surface polarization during yeast mating. Proc Natl Acad Sci U S A *99*, 14183-14188.

Beh, C.T., Cool, L., Phillips, J., and Rine, J. (2001). Overlapping functions of the yeast oxysterol-binding protein homologues. Genetics *157*, 1117-1140.

Beh, C.T., and Rine, J. (2004). A role for yeast oxysterol-binding protein homologs in endocytosis and in the maintenance of intracellular sterol-lipid distribution. J Cell Sci *117*, 2983-2996.

Belmont, L.D., and Drubin, D.G. (1998). The yeast V159N actin mutant reveals roles for actin dynamics in vivo. J Cell Biol *142*, 1289-1299.

Belmont, L.D., Patterson, G.M., and Drubin, D.G. (1999). New actin mutants allow further characterization of the nucleotide binding cleft and drug binding sites. J Cell Sci *112 (Pt 9)*, 1325-1336.

Bi, E., Chiavetta, J.B., Chen, H., Chen, G.C., Chan, C.S., and Pringle, J.R. (2000). Identification of novel, evolutionarily conserved Cdc42p-interacting proteins and of redundant pathways linking Cdc24p and Cdc42p to actin polarization in yeast. Mol Biol Cell *11*, 773-793.

Brown, M.C., Perrotta, J.A., and Turner, C.E. (1996). Identification of LIM3 as the principal determinant of paxillin focal adhesion localization and characterization of a novel motif on paxillin directing vinculin and focal adhesion kinase binding. J Cell Biol *135*, 1109-1123.

Calero, M., Chen, C.Z., Zhu, W., Winand, N., Havas, K.A., Gilbert, P.M., Burd, C.G., and Collins, R.N. (2003). Dual prenylation is required for Rab protein localization and function. Mol Biol Cell *14*, 1852-1867.

Carland, F.M., Fujioka, S., Takatsuto, S., Yoshida, S., and Nelson, T. (2002). The identification of CVP1 reveals a role for sterols in vascular patterning. Plant Cell *14*, 2045-2058.

Carlson, M., and Botstein, D. (1982). Two differentially regulated mRNAs with different 5' ends encode secreted with intracellular forms of yeast invertase. Cell *28*, 145-154.

Caviston, J.P., Longtine, M., Pringle, J.R., and Bi, E. (2003). The role of Cdc42p GTPase-activating proteins in assembly of the septin ring in yeast. Mol Biol Cell *14*, 4051-4066.

del Pozo, M.A., Price, L.S., Alderson, N.B., Ren, X.D., and Schwartz, M.A. (2000). Adhesion to the extracellular matrix regulates the coupling of the small GTPase Rac to its effector PAK. EMBO J *19*, 2008-2014.

Desrivieres, S., Cooke, F.T., Parker, P.J., and Hall, M.N. (1998). MSS4, a phosphatidylinositol-4-phosphate 5-kinase required for organization of the actin cytoskeleton in Saccharomyces cerevisiae. J Biol Chem *273*, 15787-15793.

Diederich, W., Orso, E., Drobnik, W., and Schmitz, G. (2001). Apolipoprotein AI and HDL(3) inhibit spreading of primary human monocytes through a mechanism that involves cholesterol depletion and regulation of CDC42. Atherosclerosis *159*, 313-324.

Dong, Y., Pruyne, D., and Bretscher, A. (2003). Formin-dependent actin assembly is regulated by distinct modes of Rho signaling in yeast. J Cell Biol *161*, 1081-1092.

Drubin, D.G., and Nelson, W.J. (1996). Origins of cell polarity. Cell *84*, 335-344.

Etienne-Manneville, S., and Hall, A. (2002). Rho GTPases in cell biology. Nature *420*, 629-635.

Evangelista, M., Blundell, K., Longtine, M.S., Chow, C.J., Adames, N., Pringle, J.R., Peter, M., and Boone, C. (1997). Bni1p, a yeast formin linking cdc42p and the actin cytoskeleton during polarized morphogenesis. Science *276*, 118-122.

Evangelista, M., Pruyne, D., Amberg, D.C., Boone, C., and Bretscher, A. (2002). Formins direct Arp2/3-independent actin filament assembly to polarize cell growth in yeast. Nat Cell Biol *4*, 32-41.

Fang, M., Kearns, B.G., Gedvilaite, A., Kagiwada, S., Kearns, M., Fung, M.K., and Bankaitis, V.A. (1996). Kes1p shares homology with human oxysterol binding protein and participates in a novel regulatory pathway for yeast Golgi-derived transport vesicle biogenesis. EMBO J *15*, 6447-6459.

Finger, F.P., Hughes, T.E., and Novick, P. (1998). Sec3p is a spatial landmark for polarized secretion in budding yeast. Cell *92*, 559-571.

Ford, S.K., and Pringle, J.R. (1991). Cellular morphogenesis in the Saccharomyces cerevisiae cell cycle: localization of the CDC11 gene product and the timing of events at the budding site. Dev Genet *12*, 281-292.

Fujiwara, T., Tanaka, K., Mino, A., Kikyo, M., Takahashi, K., Shimizu, K., and Takai, Y. (1998). Rho1p-Bni1p-Spa2p interactions: implication in localization of Bni1p at the bud site and regulation of the actin cytoskeleton in Saccharomyces cerevisiae. Mol Biol Cell *9*, 1221-1233.

Gao, X.D., Albert, S., Tcheperegine, S.E., Burd, C.G., Gallwitz, D., and Bi, E. (2003). The GAP activity of Msb3p and Msb4p for the Rab GTPase Sec4p is required for efficient exocytosis and actin organization. J Cell Biol *162*, 635-646.

Gao, X.D., Caviston, J.P., Tcheperegine, S.E., and Bi, E. (2004). Pxl1p, a paxillin-like protein in Saccharomyces cerevisiae, may coordinate Cdc42p and Rho1p functions during polarized growth. Mol Biol Cell *15*, 3977-3985.

Gavin, A.C., Bosche, M., Krause, R., Grandi, P., Marzioch, M., Bauer, A., Schultz, J., Rick, J.M., Michon, A.M., Cruciat, C.M.*, et al.* (2002). Functional organization of the yeast proteome by systematic analysis of protein complexes. Nature *415*, 141-147.

Gietz, R.D., and Sugino, A. (1988). New yeast-Escherichia coli shuttle vectors constructed with in vitro mutagenized yeast genes lacking six-base pair restriction sites. Gene *74*, 527-534.

Gladfelter, A.S., Bose, I., Zyla, T.R., Bardes, E.S., and Lew, D.J. (2002). Septin ring assembly involves cycles of GTP loading and hydrolysis by Cdc42p. J Cell Biol *156*, 315-326.

Godi, A., Di Campli, A., Konstantakopoulos, A., Di Tullio, G., Alessi, D.R., Kular, G.S., Daniele, T., Marra, P., Lucocq, J.M., and De Matteis, M.A. (2004). FAPPs control Golgi-

to-cell-surface membrane traffic by binding to ARF and PtdIns(4)P. Nat Cell Biol *6*, 393-404.

Gomez-Mouton, C., Abad, J.L., Mira, E., Lacalle, R.A., Gallardo, E., Jimenez-Baranda, S., Illa, I., Bernad, A., Manes, S., and Martinez, A.C. (2001). Segregation of leading-edge and uropod components into specific lipid rafts during T cell polarization. Proc Natl Acad Sci U S A *98*, 9642-9647.

Goud, B., Salminen, A., Walworth, N.C., and Novick, P.J. (1988). A GTP-binding protein required for secretion rapidly associates with secretory vesicles and the plasma membrane in yeast. Cell *53*, 753-768.

Graham, T.R., and Emr, S.D. (1991). Compartmental organization of Golgi-specific protein modification and vacuolar protein sorting events defined in a yeast sec18 (NSF) mutant. J Cell Biol *114*, 207-218.

Guan, J.L. (2004). Cell biology. Integrins, rafts, Rac, and Rho. Science *303*, 773-774.

Gulli, M.P., and Peter, M. (2001). Temporal and spatial regulation of Rho-type guanine-nucleotide exchange factors: the yeast perspective. Genes Dev *15*, 365-379.

Guo, W., Roth, D., Walch-Solimena, C., and Novick, P. (1999). The exocyst is an effector for Sec4p, targeting secretory vesicles to sites of exocytosis. EMBO J *18*, 1071-1080.

Guo, W., Tamanoi, F., and Novick, P. (2001). Spatial regulation of the exocyst complex by Rho1 GTPase. Nat Cell Biol *3*, 353-360.

Harsay, E., and Bretscher, A. (1995). Parallel secretory pathways to the cell surface in yeast. J Cell Biol *131*, 297-310.

Hazbun, T.R., Malmstrom, L., Anderson, S., Graczyk, B.J., Fox, B., Riffle, M., Sundin, B.A., Aranda, J.D., McDonald, W.H., Chiu, C.H.*, et al.* (2003). Assigning function to yeast proteins by integration of technologies. Mol Cell *12*, 1353-1365.

Higgs, H.N., and Pollard, T.D. (2001). Regulation of actin filament network formation through ARP2/3 complex: activation by a diverse array of proteins. Annu Rev Biochem *70*, 649-676.

Ho, Y., Gruhler, A., Heilbut, A., Bader, G.D., Moore, L., Adams, S.L., Millar, A., Taylor, P., Bennett, K., Boutilier, K.*, et al.* (2002). Systematic identification of protein complexes in Saccharomyces cerevisiae by mass spectrometry. Nature *415*, 180-183.

Hofmann, C., Shepelev, M., and Chernoff, J. (2004). The genetics of Pak. J Cell Sci *117*, 4343-4354.

Hsu, S.C., TerBush, D., Abraham, M., and Guo, W. (2004). The exocyst complex in polarized exocytosis. Int Rev Cytol *233*, 243-265.

Im, Y.J., Raychaudhuri, S., Prinz, W.A., and Hurley, J.H. (2005). Structural mechanism for sterol sensing and transport by OSBP-related proteins. Nature *437*, 154-158.

Imamura, H., Tanaka, K., Hihara, T., Umikawa, M., Kamei, T., Takahashi, K., Sasaki, T., and Takai, Y. (1997). Bni1p and Bnr1p: downstream targets of the Rho family small G-proteins which interact with profilin and regulate actin cytoskeleton in Saccharomyces cerevisiae. EMBO J *16*, 2745-2755.

Irazoqui, J.E., Howell, A.S., Theesfeld, C.L., and Lew, D.J. (2005). Opposing roles for actin in Cdc42p polarization. Mol Biol Cell *16*, 1296-1304.

Iwase, M., and Toh-e, A. (2001). Nis1 encoded by YNL078W: a new neck protein of Saccharomyces cerevisiae. Genes Genet Syst *76*, 335-343.

Jaquenoud, M., and Peter, M. (2000). Gic2p may link activated Cdc42p to components involved in actin polarization, including Bni1p and Bud6p (Aip3p). Mol Cell Biol *20*, 6244-6258.

Jiang, B., Brown, J.L., Sheraton, J., Fortin, N., and Bussey, H. (1994). A new family of yeast genes implicated in ergosterol synthesis is related to the human oxysterol binding protein. Yeast *10*, 341-353.

Johansson, M., Lehto, M., Tanhuanpaa, K., Cover, T.L., and Olkkonen, V.M. (2005). The oxysterol-binding protein homologue ORP1L interacts with Rab7 and alters functional properties of late endocytic compartments. Mol Biol Cell *16*, 5480-5492.

Kadota, J., Yamamoto, T., Yoshiuchi, S., Bi, E., and Tanaka, K. (2004). Septin ring assembly requires concerted action of polarisome components, a PAK kinase Cla4p, and the actin cytoskeleton in Saccharomyces cerevisiae. Mol Biol Cell *15*, 5329-5345.

Kaksonen, M., Sun, Y., and Drubin, D.G. (2003). A pathway for association of receptors, adaptors, and actin during endocytic internalization. Cell *115*, 475-487.

Kandutsch, A.A., and Shown, E.P. (1981). Assay of oxysterol-binding protein in a mouse fibroblast, cell-free system. Dissociation constant and other properties of the system. J Biol Chem *256*, 13068-13073.

Klebl, F., and Tanner, W. (1989). Molecular cloning of a cell wall exo-beta-1,3-glucanase from Saccharomyces cerevisiae. J Bacteriol *171*, 6259-6264.

Kozminski, K.G., Beven, L., Angerman, E., Tong, A.H., Boone, C., and Park, H.O. (2003). Interaction between a Ras and a Rho GTPase couples selection of a growth site to the development of cell polarity in yeast. Mol Biol Cell *14*, 4958-4970.

Kozminski, K.G., Chen, A.J., Rodal, A.A., and Drubin, D.G. (2000). Functions and functional domains of the GTPase Cdc42p. Mol Biol Cell *11*, 339-354.

Kvam, E., and Goldfarb, D.S. (2004). Nvj1p is the outer-nuclear-membrane receptor for oxysterol-binding protein homolog Osh1p in Saccharomyces cerevisiae. J Cell Sci *117*, 4959-4968.

Levine, T. (2005). A new way for sterols to walk on water. Mol Cell *19*, 722-723.

Levine, T.P., and Munro, S. (2001). Dual targeting of Osh1p, a yeast homologue of oxysterol-binding protein, to both the Golgi and the nucleus-vacuole junction. Mol Biol Cell *12*, 1633-1644.

Li, X., Rivas, M.P., Fang, M., Marchena, J., Mehrotra, B., Chaudhary, A., Feng, L., Prestwich, G.D., and Bankaitis, V.A. (2002). Analysis of oxysterol binding protein homologue Kes1p function in regulation of Sec14p-dependent protein transport from the yeast Golgi complex. J Cell Biol *157*, 63-77.

Loewen, C.J., Roy, A., and Levine, T.P. (2003). A conserved ER targeting motif in three families of lipid binding proteins and in Opi1p binds VAP. EMBO J *22*, 2025-2035.

Longtine, M.S., and Bi, E. (2003). Regulation of septin organization and function in yeast. Trends Cell Biol *13*, 403-409.

Mackin, N.A., Sousou, T.J., and Erdman, S.E. (2004). The PXL1 gene of Saccharomyces cerevisiae encodes a paxillin-like protein functioning in polarized cell growth. Mol Biol Cell *15*, 1904-1917.

Manes, S., Mira, E., Gomez-Mouton, C., Lacalle, R.A., Keller, P., Labrador, J.P., and Martinez, A.C. (1999). Membrane raft microdomains mediate front-rear polarity in migrating cells. EMBO J *18*, 6211-6220.

Marelli, M., Smith, J.J., Jung, S., Yi, E., Nesvizhskii, A.I., Christmas, R.H., Saleem, R.A., Tam, Y.Y., Fagarasanu, A., Goodlett, D.R.*, et al.* (2004). Quantitative mass spectrometry reveals a role for the GTPase Rho1p in actin organization on the peroxisome membrane. J Cell Biol *167*, 1099-1112.

Martin, S.W., and Konopka, J.B. (2004). Lipid raft polarization contributes to hyphal growth in Candida albicans. Eukaryot Cell *3*, 675-684.

Matheos, D., Metodiev, M., Muller, E., Stone, D., and Rose, M.D. (2004). Pheromone-induced polarization is dependent on the Fus3p MAPK acting through the formin Bni1p. J Cell Biol *165*, 99-109.

Merlot, S., and Firtel, R.A. (2003). Leading the way: Directional sensing through phosphatidylinositol 3-kinase and other signaling pathways. J Cell Sci *116*, 3471-3478.

Misu, K., Fujimura-Kamada, K., Ueda, T., Nakano, A., Katoh, H., and Tanaka, K. (2003). Cdc50p, a conserved endosomal membrane protein, controls polarized growth in Saccharomyces cerevisiae. Mol Biol Cell *14*, 730-747.

Mondesert, G., Clarke, D.J., and Reed, S.I. (1997). Identification of genes controlling growth polarity in the budding yeast Saccharomyces cerevisiae: a possible role of N-glycosylation and involvement of the exocyst complex. Genetics *147*, 421-434.

Munn, A.L., Heese-Peck, A., Stevenson, B.J., Pichler, H., and Riezman, H. (1999). Specific sterols required for the internalization step of endocytosis in yeast. Mol Biol Cell *10*, 3943-3957.

Munn, A.L., and Riezman, H. (1994). Endocytosis is required for the growth of vacuolar H(+)-ATPase-defective yeast: identification of six new END genes. J Cell Biol *127*, 373-386.

Nicholson-Dykstra, S., Higgs, H.N., and Harris, E.S. (2005). Actin dynamics: growth from dendritic branches. Curr Biol *15*, R346-357.

Novick, P., Field, C., and Schekman, R. (1980). Identification of 23 complementation groups required for post-translational events in the yeast secretory pathway. Cell *21*, 205-215.

Novick, P., and Schekman, R. (1979). Secretion and cell-surface growth are blocked in a temperature-sensitive mutant of Saccharomyces cerevisiae. Proc Natl Acad Sci U S A *76*, 1858-1862.

Novick, P., and Schekman, R. (1983). Export of major cell surface proteins is blocked in yeast secretory mutants. J Cell Biol *96*, 541-547.

Olkkonen, V.M., and Levine, T.P. (2004). Oxysterol binding proteins: in more than one place at one time? Biochem Cell Biol *82*, 87-98.

Ozaki-Kuroda, K., Yamamoto, Y., Nohara, H., Kinoshita, M., Fujiwara, T., Irie, K., and Takai, Y. (2001). Dynamic localization and function of Bni1p at the sites of directed growth in Saccharomyces cerevisiae. Mol Cell Biol *21*, 827-839.

Palazzo, A.F., Eng, C.H., Schlaepfer, D.D., Marcantonio, E.E., and Gundersen, G.G. (2004). Localized stabilization of microtubules by integrin- and FAK-facilitated Rho signaling. Science *303*, 836-839.

Palmgren, S., Vartiainen, M., and Lappalainen, P. (2002). Twinfilin, a molecular mailman for actin monomers. J Cell Sci *115*, 881-886.

Pierini, L.M., Eddy, R.J., Fuortes, M., Seveau, S., Casulo, C., and Maxfield, F.R. (2003). Membrane lipid organization is critical for human neutrophil polarization. J Biol Chem *278*, 10831-10841.

Pruyne, D., Gao, L., Bi, E., and Bretscher, A. (2004a). Stable and dynamic axes of polarity use distinct formin isoforms in budding yeast. Mol Biol Cell *15*, 4971-4989.

Pruyne, D., Legesse-Miller, A., Gao, L., Dong, Y., and Bretscher, A. (2004b). Mechanisms of polarized growth and organelle segregation in yeast. Annu Rev Cell Dev Biol *20*, 559-591.

Ramirez, R.M., Ishida-Schick, T., Krilowicz, B.L., Leish, B.A., and Atkinson, K.D. (1983). Plasma membrane expansion terminates in Saccharomyces cerevisiae secretion-defective mutants while phospholipid synthesis continues. J Bacteriol *154*, 1276-1283.

Raychaudhuri, S., Im, Y.J., Hurley, J.H., and Prinz, W.A. (2006). Nonvesicular sterol movement from plasma membrane to ER requires oxysterol-binding protein-related proteins and phosphoinositides. J Cell Biol *173*, 107-119.

Ridgway, N.D., Dawson, P.A., Ho, Y.K., Brown, M.S., and Goldstein, J.L. (1992). Translocation of oxysterol binding protein to Golgi apparatus triggered by ligand binding. J Cell Biol *116*, 307-319.

Roberts, C.J., Raymond, C.K., Yamashiro, C.T., and Stevens, T.H. (1991). Methods for studying the yeast vacuole. Methods Enzymol *194*, 644-661.

Robinson, J.S., Klionsky, D.J., Banta, L.M., and Emr, S.D. (1988). Protein sorting in Saccharomyces cerevisiae: isolation of mutants defective in the delivery and processing of multiple vacuolar hydrolases. Mol Cell Biol *8*, 4936-4948.

Rodal, A.A., Kozubowski, L., Goode, B.L., Drubin, D.G., and Hartwig, J.H. (2005). Actin and septin ultrastructures at the budding yeast cell cortex. Mol Biol Cell *16*, 372-384.

Sagot, I., Klee, S.K., and Pellman, D. (2002). Yeast formins regulate cell polarity by controlling the assembly of actin cables. Nat Cell Biol *4*, 42-50.

Schiestl, R.H., and Gietz, R.D. (1989). High efficiency transformation of intact yeast cells using single stranded nucleic acids as a carrier. Curr Genet *16*, 339-346.

Schmalix, W.A., and Bandlow, W. (1994). SWH1 from yeast encodes a candidate nuclear factor containing ankyrin repeats and showing homology to mammalian oxysterol-binding protein. Biochim Biophys Acta *1219*, 205-210.

Servant, G., Weiner, O.D., Herzmark, P., Balla, T., Sedat, J.W., and Bourne, H.R. (2000). Polarization of chemoattractant receptor signaling during neutrophil chemotaxis. Science *287*, 1037-1040.

Sheu, Y.J., Barral, Y., and Snyder, M. (2000). Polarized growth controls cell shape and bipolar bud site selection in Saccharomyces cerevisiae. Mol Cell Biol *20*, 5235-5247.

Sheu, Y.J., Santos, B., Fortin, N., Costigan, C., and Snyder, M. (1998). Spa2p interacts with cell polarity proteins and signaling components involved in yeast cell morphogenesis. Mol Cell Biol *18*, 4053-4069.

Sikorski, R.S., and Hieter, P. (1989). A system of shuttle vectors and yeast host strains designed for efficient manipulation of DNA in Saccharomyces cerevisiae. Genetics *122*, 19-27.

Sugawara, K., Morita, K., Ueno, N., and Shibuya, H. (2001). BIP, a BRAM-interacting protein involved in TGF-beta signalling, regulates body length in Caenorhabditis elegans. Genes Cells *6*, 599-606.

Taylor, F.R., and Kandutsch, A.A. (1985). Oxysterol binding protein. Chem Phys Lipids *38*, 187-194.

TerBush, D.R., Maurice, T., Roth, D., and Novick, P. (1996). The Exocyst is a multiprotein complex required for exocytosis in Saccharomyces cerevisiae. EMBO J *15*, 6483-6494.

Tinkelenberg, A.H., Liu, Y., Alcantara, F., Khan, S., Guo, Z., Bard, M., and Sturley, S.L. (2000). Mutations in yeast ARV1 alter intracellular sterol distribution and are complemented by human ARV1. J Biol Chem *275*, 40667-40670.

Turner, C.E. (2000). Paxillin interactions. J Cell Sci *113 Pt 23*, 4139-4140.

Uetz, P., Giot, L., Cagney, G., Mansfield, T.A., Judson, R.S., Knight, J.R., Lockshon, D., Narayan, V., Srinivasan, M., Pochart, P.*, et al.* (2000). A comprehensive analysis of protein-protein interactions in Saccharomyces cerevisiae. Nature *403*, 623-627.

Ungermann, C., Nichols, B.J., Pelham, H.R., and Wickner, W. (1998). A vacuolar v-t-SNARE complex, the predominant form in vivo and on isolated vacuoles, is disassembled and activated for docking and fusion. J Cell Biol *140*, 61-69.

Valdez-Taubas, J., and Pelham, H.R. (2003). Slow diffusion of proteins in the yeast plasma membrane allows polarity to be maintained by endocytic cycling. Curr Biol *13*, 1636-1640.

Van Aelst, L., and Symons, M. (2002). Role of Rho family GTPases in epithelial morphogenesis. Genes Dev *16*, 1032-1054.

Vasanji, A., Ghosh, P.K., Graham, L.M., Eppell, S.J., and Fox, P.L. (2004). Polarization of plasma membrane microviscosity during endothelial cell migration. Dev Cell *6*, 29-41.

Versele, M., and Thorner, J. (2004). Septin collar formation in budding yeast requires GTP binding and direct phosphorylation by the PAK, Cla4. J Cell Biol *164*, 701-715.

Wach, A., Brachat, A., Pohlmann, R., and Philippsen, P. (1994). New heterologous modules for classical or PCR-based gene disruptions in Saccharomyces cerevisiae. Yeast *10*, 1793-1808.

Wachtler, V., Rajagopalan, S., and Balasubramanian, M.K. (2003). Sterol-rich plasma membrane domains in the fission yeast Schizosaccharomyces pombe. J Cell Sci *116*, 867-874.

Wang, P., Zhang, Y., Li, H., Chieu, H.K., Munn, A.L., and Yang, H. (2005a). AAA ATPases regulate membrane association of yeast oxysterol binding proteins and sterol metabolism. EMBO J *24*, 2989-2999.

Wang, P.Y., Weng, J., and Anderson, R.G. (2005b). OSBP is a cholesterol-regulated scaffolding protein in control of ERK 1/2 activation. Science *307*, 1472-1476.

Weiner, O.D., Neilsen, P.O., Prestwich, G.D., Kirschner, M.W., Cantley, L.C., and Bourne, H.R. (2002). A PtdInsP(3)- and Rho GTPase-mediated positive feedback loop regulates neutrophil polarity. Nat Cell Biol *4*, 509-513.

Welch, M.D., and Mullins, R.D. (2002). Cellular control of actin nucleation. Annu Rev Cell Dev Biol *18*, 247-288.

Wennerberg, K., Rossman, K.L., and Der, C.J. (2005). The Ras superfamily at a glance. J Cell Sci *118*, 843-846.

Wild, A.C., Yu, J.W., Lemmon, M.A., and Blumer, K.J. (2004). The p21-activated protein kinase-related kinase Cla4 is a coincidence detector of signaling by Cdc42 and phosphatidylinositol 4-phosphate. J Biol Chem *279*, 17101-17110.

Willemsen, V., Friml, J., Grebe, M., van den Toorn, A., Palme, K., and Scheres, B. (2003). Cell polarity and PIN protein positioning in Arabidopsis require STEROL METHYLTRANSFERASE1 function. Plant Cell *15*, 612-625.

Winter, D., Podtelejnikov, A.V., Mann, M., and Li, R. (1997). The complex containing actin-related proteins Arp2 and Arp3 is required for the motility and integrity of yeast actin patches. Curr Biol *7*, 519-529.

Winzeler, E.A., Shoemaker, D.D., Astromoff, A., Liang, H., Anderson, K., Andre, B., Bangham, R., Benito, R., Boeke, J.D., Bussey, H.*, et al.* (1999a). Functional characterization of the S. cerevisiae genome by gene deletion and parallel analysis. Science *285*, 901-906.

Winzeler, E.A., Shoemaker, D.D., Astromoff, A., Liang, H., Anderson, K., Andre, B., Bangham, R., Benito, R., Boeke, J.D., Bussey, H.*, et al.* (1999b). Functional characterization of the S. cerevisiae genome by gene deletion and parallel analysis. Science *285*, 901-906.

Wyles, J.P., McMaster, C.R., and Ridgway, N.D. (2002). Vesicle-associated membrane protein-associated protein-A (VAP-A) interacts with the oxysterol-binding protein to modify export from the endoplasmic reticulum. J Biol Chem *277*, 29908-29918.

Yamochi, W., Tanaka, K., Nonaka, H., Maeda, A., Musha, T., and Takai, Y. (1994). Growth site localization of Rho1 small GTP-binding protein and its involvement in bud formation in Saccharomyces cerevisiae. J Cell Biol *125*, 1077-1093.

Zajac, A., Sun, X., Zhang, J., and Guo, W. (2005). Cyclical regulation of the exocyst and cell polarity determinants for polarized cell growth. Mol Biol Cell *16*, 1500-1512.

Zhang, X., Bi, E., Novick, P., Du, L., Kozminski, K.G., Lipschutz, J.H., Guo, W. (2001). Cdc42 interacts with the exocyst and regulates polarized secretion. J Biol Chem *276*, 46745-46750.

Zhang, X., Orlando, K., He, B., Xi, F., Zhang, J., Zajac, A., and Guo, W. (2008). Membrane association and functional regulation of Sec3 by phospholipids and Cdc42. J Cell Biol *180*, 145-158.

3: **Genome-Wide Analysis of Sterol-Lipid Storage and Trafficking in *Saccharomyces cerevisiae***

Author list: Weihua Fei*, **Gabriel Alfaro***, Baby-Periyanayaki Muthusamy, Zachary Klaassen, Todd R. Graham, Hongyuan Yang, and Christopher T. Beh.

*Contributed equally to work

Author contribution: The initial lovastatin and nystatin screen for sterol homeostasis mutants was performed by C.T.B. All aspects of the experiments to generate figure 3.5.2, 3.5.3, 3.5.4, and 3.5.7 was performed by W.F and H.Y. The experiments to generate figures 3.5.1, 3.5.6, 3.5.8, and tables 3.6.4, and 3.6.5 were performed by G.A and undergraduate student Z.K. The electron microscopy to generate figure 3.5.5 was performed by B.M and T.G. I contributed to materials and methods and figure legends while the text was written by C.T.B.

 Abstract

The pandemic of lipid-related disease necessitates a determination of how cholesterol and other lipids are transported and stored within cells. The first step in this determination is the identification of the genes involved in these transport and storage processes. Using genome-wide screens, we identified 56 yeast (*Saccharomyces cerevisiae*) genes involved in sterol-lipid biosynthesis, intracellular trafficking, and/or neutral-lipid storage. Direct biochemical and cytological examination of mutant cells revealed an unanticipated link between secretory protein glycosylation and triacylglycerol (TAG)/steryl ester (SE) synthesis for the storage of lipids. Together with the analysis of

other deletion mutants, these results suggested at least two distinct events for the biogenesis of lipid storage particles: a step affecting neutral-lipid synthesis, generating the lipid core of storage particles, and another step for particle assembly. In addition to the lipid storage mutants, we identified mutations that affect the localization of unesterified sterols, which are normally concentrated in the plasma membrane. These findings implicated phospholipase C and the protein phosphatase Ptc1p in the regulation of sterol distribution within cells. This study identified novel sterol-related genes that define several distinct processes maintaining sterol homeostasis.

3.1 Introduction

Both cholesterol biosynthesis and storage are controlled in response to levels and localization of regulatory pools of sterols (Lum et al., 2004; Maxfield and Menon, 2006; Prinz, 2002; Soccio and Breslow, 2004). In response to high cholesterol levels in the endoplasmic reticulum (ER) membrane, the enzyme acyl coenzyme A (CoA):sterol *O*-acyltransferase (ASAT) initiates sterol esterification and storage by covalently coupling fatty acids to cholesterol. Through an active process, the esterified cholesterol is amalgamated with other neutral lipids into lipid storage droplets that are released from the ER membrane (Murphy and Vance, 1999; Zweytick et al., 2000). The trafficking of unesterified sterols also affects the sterol distribution in regulatory pools. Although cholesterol is synthesized in the ER, the highest level of unesterified cholesterol is found in the plasma membrane (Liscum and Munn, 1999) and maintenance of normal sterol levels requires the efficient transport of cholesterol from the ER membrane to the plasma membrane. The maintenance of cholesterol levels in the plasma membrane is affected by sorting from endosomal compartments and recycling back to the cell surface (Liscum and

Munn, 1999; Prinz, 2002), and feedback regulation of cholesterol on its own biosynthesis and storage also controls levels of cellular sterols (Du et al., 2004; Steck and Lange, 2002). These findings suggest that the maintenance of cellular cholesterol homeostasis requires the regulatory integration of cholesterol synthesis, storage, and transport pathways.

As in mammalian cells, the budding yeast *Saccharomyces cerevisiae* synthesizes its own cholesterol-like lipids but, under normal aerobic conditions, yeast does not internalize exogenous sterol lipids. Apart from this difference, other elements of sterol homeostasis, including lipid storage and transport pathways, appear to be conserved (Sturley, 2000). In yeast, ASAT is encoded by two homologous genes, *ARE1* and *ARE2*, which together generate steryl esters for lipid storage droplets (Yang et al., 1996). Lipid droplets are also comprised of triacylglycerols, which in yeast are produced by the acyl-CoA:diacylglycerol acyltransferase 2 (DGAT2) homologue encoded by *DGA1* and by the phospholipid:diacylglycerol acyltransferase (PDAT) homologue encoded by *LRO1* (Oelkers et al., 2000). The genes encoding sterol and diacylglycerol acyltransferases are not essential, and a viable strain has been constructed that lacks all genes required for neutral-lipid biosynthesis (Sandager et al., 2002; Sorger and Daum, 2003). These findings indicate that lipid storage is itself not required for yeast growth under normal culture conditions. A likely explanation for why neutral-lipid/ sterol storage is dispensable for yeast viability is that it represents only one of several independent mechanisms that contribute to the maintenance of lipid and sterol homeostasis. This leads to the prediction that sterol regulatory pathways are functionally redundant and that growth defects occur only when several of these pathways are disrupted in concert.

In the case of sterol storage and other sterol regulatory pathways, functional redundancy has been successfully exploited to identify novel sterol-associated genes in yeast. *ARV1*, which affects the distribution of unesterified sterols, was originally identified as a deletion mutation that is lethal in combination with deletions of both *ARE1* and *ARE2* (Tinkelenberg et al., 2000). This finding suggests that both sterol storage and trafficking make overlapping contributions to sterol homeostasis. *ECM22* and *UPC2* encode transcription factors that control another aspect of sterol homeostasis through the coordinate regulation of several sterol biosynthesis genes (Vik and Rine, 2001). Although the combined deletion of *ECM22* and *UPC2* is not lethal, *upc2Δ ecm22Δ* cells are inviable with the additional perturbation of sterols caused by the deletion of *ERG2*, which encodes the otherwise nonessential enzyme C-8 sterol isomerase (Vik and Rine, 2001). Together these results affirm that the disruption of just one sterol regulatory pathway is not detrimental unless there are additional defects in sterol homeostasis.

In this study, we carried out a functional genomics screen to identify yeast deletion mutants that cannot tolerate drug-induced disruptions in sterol homeostasis. This screen successfully identified 56 known and novel genes that are required for maintenance of sterol homeostasis. The identified deletion mutants were analyzed by cellular and biochemical approaches to establish their specific roles in sterol-lipid biosynthesis, trafficking, and/or storage. In this study, we defined distinct steps required for lipid storage droplet biogenesis and established a link between ASAT/DGAT lipid esterification and secretory protein glycosylation. Our findings provide insights into mechanisms affecting sterol transport, synthesis, and neutral-lipid storage, which together maintain sterol homeostasis and are potentially linked to human lipid disorders.

3.2 Materials and Methods

3.2.1 Strains and microbial and genetic techniques

Culture media and genetic manipulations were as described previously (Adams et al. 1997). To select for the *kan-MX4* gene, yeast were grown on yeast rich medium (YPD) containing 200 μg/ml Geneticin sulfate (G418) (Gibco BRL Life Technologies, Inc., Rockville, MD). YPD solid medium containing nystatin (Sigma Chemicals, Inc., St. Louis, MO) or lovastatin (a gift of Merck & Co., Inc., NJ) was prepared as previously described (Beh et al., 2001). Functional genomics screens were conducted using the nonessential *kan-MX4*-marked homozygous diploid deletion collection (isogenic derivates of BY4743), and subsequent analysis involved the *MAT*a nonessential haploid deletion strain collection (isogenic derivates of BY4741) (Winzeler et al., 1999b). The genotypes of other yeast mutant strains not obtained from the deletion mutant collections are listed in Table 3.6.1. Strains bearing multiple gene disruptions were generated through standard genetic crosses.

3.2.2 Cloning and recombinant techniques

DNA cloning techniques and bacterial transformations were performed by standard procedures (Sambrook et al., 1989) (Table 3.6.2). Restriction enzymes were obtained from New England Biolabs (Beverly, MA). Oligonucleotide primers for PCR were purchased from Operon Biotechnologies, Inc. (Huntsville, AL), and the yeast genomic DNA template for amplification was isolated from BY4741. All oligonucleotide primers used for PCR amplifications are listed in Table 3.6.3.

To construct a yeast plasmid that would rescue *CNB1* mutant defects, the primer combination of CBP263 and CBP264 was used to amplify the *CNB1* gene by PCR. The

123

amplified 1.1-kb fragment included all promoter and terminator sequences for wild-type expression and was cloned into the EcoRI-XhoI sites of pRS416 (Sikorski and Hieter, 1989) to generate the plasmid pCB456. One set of primers used to amplify the *CAX4* gene were CBP267 and CBP268, and the amplified 1.9-kb fragment was cloned into the BamHI site of pRS416 to generate pCB419. The YHP1 and YHP2 primers were used to generate the *CAX4* gene, after which the amplified fragment was cloned into the HindIII and BamHI restriction sites of YCplac111 to generate the plasmid YCplac111-CWH8. The primer combination used to amplify *VMA21* was CBP287 and CBP288, which produced a 0.6-kb fragment that was cloned into the EcoRI site of pRS416 to generate pCB523. Using primers CBP276 and CBP277, a 3.1-kb *PLC1* fragment was amplified and cloned into the EcoRI site of pRS416, producing pCB526.

3.2.3 Lovastatin and nystatin functional genomic screen

To screen the homozygous deletion collection for sterol-sensitive mutants, a pin replicator was used to transfer equivalent inocula from strains arrayed and grown on solid medium into 200 μl of sterile water. The resuspended cells were further diluted 100-fold in sterile water into individual wells of microtiter plates. Using a pin replicator, strains were spotted and arrayed onto YPD solid rich medium and onto YPD containing 5 U/ml nystatin or 20 U/ml nystatin. Strains cultured on YPD solid medium or YPD containing 5 U/ml nystatin were incubated for 1, 1 to 2, and 3 days at 37, 30, and 23°C, respectively. Strains cultured on YPD solid medium containing 20 U/ml nystatin were incubated at 37, 30, or 23°C for 2, 3, and 4 days, respectively. Resistance to nystatin was recorded only if the mutant grew in the presence of 20 U/ml nystatin, whereas sensitivity was recorded only for strains that grew poorly on medium containing 5 U/ml nystatin. Growth defects

were assessed relative to the wild-type control (BY4743) and in comparison to growth of each respective deletion strain on YPD without nystatin. If the growth of a specific deletion strain was affected by nystatin when cultured at two or more of the temperatures tested, the strain was picked and retested on nystatin-containing medium to confirm the results. Once confirmed, these deletion strains were then arrayed on solid medium and equivalent inocula were transferred to wells of microtiter plates and diluted 100-fold in sterile water. Using a pin replicator, these strains were spotted onto YPD solid rich medium and YPD medium containing 150 μg/ml lovastatin and incubated at 37, 30, and 23°C for 2, 3, and 4 days, respectively. Relative to the wild-type control (BY4743), deletion mutants that were susceptible to lovastatin for at least two of the three culture temperatures tested were retested (no lovastatin-resistant deletion mutants were identified). The confirmed list of nystatin/lovastatin-affected homozygous deletion mutants includes all of the deletions shown in Table 3.6.4.

3.2.4 Filipin/sterol and Nile red fluorescence microscopy

To examine sterol-lipid distribution, yeast cells were fixed and treated with filipin complex as previously described (Beh and Rine, 2004). For filipin and FM4-64 colocalization, 5.0 units of log-phase cells at an optical density at 600 nm grown in synthetic complete medium at 30°C were pelleted and cultured at 30°C with 32 μM FXM4-64 (Molecular Probes/Invitrogen, Carlsbad, CA) (Vida and Emr, 1995) for either 5 or 25 min. After the timed FXM4-64 uptake, cells were washed once with water, pelleted, and diluted to an optical density at 600 nm of 0.7 units/ml with fresh medium. Cells were then fixed for 10 min following the addition of formaldehyde to a final concentration of 3.75%. These cells were treated with filipin complex as described

previously (Beh and Rine, 2004).

Lipid storage droplets were visualized by fluorescence microscopy after treatment with the lipophilic dye Nile red (Sigma Chemicals, St. Louis, MO). Cells from mid-logarithmic-phase-grown cultures were centrifuged, and the cell pellet was resuspended with water before the addition of Nile red to a final concentration of 2 μg/ml. Nile red-stained cells were washed once with water before visualization. Osmotically susceptible mutant strains were fixed with 3.75% formaldehyde for 15 min and washed in an equal volume of water before and after Nile red addition.

For all fluorescence microscopy, samples were mounted on poly-lysine-coated slides, sealed under coverslips with nail polish, and imaged on a Leica DMRA2 microscope microscope (Leica Microsystems, Wetzlar, Germany) equipped with a Orca-ER charge-coupled device digital camera (Hamamatsu Photonics, Hamamatsu City, Japan). Filipin and FM4-64 fluorescence was observed with a UV and fluorescein isothiocyanate (FITC) filter set using neutral-density filters to preserve fluorescence. For each experimental trial shown, equal exposure times were used to compare cellular fluorescence. Image analysis was performed using Improvision (Lexington, MA) Open Lab image analysis software.

3.2.5 In vivo assay for oleate incorporation into steryl esters and triacylglycerol

The incorporation of [^{3}H]oleate into steryl ester and triacylglycerol was used as a measurement of sterol and diacylglycerol esterification rates as described previously (Oelkers et al., 2000). Cells (5 ml) were grown in YPD liquid medium to mid-logarithmic phase and then incubated at 30°C for 30 min with 5 μCi of [^{3}H]oleate. To remove

126

residual [^{3}H]oleate, cells were washed twice with 0.5% Tergitol, washed once with water, and then lyophilized. Dried cell pellets were resuspended in 50 μl of lyticase solution (1,700 U/ml in 10% glycerol, 0.02% sodium azide), chilled for 1h at -70°C, and then incubated at 30°C for 15 min. Lipids were extracted by hexane and analyzed by thin-layer chromatography (TLC). The plates were developed in hexane-diethyl ether-acetic acid (70:30:1) and stained with iodine vapor. Incorporation of label into lipids was determined after scintillation counting and normalization to a [^{14}C]cholesterol internal standard and cell dry weight. For each assay, at least three independent strains of each genotype were used. Statistical analysis was performed using the paired t test.

3.2.6 Measurements of steady-state levels of unesterified sterol and neutral lipids

Lipid extractions were performed as described (Zhang et al., 2003), and the quantification of neutral lipids and unesterified sterols were assayed by the methods of Zweytick et al. (Zweytick et al., 2000) with modifications. Log-phase cells were grown in rich medium and pelleted and then resuspended and pelleted twice in 0.5% Nonidet P-40 and once in distilled water before lyophilization. The dried cell pellets were resuspended in 50 μl of lyticase (1,700 U/ml in 10% glycerol; Sigma Chemicals), incubated at 37°C for 15 min, and then freeze/thaw lysed at -70°C for 1 h and then at 37°C for 15 min. Lipids were extracted with hexane, blown dry with N2, and dissolved in 100 μl of chloroform-methanol (2:1 [vol/vol]). Samples were applied to Silica gel 60 F254 plates (Merck), and chromatograms were developed in hexane-diethyl ether-acetic acid (85:15:1) with cholesterol, triolein, and cholesteryl ester (Sigma Chemicals) as the standard. Quantitative analysis of unesterified sterol was carried out by densitometric scanning at 275 nm with a CAMAG TLC scanner. For quantitation of steryl ester and

TAG, plates were dipped into methanolic MnCl2 solution (0.63 g MnCl2 ·4H2O, 60 ml water, 60 ml methanol, and 4 ml concentrated sulfuric acid), dried, and heated at 120°C for 15 min. Densitometric scanning was performed at 500 nm.

3.2.7 Immunoblots

Yeast extracts for Western blots were prepared as described (Ohashi et al., 1982). Prior to loading for sodium dodecyl sulfate-polyacrylamide gel electrophoresis (SDS-PAGE), samples were incubated in sample buffer at 60°C for 10 min before loading. Transfer and immunoblot wash conditions were as previously described (Beh et al., 1997). Polyclonal antibodies were raised in rabbits against glutathione *S*-transferase (GST)-fused Are1p (amino acids 12 to 191) and against GST-fused Lro1p (amino acids 440 to 661). Rabbit anti-Are1p polyserum was used at a 1:500 dilution; rabbit anti-Lro1p polyserum was used at 1:1,000. Rabbit anti-Vti1p was a gift from Wanjin Hong (Institute of Molecular and Cell Biology, Singapore) and was used at a dilution of 1:3,000. Bands were visualized with a 1:3,000 dilution of horseradish peroxidase-conjugated antirabbit secondary antibody, followed by chemiluminescent detection (Pierce Chemical Co., Rockford, IL). Endoglycosidase H (endo H) removal of N-linked glycosylation was performed on protein extracts as described by the manufacturer (Sigma Chemicals, Inc.). Following deglycosylation, equivalent amounts of protein (20 μg) were loaded per lane for SDS-PAGE and, after transfer, immunoblots were probed with anti-Are1p and anti-Lro1p antibodies and detected by chemiluminescence as described above.

3.2.8 Transmission electron microscopy

Samples were prepared for electron microscopy as described previously (Rieder et

al., 1996). In brief, cells were fixed and embedded after treatment with osmium-thiocarbohydrazide and dehydration. Thin sections were stained with uranyl acetate and lead citrate prior to viewing on a Philips CM12 transmission electron microscope.

3.3 Results

3.3.1 Identification of deletion mutants susceptible to sterol-lipid perturbation

Sterol lipids are essential for viability in almost all eukaryotic cells. The overall regulation of sterols, however, involves the control of sterol synthesis, as well as sterol transport and storage pathways. The individual pathways appear to be dispensable for normal cell growth only because each pathway compensates for the others. We predicted that yeast mutations that disrupt any of these pathways might result in cells that are sensitized to further sterol perturbations and would be unable to compensate for imbalances in sterol homeostasis. With this in mind, a yeast functional/chemical genomics approach was applied to identify nonessential genes representing each of the general pathways that conspire to maintain sterol homeostasis.

Ergosterol is a cholesterol-like sterol that is the bulk product of sterol biosynthesis in yeast. To identify potential candidate sterol-regulatory genes, we screened the ~4,700 diploid homozygous deletion strains (Winzeler et al., 1999b) for sterol-related defects. This mutant collection represents deletions corresponding to almost all individual nonessential genes in the yeast genome (Winzeler et al., 1999b). We screened the homozygous diploid collection, as opposed to haploid deletions, to reduce false mutant identifications due to nonspecific spontaneous recessive mutations. For the initial screening of the deletion collection, we analyzed mutant growth in the presence of the ergosterol-binding antibiotic, nystatin (Walker-Caprioglio et al., 1989; Woods, 1971).

Although the mechanism of nystatin toxicity is complex, it exerts its effects by direct binding to plasma membrane ergosterol and nystatin has been successfully used to select viable mutants defective in ergosterol biosynthesis (McCammon et al., 1984). In this broad-based screen (see Materials and Methods), we identified 262 nystatin-susceptible mutants and 95 nystatin-resistant mutants. Some of the same deletion mutants (e.g., *ARV1*, *ERG3*, *CDC50*, *CNB1*, *DRS2*, *NUT1*, *PHO88*, *RIM9*, *SIF2*, *UME6*, *ZAP1*, etc.) were independently identified in previous genomic studies that examined the effects of various sterol-affecting drugs on yeast growth (Giaever et al., 2002; Lum et al., 2004; Parsons et al., 2004; Parsons et al., 2006). However, to eliminate from consideration those deletion mutants that did not specifically affect sterols, we performed a secondary screen using lovastatin. In yeast (and mammals), lovastatin reduces total amounts of sterols by inhibiting the rate-limiting enzyme in sterol synthesis, 3-hydroxy-3-methyl-glutaryl-CoA reductase (Basson et al., 1986; Tobert, 2003). In this regard, nystatin and lovastatin have different inhibitory mechanisms but, because both drugs disrupt normal sterol regulation, both would affect deletion strains defective in sterol homeostasis. Thus, the 357 deletion strains affected by nystatin were tested for lovastatin sensitivity (none were lovastatin resistant). Fifty-seven of the nystatin-susceptible deletion strains were lovastatin sensitive, whereas only 5 nystatin-resistant strains were also lovastatin sensitive. Six of the mutants had been previously reported to exhibit nonspecific multidrug sensitivities (Parsons et al., 2004), and they were not analyzed further unless independent evidence suggested otherwise (see below). Therefore, the 56 deletion mutations that affected sterol regulation or homeostasis are listed in Table 3.6.4; 8 of these mutants had mutations that corresponded to genes with established links to lipid

synthesis, regulation, or transport (*ARV1*, *BTS1*, *CDC50*, *DRS2*, *ERG3*, *ERG6*, *PLC1*, and *RAM1*), whereas 3 corresponded to novel genes (YEL045C, YDL133W, and YJL175W). The remainder of mutants represented known genes that have not been previously reported to have a role in sterol or lipid function. Our study is complementary to a previous genomic approach that surveyed all nonessential deletion mutants for those that affected sterol uptake during anaerobic growth conditions (Reiner et al., 2006). Except for the *tkl1Δ* and *rlr1Δ* mutants, the subset of mutants identified by these different approaches had no overlap. To determine how the deletion mutations we identified affect sterols, each of the 56 deletion mutants was analyzed for specific cellular defects in sterol storage, sterol synthesis, or in the intracellular membrane distribution of sterols.

3.3.2 Mutant defects in neutral-lipid storage disrupt sterol homeostasis

Esterified sterols within lipid droplets represent a major pool of cellular sterols in most eukaryotes, including yeast (Murphy and Vance, 1999; Zweytick et al., 2000). To determine if lipid storage was affected by any of the deletion mutations we identified, mutant cells were examined after incubation with Nile red, a fluorescent dye that stains neutral-lipid storage droplets. Nile red has been successfully used both in yeast (Yang et al., 1996) and in *Caenorhabditis elegans* genomic screens to examine lipid storage defects (Ashrafi et al., 2003). Haploid deletion mutants, representing each of the 56 sterol-related homozygous deletion strains identified in the genomic screens, were individually cultured in rich medium to the logarithmic phase and stained with Nile red. The number, size, and intensity of Nile red-stained lipid droplets were determined by fluorescence microscopy and image analysis (Table 3.6.4). In wild-type cells, an average of 2.7 Nile red droplets was observed by fluorescence microscopy in a single optical

131

section. Although many of the deletion strains had relatively modest but reproducible deviations from the wild-type control in droplet number or Nile red staining intensity, seven deletion mutants had severely reduced numbers of lipid droplets (fewer than half that of wild type) and 2 strains (*ume6Δ* and *cdc50Δ*) had a significant increase in both intensity and droplet number (Table 3.6.4). These findings suggested that at least some of the deletion mutants originally identified were susceptible to sterol-specific inhibitors because of lipid storage defects. As a pragmatic approach, we conducted detailed analyses on just those mutants having the greatest effects on the number and fluorescence intensity of Nile red-stained lipid droplets.

As shown in Figure 3.5.1, the deletion of *CAX4* drastically reduced lipid storage droplets. *CAX4* encodes dolichyl pyrophosphate phosphatase (Fernandez et al., 2001), and the corresponding deletion mutant exhibited the greatest reduction in lipid droplet numbers of those analyzed. Compared to wild-type cells, there were 9.1-fold-fewer lipid droplets in *cax4Δ* cells (Table 3.6.4 and Figure 3.5.1). Of all the deletion mutants with reduced numbers of lipid droplets, the deletion of *CAX4* had the greatest impact. To confirm that the observed Nile red staining defects were a direct result of the specified deletion and were not due to another unlinked random mutation, we transformed the *cax4Δ* strain with a low-copy plasmid containing its respective wild-type gene. The *cax4Δ* strain transformed with the *CAX4* gene, but not the vector alone control, fully rescued the lipid droplet defect phenotype (Figure 3.5.1). These results implicated *CAX4* as being required for lipid droplet biogenesis. In contrast to *cax4Δ* cells, deletion of either *UME6* or *CDC50* caused enhanced Nile red fluorescence and a proliferation of lipid droplets relative to wild-type cells (Table 3.6.4). In this regard, the *ume6Δ* and *cdc50Δ*

132

mutants were unique in that, in addition to the many lipid droplets, the intensity of Nile red fluorescence was significantly greater than those observed in the other mutants. For these reasons, the sterol defects in *ume6Δ* and *cdc50Δ* cells were analyzed in detail. *CDC50* encodes a protein that is involved in cell polarization and also regulates the cellular localization of Drs2p, a lipid translocase (Natarajan et al., 2004; Saito et al., 2004). The finding that the number of lipid droplets increased in *cdc50Δ* cells was particularly noteworthy because it was recently shown that *CDC50* genetically interacts with sterol biosynthetic genes (Kishimoto et al., 2005). In *cdc50Δ* cells, wild-type *CDC50* expressed from a plasmid rescued the lipid droplet proliferation and the observed increase in Nile red staining (Figure 3.5.1). These findings indicated that the lipid droplet defect was linked to the *CDC50* locus. Significant increases in both lipid droplet number and intensity were also observed in *ume6Δ* cells (Table 3.6.4). *UME6* encodes a transcriptional regulator that induces early meiotic genes (Vershon and Pierce, 2000), but it also has a role as a regulator of specific mitotic genes (Einerhand et al., 1995; Strich et al., 1994; Sweet et al., 1997). All told, our results established that several yeast genes, in addition to those directly involved in neutral-lipid biosynthesis, are required for lipid storage particle biogenesis.

3.3.3 Neutral-lipid synthesis is susceptible to defects in secretory protein glycosylation

A core component of lipid storage particles is esterified ergosterol and the enzyme ASAT catalyzes the coupling of sterols with fatty acids (Xu and Tabas, 1991; Yang et al., 1996). If *cax4Δ* mutations inhibit lipid droplet formation by blocking sterol trans-esterification, then ASAT activity might be reduced in mutant cells. To measure ASAT

activity, the rate of [3H]oleate incorporation into steryl esters was determined for wild-type and mutant strains. Compared to the wild-type strain and the other deletion mutants tested, the *cax4Δ* mutant had significantly reduced ASAT activity (Figure 3.5.2A). After a pulse-labeling for 30 min at 30°C, the amount of [3H]oleate incorporated into steryl esters in the *cax4Δ* mutant was only 32% of that measured for the wild-type strain. Consistent with the reduction in ASAT activity, steady-state levels of steryl esters in log-phase *cax4Δ* cells were markedly reduced when separated and measured by TLC after lipid extraction (Figure 3.5.3). These findings indicated that the lipid droplet defect observed in *cax4Δ* cells was caused at least in part by a reduction in ASAT activity.

Another major lipid component of yeast lipid droplets is triacylglycerol, which is synthesized by DGAT and PDAT (Sorger and Daum, 2003). To determine whether defects in DGAT/PDAT activity contributed to the observed reduction of lipid storage particles in the *cax4Δ* strain, cells were pulse-labeled with [3H]oleate to measure the rate of its incorporation into triacylglycerol. In the *cax4Δ* strain, DGAT/PDAT activity was reduced (29% of wild type) (Figure 3.5.2B) and steady-state levels of triacylglycerol were barely detectable by TLC (Figure 3.5.3). These results indicated that the *CAX4* deletion affects all aspects of neutral-lipid synthesis, including ASAT and DGAT/PDAT activities.

Cax4p is a dolichyl pyrophosphate phosphatase that regenerates free dolichol, a lipid required for N-linked core glycosylation of secretory proteins in the ER (Fernandez et al., 2001; van Berkel et al., 1999). To determine whether the generation of lipid storage particles is linked to secretory protein glycosylation, or to another aspect of dolichol metabolism, we examined temperature-sensitive (ts) *sec53-6ts* mutant cells (RSY12) for

lipid droplet defects. *SEC53* encodes an essential phosphomannomutase required for core glycosylation of secretory proteins, but *SEC53* is not directly associated with dolichol metabolism (Kepes and Schekman, 1988). If protein glycosylation and lipid particle generation are indeed linked, then *sec53-6ts* cells might be defective for both. After 1 h at 37°C, *sec53-6ts* cells stained with Nile red exhibited a clear reduction in lipid droplets of 0.54 per cell (standard deviation [SD], 1.2; n = 100) compared to the wild-type control (RSY255) (2.5 droplets per cell [SD, 1.6; n = 100]). Even under permissive growth conditions, *sec53-6ts* cells had a reduction in lipid droplets comparable to the *cax4Δ* mutant. To test whether a general block in secretion would also block lipid droplet biogenesis, lipid droplets were counted after Nile red staining in *sec18ts* cells (JRY4130). After 1 h at 37°C, *sec18ts* cells are defective in multiple secretory transport events (Graham and Emr, 1991), but under these conditions there were no detectable defects in lipid droplet number or intensity of Nile red staining (2.7 lipid droplets per cell [SD, 1.3] compared to the wild-type, RSY255, value above). Thus, there is a specific link between core glycosylation and lipid droplet biogenesis that is independent of general secretory transport.

3.3.4 *CAX4* is required for acyltransferase expression.

The *CAX4* dependence of neutral-lipid synthesis might reflect a requirement for Cax4p in the enzymatic activation of ASAT and DGAT/PDAT or for the expression of these proteins. To determine if *CAX4* is required for ASAT or PDAT protein expression, we examined *cax4Δ* cells for the expression levels of Are1p, which is a representative ASAT protein (Yang et al., 1996), and Lro1p, a phospholipid diacylglycerol (DAG) acyltransferase (Oelkers et al., 2000). By immunoblot analysis, Are1p and Lro1p were

135

expressed at comparable levels in protein extracts derived from either wild-type cells or a *cax4Δ* strain transformed with a plasmid containing the wild-type *CAX4* gene (Figure 3.5.4A). In contrast, levels of both Are1p and Lro1p were significantly reduced in protein extracts from the *cax4Δ* strain, whereas levels of the internal control protein (Vti1p) remained unchanged (Figure 3.5.4A). These results suggested that in the *cax4Δ* mutant, inhibition of neutral-lipid synthesis was a result of a global reduction in ASAT and DGAT/PDAT protein expression. Thus, *CAX4* defines a mechanism that links secretory protein glycosylation with neutral-lipid acyltransferase expression.

A trivial explanation for these results is that the various neutral-lipid acyltransferases are all glycosylated, and their stability is sensitive to even small perturbations in glycosylation. To test whether Are1p or Lro1p is glycosylated and whether their glycosylation state is affected by *CAX4*, protein extracts from wild-type and *cax4Δ* cells were treated with endo H to remove N-linked oligosaccharides. The molecular weight of Are1p was unchanged whether in *cax4Δ* cells or in wild-type cells treated with endo H, which suggested that Are1p is not an N-linked glycoprotein (Figure 3.5.4B). This result also suggested that *CAX4* does not affect Are1p stability through glycosylation. Although the molecular weight of Lro1p was reduced by endo H treatment, indicating that Lro1p is a glycoprotein, only the glycosylated form of Lro1p was detected in *cax4Δ* cells (Figure 3.5.4B). Given these results, *CAX4* does not appear to affect neutral- lipid acyltransferase expression through their glycosylation.

In *cax4Δ* cells and in cells where N-linked glycosylation has been otherwise compromised, sphingolipid composition is significantly altered (Pittet et al., 2006). Specifically, in *cax4Δ* cells there is a considerable reduction in

inositolphosphorylceramides (IPCs), which represent a major class of sphingolipids (Pittet et al., 2006). To test whether the effect of *CAX4* on sphingolipid composition has a bearing on neutral lipid storage, lipid droplets in *lcb1-100ts* (YJN63), *lcb2ts* (YJN64), and wild-type (W303-1A) cells were visualized using Nile red fluorescence microscopy. The *lcb1-100ts* and *lcb2ts* mutants are defective in the first commitment step for the biosynthesis of all sphingolipids (Nagiec et al., 1994). After cultures were incubated at 37°C for 3 h, both the number and fluorescence intensity of Nile red-stained lipid droplets markedly increased in *lcb1-100ts* (average number of droplets per cell, 9.5; $n = 101$) and *lcb2ts* cells (average number of droplets per cell, 7.9; $n = 251$) as compared to the congenic wild-type control (average number of droplets per cell, 5.2; $n = 228$). When cultured at 23°C, all strains had a comparable number of lipid droplets (4.4 to 4.8 per cell). These findings indicated that the inhibition of all sphingolipid biosynthesis results in a concomitant proliferation in lipid droplets. These results were, however, opposite to those observed in *cax4Δ* cells, in which reduced IPC levels correlated with an absence of neutral lipids and lipid droplets.

3.3.5 Sterol homeostasis is disrupted in mutants that accumulate lipid storage particles

In the genomic screen, several but not all deletion mutants corresponding to vacuolar H^+-ATPase subunits (e.g., *vma2Δ*, *vma9Δ*, *vma21Δ*, and *tfp1Δ*) were susceptible to sterol inhibitors. To determine whether the vacuolar H^+-ATPase is required for lipid storage, we inspected these deletion mutants for defects in neutral-lipid synthesis. In particular, a significant increase in the number of lipid droplets was observed in *vma9Δ* cells (Table 3.6.4). *VMA9* encodes subunit e of the V0 vacuolar H^+-ATPase (Sambade

and Kane, 2004). Deletion of *VMA9* resulted in significant increases in ASAT activity (2.5-fold) and steryl ester levels (3.4-fold) compared to wild-type cells (Figure 3.5.2A and Figure 3.5.3). These increases in steryl esters were specific since no change in triacylglycerol synthesis or levels was detected in *vma9Δ* cells (Figure 3.5.2B and Figure 3.5.3). The results suggested that other vacuolar H^+-ATPase deletion mutants might also have specific effects on steryl ester storage. In *vma21Δ* cells, a modest increase in lipid droplet number and increases in steryl ester synthesis and levels were detected (Figure 3.5.2A and 3). *VMA21* encodes an ER-localized protein required for the assembly of the vacuolar H^+-ATPase complex (Hill and Stevens, 1994; Maeda et al., 1994). None of the other vacuolar H^+-ATPase deletion mutants had significant effects on lipid droplets, as determined by Nile red staining (Table 3.6.4). These results indicated that steryl ester storage is not dependent on vacuolar H^+-ATPase function per se. However, in *vma9Δ* cells, and to a lesser degree *vma21Δ* cells, steryl ester storage and triacylglycerol storage are uncoupled. The proliferation of lipid droplets is consistent with the increased steryl ester synthesis measured in these particular vacuolar H^+-ATPase mutants.

In contrast to *vma9Δ* cells, the profusion of lipid droplets in *ume6Δ* and *cdc50Δ* cells was coupled with a striking increase in Nile red fluorescence intensity (Table 3.6.4). Cdc50p regulates and physically interacts with the Drs2p P-type ATPase aminophospholipid translocase (Chen et al., 1999; Graham, 2004; Natarajan et al., 2004), which generates phospholipid asymmetry in membranes (Pomorski et al., 2003; Saito et al., 2004). This suggested that the lipid droplet proliferation in *cdc50Δ* cells might be a consequence of defects in Drs2p phospholipid translocase activity. Consistent with this possibility, *drs2Δ* was identified in our sterol genomic screen and others have reported

sterol defects in *drs2Δ* cells (Reiner et al., 2006). However, we observed a very minor

increase in lipid droplet numbers (albeit statistically significant [$P = 0.04$]) in *drs2Δ* cells

stained with Nile red (Table 3.6.4), and insignificantlipid defects were detected in

biochemical assays (Figure 3.5.2 and 3 [see below]). Because the *S. cerevisiae* genome

contains four other potential aminophospholipid translocases that, in some cases, have

functional overlap with *DRS2 (Huh et al., 2003)*, we tested whether these P-type ATPases

(*DNF1* to *DNF3*, *NEO1*) affected lipid droplets. As observed by Nile red staining, no

appreciable changes in the number of lipid droplets were observed in *neo1-1* (ZHY628-

15B), *neo1-2* (ZHY628-34A), *dnf1Δ dnf2Δ dnf3Δ* (PFY3273A), or *dnf1Δ dnf2Δ dnf3Δ*

drs2-31ts (ZHY410-3A) mutants, regardless of temperature (unpublished data). These

results suggested that *CDC50* affects lipid droplets through a mechanism that is

independent of the P-type aminophospholipid translocases.

To determine how lipid droplets are affected in *cdc50Δ* cells, lipid esterification

activities and neutral lipid levels were analyzed. To test if increased ASAT and

DGAT/PDAT activities caused the increase in lipid droplets, *cdc50Δ* cultures were pulse-

labeled with [3H]oleate to measure the rate of steryl ester and triacylglycerol synthesis.

Compared to the wild-type strain, the *cdc50Δ* strain had a 3-fold increase in ASAT

activity and a 1.9-fold increase in DGAT activity (Figure 3.5.2A and B). However, these

increases in enzyme activities manifested only a modest 1.4-fold increase in both steady-

state steryl ester and triacylglycerol levels (Figure 3.5.3). Thus, the proliferation of lipid

droplets in *cdc50Δ* cells as observed with Nile red is not entirely attributable to increases

in neutral-lipid levels.

In *ume6Δ* cells, neutral-lipid levels were also unaffected (Figure 3.5.3) despite the

observed increase in the number and fluorescence intensity of Nile red-stained lipid droplets (Table 3.6.4). Similar to *cdc50Δ* cells, in *ume6Δ* cells ASAT activity was markedly induced (3-fold) relative to the wild-type control, while DGAT activity was elevated only by 1.3-fold (Figure 3.5.2). Despite the induction of ASAT activity in *ume6Δ* cells, no meaningful changes in steady-state steryl ester levels were detected and triacylglycerol levels were normal. Based on these results, the lipid droplet defects observed by fluorescence microscopy in *ume6Δ* cells are not attributable to changes in neutral-lipid levels. Based on these findings, the biogenesis of lipid storage particles is affected by two distinct classes of mutants: one group that affects neutral-lipid synthesis (e.g., *cax4Δ* and *vma9Δ*), and another that is independent of lipid synthesis (e.g., *cdc50Δ* and *ume6Δ*).

3.3.6 *CDC50* and *UME6* deletions disrupt lipid storage particle ultrastructure.

In addition to the enzymes that synthesize neutral lipids, lipid storage also involves lipases that hydrolyze and release lipids from storage and structural factors for storage particle assembly (Murphy and Vance, 1999). Because steady-state levels of neutral lipids were not grossly affected in *cdc50Δ* and *ume6Δ* cells, we examined lipid storage particles in these mutants for structural defects by using electron microscopy (Figure 3.5.5). Consistent with Nile red staining, the number of lipid droplets in *cdc50Δ* cells was greater than wild type when viewed by electron microscopy. In wild-type cells, we observed 0.9 lipid droplet per cell section ($n = 186$), whereas in *cdc50Δ* cells there were 1.8 droplets per cell section ($n = 84$). In *ume6Δ* cells, the number of lipid droplets observed by electron microscopy was also greater than wild type (2.1 droplets per cell section; $n = 40$). Because optical sections of Nile red-stained cells represent a greater

thickness through the cell than thin sections for electron microscopy, the average number of lipid droplets counted on electron micrographs was fewer than those observed by fluorescence microscopy. When observed by electron microscopy, the lipid droplet cortex in wild-type cells was surrounded by a discrete darkly stained "shell" (Figure 3.5.5). In *ume6Δ* cells, the lipid droplet shell was exaggerated and clearly thicker than in wild-type cells (Figure 3.5.5). In *cdc50Δ* cells, however, lipid droplets appeared less well defined and had no distinct border (Figure 3.5.5). These results not only confirmed previous results showing an increase in Nile red-stained lipid droplets in *cdc50Δ* and *ume6Δ* cells, but indicated lipid storage particle assembly was defective in both mutants. These findings also indicated that *CDC50* and *UME6* have dramatically different effects on lipid droplet ultrastructure.

3.3.7 Sterol homeostasis is disrupted by mutations affecting the intracellular distribution of unesterified sterols.

One of the deletion mutants identified (*arv1Δ*) has an established defect in ergosterol localization (Beh and Rine, 2004; Tinkelenberg et al., 2000). To determine if any of other deletion mutations we identified disrupt the normal ergosterol distribution, cells were fixed and treated with filipin complex to visualize unesterified sterol lipids. Filipin is a specific fluorescent probe for unesterified sterol localization in both mammalian cells and yeast (Beh and Rine, 2004; Severs, 1997). In wild-type yeast, filipin fluorescence is observed at the plasma membrane (Beh and Rine, 2004) and this pattern of localization is consistent with previous studies that showed that ergosterol, the most abundant yeast sterol, is concentrated in the plasma membrane (Zinser et al., 1993). In addition to the plasma membrane staining, 15.7% of wild-type cells exhibited small

filipin-fluorescent cytoplasmic spots. In 8.5% of wild-type cells, membrane strands were also observed (Table 3.6.5 and Figure 3.5.6). In terms of morphology and localization, the membrane strands are consistent with peripheral ER. This could not be confirmed because of technical limitations of using filipin, which prevented costaining with ER markers. Nonetheless, these results affirmed that the plasma membrane is the primary repository of unesterified sterols in *S. cerevisiae*, but additional filipin-stained structures were also evident.

As listed in Table 3.6.5, the normal pattern of filipin fluorescence was defective in several mutants other than the *arv1Δ* strain. Cytoplasmic spots were infrequently observed in wildtype cells, but a significant number were observed in *erg3Δ*, *ptc1Δ*, and *plc1Δ* cells (Table 3.6.5 and Figure 3.5.6). *ERG3* encodes a sterol biosynthetic enzyme (Arthington et al., 1991), *PTC1* encodes a protein phosphatase type 2C (Maeda et al., 1994; Robinson et al., 1994), and *PLC1* encodes phospholipase C (Flick and Thorner, 1998). Compared to wild-type cells, 3.2-fold more *erg3Δ* cells contained internal filipin-fluorescent spots, 2.6-fold more *ptc1Δ* cells and 2.2-fold more *plc1Δ* cells contained spots. In contrast, 3.7-fold fewer filipin/ergosterol spots and 4.4-fold more filipin-fluorescent membrane strands were observed in *arv1Δ* cells, compared to wild-type cells. Eleven deletion mutants accumulated filipin-fluorescent membrane strands, whereas strands were all but absent in *erg3Δ* cells (Table 3.6.5 and Figure 3.5.6). These results suggested that different deletion mutations had distinct effects on the intracellular distribution of sterols.

To determine whether changes in unesterified ergosterol levels were associated with abnormal sterol distributions, sterols were extracted from those deletion mutants

with pronounced sterol/filipin localization defects. In *ptc1Δ* and *plc1Δ* cells, ergosterol levels were somewhat elevated (150 and 154%, respectively) compared to wild-type cells. These values were similar in magnitude to the 176% increase in *arv1Δ* cells, which is in agreement with previous studies (Figure 3.5.7) (Tinkelenberg et al., 2000). Thus, in *ptc1Δ, plc1Δ,* and *arv1Δ* cells the internal accumulation of sterols observed by filipin fluorescence microscopy was associated with modest increases in unesterified ergosterol within cells. As predicted, the *erg3Δ* control that does not synthesize ergosterol had no detectable ergosterol. These findings suggested that like *ARV1, PTC1* and *PLC1* play a role in sterol trafficking within yeast cells.

We also investigated whether any of the lipid storage mutations affected unesterified ergosterol levels. Compared to the wild-type control, the level of unesterified ergosterol in *cdc50Δ* cells was unchanged and the ergosterol levels in *cax4Δ* and *ume6Δ* strains were only a little higher (Figure 3.5.7). These findings indicated that in the mutants with lipid droplet mutations, increased concentrations of unesterified ergosterol were not necessarily coupled with defects in sterol storage.

In mammalian cells, the late endosome represents a sorting compartment for internalized cholesterol (Prinz, 2002). To determine whether the cytoplasmic filipin-fluorescent spots observed in yeast correspond to an endosomal compartment, cells were incubated with the endosome-specific dye FM4-64 (Vida and Emr, 1995) and then fixed and stained with filipin. FM4-64 is a fluorescent lipophilic dye that is internalized from the yeast plasma membrane, through endosomal compartments, to the vacuole (Vida and Emr, 1995). Colocalization of filipin and FM4-64 fluorescence was detected 25 min after FM4-64 internalization but not at earlier times of endocytosis (Figure 3.5.8). This finding

suggested that in wild-type cells, filipin stains both ergosterol in the plasma membrane and, in a minority of cells, sterols in late endosomes.

To determine whether the excess filipin-stained spots observed in *plc1Δ* and *ptc1Δ* cells corresponded to endosomes, cells were incubated with FM4-64 prior to fixation and then filipin stained. After 25 min (and not before), the colocalization of FM4-64- and filipin-stained spots was significantly greater in *plc1Δ* and *ptc1Δ* cells than in wild-type cells (Figure 3.5.8). In wild-type cells ($n = 239$), filipin fluorescence was detected in 8% of FM4-64-stained late endosomes. In contrast, 41% of late endosomes costained with filipin in *plc1Δ* cells ($n = 310$) and 27% costained with filipin in *ptc1Δ* cells ($n = 255$). These results suggested that in the absence of *PLC1* or *PTC1* function, unesterified sterols accumulated in late endosomes, though not exclusively.

3.4 Discussion

In a genome-wide screen, we identified 56 mutants from the yeast nonessential deletion collection that were susceptible to drug-induced perturbations in sterol homeostasis. Sterol homeostasis is maintained through the interplay of several processes: sterol transport between membranes, the regulation of sterol biosynthesis, and the storage of sterol esters in lipid droplets/lipid storage particles (Figure 3.5.9). Some of the mutants we identified affected sterol homeostasis as a result of defects in lipid droplet generation (Figure 3.5.9). Direct examination of specific mutants defined at least two distinct events in lipid storage particle biogenesis, namely neutral lipid synthesis and lipid droplet organelle assembly (Figure 3.5.10). Further biochemical analysis of neutral-lipid synthesis in some of these mutants revealed an unanticipated link between neutral-lipid synthesis and secretory protein glycosylation. Yet another group of mutants we identified

had mutations that affected sterol homeostasis through defects in the membrane localization of unesterified sterols (Figure 3.5.9). These results implicated phospholipase C (Plc1p) and protein phosphatase type 2C (Ptc1p) in the intracellular trafficking of unesterifed sterols. These findings affirmed that multiple independent pathways contribute to the maintenance of cellular sterol-lipid homeostasis.

Previous genomic studies have analyzed the pharmacological effects of sterol-targeting drugs on yeast deletion strains (Giaever et al., 2002; Lum et al., 2004; Parsons et al., 2006), but the causal basis for the drug sensitivity was not explored. The nonessential deletion collection was also screened for mutants that cannot grow in anaerobic cultures in order to identify sterol uptake mutants (Reiner et al., 2006). Oxygen is essential for sterol synthesis, and under anaerobic conditions yeast must import sterols from the medium to survive. Under these anaerobic conditions, however, sterol-esterification-defective mutants grow normally, which explains why lipid storage mutants were not represented in the list of 37 anaerobically sensitive mutants (Reiner et al., 2006). In fact, only 2 of these 37 deletion mutants (*tkl1Δ* and *rlr1Δ*) were also identified by our approach. As such, our study complements previous genome-wide screens and identifies novel sterol-associated genes.

As a confirmation of the efficacy of our approach, we identified several deletion mutants that correspond to previously identified sterol-related genes. Deletion mutations that affect isoprenoid and sterol biosynthesis were identified, including *bts1Δ*, *ram1Δ*, *erg3Δ*, and *erg6Δ* (Daum et al., 1998), as well as *arv1Δ*, which affects the normal distribution of unesterified sterols (Tinkelenberg et al., 2000). Many of the deletion mutations corresponded to general transcription factors that could affect the expression of

genes required for sterol biosynthesis and homeostasis. However, the deletion of *UME6*, a transcriptional regulator in mitotic and meiotic cells (Einerhand et al., 1995; Strich et al., 1994; Sweet et al., 1997; Vershon and Pierce, 2000), had pronounced and specific effects on sterol-lipid storage. Thus, our unbiased analysis of yeast nonessential gene deletions identified both predicted targets as well as novel mutations not previously linked to sterol homeostasis.

In our mutant identification, there were some genes with direct and inferred connections to sterol homeostasis that were not detected. Because the screen was performed under aerobic conditions, most anaerobic mutations that affect sterol uptake were not identified (Reiner et al., 2006), and of course essential genes or those with redundant/overlapping functions would also not be detected. We note that deletion mutations representing lipid droplet-localized proteins were not detected. From genomewide protein localization studies (Athenstaedt et al., 1999; Huh et al., 2003), we compiled a list of 29 potential lipid droplet proteins. Of the 29 corresponding deletion mutants, only 2 mutants had lipid droplet defects as observed by Nile red fluorescence microscopy. In *tgl3Δ* cells, an increase in Nile red/lipid droplet fluorescence was detected whereas *ldb16/ycl005wΔ* cells had decreased numbers of lipid droplets (unpublished results); *TGL3* encodes a TAG lipase (Athenstaedt et al., 1999) and *LDB16* has a potential role in protein glycosylation (Corbacho et al., 2005). These results suggested that the vast majority of lipid droplet proteins are either functionally redundant or not required for lipid droplet formation/maintenance. Since proteins on lipid droplets have such limited effects, the implication is that lipid droplet biogenesis is mainly regulated by nonresident proteins.

3.4.1 Two distinct steps in lipid storage particle biogenesis

From the studies of many different cell types, a general model for lipid droplet biogenesis has been established ((Czabany et al., 2007), reviewed in reference (Murphy and Vance, 1999)). This model posits that neutral lipid synthesis occurs in specific ER microdomains wherein lipid droplets coalesce between the bilayer leaflets. Lipid storage particle maturation results after the neutral lipid core is sheathed with a phospholipid monolayer and buds from the ER surface into the cytoplasm. In Figure 3.5.10, our findings are integrated into this model to depict the distinct events in yeast lipid droplet biogenesis revealed by the defects in *cax4Δ*, *cdc50Δ*, *ume6Δ*, *vma9Δ*, and *vma21Δ* cells.

The first requisite step in lipid droplet biogenesis is the synthesis of its bulk neutral lipid components by the acyltransferases ASAT (Are1p and Are2p) and DGAT/PDAT (Dga1p and Lro1p). Remarkably, the expression of these enzymes was dependent on *CAX4*, which otherwise has a secondary role in secretory protein N glycosylation (Fernandez et al., 2001; van Berkel et al., 1999). Lipid droplet biogenesis was also dependent on *SEC53*, which also affects N-linked glycosylation (Kepes and Schekman, 1988). However, direct glycosylation did not appear to play a role in regulating the expression or turnover of the neutral lipid acyltransferases. Alternatively, acyltransferase expression might be indirectly affected by signaling pathways that respond to unfolded and/or unglycosylated secretory proteins. However, none of the glycoprotein folding and/or quality control mutants we tested (i.e., *ire1Δ*, *HAC1-238* [S238A] (Mori et al., 2000), and *cne1Δ*) had significant lipid droplet defects (unpublished results). Another less-understood consequence of N-glycosylation defects is a concomitant change in sphingolipid composition (Pittet et al., 2006). Whereas in *cax4Δ* cells, the reduction in sphingolipid (IPC) levels was associated with fewer lipid droplets,

we found that the number of lipid droplets dramatically increased in mutants that block sphingolipid biosynthesis. These findings suggest a potential link between sphingolipids, N glycosylation, and neutral-lipid storage, but the mechanism is anything but straightforward.

Other mutants were defective in another aspect of yeast lipid droplet biogenesis, the structural assembly of the lipid-storage particle (Figure 3.5.10). Both *CDC50* and *UME6* deletion mutations had striking effects on lipid droplet structure. In addition to a marked increase in the number of lipid droplets and a modest increase in neutral lipids, the lipid storage particles in *cdc50Δ* cells exhibited a distinctive morphological defect. Lipid droplets in *cdc50Δ* cells lacked the discrete electron-dense cortex, suggesting that *CDC50* affects the addition of protein(s) onto lipid droplets. In contrast, *UME6* had the opposite effect on the structural assembly of lipid droplet organelles. In *ume6Δ* cells, the intensity of Nile red fluorescence was more intense and the electron-dense shell surrounding the lipid storage particles was more prominent than in wild-type cells. Since Ume6p is a Cys[6] zinc binuclear transcription factor that coordinates mitotic and meiotic gene expression (Strich et al., 1994), these findings suggest a role for Ume6p in regulating the mitotic and meiotic proliferation of lipid storage particles. *UME6* might affect lipid droplet maturation during meiosis and sporulation, when large increases in neutral-lipid content occur (Illingworth et al., 1973). Despite their different effects, both *UME6* and *CDC50* define new processes in lipid storage particle assembly.

3.4.2 Potential regulators of intracellular ergosterol distribution

In wild-type yeast, sterol lipids are concentrated in the plasma membrane (Zinser et al., 1993), but some filipin/sterol fluorescence was observed in internal membranes.

Based on the overlap of filipin/ FM4-64 fluorescence, some of the internalized sterols correspond to the late endosome. Many deletion mutants affected the normal pattern of filipin/sterol staining, but *plc1Δ* and *ptc1Δ* cells exhibited the most striking defects. In these deletion mutants, a significant increase in filipin fluorescence was observed, most of which corresponded to endosomes. Since unesterified and esterified sterol levels in *plc1Δ* and *ptc1Δ* cells were only modestly higher than wild type, increases in internal filipin fluorescence were not caused by larger amounts of sterols but rather by sterol redistribution. A simple explanation for this redistribution is that endosomal sorting of sterols is defective in *PLC1* and *PTC1* mutants. Of the many endosomal mutants represented in the deletion collection, however, none were identified in our screen, suggesting that the role of *PLC1* and *PTC1* in sterol sorting is independent of established endosomal trafficking pathways.

Tentative connections have been reported that link *PLC1* and *PTC1* to endosomal function. *PTC1* encodes a PP2C phosphatase that is best described as a negative regulator of the HOG mitogen-activated protein kinase pathway, which responds to osmotic stress by increasing cellular glycerol concentrations (Young et al., 2002). Independent of this function, however, *ptc1Δ* genetically interacts with conditional alleles of the clathrin heavy chain gene (Bensen et al., 2000), which affect Golgi and endocytic trafficking (Payne et al., 1988). Ptc1p purportedly binds the ASAT Are2p (Ho et al., 2002), although no lipid droplet defects were detected in our analysis of *ptc1Δ* cells. Plc1p, the phospholipase C homologue, hydrolyzes phosphatidylinositol bisphosphate to produce DAG (Flick and Thorner, 1998), which in turn stimulates vacuolar membrane dynamics (Jun et al., 2004). In *plc1Δ* cells, fragmented vacuoles accumulate, suggesting a defect in

vacuolar/endosomal trafficking or vacuole fusion (Jun et al., 2004). Both Ptc1p and Plc1p also share a link to osmoregulation (Lin et al., 2002), and both *PTC1* and *PLC1* are linked to calcium signaling (Jun et al., 2004; Shitamukai et al., 2004; Tisi et al., 2004). Regardless of whether sterol trafficking involves these or a novel function, Ptc1p and Plc1p appear to play an important role in how sterols are distributed within cells.

Another potential regulator of sterols that was identified is calcineurin. In the absence of the calcineurin regulatory subunit, encoded by *CNB1*, cells were lovastatin sensitive but nystatin resistant. However, no significant sterol biosynthesis, sterol transport, or sterol storage defects were detected in our analysis of *cnb1Δ* cells. This finding is noteworthy only because several of the other deletion mutations identified (i.e., *bts1Δ, bck1Δ, cax4Δ, drs2Δ, ptc1Δ, van1Δ, vma2Δ,* and *vma21Δ*) are lethal in combination with *cnb1Δ* (Nakamura et al., 1996; Natarajan et al., 2004; Parsons et al., 2004; Shitamukai et al., 2004; Tong et al., 2001). In both *S. cerevisiae* and *Candida* species, calcineurin has been previously implicated in promoting resistance to sterol biosynthetic inhibitors through an adaptive mechanism (Cowen and Lindquist, 2005; Cruz et al., 2002; Edlind et al., 2002; Heitman, 2005; Onyewu et al., 2003). Perhaps calcineurin plays a similar role in adaptation to the defects in sterol homeostasis caused by some nonessential deletion mutants.

We note that many of the sterol homeostasis genes that were identified by this yeast functional/chemical genomics approach are conserved in mammals. In particular, yeast genes that affect lipid droplet biogenesis might play a conserved role in humans. For instance, the link between neutral-lipid synthesis and secretory protein glycosylation might be applicable to human adipocytes, as in yeast. Thus, the study of sterol

homeostasis in yeast might not only be pertinent to human cholesterol regulation, but also

valuable for providing novel gene targets for treating obesity.

3.5 Figures

Figure 3.5.1: Examples of deletion mutants with defects in lipid droplets and sterol lipid storage.
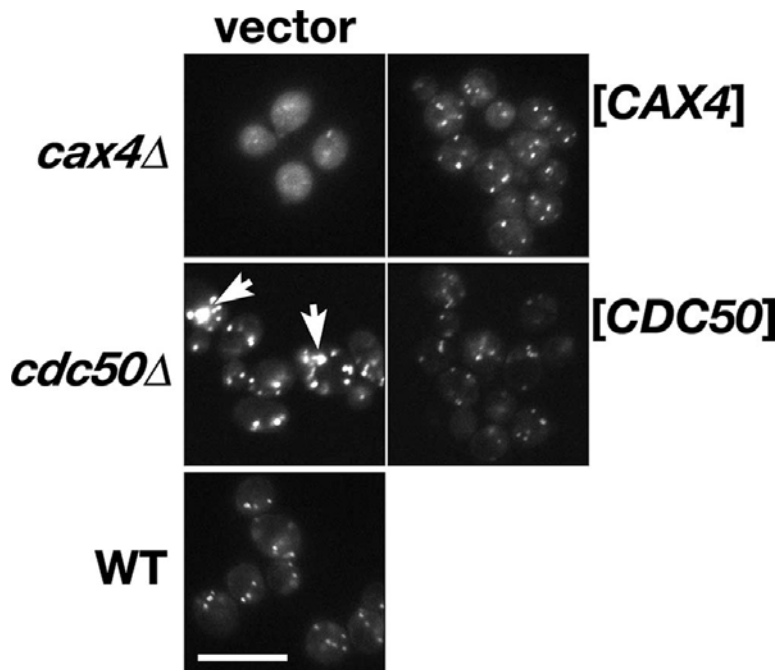
Figure 3.5.1: Nile red-stained lipid droplets were visualized by fluorescence microscopy in *cax4Δ* (CBY2346), *cdc50Δ* (CBY2408), and isogenic wild-type (WT; CBY2342) cells. (Left panels) Strains were transformed with the vector control, and log-phase cells were stained with Nile red. (Right panels) Wild-type *CDC50* and *CAX4* genes rescued the corresponding lipid droplet defects in the *cax4Δ* [*CAX4*] (CBY2404) and *cdc50Δ* [*CDC50*] (CBY2439) cells. The *cax4Δ* cells are an example of mutants that reduced the number of lipid droplets, whereas an excess of lipid droplets were observed in the *cdc50Δ* example. In the *cax4Δ* mutant, few lipid droplets were ever observed, although a cytoplasmic background fluorescence was sometimes seen. Arrows indicate increased lipid droplet size and staining intensity. The scale bar for all panels is 10 μm.**This work was performed by G.A. and Z.K**

Figure 3.5.2: Measurement of enzymatic activities for neutral lipid synthesis in selected sterol mutants.
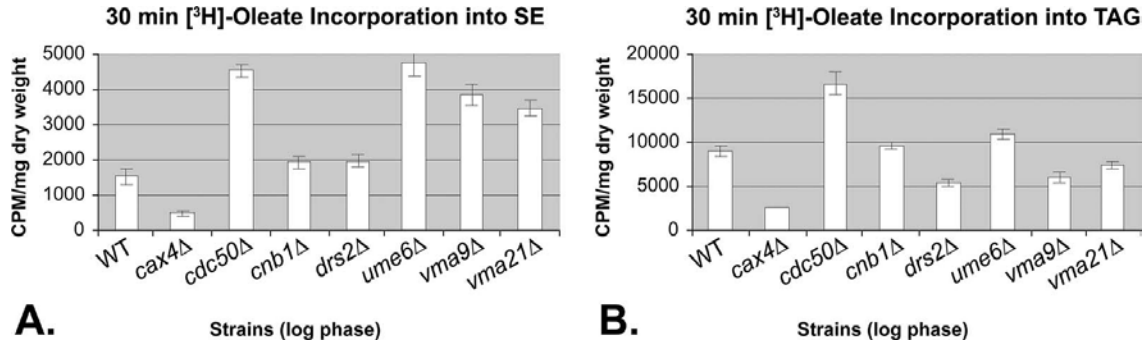
Figure 3.5.2: Steryl ester (SE) synthesis by ASAT (A) and triacylglycerol (TAG) synthesis by DGAT/PDAT (B) were determined by measuring [3H]oleate incorporation into steryl ester or triacylglycerol neutral lipids after cells were pulse-labeled for 30 min. WT, wild type. ***This work was performed by W.F.**

Figure 3.5.3: Steady-state levels of steryl esters and triacylglycerol in lipid droplet-defective mutants.
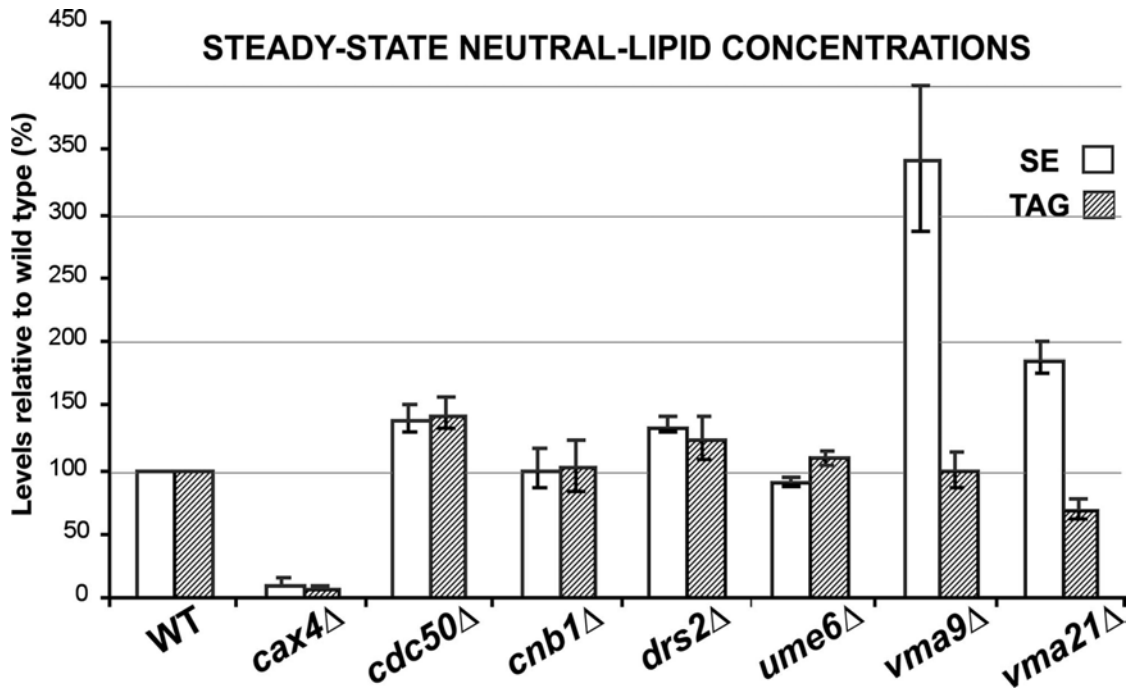
Figure 3.5.3: For all deletion strains shown, relative levels of steryl esters (SE; white bars) and triacylglycerol (TAG; hatched bars) were determined by TLC and are shown as a percentage of wild-type (WT) levels. ***This work was performed by W.F.**

Figure 3.5.4: Immunoblot analysis of Are1p and Lro1p expression in the *cax4Δ* mutant.
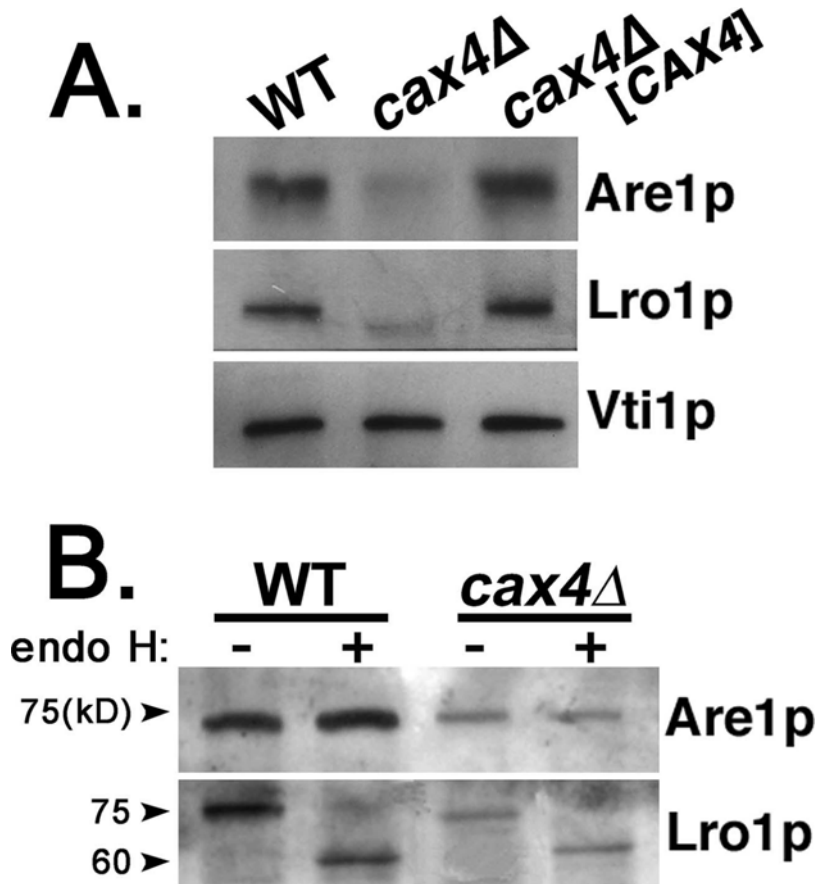
Figure 3.5.4: (A) As shown by anti-Are1p immunoblotting, Are1p levels were equivalent in the wild-type control (WT; BY4741) and the *cax4Δ* mutant rescued with a *CAX4*-containing plasmid (Yplac111- CWH8). Are1p levels, however, were clearly reduced in the *cax4Δ* mutant. As shown by anti-Lro1p immunoblotting, Lro1p levels were also reduced in the *cax4Δ* mutant compared to the wild-type strain or the *cax4Δ* transformant strain containing an episomal copy of *CAX4*. As an internal control for loading, samples were probed by immunoblotting for Vti1p, which is a Golgi v-SNARE that has no direct association with neutral lipid synthesis. (B.) Treatment of protein

extracts with endo H demonstrated that Are1p was not N-linked glycosylated, whereas Lro1p was an N-linked glycosylated protein. Without added endo H (-), the molecular mass of Are1p was consistent with its predicted unmodified molecular mass (72 kDa) and Lro1p was 75 kDa. With the addition of endo H (+), the position of Are1p on the gel was unchanged but the migration of Lro1p indicated a reduction in molecular mass. Equal amounts of protein were added to each lane. **This work was performed by W.F.**

Figure 3.5.5: Ultrastructure of *ume6Δ* and *cdc50Δ* lipid droplet defects.
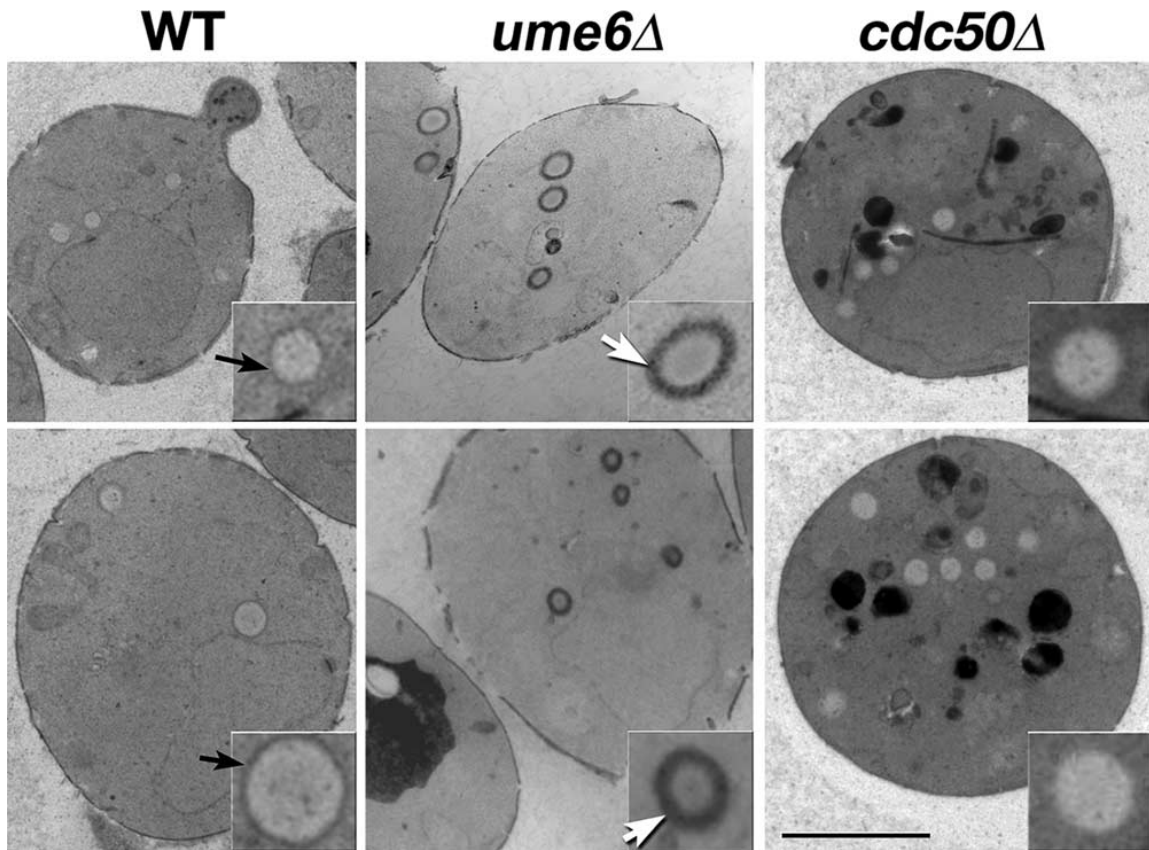
Figure 3.5.5: Wild-type (WT; left panels), *ume6Δ* (middle panels), and *cdc50Δ* (right panels) cells were examined by electron microscopy. In wild-type cells, lipid droplets are distinguished by their light gray/white appearance encircled by a thin, dark, electron-dense border (black arrows). The discrete border surrounding the cortex of lipid droplets is exaggerated in *ume6Δ* cells (white arrows) and absent in *cdc50Δ* cells. The large electron-dense structures are vacuoles, and, consistent with previous reports (Misu et al., 2003), vacuolar fragmentation was observed in *cdc50Δ* cells. The scale bar is 2 μm.

*This work was performed by B.M.

Figure 3.5.6: Deletion strains defective for ergosterol localization.
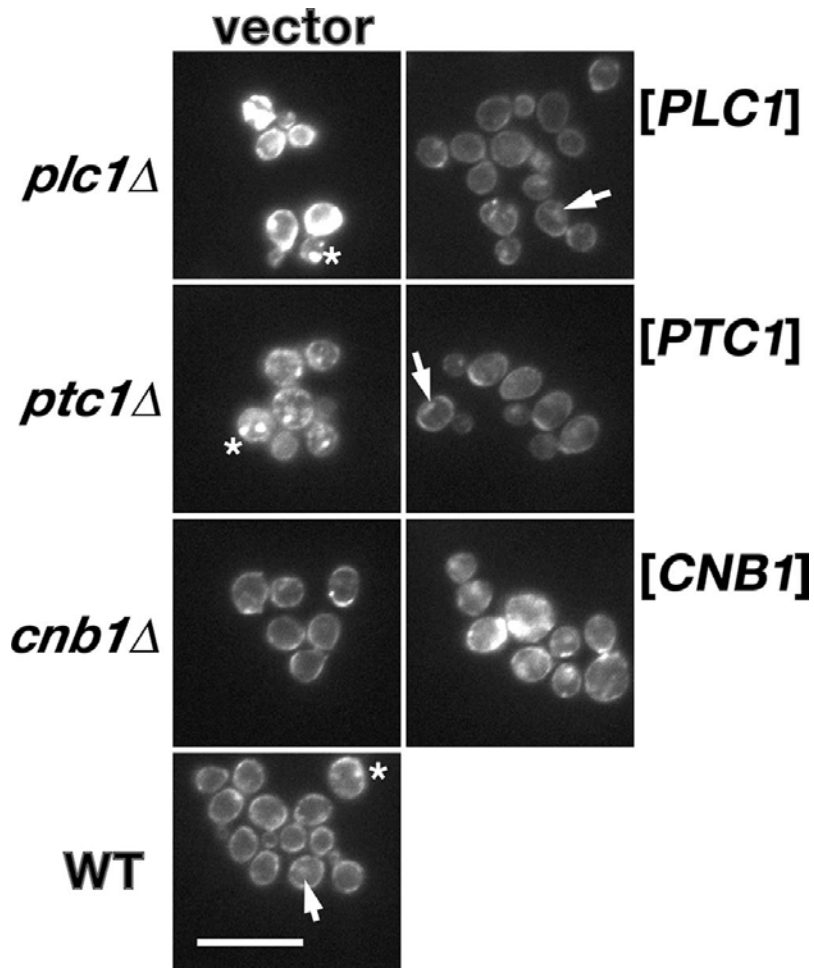
Figure 3.5.6: (Left panels) Filipin-stained unesterified sterol distribution visualized by fluorescence microscopy shown for *plc1Δ* (CBY2413), *ptc1Δ* (CBY2346), and wild-type (WT; CBY2342) log-phase cells transformed with the vector or (right panels) the corresponding wild-type genes. In the corresponding mutant, each wild-type gene rescued the sterol defects observed. Arrows indicate membranous strands, whereas asterisks (*) indicate internal filipin-stained spots. The scale bar for all panels is 10 μm.

*This work was performed by G.A. and Z.K.

Figure 3.5.7: Unesterified ergosterol levels in selected sterol-defective deletion mutants.
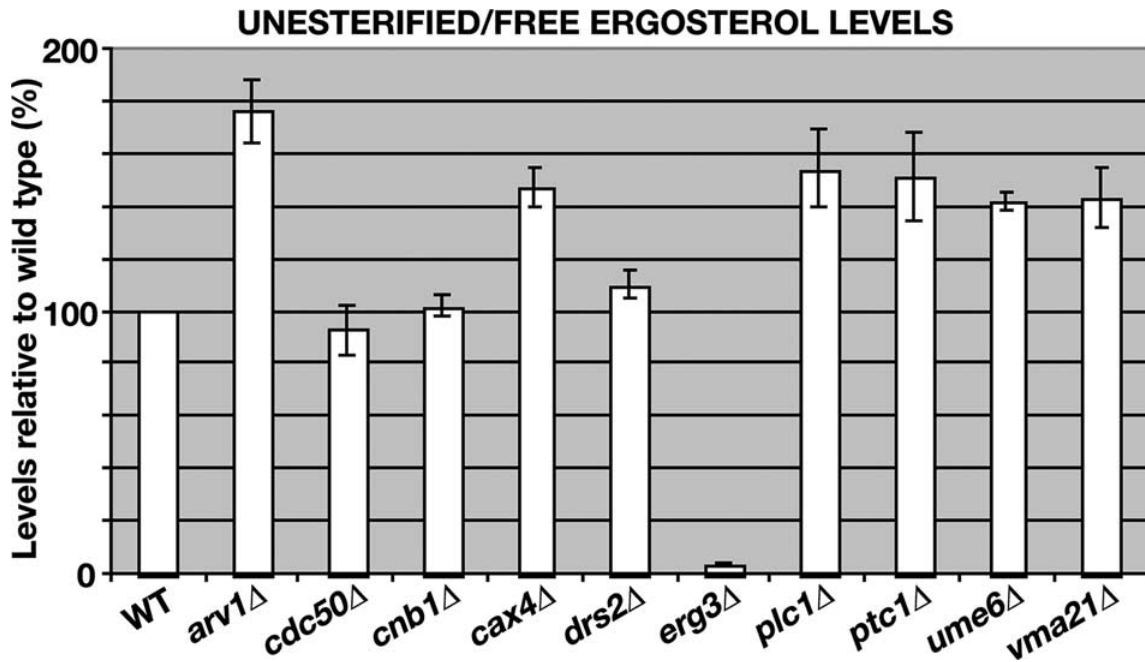
Figure 3.5.7: Levels of unesterified ergosterol were determined (see Materials and Methods) for log-phase cultures of each deletion strain shown. Amounts are expressed as a percentage relative to the wild-type (WT) level. ***This work was performed by W.F.**

Figure 3.5.8: Colocalization of FM4-64 late endosome fluorescence and internal filipin fluorescence.
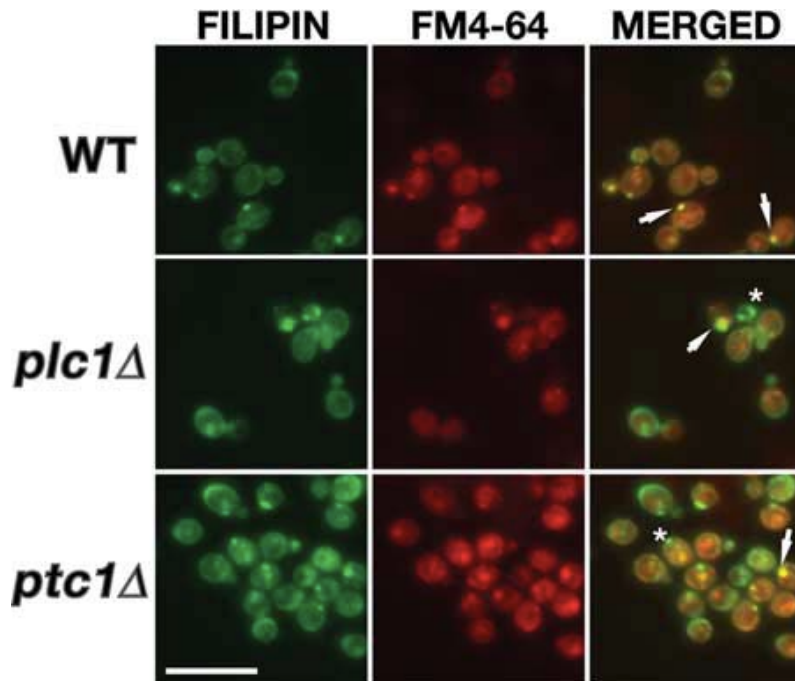
Figure 3.5.8: Wild-type (WT; BY4741), *ptc1Δ* (CBY2448), and *plc1Δ* (CBY2464) strains were incubated with FM4-64 in synthetic medium for 25 min at 30°C. Cells were fixed and stained with filipin, and the coincident staining of FM4-64-fluorescent endosomes (red) and filipin-stained membranes (false-colored green) was observed by fluorescence microscopy. In wild-type cells, internal filipin-stained spots overlapped with FM4-64-fluorescent late endosomes, as shown by arrows pointing to overlapping yellow spots in the merged image. Asterisks (*****) indicate examples of filipin-stained spots that did not colocalize with FM4-64. The colocalizations detected did not represent fluorescence bleed-through since FM4-64 was not detected by DAPI (4`,6-diamidino-2-phenylindole) fluorescence and filipin was not detected by Texas red fluorescence channels (data not shown). The scale bar for all panels is 10 μm. ***This work was performed by G.A. and Z.K.**

Figure 3.5.9: Processes and genes contributing to the maintenance of ergosterol homeostasis.
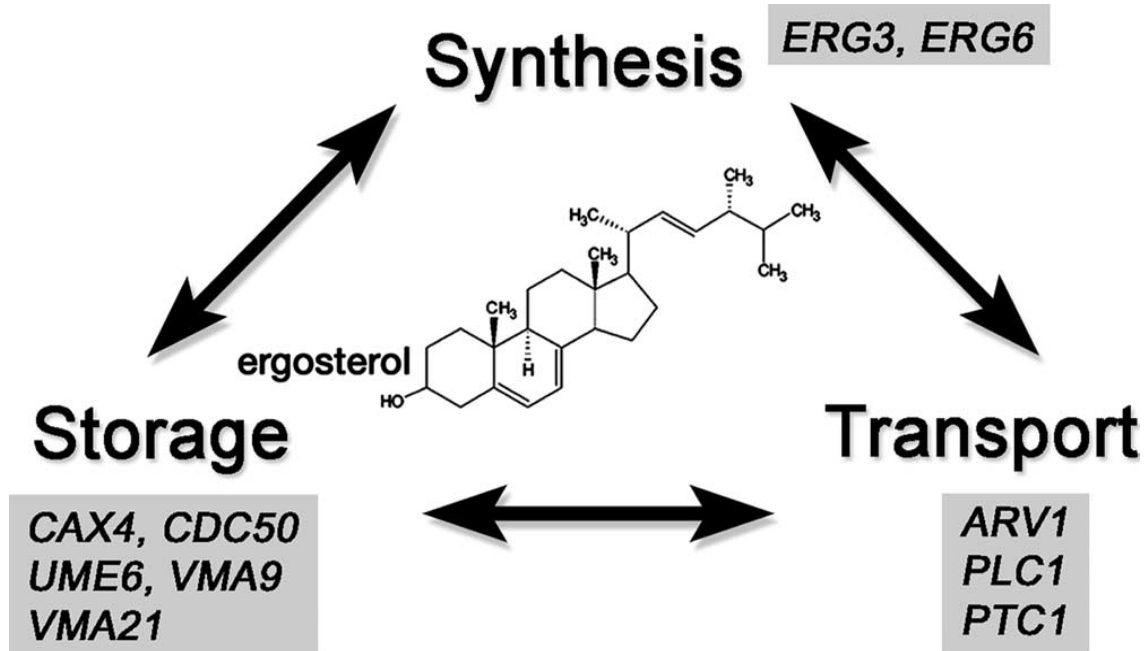
Figure 3.5.9: The control of sterol synthesis, sterol transport between membranes, and the storage of sterols as neutral lipid esters all contribute to sterol homeostasis. The functional redundancy between these processes was the premise for the genomic screen that identified 56 sterol homeostasis genes. Of the 56 genes, those whose sterol-related function was previously established, as well as those whose specific role in sterol homeostasis was determined in this study, are shown. ***This work was performed by C.T.B.**

Figure 3.5.10: A model for the initial steps in lipid storage particle biogenesis in yeast.
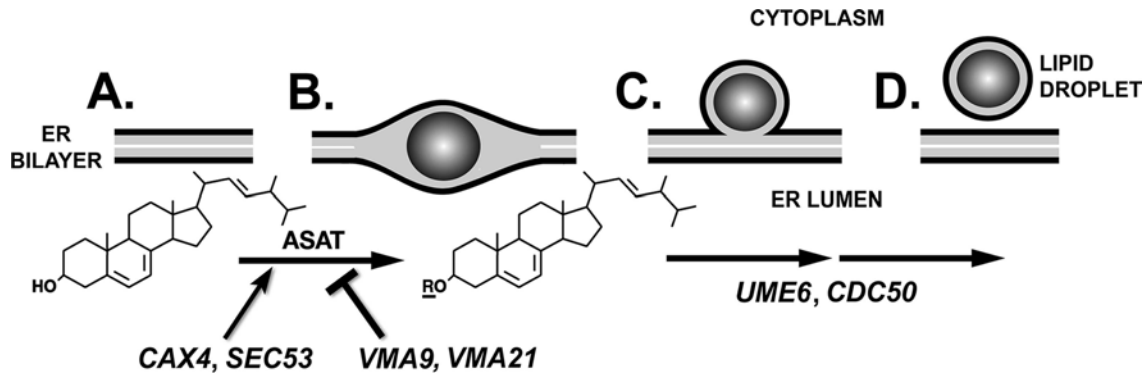
Figure 3.5.10: (A) The requisite first step in lipid droplet formation in the ER is the synthesis of neutral lipids, the core component of storage particles. (B) ASAT, encoded by *ARE1* and *ARE2*, esterifies sterols with fatty acids (*R*), which produces a major lipid component of the emerging lipid droplet. The other neutral-lipid component is triacylglycerol, which is synthesized by DGAT/PDAT. Neutral-lipid synthesis is dependent on *CAX4* and *SEC53*, whereas *VMA9* negatively affected ASAT but not DGAT/PDAT activities. (C) After synthesis, neutral lipids either coalesce spontaneously within the membrane bilayer or are actively amalgamated. The deletion of *UME6* or *CDC50* disrupted lipid droplet morphology. (D) After release from the ER, neutral lipids are sheathed in a phospholipid monolayer and resident lipid droplet proteins are associated with the periphery (Czabany et al., 2007; McCammon et al., 1984). As in mammalian cells, mature lipid droplet organelles might arise from the fusion of smaller particles and the release of stored lipid esters from formed lipid droplets is mediated by acyl-lipases. ***This work was performed by C.T.B.**

163

Tables

Table of Yeast strains used in this study

Strain	Genotype	Source or reference[a]
BY4741	*MAT*a *ura3Δ0 leu2Δ0 his3Δ1 met15Δ0*	
BY4743	*MAT*a/*MAT*α *ura3Δ0/ura3Δ0 leu2Δ0/leu2Δ0 his3Δ1/his3Δ1 met15Δ0/MET15 lys2Δ0/LYS2*	
CBY2342	BY4741/pRS416	
CBY2344	BY4741 *cnb1Δ::kan-MX4*/pRS416	
CBY2346	BY4741 *cax4Δ::kan-MX4*/pRS416	
CBY2400	BY4741/pCB419	
CBY2404	BY4741 *cax4Δ::kan-MX4*/pCB419	
CBY2408	BY4741 *cdc50Δ::kan-MX4*/pRS416	
CBY2439	BY4741 *cdc50Δ::kan-MX4*/pKT1265	
CBY2443	BY4741/pCB456	
CBY2445	BY4741 *cnb1Δ::kan-MX4*/pCB456	
CBY2446	BY4741/pPTC1-1	
CBY2448	BY4741 *ptc1Δ::kan-MX4*/pRS416	
CBY2450	BY4741 *ptc1Δ::kan-MX4*/pPTC1-1	
CBY2464	BY4741 *plc1Δ::kan-MX4*/pRS416	
CBY2485	BY4741/pKT1265	
CRY1	*MAT*a *ade2-1 can1-100 his3-11,15 leu2-3,112 trp1-1 ura3-1*	B. Fuller
JGY149	*MAT*a *ade2-1 can1-100 his3-11,15 leu2-3,112 trp1-1 ura3-1 cmd1-6*	41
JRY4130	*MAT*a *sec18 ura3-52 his4-619*	6
MMY09	*MAT*a *ade2-1 can1-100 his3-11,15 leu2-3,112 trp1-1 ura3-1 cna1::LEU2 cna2::URA3*	41
MMY41-10B	*MAT*a *ade2-1 can1-100 his3-11,15 leu2-3,112 trp1-1 ura3-1 CAN2ΔC*	41
MMY71	*MAT*a *ade2-1 can1-100 his3-11,15 leu2-3,112 trp1-1 ura3-1 cmk1Δ1::HIS3 cmk2::TRP1*	41
RSY12	*MAT*α *ura3-52 leu2-3,112 sec53-6*	R. Schekman
RSY255	*MAT*α *ura3-52 leu2-3,112*	R. Schekman
W303-1A	*MAT*a *ade2 his3 leu2 trp1 ura3 can1*	J. Nickels
YJN62	*MAT*a *ade2 his3 leu2 trp1 ura3 can1 lcb2ts*	J. Nickels
YJN63	*MAT*a *ade2 his3 leu2 trp1 ura3 can1 lcb1-100ts*	J. Nickels

[a] Unless otherwise stated, all yeast strains were created as part of this study.

Table of Plasmids used in this study

Plasmid	Markers	Source or reference[a]
pCB419	*CAX4 URA3 CEN*	
pCB456	*CNB1 URA3 CEN*	
pCB523	*VMA21 TRP1 CEN*	
pCB526	*PLC1 TRP1 CEN*	
pKT10-GAL-HA	P^{GAL}-HA *URA3* 2 μm	39
pRS416	*URA3 CEN*	
pKT1265	*CDC50 URA3 CEN*	39
pPTC1-1	*PTC1 URA3 CEN*	J. Shaw
YCplac111	*LEU2 CEN*	
YCplac111-CWH8	*CAX4 LEU2 CEN*	

[a] Unless otherwise stated, all plasmids were created as part of this study.

Table of Oligonucleotides used in this study

Primer	Corresponding gene	Sequence
CBP267	*CAX4*	5′ TGCGGATCCAGTTCACCCGC GGCG 3′
CBP268	*CAX4*	5′ CTAGGATCCGGGTATACTAGCTC CATGTAAGGAGT 3′
CBP276	*PLC1*	5′ CTAGAATTCGTCCATGAAGATTC CGCACG 3′
CBP277	*PLC1*	5′ CTAGAATTCCCAAAGGATCCTAA TTCAGTAATGCT 3′
CBP287	*VMA21*	5′ CTTCTTTAATATGGAATACCTTGG CTGG 3′
CBP288	*VMA21*	5′ ATCGTTATATATACTCATATATTT GAAAGAAAC 3′
YHP1	*CAX4*	5′ CCCAAGCTTGGGAGATTCGCATG TAATT 3′
YHP2	*CAX4*	5′ GCGGATCCCACAAACGCTCAAGA TCGC 3′

Table of Lipid droplet defects

[a] All deletion mutants identified by sterol functional/chemical genomic arrays are listed. Deletion mutants that were further analyzed for lipid storage particle defects are in boldface.

[b] Significant differences compared to wild type, as indicated by particularly low P values, are shown in boldface. P values and statistical significances compared to wild-type cells were determined by unpaired t test computed at a 95% confidence interval. P values representing trivial differences are not shown.

[c] Compared to the wild-type control (+), the observed range of Nile red fluorescence intensity is indicated by a minimum (-) to a maximum (++++).**This work was performed by G.A. and Z.K.

Strain type[a]	Avg no. of droplets/ cell[b]	Variability (SD)	P value[b]	Relative staining intensity[c]	No. counted (n)
Wild type	2.7	1.7	NA	+	363
cax4Δ	0.3	1.2	<0.0001	+	144
rad51Δ	0.5	2.1	<0.0001	+/−	100
lge1Δ	1.2	1.6	<0.0001	+	100
hof1Δ	1.3	1.5	<0.0001	+/−	100
rpl31aΔ	1.4	1.2	<0.0001	+/−	100
rmd7Δ	1.5	1.1	<0.0001	+	200
rim8Δ	1.6	1.7	<0.0001	+	100
tkl1Δ	1.6	1.8	<0.0001	+/−	100
srv2Δ	1.9	2.0	<0.0001	+	100
stp1Δ	1.9	1.5	<0.0001	+	100
van1Δ	2.1	1.9	0.002	+	100
yel045cΔ	2.2	1.7	0.02	+	63
zap1Δ	2.2	1.9	0.0051	+	100
ydl133wΔ	2.2	1.6	0.006	++	100
yjl175wΔ	2.2	2.1	0.02	+	100
tup1Δ	2.3	1.9	0.04	+	77
tfp1Δ	2.3	1.4	0.03	+	100
nut1Δ	2.5	1.3		+	100
sif2Δ	2.6	2.1		+	100
rim9Δ	2.6	1.6		+	100
vma2Δ	2.6	1.6		+	200
trp1Δ	2.7	1.6		+	100
mck1Δ	2.7	1.7		+	100
lbd7Δ	2.7	2.0		+	100
yaf9Δ	2.8	1.8		+	100
cnb1Δ	2.8	1.4		+	100
erg6Δ	2.8	1.8		++	100
plc1Δ	2.9	1.4		+	100
bck1Δ	2.9	2.8		+	92
vps28Δ	3.0	1.5		+	100
ram1Δ	3.1	1.9		+	100
soh1Δ	3.1	1.9		+	100
fyv4Δ	3.1	1.9		+	100
sac3Δ	3.1	2.6		++	100
drs2Δ	3.1	2.0	0.04	+	100
mdm39Δ	3.2	2.0	0.03	+	100
bts1Δ	3.2	2.2	0.03	+	100
erg3Δ	3.2	1.9	0.002	+	235
cin4Δ	3.5	2.0	0.0004	+	100
vma21Δ	3.5	2.3	<0.0001	+	300
taf14Δ	3.5	2.1	0.0003	+	100
cdc50Δ	3.5	1.9	<0.0001	+++	445
ptc1Δ	3.5	2.0	<0.0001	+	100
rlr1Δ	3.6	3.1	0.0005	+	100
srb5Δ	3.7	1.7	<0.0001	+	100
sin4Δ	3.9	2.5	<0.0001	+	100
pop2Δ	4.1	2.4	<0.0001	++	100
bud27Δ	4.1	3.1	<0.0001	+	100
rsc2Δ	4.1	2.4	<0.0001	+	100
vps69Δ	4.2	3.1	<0.0001	++	100
arv1Δ	4.2	3.3	<0.0001	++	171
ume6Δ	4.2	2.1	<0.0001	++++	100
vma9Δ	4.3	2.6	<0.0001	+	100
vps65Δ	4.4	2.8	<0.0001	+	92
bub1Δ	4.9	2.8	<0.0001	+	100
pho88Δ	4.9	3.3	<0.0001	+	100

166

Table of Sterol/Filipin Defects

Strain type	% Cells with internal filipin fluorescence:		No. counted (n)
	In the form of discrete spots	In membrane strands	
Wild type	15.7	8.5	363
erg3Δ	**50.0**	**1.6**	122
ptc1Δ	**41.5**	6.1	82
plc1Δ	**34.0**	12.1	215
stp1Δ	31.2	**26.6**	109
tfp1Δ	29.8	**20.2**	84
vma2Δ	27.8	**29.5**	148
srv2Δ	22.5	**28.8**	111
bts1Δ	21.3	**17.0**	141
rlr1Δ	19.9	**17.0**	171
rim8Δ	16.8	**23.2**	95
tkl1Δ	14.8	**20.4**	108
van1Δ	13.6	**16.4**	176
vps69Δ	11.5	**16.7**	96
cnb1Δ	9.7	**0.7**	298
arv1Δ	**4.3**	37.2	253

[a] The mutants listed had >2-fold the number of cells with defective intracellular sterol/filipin distribution (defined in either of the filipin fluorescence columns) compared to wild-type cells. All percentages in boldface represent statistically significant differences compared to the wild-type control ($P < 0.0001$; 95% confidence). The remaining 41 deletion mutants identified in the genomic screen had no significant differences.

*This work was performed by G.A. and Z.K.

3.6 Reference list:

Adams, A., Gottsschling, D., Kaiser, C., and Stearns, T. (1997). Methods in yeast genetics. Cold Spring Harbor Laboratory Press, Cold Spring Harbor, NY.

Arthington, B.A., Bennett, L.G., Skatrud, P.L., Guynn, C.J., Barbuch, R.J., Ulbright, C.E., and Bard, M. (1991). Cloning, disruption and sequence of the gene encoding yeast C-5 sterol desaturase. Gene *102*, 39-44.

Ashrafi, K., Chang, F.Y., Watts, J.L., Fraser, A.G., Kamath, R.S., Ahringer, J., and Ruvkun, G. (2003). Genome-wide RNAi analysis of Caenorhabditis elegans fat regulatory genes. Nature *421*, 268-272.

Athenstaedt, K., Zweytick, D., Jandrositz, A., Kohlwein, S.D., and Daum, G. (1999). Identification and characterization of major lipid particle proteins of the yeast Saccharomyces cerevisiae. J Bacteriol *181*, 6441-6448.

Basson, M. E., M. Thorsness, and J. Rine. (1986). *Saccharomyces cerevisiae* contains two functional genes encoding 3-hydroxy-3-metyhylglutaryl-coenzyme A reductase. Proc. Natl. Acad. Sci. USA *83*,5563-5567.

Beh, C.T., Brizzio, V., and Rose, M.D. (1997). KAR5 encodes a novel pheromone-inducible protein required for homotypic nuclear fusion. J Cell Biol *139*, 1063-1076.

Beh, C.T., Cool, L., Phillips, J., and Rine, J. (2001). Overlapping functions of the yeast oxysterol-binding protein homologues. Genetics *157*, 1117-1140.

Beh, C.T., and Rine, J. (2004). A role for yeast oxysterol-binding protein homologs in endocytosis and in the maintenance of intracellular sterol-lipid distribution. J Cell Sci *117*, 2983-2996.

Bensen, E.S., Costaguta, G., and Payne, G.S. (2000). Synthetic genetic interactions with temperature-sensitive clathrin in Saccharomyces cerevisiae. Roles for synaptojanin-like Inp53p and dynamin-related Vps1p in clathrin-dependent protein sorting at the trans-Golgi network. Genetics *154*, 83-97.

Chen, C.Y., Ingram, M.F., Rosal, P.H., and Graham, T.R. (1999). Role for Drs2p, a P-type ATPase and potential aminophospholipid translocase, in yeast late Golgi function. J Cell Biol *147*, 1223-1236.

Corbacho, I., Olivero, I., and Hernandez, L.M. (2005). A genome-wide screen for Saccharomyces cerevisiae nonessential genes involved in mannosyl phosphate transfer to mannoprotein-linked oligosaccharides. Fungal Genet Biol *42*, 773-790.

Cowen, L.E., and Lindquist, S. (2005). Hsp90 potentiates the rapid evolution of new traits: drug resistance in diverse fungi. Science *309*, 2185-2189.

Cruz, M.C., Goldstein, A.L., Blankenship, J.R., Del Poeta, M., Davis, D., Cardenas, M.E., Perfect, J.R., McCusker, J.H., and Heitman, J. (2002). Calcineurin is essential for survival during membrane stress in Candida albicans. EMBO J *21*, 546-559.

Czabany, T., Athenstaedt, K., and Daum, G. (2007). Synthesis, storage and degradation of neutral lipids in yeast. Biochim Biophys Acta *1771*, 299-309.

Daum, G., Lees, N.D., Bard, M., and Dickson, R. (1998). Biochemistry, cell biology and molecular biology of lipids of Saccharomyces cerevisiae. Yeast *14*, 1471-1510.

Du, X., Pham, Y.H., and Brown, A.J. (2004). Effects of 25-hydroxycholesterol on cholesterol esterification and sterol regulatory element-binding protein processing are dissociable: implications for cholesterol movement to the regulatory pool in the endoplasmic reticulum. J Biol Chem *279*, 47010-47016.

Edlind, T., Smith, L., Henry, K., Katiyar, S., and Nickels, J. (2002). Antifungal activity in Saccharomyces cerevisiae is modulated by calcium signalling. Mol Microbiol *46*, 257-268.

Fernandez, F., Rush, J.S., Toke, D.A., Han, G.S., Quinn, J.E., Carman, G.M., Choi, J.Y., Voelker, D.R., Aebi, M., and Waechter, C.J. (2001). The CWH8 gene encodes a dolichyl pyrophosphate phosphatase with a luminally oriented active site in the endoplasmic reticulum of Saccharomyces cerevisiae. J Biol Chem *276*, 41455-41464.

Flick, J.S., and Thorner, J. (1998). An essential function of a phosphoinositide-specific phospholipase C is relieved by inhibition of a cyclin-dependent protein kinase in the yeast Saccharomyces cerevisiae. Genetics *148*, 33-47.

Giaever, G., Chu, A.M., Ni, L., Connelly, C., Riles, L., Veronneau, S., Dow, S., Lucau-Danila, A., Anderson, K., Andre, B.*, et al.* (2002). Functional profiling of the Saccharomyces cerevisiae genome. Nature *418*, 387-391.

Graham, T.R. (2004). Flippases and vesicle-mediated protein transport. Trends Cell Biol *14*, 670-677.

Graham, T.R., and Emr, S.D. (1991). Compartmental organization of Golgi-specific protein modification and vacuolar protein sorting events defined in a yeast sec18 (NSF) mutant. J Cell Biol *114*, 207-218.

Heitman, J. (2005). Cell biology. A fungal Achilles' heel. Science *309*, 2175-2176.

Hill, K.J., and Stevens, T.H. (1994). Vma21p is a yeast membrane protein retained in the endoplasmic reticulum by a di-lysine motif and is required for the assembly of the vacuolar H(+)-ATPase complex. Mol Biol Cell *5*, 1039-1050.

Ho, Y., Gruhler, A., Heilbut, A., Bader, G.D., Moore, L., Adams, S.L., Millar, A., Taylor, P., Bennett, K., Boutilier, K.*, et al.* (2002). Systematic identification of protein complexes in Saccharomyces cerevisiae by mass spectrometry. Nature *415*, 180-183.

Huh, W.K., Falvo, J.V., Gerke, L.C., Carroll, A.S., Howson, R.W., Weissman, J.S., and O'Shea, E.K. (2003). Global analysis of protein localization in budding yeast. Nature *425*, 686-691.

Illingworth, R.F., Rose, A.H., and Beckett, A. (1973). Changes in the lipid composition and fine structure of Saccharomyces cerevisiae during ascus formation. J Bacteriol *113*, 373-386.

Jun, Y., Fratti, R.A., and Wickner, W. (2004). Diacylglycerol and its formation by phospholipase C regulate Rab- and SNARE-dependent yeast vacuole fusion. J Biol Chem *279*, 53186-53195.

Kepes, F., and Schekman, R. (1988). The yeast SEC53 gene encodes phosphomannomutase. J Biol Chem *263*, 9155-9161.

Kishimoto, T., Yamamoto, T., and Tanaka, K. (2005). Defects in structural integrity of ergosterol and the Cdc50p-Drs2p putative phospholipid translocase cause accumulation of endocytic membranes, onto which actin patches are assembled in yeast. Mol Biol Cell *16*, 5592-5609.

Lin, H., Nguyen, P., and Vancura, A. (2002). Phospholipase C interacts with Sgd1p and is required for expression of GPD1 and osmoresistance in Saccharomyces cerevisiae. Mol Genet Genomics *267*, 313-320.

Liscum, L., and Munn, N.J. (1999). Intracellular cholesterol transport. Biochim Biophys Acta *1438*, 19-37.

Lum, P.Y., Armour, C.D., Stepaniants, S.B., Cavet, G., Wolf, M.K., Butler, J.S., Hinshaw, J.C., Garnier, P., Prestwich, G.D., Leonardson, A.*, et al.* (2004). Discovering modes of action for therapeutic compounds using a genome-wide screen of yeast heterozygotes. Cell *116*, 121-137.

Maeda, T., Wurgler-Murphy, S.M., and Saito, H. (1994). A two-component system that regulates an osmosensing MAP kinase cascade in yeast. Nature *369*, 242-245.

Malkus, P. Graham, L., Stevens, T., and Schekman, R. (2004). Role of Vma21p in assembly and transport of the yeast vacuolar ATPase. Mol. Biol. Cell. *15*,5075-5091.

Maxfield, F.R., and Menon, A.K. (2006). Intracellular sterol transport and distribution. Curr Opin Cell Biol *18*, 379-385.

McCammon, M.T., Hartmann, M.A., Bottema, C.D., and Parks, L.W. (1984). Sterol methylation in Saccharomyces cerevisiae. J Bacteriol *157*, 475-483.

Misu, K., Fujimura-Kamada, K., Ueda, T., Nakano, A., Katoh, H., and Tanaka, K. (2003). Cdc50p, a conserved endosomal membrane protein, controls polarized growth in Saccharomyces cerevisiae. Mol Biol Cell *14*, 730-747.

Mori, K., Ogawa, N., Kawahara, T., Yanagi, H., and Yura, T. (2000). mRNA splicing-mediated C-terminal replacement of transcription factor Hac1p is required for efficient activation of the unfolded protein response. Proc Natl Acad Sci U S A *97*, 4660-4665.

Moser, M., Geiser, J., and Davis, T. (1996). Calcium-calmodulin promotes survival of pheromone-induced growth arrest by activation of calcineurin and calcium-calmodulin-dependent protein kinase. Mol. Cell. Biol. *16*,4824-4831.

Murphy, D.J., and Vance, J. (1999). Mechanisms of lipid-body formation. Trends Biochem Sci *24*, 109-115.

Nagiec, M.M., Baltisberger, J.A., Wells, G.B., Lester, R.L., and Dickson, R.C. (1994). The LCB2 gene of Saccharomyces and the related LCB1 gene encode subunits of serine palmitoyltransferase, the initial enzyme in sphingolipid synthesis. Proc Natl Acad Sci U S A *91*, 7899-7902.

Nakamura, T., Ohmoto, T., Hirata, D., Tsuchiya, E., and Miyakawa, T. (1996). Genetic evidence for the functional redundancy of the calcineurin- and Mpk1-mediated pathways in the regulation of cellular events important for growth in Saccharomyces cerevisiae. Mol Gen Genet *251*, 211-219.

Natarajan, P., Wang, J., Hua, Z., and Graham, T.R. (2004). Drs2p-coupled aminophospholipid translocase activity in yeast Golgi membranes and relationship to in vivo function. Proc Natl Acad Sci U S A *101*, 10614-10619.

Oelkers, P., Tinkelenberg, A., Erdeniz, N., Cromley, D., Billheimer, J.T., and Sturley, S.L. (2000). A lecithin cholesterol acyltransferase-like gene mediates diacylglycerol esterification in yeast. J Biol Chem *275*, 15609-15612.

Ohashi, A., Gibson, J., Gregor, I., and Schatz, G. (1982). Import of proteins into mitochondria. The precursor of cytochrome c1 is processed in two steps, one of them heme-dependent. J Biol Chem *257*, 13042-13047.

Onyewu, C., Blankenship, J.R., Del Poeta, M., and Heitman, J. (2003). Ergosterol biosynthesis inhibitors become fungicidal when combined with calcineurin inhibitors against Candida albicans, Candida glabrata, and Candida krusei. Antimicrob Agents Chemother *47*, 956-964.

Parsons, A.B., Brost, R.L., Ding, H., Li, Z., Zhang, C., Sheikh, B., Brown, G.W., Kane, P.M., Hughes, T.R., and Boone, C. (2004). Integration of chemical-genetic and genetic interaction data links bioactive compounds to cellular target pathways. Nat Biotechnol *22*, 62-69.

Parsons, A.B., Lopez, A., Givoni, I.E., Williams, D.E., Gray, C.A., Porter, J., Chua, G., Sopko, R., Brost, R.L., Ho, C.H.*, et al.* (2006). Exploring the mode-of-action of bioactive compounds by chemical-genetic profiling in yeast. Cell *126*, 611-625.

Payne, G.S., Baker, D., van Tuinen, E., and Schekman, R. (1988). Protein transport to the vacuole and receptor-mediated endocytosis by clathrin heavy chain-deficient yeast. J Cell Biol *106*, 1453-1461.

Pittet, M., Uldry, D., Aebi, M., and Conzelmann, A. (2006). The N-glycosylation defect of cwh8Delta yeast cells causes a distinct defect in sphingolipid biosynthesis. Glycobiology *16*, 155-164.

Reiner, S., Micolod, D., Zellnig, G., and Schneiter, R. (2006). A genomewide screen reveals a role of mitochondria in anaerobic uptake of sterols in yeast. Mol Biol Cell *17*, 90-103.

Rieder, S.E., Banta, L.M., Kohrer, K., McCaffery, J.M., and Emr, S.D. (1996). Multilamellar endosome-like compartment accumulates in the yeast vps28 vacuolar protein sorting mutant. Mol Biol Cell *7*, 985-999.

Robinson, M.K., van Zyl, W.H., Phizicky, E.M., and Broach, J.R. (1994). TPD1 of Saccharomyces cerevisiae encodes a protein phosphatase 2C-like activity implicated in tRNA splicing and cell separation. Mol Cell Biol *14*, 3634-3645.

Saito, K., Fujimura-Kamada, K., Furuta, N., Kato, U., Umeda, M., and Tanaka, K. (2004). Cdc50p, a protein required for polarized growth, associates with the Drs2p P-type ATPase implicated in phospholipid translocation in Saccharomyces cerevisiae. Mol Biol Cell *15*, 3418-3432.

Sambade, M., and Kane, P.M. (2004). The yeast vacuolar proton-translocating ATPase contains a subunit homologous to the Manduca sexta and bovine e subunits that is essential for function. J Biol Chem *279*, 17361-17365.

Sambrook, J., Fritsch, E., and Maniatis, T. (1989). Molecular cloning: a laboratory manual, 2nd ed. Cold Spring Harbor Laboatory Press, Col Spring Harbor, NY.

Sandager, L., Gustavsson, M.H., Stahl, U., Dahlqvist, A., Wiberg, E., Banas, A., Lenman, M., Ronne, H., and Stymne, S. (2002). Storage lipid synthesis is non-essential in yeast. J Biol Chem *277*, 6478-6482.

Severs, N. (1997). Cholesterol cytochemistry in cell biology and disease. Cubcell. Biochem. *28,*477-505.

Shitamukai, A., Hirata, D., Sonobe, S., and Miyakawa, T. (2004). Evidence for antagonistic regulation of cell growth by the calcineurin and high osmolarity glycerol pathways in Saccharomyces cerevisiae. J Biol Chem *279*, 3651-3661.

Sikorski, R.S., and Hieter, P. (1989). A system of shuttle vectors and yeast host strains designed for efficient manipulation of DNA in Saccharomyces cerevisiae. Genetics *122*, 19-27.

Soccio, R.E., and Breslow, J.L. (2004). Intracellular cholesterol transport. Arterioscler Thromb Vasc Biol *24*, 1150-1160.

Sorger, D., Athenstaedt, K., Hrastnik, C., and Daum, G. (2004). A yeast strain lacking lipid particles bears a defect in ergosterol formation. J Biol. Chem. *279,*31190-31196.

Sorger, D., and Daum, G. (2003). Triacylglycerol biosynthesis in yeast. Appl Microbiol Biotechnol *61*, 289-299.

Steck, T.L., and Lange, Y. (2002). SCAP, an ER sensor that regulates cell cholesterol. Dev Cell *3*, 306-308.

Strich, R., Surosky, R.T., Steber, C., Dubois, E., Messenguy, F., and Esposito, R.E. (1994). UME6 is a key regulator of nitrogen repression and meiotic development. Genes Dev *8*, 796-810.

Sturley, S.L. (2000). Conservation of eukaryotic sterol homeostasis: new insights from studies in budding yeast. Biochim Biophys Acta *1529*, 155-163.

Sweet, D.H., Jang, Y.K., and Sancar, G.B. (1997). Role of UME6 in transcriptional regulation of a DNA repair gene in Saccharomyces cerevisiae. Mol Cell Biol *17*, 6223-6235.

Tinkelenberg, A.H., Liu, Y., Alcantara, F., Khan, S., Guo, Z., Bard, M., and Sturley, S.L. (2000). Mutations in yeast ARV1 alter intracellular sterol distribution and are complemented by human ARV1. J Biol Chem *275*, 40667-40670.

Tisi, R., Belotti, F., Wera, S., Winderickx, J., Thevelein, J.M., and Martegani, E. (2004). Evidence for inositol triphosphate as a second messenger for glucose-induced calcium signalling in budding yeast. Curr Genet *45*, 83-89.

Tolbert, J. (2003) Lovastatin and beyond: the history of the HMG-CoA reductase inhibitors. Nat. Rev. Drug Discov. *2,* 517-526Tong, A.H., Evangelista, M., Parsons, A.B., Xu, H., Bader, G.D., Page, N., Robinson, M., Raghibizadeh, S., Hogue, C.W., Bussey, H.*, et al.* (2001). Systematic genetic analysis with ordered arrays of yeast deletion mutants. Science *294*, 2364-2368.

van Berkel, M.A., Rieger, M., te Heesen, S., Ram, A.F., van den Ende, H., Aebi, M., and Klis, F.M. (1999). The Saccharomyces cerevisiae CWH8 gene is required for full levels of dolichol-linked oligosaccharides in the endoplasmic reticulum and for efficient N-glycosylation. Glycobiology *9*, 243-253.

Vershon, A.K., and Pierce, M. (2000). Transcriptional regulation of meiosis in yeast. Curr Opin Cell Biol *12*, 334-339.

Vida, T.A., and Emr, S.D. (1995). A new vital stain for visualizing vacuolar membrane dynamics and endocytosis in yeast. J Cell Biol *128*, 779-792.

Vik, A., and Rine, J. (2001). Upc2p and Ecm22p, dual regulators of sterol biosynthesis in Saccharomyces cerevisiae. Mol Cell Biol *21*, 6395-6405.

Wach, A., Brachat, A., Pohlmann, R., and Philippsen, P. (1994). New heterologous modules for classical or PCR-based gene disruptions in Saccharomyces cerevisiae. Yeast *10*, 1793-1808.

Walker-caprioglio. H., Mackenzie, J., and Parks, L. (1989). Anti-bodies to nystatin demonstrate polyene sterol specificity and allow immunolabeling of sterols in *Saccharomyces cerevisiae.* Antimicrob. Agents Chemother. *33,*2092-2095

Winzeler, E.A., Shoemaker, D.D., Astromoff, A., Liang, H., Anderson, K., Andre, B., Bangham, R., Benito, R., Boeke, J.D., Bussey, H.*, et al.* (1999b). Functional characterization of the S. cerevisiae genome by gene deletion and parallel analysis. Science *285*, 901-906.

Woods, R. (1971). Nystatin-resistant mutants of yeast: alterations in sterol contant. J. Bacteriol. *108,*69-73.

Xu, X.X., and Tabas, I. (1991). Sphingomyelinase enhances low density lipoprotein uptake and ability to induce cholesteryl ester accumulation in macrophages. J Biol Chem *266*, 24849-24858.

Yang, H., Bard, M., Bruner, D.A., Gleeson, A., Deckelbaum, R.J., Aljinovic, G., Pohl, T.M., Rothstein, R., and Sturley, S.L. (1996). Sterol esterification in yeast: a two-gene process. Science *272*, 1353-1356.

Young, C., Mapes, J., Hanneman, J., Al-Zarban, S., and Ota, I. (2002). Role of Ptc2 type 2C Ser/Thr phosphatase in yeast high-osmolarity glycerol pathway inactivation. Eukaryot Cell *1*, 1032-1040.

Zhang, Q., Chieu, H.K., Low, C.P., Zhang, S., Heng, C.K., and Yang, H. (2003). Schizosaccharomyces pombe cells deficient in triacylglycerols synthesis undergo apoptosis upon entry into the stationary phase. J Biol Chem *278*, 47145-47155.

Zinser, E., Paltauf, F., and Daum, G. (1993). Sterol composition of yeast organelle membranes and subcellular distribution of enzymes involved in sterol metabolism. J Bacteriol *175*, 2853-2858.

Zweytick, D., Athenstaedt, K., and Daum, G. (2000). Intracellular lipid particles of eukaryotic cells. Biochim Biophys Acta *1469*, 101-120.

4: The Sterol-Binding Protein Kes1/Osh4p is a Regulator of Polarized Exocytosis

Author List: Gabriel Alfaro, Jesper Johansen, Shuba Dighe, Giselle Duamel, Keith G. Kozminski, and Christopher T. Beh.

Author Contribution: G.A designed and performed all the experiments to generate figures 4.6.1, 4.6.2, 4.6.3, 4.6.4, 4.6.7, 4.6.10, and 4.6.11. GA made the strains and performed the experiment to generate figure 4.6.6 however the $OSH2^{Y963F}$ mutant used in these strains was made by J.J. The work to generate figure 4.6.5b was performed by G.D. Although the work to generate figure 4.6.5c was done by G.A., the initial characterization of the mutant allele was performed by G.D. All work required to generate 4.6.5d was done by G.A. All aspects of the work to generate figure 4.6.8 were performed by J.J. and C.T.B. All aspects of the work to generate figures 4.6.9 and 4.6.12 was done by S.D. The majority of the writing of the manuscript was performed by C.T.B while I contributed to the results, materials and methods, and figure legends.

Abstract
Oxysterol-binding protein (OSBP)-related protein Kes1/Osh4p is implicated in nonvesicular sterol transfer between membranes in *Saccharomyces cerevisiae*. However, we found that Osh4p associated with exocytic vesicles that move from the mother cell into the bud, where Osh4p facilitated vesicle docking by the exocyst tethering complex at sites of polarized growth on the plasma membrane. Osh4p formed complexes with the small GTPases Cdc42p, Rho1p, and Sec4p, and the exocyst complex subunit Sec6p,

which was also required for Osh4p association with vesicles. Although Osh4p directly affected polarized exocytosis, its role in sterol trafficking was less clear. Contrary to what is predicted for a sterol-transfer protein, inhibition of sterol binding by the Osh4p Y97F mutation did not cause its inactivation. Rather, $OSH4^{Y97F}$ is a gain-of-function mutation that causes dominant lethality. We propose that in response to sterol binding and release Osh4p promotes efficient exocytosis through the coordinate regulation of Sac1p, a phosphoinositide 4-phosphate (PI4P) phosphatase, and the exocyst complex. These results support a model in which Osh4p acts as a sterol-dependent regulator of polarized vesicle transport, as opposed to being a sterol-transfer protein.

4.1 Introduction

As a principal component of the plasma membrane (PM), cholesterol is a key determinant of PM structure and function (Mesmin and Maxfield, 2009). Despite the overall importance of cholesterol to membrane organization, the mechanism for the intracellular trafficking of sterols between organelles is poorly understood. Apart from the exocytic vesicles that transport most proteins and phospholipids destined for the PM, a parallel "nonvesicular" pathway transfers cholesterol from its site of synthesis in the endoplasmic reticulum (ER) membrane to the PM, where sterols are concentrated (Baumann et al., 2005; Urbani and Simoni, 1990). An appealing model for nonvesicular sterol transport envisions that soluble lipid-transfer proteins ferry sterols through the cytoplasm to the PM, after their extraction from the cytoplasmic leaflets of intracellular membranes (Maxfield and Menon, 2006).

Oxysterol-binding protein-related proteins (ORPs) represent perhaps the most promising candidates for sterol-transfer proteins. The 7 ORPs in *Saccharomyces cerevisiae*, encoded by the *OSH1-OSH7* genes, and the 19 human ORPs (encoded by 12 different ORP genes), bind sterols and many are implicated in sterol-dependent regulatory pathways (Fairn and McMaster, 2008; Olkkonen and Levine, 2004). In vivo and in vitro studies suggest that the yeast ORP Kes1/Osh4p (hereafter Osh4p) affects sterol transfer between the ER and PM (Beh and Rine, 2004; Raychaudhuri et al., 2006). However, other investigations point to a role for Osh4p in post-Golgi vesicle transport (Fairn et al., 2007; Fang et al., 1996; Kozminski et al., 2006; Li et al., 2002; Muthusamy et al., 2009). Deletion of *OSH4*, for example, bypasses the essential requirement for *SEC14*, which encodes a phosphatidylcholine/phosphatidylinositol (PC/PI) transfer protein required for vesicle budding from the Golgi (Fang et al., 1996). The deletion of *OSH4* by itself, however, does not block vesicle transport from the Golgi, though Osh4p and Golgi P4-ATPase lipid-flippases have mutually antagonistic functions that affect membrane biogenesis (Muthusamy et al., 2009). These findings raise further questions about how Osh proteins and their binding of sterols might affect both nonvesicular sterol trafficking and vesicle-mediated exocytosis.

Apart from Osh4p functions at the Golgi, the *OSH* gene family is collectively required for polarized exocytosis during the last steps of polarized transport (Kozminski et al., 2006). In budding yeast cells, the release of exocytic vesicles from the actomyosin cytoskeleton is coordinated with vesicle docking at the PM, specifically at the bud tip or mother-bud junction (Park and Bi, 2007). These dynamic events can be tracked by observing the motility of Sec4p (Boyd et al., 2004), a vesicle-anchored Rab GTPase that

links exocytic vesicles to actin cables via the myosin motor Myo2p, which facilitates transport to specific docking sites in the bud (Pruyne and Bretscher, 2000; Pruyne et al., 1998; Wagner et al., 2002). When temperature-sensitive *osh*Δ *osh4-1*[ts] cells (*osh*Δ refers to the deletion of all *OSH* genes) are incubated at elevated temperatures, the entire, functionally redundant, *OSH* gene family is inactivated and GFP-Sec4p-marked vesicles transit into the bud but do not fuse with the PM (Kozminski et al., 2006). This result is consistent with the observed buildup of polarized exocytic cargo within cells after *OSH* gene inactivation (Kozminski et al., 2006)and suggests a defect in vesicle docking with the PM, as mediated by the exocyst complex. When a vesicle is closely juxtaposed to the PM, interactions between membrane- and vesicle-bound exocyst complex subunits result in vesicle docking, which actuates SNARE-mediated fusion with the PM (He and Guo, 2009). When vesicles are docked at the PM, the final assembled exocyst complex includes Sec3p and Exo70p, the Rho family GTPases Cdc42p and Rho1p (He et al., 2007; Zhang et al., 2008), and the six other subunits that are tethered to vesicles by an association with Sec4p (Novick et al., 2006). Several *OSH* family members, including *OSH4*, genetically interact with genes encoding exocyst complex subunits and their small GTPase regulators (Fang et al., 1996; Kozminski et al., 2006). Thus, there are compelling indications of a link between Osh proteins and the exocyst complex.

In this study, we describe a direct role for Osh proteins in the regulation of exocytic vesicle docking at the PM during polarized transport. We found that Osh4p is attached to post-Golgi exocytic vesicles as they are released from the Golgi and are targeted to the PM in the growing bud. Once at the PM, Osh4p facilitates vesicle docking through physical interactions with the exocyst complex and its regulators.

Structure/function analysis of mutant Osh4 proteins indicated that sterol binding is dispensable for at least some Osh4p functions, and these results present an alternative to current models positing that Osh4p acts solely as a sterol transfer protein for the nonvesicular transport of sterols. Instead, Osh4p appears to be a lipid-dependent regulator of the Sac1p PI4P phosphatase and of downstream events involving vesicle docking at sites of polarized growth at the PM.

4.2 Results

4.2.1 Docking of exocytic vesicles is defective in cells lacking functional Osh proteins

The elimination of all Osh protein function results in the depolarized localization of both Rho1p and Cdc42p, and the aberrant accumulation of Sec4p-marked vesicles within yeast cell buds (Kozminski et al., 2006). These defects are consistent with a block in vesicle/PM docking in which vesicle-bound exocyst complex subunits (Sec5p, Sec6p, Sec8p, Sec10p, Sec15p, Exo70p, Exo84p) fail to assemble with PM-bound exocyst subunits (Sec3p and Exo70p) at sites of polarized growth (Boyd et al., 2004). Other predicted defects resulting from such a failure include an accumulation of vesicle-associated exocyst complex subunits within buds, a reduction in the turn-over of these subunits after vesicle docking, and the depolarized localization of undocked subunits.

To determine how *OSH* mutants affect exocyst complex assembly, the dynamic localization of Sec5p-3xGFP, GFP-Sec4p, and GFP-Exo70p particles was analyzed in detail in wild-type, *osh∆ OSH4*, and *osh∆ osh4-1*[ts] cells cultured at 23˚C and then incubated at 37˚C for 4 h. In small-, medium-, and large-budded wild-type cells, these

179

proteins are observed at sites of polarized membrane growth corresponding to the bud tip, around the bud cortex, and at the mother-bud junction, depending on cell-cycle stage (Boyd et al., 2004) (Figure 4.6.1A,C,E). In *osh*Δ *OSH4* cells, the localization of Sec5p-3xGFP, GFP-Sec4p, and GFP-Exo70p particles to these polarized sites was similar to wild type (Figure 4.6.1A,C,E). Thus, despite the deletion of six *OSH* genes, *OSH4* expression alone was sufficient for polarized exocytosis, presumably due to functional redundancy among *OSH* genes (Beh et al., 2001). In contrast, when *osh*Δ *osh4-1*[ts] cells were incubated at 37˚C, we observed a 3-fold increase in Sec5p-3xGFP aggregation within buds relative to wild type (n > 180 cells; $p = 0.0003$), similar to the reported aggregation in GFP-Sec4p-expressing cells (Kozminski et al., 2006) (Figure 4.6.1C). Furthermore, if we quantified just discrete non-aggregated particles, in *osh*Δ *osh4-1*[ts] cells incubated at 37˚C many were mislocalized from buds into mother cells as shown by increased ratio of Sec5p-3xGFP and GFP-Sec4p particles in mother cells relative to buds (Figure 4.6.1A,C). Sec15p-3xGFP, another vesicle-associated exocyst complex subunit, was also mislocalized in *osh*Δ *osh4-1*[ts] cells (data not shown). When cultured at 23˚C, no statistically significant differences were observed for the polarized localization of GFP-Sec4p, Sec5p-3xGFP, or Sec15p-3xGFP in *osh*Δ *osh4-1*[ts] cells relative to *osh*Δ *OSH4* or wild-type cells (n > 40 cells for each strain and each marker; $p > 0.05$). For PM-associated exocyst complex subunits, the polarized localization of GFP-Sec3p was not affected in *osh*Δ *osh4-1*[ts] cells (Fang et al., 1996; Kozminski et al., 2006) and the defect in GFP-Exo70p polarized localization was moderate (2.5 fold) as compared to the 3.8-fold and 3.5-fold increases in mother/bud ratios for Sec4p and Sec5p, respectively (Figure 4.6.1E). Because Sec3p localization to the PM does not require vesicle transport,

and Exo70p is only partially dependent (Boyd et al., 2004; He et al., 2007), these results indicated that Osh protein inactivation mainly affects the localization of exocyst complex-associated proteins carried on exocytic vesicles, consistent with a vesicle-docking defect.

In Osh deficient cells, the observed accumulation of vesicles in the mother cell might result either from defective vesicle movement into the bud or a return of vesicles back into the mother cell because of the failure of vesicles to attach and then fuse with the PM. Compared to wild-type cells, 89% of Sec5p-3xGFP and 79% of GFP-Sec4p particles were properly targeted into the bud in *osh*Δ *osh4-1*[ts] cells at 37˚C, when tracked by wide-field video microscopy (n ≥ 20 vesicles). In these *osh*Δ *osh4-1*[ts] cells, the small ~10-20% of particles that stay within the mother cell do not account for the large increase in the ratio of particles in the mother cell versus the bud. Thus, in Osh deficient cells the backlog of undocked polarized exocytic vesicles results in both their accumulation within buds and their overflow back out into the mother cell.

To determine whether Osh proteins affected the lifespan/turn-over of exocyst complex proteins within the bud, wide-field video microscopy was used to monitor individual particles at the PM. In comparison to wild-type and *osh*Δ *OSH4* cells, in *osh*Δ *osh4-1*[ts] cells incubated at 37˚C we observed 1.9 to 3.4-fold increases in the lifespan of Sec5p-3xGFP, GFP-Sec4p, and GFP-Exo70p particles within the bud ($p < 0.001$), as timed immediately after particles first reached the cell cortex (Figure 4.6.1B,D,F). These findings suggested that without Osh proteins exocyst complex subunits do not dissociate from vesicles as a result of incomplete vesicle/PM docking, and the subunits therefore persist on these undocked vesicles.

4.2.2 Osh4p associates with vesicles targeted to sites of polarized growth

To address whether Osh proteins themselves associate with exocytic vesicles, we analyzed the localization of Osh4p fused to RFP (red fluorescent protein) or YFP (yellow fluorescent protein) using three-dimensional time-lapsed (4D) video confocal microscopy. Consistent with previous studies (Li et al., 2002), Osh4p-YFP was observed in wild-type cells both throughout the cytoplasm and in association with a population of punctate structures co-localizing with the Golgi-marker Kex2p-CFP (cyan fluorescent protein) (Figure 4.6.2A). In addition, we found a population of small highly motile Osh4p-YFP particles that did not co-localize with Kex2p-CFP (Figure 4.6.2A). The dynamic behavior of these smaller particles suggested they correspond to exocytic vesicles. When the motile Osh4p-RFP particles were tracked by 4D confocal microscopy (Figure 4.6.2B,C), most co-localized with the post-Golgi vesicle marker GFP-Sec4p (Schott et al., 2002). These Osh4p-RFP/GFP-Sec4p particles moved together into the bud (Figure 4.6.2 C) and congregated at sites of polarized growth on the PM (Figure 4.6.1B, arrows). This result is also consistent with previous observations using electron microscopy in which an accumulation of vesicles was seen within buds of cells lacking functional Osh proteins (Beh and Rine, 2004). These findings established that Osh4p associates with post-Golgi vesicles, providing further support for a role of Osh4p in polarized vesicular transport.

4.2.3 Osh4p association with polarized exocytic vesicles is SEC6-dependent

To test whether Osh4p association with vesicles was dependent on the exocyst complex, the association of Osh4p with exocytic vesicles was analyzed following the

disruption of exocyst complex assembly. At 37°C, the *sec6-4*[ts] mutation causes Sec6p destabilization and disrupts exocyst complex assembly (Songer and Munson, 2009), which results in the accumulation of Sec4p-marked exocytic vesicles within the bud (Walch-Solimena et al., 1997). Using *sec6-4*[ts] cells (TerBush and Novick, 1995) expressing Osh4p-YFP, we tested if the disruption of the exocyst complex affected Osh4p localization on vesicles or at sites of polarized growth at the PM. Consistent with the data above (Figure 4.6.2B), in wild-type and *sec6-4*[ts] cells cultured at 25°C, Osh4p-YFP was observed on motile particles/vesicles targeted to sites of polarized growth. Osh4p-YFP was also observed on immotile particles that co-localized with the Golgi marker Sec7p-dsRED (Losev et al., 2006)(Figure 4.6.3). After incubating *sec6-4*[ts] cells at 37°C, the motile population of Osh4p-YFP particles decreased 8.7-fold relative to that observed in wild-type cells at 37°C. Conversely, the population of immotile particles in these cells containing both Osh4p-YFP and Sec7p-dsRED increased 1.5-fold relative to wild type (Figure 4.6.3). Thus, Osh4p-YFP association with the Golgi was largely unaffected in *sec6-4*[ts] cells at 37°C, despite the increased size of Golgi as visualized with the Sec7p-dsRED marker (Figure 4.6.3). Consistent with these results, we found that Osh4p co-fractionates with membrane fractions containing exocytic vesicles, and this co-fractionation was also *SEC6* dependent. Using extracts of yeast grown at 25°C, Osh4p co-fractionated with markers of polarized exocytic vesicles (i.e. Sec4p) on 18-34% Nycodenz-sorbitol bouyant density gradients (Figure 4.6.9). When membrane extracts derived from *sec6-4*[ts] cells incubated at 37°C for 1.5 hr were centrifuged in a 18-34% Nycodenz-sorbitol buoyant density gradient, Osh4p no longer co-fractionated with markers of polarized exocytic vesicles (i.e. Sec4p and Bgl2p) (Figure 4.6.9). All together,

these results suggested that the recruitment or maintenance of Osh4p on exocytic vesicles is affected by *SEC6* and the integrity of the exocyst complex, whereas Osh4p association with the Golgi is *SEC6* independent.

4.2.4 Osh4p forms complexes with exocyst-associated proteins

Osh4p and Sec4p co-localization and co-fractionation, and genetic interactions between *OSH4* and exocyst complex regulators (Kozminski et al., 2006), suggested that Osh4p physically interacts with proteins required for vesicle docking. We first tested whether Osh4p interacts in vivo with the small GTPases required for exocyst complex formation. We found by tandem affinity purification (TAP) that the small GTPases Cdc42p and Rho1p co-purified with TAP-tagged Osh4p from detergent-treated yeast extracts, but not with TAP-tagged Tdh1p (glyceraldehyde-3-phosphate dehydrogenase [GAPDH]), which is not involved in cell polarization (Figure 4.6.4A). Non-ionic detergent was added to all extracts (unless otherwise indicated) to ensure membrane disruption and solubilization of membrane-associated proteins. These results were also confirmed by co-immunoprecipitation (coIP). An anti-Osh4p antibody immunoprecipitated endogenous Osh4p and co-precipitated endogenous Rho1p, whereas an anti-HA antibody precipitated Osh4p-2xHA and co-precipitated endogenously expressed Cdc42p (Figure 4.6.4B). Therefore, we also tested whether Osh4p might co-purify with Sec4p, the GTPase that binds exocyst subunits to the vesicle membrane (Boyd et al., 2004). Using TAP, we found that GFP-Sec4p co-purified with Osh4p-TAP from detergent-treated yeast extracts, but not with the Tdh1p-TAP control (Figure 4.6.4C). As confirmation of this result, an antibody that immunoprecipitated endogenous

Osh4p also co-precipitated Sec4p (Figure 4.6.4D). Independent from the exocyst complex, Sec4p associates with the type V myosin Myo2p (TerBush and Novick, 1995). However, in TAP experiments Osh4p did not co-purify with Myo2p (data not shown). Again this result indicated that Osh4p specifically co-precipitates exocyst complex subunits and does not interact with other Sec4p-associated complexes – even those affecting related but separate aspects of vesicle transport.

Given that Osh4p co-purified with vesicle- and PM-associated GTPases that regulate the exocyst complex, we also tested if Osh4p physically associates with Sec6p, the exocyst subunit that stabilizes the assembled exocyst complex at sites of secretion (Songer and Munson, 2009). By TAP, Osh4p-2xHA co-purified from detergent-solubilized yeast extracts with Sec6p-TAP, but not Tdh1p-TAP (Figure 4.6.4E). Similarly, an anti-GFP antibody that precipitated Sec6p-GFP also co-precipitated Osh4p-2xHA (Figure 4.6.4F). Using the same extracts and conditions, we also found that lipid-modified Ras2p did not co-precipitate with Osh4p-2xHA, indicating that Osh4p does not have a general affinity for prenylated small GTPases (Figure 4.6.4F). We also found that the exocyst subunit Sec8p-Myc coIPed with Osh4p-2xHA (data not shown). Finally, we tested whether Osh4p interactions were affected by $sec6-4^{ts}$, a mutation that reduces the association of some, but not all, exocyst complex associations (Songer and Munson, 2009; TerBush and Novick, 1995). In coIPs from extracts isolated after $sec6-4^{ts}$ cells were incubated at 37˚C, there was a 2.2-fold reduction in the amount of Osh4p-2xHA that co-purified with native Rho1p relative to coIPs from wild-type extracts (Figure 4.6.4G). In similar coIP experiments from $sec6-4^{ts}$ and wild-type cell extracts, the relative amount of Osh4p-2xHA that co-precipitated with native Sec4p was equivalent (data not shown).

Altogether, these experiments strongly suggested that Osh4p forms a functional complex in vivo with the assembled exocyst complex, and this association is affected in part by *SEC6*.

4.2.5 The Osh4(Y97F)p sterol-binding mutant increases Osh4p activity causing lethality

Sterol binding is clearly an important determinant of ORP localization and presumably for the role ORPs play in nonvesicular transfer of sterols between membranes (Beh et al., 2009). To determine how sterol binding affects Osh4p activities with respect to *SEC14* or the essential overlapping function of all *OSH* genes, we analyzed two previously engineered mutations, Osh4(L111D)p and Osh4(Y97F)p (Im et al., 2005)(Figure 4.6.5A). These mutations were designed to prevent Osh4p association with sterols (Im et al., 2005). As previously reported (Im et al., 2005), neither of these *OSH4* mutations rescued *oshΔ osh4-1*[ts] growth defects nor reversed the *osh4Δ* bypass suppression of *sec14-3*[ts] at elevated temperatures (Figure 4.6.5B). Consistent with a loss-of-function mutation, Osh4(L111D)p expression also had little impact on growth when expressed in wild-type cells (Figure 4.6.5B). At first glance, these results suggested that sterol binding is generally required for Osh4p function. However, we extended this analysis and discovered that the Y97F substitution had quite different effects. We verified that Osh4(Y97F)p does not bind sterols in vitro ((Im et al., 2005); data not shown), but our in vivo data indicated that the Y97F substitution was not a loss-of-function mutation that inactivates the Osh4 protein. When methionine was absent from the medium, the induction of P^{MET3}-*OSH4*^{Y97F} expression was lethal in *sec14-3*[ts] and *osh4Δ sec14-3*[ts] cells

even at 25˚C, a temperature at which these cells otherwise grow (Figure 4.6.5B). Expression of Osh4(Y97F)p was also lethal in *oshΔ osh4-1*[ts] cells at 25˚C, which is also a temperature at which these cells are viable (Figure 4.6.5B). Even more surprising, the expression of P[*MET3*]-*OSH4*[Y97F] at equivalent levels to endogenous *OSH4* expression caused dominant lethality in all wild-type strains tested, regardless of genotype, genetic background, or temperature and/or growth medium (Figure 4.6.5B and Figure 4.6.10; data not shown). Thus, a higher total level of Osh4 protein, or genotypic differences between strain backgrounds, was not the cause of *OSH4*[Y97F] lethality. In short, in contrast to the Osh4(L111D)p loss-of-function mutant, Osh4(Y97F)p cannot bind sterols and is a dominant mutant protein.

A possible mechanism for how *OSH4*[Y97F] affects cell growth is simply by interfering with the formation of a presumptive sterol-transport complex, acting as a dominant-negative (antimorphic) mutation (as defined by Müller (Muller, 1932)). Operationally, it is predicted that such a mutation is suppressed by increased wild-type gene dosage (Wilkie, 1994). In contrast, a dominant mutation that has acquired a completely new function (neomorph) is unaffected by increased wild-type gene dosage, whereas a dominant mutation increasing gene function (hypermorph) exhibits worsened phenotypic defects (Muller, 1932; Wilkie, 1994). Examples of the latter include gain-of-function mutations in cell signaling genes such as transforming alleles of ras (Beitel et al., 1990). To test how the dominant Y97F mutation affects *OSH4* function, we transformed P[*MET3*]-*OSH4*[Y97F] cells with a low-copy plasmid thereby increasing wild-type *OSH4* dosage (stable transformants containing both P[*MET3*]-*OSH4*[Y97F] and a multicopy *OSH4* plasmid were inviable, regardless of culture condition). At moderate (20 mg/L [+ Met])

and high methionine (100 mg/mL [++ Met]) concentrations, the P^{MET3}-$OSH4^{Y97F}$ construct was repressed, permitting cell growth (Figure 4.6.5C). In cells containing both P^{MET3}-$OSH4^{Y97F}$ and wild-type $OSH4$ plasmids, no growth was observed except at the highest levels of $OSH4^{Y97F}$ repression (++ Met) (Figure 4.6.5C). Because increased $OSH4$ dosage worsened P^{MET3}-$OSH4^{Y97F}$ defects, the Y97F substitution functions as a hypermorphic mutation that increases Osh4p activity. In addition, P^{MET3}-$OSH4^{Y97F}$ expression was still lethal in $osh4\Delta$ cells (Figure 4.6.10), which also indicated that $OSH4^{Y97F}$ is not a dominant-interfering mutation that counteracts wild-type Osh4p function. Together these findings suggested that despite its inability to bind sterols, the Osh4(Y97F)p mutation did not abolish Osh4p function, but rather amplified it.

To determine whether Osh4(Y97F)p caused specific defects in polarized exocytosis, we analyzed PM docking of GFP-Sec4p-marked exocytic vesicles in cells expressing P^{MET3}-$OSH4^{Y97F}$. After induction of P^{MET3}-$OSH4^{Y97F}$ expression, GFP-Sec4p distribution was depolarized and diffuse, and no longer detected on any particles, let alone on vesicles transiting into the bud (Figure 4.6.5D; -Met). The induced $OSH4^{Y97F}$ construct was also lethal in conditional $CDC42$, $RHO1$, and all exocyst complex mutants tested (data not shown). Together these findings suggested the increased activity of the $OSH4^{Y97F}$ mutant disrupted Sec4p-mediated polarized vesicular transport, which resulted in the observed growth defect.

The dominant-lethal $OSH4^{Y97F}$ mutation involves the substitution of a conserved tyrosine found in all Osh proteins and likely in all other ORPs regardless of species (Figure 4.6.6A). To determine whether the same residue substitution in the context of another Osh protein also confers dominant-lethality, we generated an inducible $OSH2$

allele with a substitution analogous to Y97F in Osh4p (Figure 4.6.6A). In contrast to $OSH4^{Y97F}$, P^{MET3}-$OSH2^{Y963F}$ expression in wild-type yeast did not cause any growth defects (Figure 4.6.6B). Moreover, the P^{MET3}-$OSH2^{Y963F}$ construct was able to suppress the growth defects of $osh\Delta$ $osh4$-1^{ts} (Figure 4.6.6B), indicating P^{MET3}-$OSH2^{Y963F}$ was both expressed and functional. These experiments indicated that the $OSH4^{Y97F}$ dominant growth defect was specific to that mutation in Osh4p, and the corresponding mutation in other ORPs might not have the same effect.

4.2.6 The dependence of Sec4p and Osh4p localization on sterols

The polarized exocytosis defect in $osh\Delta$ $osh4$-1 cells only affects the last steps of vesicle docking at the PM. If this defect was an indirect consequence of either diminished sterol trafficking to the PM or a general disruption in sterol homeostasis, then reduced cellular sterol concentrations would also be predicted to cause similar vesicle docking defects. First, to test whether sterol levels influence polarized exocytosis, the localization of GFP-Sec4p-marked vesicles was examined by fluorescence microscopy in $erg9\Delta$ P^{MET3}-$ERG9$ cells. In these mutant cells sterols are depleted upon methionine addition to the medium, which represses expression of Erg9p/squalene synthase (Beh and Rine, 2004). Erg9p is the first enzyme in the isoprenoid biosynthetic pathway specifically required for sterol production and it acts after the enzymatic steps that produce prenyl lipids such as those covalently attached to small GTPases (Sturley, 2000). For this reason, repression of $ERG9$ expression was used to deplete sterols because it would not directly impact the synthesis of the non-sterol isoprenoid precursors needed for other cellular processes, including the lipid modification of Sec4p. As shown in Figure 4.6.7A, GFP-

Sec4p fluorescence in the cytoplasm markedly increased in cells following Erg9p repression (Erg9p "off"). In these sterol-depleted cells, any remaining cortical GFP-Sec4p was not concentrated at sites of polarized growth. A minor amount of GFP-Sec4p perinuclear membrane fluorescence was detected in 33% of cells before Erg9p repression (n = 76 cells) and in 91% of cells after Erg9p repression (n = 108 cells). These results were in stark contrast to those observed in cells lacking Osh proteins, in which polarized exocytosis was defective but GFP-Sec4p still entered the bud and accumulated on exocytic vesicles (Kozminski et al., 2006). The differences in GFP-Sec4p distribution between *OSH* mutant cells and sterol-depleted cells suggested the role of Osh proteins in polarized exocytosis is not caused by gross changes in sterol homeostasis.

The localization of the canonical mammalian OSBP is affected by oxysterol binding (Ridgway et al., 1992), and models for ORP translocation between membranes involve a sterol binding and release cycle (Im et al., 2005). We tested whether sterol levels also influence Osh4p localization. As previously shown (Figure 4.6.1A), in wild-type cells Osh4p-YFP resides in the cytoplasm, the Golgi, and on exocytic vesicles targeted to sites of polarized growth. In sterol-depleted *erg9Δ* P^{MET3}-*ERG9* cells, however, less Osh4p-YFP was associated with motile particles (vesicles) and Osh4p-YFP was largely redistributed into the cytoplasm and to immotile particles (Figure 4.6.7B). These findings indicated that sterols influence Osh4p association with vesicles.

4.2.7 Sterols affect OSH4 regulation of SAC1 lipid signaling

In addition to binding sterols, Osh4p associates with PI lipids and several findings suggest that Osh proteins regulate Sac1p, a PI4P phosphatase (Curwin et al., 2009;

LeBlanc and McMaster, 2010; Li et al., 2002). High-level *OSH4* expression from a galactose-inducible promoter (P^{GAL}) results in reductions of PI4P and PI3P levels (LeBlanc and McMaster, 2010). Many of the same reported cellular defects in *oshΔ osh4-1* cells (Beh and Rine, 2004) are also observed in *sac1Δ* cells (Foti et al., 2001; Novick et al., 1989; Tahirovic et al., 2005). To determine if *OSH4* affects *SAC1* regulation in vivo, we tested the functional relationship of *OSH4* and *SAC1* by epistasis analysis.

If *OSH4* is an upstream regulator of *SAC1*, and if *OSH4*^{Y97F} dominant lethality is manifested through *SAC1*, then deletion of *SAC1* is predicted to suppress growth defects caused by either high-level *OSH4* expression or expression of the dominant activated allele. In wild-type cells, P^{GAL}-*OSH4* induction on galactose medium resulted in a significant growth defect, relative to growth on glucose medium in which P^{GAL}-*OSH4* expression was repressed (Figure 4.6.8A) (LeBlanc and McMaster, 2010). In contrast, the growth defect caused by P^{GAL}-*OSH4* overexpression is suppressed in *sac1Δ* cells cultured with galactose. This result is consistent with *OSH4* being an upstream regulator of *SAC1*, though both genes still might operate in parallel pathways. If *OSH* genes only function to induce *SAC1* and downstream effectors, then increasing *SAC1* expression might remove the cellular requirement for *OSH* genes. On galactose medium, the induction of P^{GAL}-*SAC1* caused a modest growth defect in wild-type, *oshΔ OSH4*, and *oshΔ osh4-1*^{ts} cells (Figure 4.6.8B). More to the point, P^{GAL}-*SAC1* did not suppress the growth defect of *oshΔ osh4-1*^{ts} cells, regardless of temperature. This finding suggests that *OSH4* and other *OSH* genes are not just upstream activators of *SAC1*, but *OSH* genes must have additional regulatory effects that are downstream or independent of *SAC1*. It is important to note that *sac1Δ* cells grow poorly in media containing non-fermentable carbon sources or

galactose (Dudley et al., 2005) and, relative to the vector control, the expression of P^{GAL}-*OSH4* partially suppresses the *sac1Δ* growth defect on galactose medium (Figure 4.6.8A). This observation again supports the conclusion that *OSH* genes have effects downstream of *SAC1*, in addition to their upstream role.

To test whether the Osh4(Y97F)p sterol-binding mutation affects *SAC1* signaling and/or other functions during polarized exocytosis, the growth of *sac1Δ* cells was analyzed in response to *OSH4*^{Y97F} expression (Figure 4.6.8C). As previously determined, in wild-type cells cultured in the absence of methionine the induction of P^{MET3}-*OSH4*^{Y97F} expression was lethal. In contrast, the deletion of *SAC1* suppressed P^{MET3}-*OSH4*^{Y97F} dominant lethality and *sac1Δ* cells expressing *OSH4*^{Y97F} were viable. These results again point to *OSH4* as an upstream activator of *SAC1*. However, a clear growth defect was still evident in *sac1Δ* cells expressing *OSH4*^{Y97F} (as compared to the vector alone control) (Figure 4.6.8B) indicating that the *OSH4*^{Y97F} allele also impacts growth through another pathway independent of *SAC1* (e.g. exocyst complex assembly).

Sac1p dephosphorylates PI4P, which is generated in vivo by the Pik1p and Stt4p PI4P kinases (Foti et al., 2001; Novick et al., 1989; Schorr et al., 2001; Tahirovic et al., 2005). Similar to *sac1Δ*, the deletion of *OSH4* suppresses the growth defects of *pik1*^{ts} cells and Osh4p directly binds PI4P (Fairn et al., 2007; Faulhammer et al., 2007; Li et al., 2002; Ridgway et al., 1992). Given the antagonistic relationship between the PI4P kinases and the Sac1p PI4P phosphatase, we predicted that constitutive activation of *SAC1* by the *OSH4*^{Y97F} mutation might negatively affect Pik1p and/or Stt4p function. As shown in Figure 4.6.8D, under conditions where the P^{MET3}-*OSH4*^{Y97F} is repressed, even the small residual expression of *OSH4*^{Y97F} was enough to severely inhibit growth of *pik1*-

101[ts] cells and, to a minor degree, *stt4-4*[ts] cells. Because Pik1p resides in the Golgi, and Stt4p localizes and affects PM PI4P levels, these results suggested that Osh4p primarily affects Pik1p function at the Golgi.

4.3   Discussion

Previous work implicated the *OSH* gene family in the maintenance of Cdc42p-dependent cell polarization and polarized exocytosis (Kozminski et al., 2006). In this study, we found that: (i) Osh4p is present on vesicles as they move from the mother cell to sites of polarized growth in the bud; (ii) in response to sterol binding Osh4p regulates the function of the Sac1p lipid phosphatase; (iii) Osh proteins interact in vivo with exocyst complex subunits and associated Rho- and Rab-family GTPases. In concert with the other Osh proteins, Osh4p facilitates exocyst complex interactions required for vesicle docking with the PM. Whereas Osh4p clearly affected polarized vesicular transport, the results did not support a direct role for Osh4p as a nonvesicular sterol-transfer protein. It stands to reason that without the capacity to bind sterols a sterol-transfer protein would be nonfunctional. Contrary to this prediction, however, an Osh4p mutant that blocked sterol binding had increased Osh4p activity. Although other studies have established that Osh proteins are in fact involved in sterol transfer (Beh and Rine, 2004; Raychaudhuri et al., 2006), our results suggest a regulatory role for Osh4p. Consistent with this conclusion, *OSH4* acts as an upstream regulator of the *SAC1* PI4P phosphatase pathway. These results thus add to other studies implicating ORPs in cell signaling, such as the role of mammalian OSBP in extracellular signal-regulated kinase (ERK) regulation (Wang et al., 2005b).

4.3.1 Osh4p is directly involved in exocyst-dependent vesicle docking

In the absence of all *OSH* function, GFP-Sec4p vesicles accumulate within the bud indicating a late defect in polarized exocytosis (Kozminski et al., 2006). In these cells, vesicles and associated Sec4 protein were no longer localized at sites of polarized growth, even though the PM exocyst components Sec3p and Exo70p were properly polarized. A simple explanation for this result is that Osh proteins activate or stabilize vesicle docking at the PM by facilitating the interaction of exocyst subunits from each membrane. However, we cannot exclude the possibility that Osh proteins are required for exocyst complex disassembly, which is likely a precondition for membrane fusion. The fact that Osh4p co-precipitated in vivo with proteins associated with the fully assembled exocyst complex also supports the conclusion that Osh proteins promote final events in the docking and assembly of the entire exocyst complex.

In addition to its observation at the Golgi and in the cytoplasm (Li et al., 2002), we detected Osh4p on moving exocytic vesicles and near sites of polarization on the PM. Our analysis showed that polarized exocytosis is a shared overlapping function of all Osh proteins, but we do not yet know if Osh proteins other than Osh4p also associate with exocytic vesicles. However, because almost all Osh proteins are free to diffuse through the cytoplasm, any Osh protein could encounter the exocyst complex if only by a stochastic mechanism. However, simple diffusion would presumably be less effective than directed transport on vesicles, which might explain why Osh4p is the most effective Osh protein at supporting vegetative growth (Beh et al., 2001). Regardless of the mechanism, Osh proteins other than Osh4p also co-precipitated with exocyst complex

subunits from yeast extracts (data not shown). These findings again suggested that the interaction with the exocyst complex is a shared property of the Osh protein family.

At the Golgi complex, none of the *OSH* genes other than *OSH4* affects *SEC14*-dependent vesicle biogenesis (Beh and Rine, 2004; Li et al., 2002), and a recent report links Sec14p to the regulation of Bgl2p polarized exocytosis (Curwin et al., 2009). As such, the genetic interaction between *OSH4* and *SEC14* might reflect a functional interaction at the trans-Golgi required for the biogenesis of Bgl2p-containing vesicles. Because the Sac1p PI4P phosphatase localizes to the ER and Golgi, and appears to act downstream of Osh4p, the role of *OSH4* in *SAC1* signaling would also be likely to occur at the Golgi. In contrast, the functional interactions between Osh4p and Sec6p (or other exocyst complex-associated subunits) involve post-Golgi events during vesicle exocytosis. With a unique role at the Golgi and a role at the PM during exocyst complex docking, Osh4p appears to coordinate polarized exocytosis both at the beginning and end of polarized vesicle transport.

4.3.2 The role of sterols in Osh4p regulation of vesicular and nonvesicular transport

In its sterol-free state, a sterol transfer protein is predicted to associate with the donor membrane where sterol binding triggers translocation of the protein with its bound lipid through the cytoplasm to the recipient membrane (Maxfield and Menon, 2006). Consistent with this model, the canonical mammalian OSBP translocates to the Golgi when bound to 25-hydroxycholesterol (Ridgway et al., 1992), though it is argued that cholesterol (not oxysterols) is the physiological ligand for ORPs (Im et al., 2005).

Accordingly, if Osh proteins are sterol transfer proteins in yeast cells, then sterol depletion would cause the translocation of Osh proteins to donor membranes to acquire sterol cargo. Instead, we found that Osh4p mainly accumulated in the cytoplasm in response to sterol depletion (Figure 4.6.7B). This result represented another challenge to models that propose Osh4p as a soluble sterol transfer protein.

Although Sec4p localization was disrupted both in cells where all *OSH* genes were inactivated and in sterol-depleted cells, the pattern of Sec4p depolarization was completely different. In sterol-depleted cells, Sec4p was dispersed into the cytoplasm indicating that Sec4p was no longer associated with membranes. In contrast, *OSH* inactivation did not affect Sec4p association with membranes, but rather Sec4p polarization along the PM was affected because of the block in exocytic vesicle docking. These differences in Sec4p localization suggested that the action of Osh proteins during vesicle docking is not an indirect effect of homeostatic changes in bulk sterol levels. On the basis of these findings, we propose that sterol binding primarily acts to regulate Osh4p signaling.

Our structure/function analysis of Osh4p indicated that its activity was dependent on membrane association, but not sterol binding per se. This conclusion was based on comparing the effects of *osh4*^{L111D} and *OSH4*^{Y97F} mutations on cell growth. The Osh4(L111D)p cannot associate with membranes irrespective of sterol binding (Im et al., 2005) and, as predicted if membrane association is required for Osh4p function, *osh4*^{L111D} was defective for all *OSH4* genetic interactions tested (Figure 4.6.5B; data not shown). In contrast, the Osh4(Y97F) protein was specifically engineered to abolish sterol binding (Im et al., 2005). Our in vivo functional tests indicated the Osh4(Y97F)p protein had

increased function, as opposed to no activity. This conclusion was supported by the finding that $OSH4^{Y97F}$ lethality was suppressed by the deletion of $SAC1$, which mimicked $sac1\Delta$ suppression of growth defects caused by $OSH4$ overexpression. Thus, the deletion of $SAC1$ suppressed growth defects whether from increases in Osh4p levels or activity. Osh4(Y97F)p expression also affected Sec4p distribution on vesicles, which is consistent with data that high-level Osh4p expression causes vesicular trafficking defects to the PM (LeBlanc and McMaster, 2010).

Because Osh4(Y97F)p exhibited increased function but cannot bind sterols, the most straightforward conclusion is that in the sterol-unbound form the wild-type Osh4 protein is activated. However, the Osh4(Y97F) protein might mimic wild-type Osh4p in a sterol-bound conformation and might bypass the requirement for sterols for its activation. Regardless, analysis of Osh4(Y97F)p showed that binding of sterols as regulatory ligands affects Osh4p activity with respect to downstream Sac1p function.

4.3.3 A model for Osh4p activities during vesicle docking

$OSH4$ was originally designated $KES1$ (<u>kre</u>11-1 <u>s</u>uppressor) because its deletion partially suppresses the resistance of $kre11-1$ cells to the antifungal protein, K1 killer toxin (Jiang et al., 1994). Kre11/Trs65p is a subunit of the TRAPPII complex, which is the guanine nucleotide exchange complex that activates the Rab GTPases Ypt31p and Ypt32p (Jones et al., 2000). The genetic interaction between $KRE11$/$TRS65$ and $OSH4$ might be an indirect effect of PI4P regulation on Ypt32p inhibition of Sec4p function. During exocytosis, the decline in PI4P levels in vesicles signals the dissociation of Ypt32p from specific Sec4p activators, which releases them to bind Sec4p. The

197

subsequent activation of Sec4p initiates the first steps in exocyst complex assembly (Mizuno-Yamasaki et al., 2010). We propose that Osh4p plays two roles in exocyst complex assembly: (i) by acting as an upstream regulator of Sac1p PI4P phosphatase activity, Osh4p affects the initial stages of exocyst complex assembly by promoting the decrease in PI4P on exocytic vesicles that releases Ypt32p from Sec4p activators; (ii) because Osh4p physically associates with exocyst complex subunits and their PM-associated regulators, and because Osh4p travels to the PM on vesicles that accumulate at the cell cortex in the absence of Osh proteins, Osh4p also affects exocyst complex assembly at the last steps of membrane docking at the PM. Consistent with this latter role, the deletion of *SAC1* did not completely suppress the growth defects caused by *OSH4* activation, indicating that *OSH4* has a secondary *SAC1*-independent function/s during polarized exocytosis.

The sterol-bound state of Osh4p affects the function of Sac1p and Pik1p, both of which reside at the Golgi. Thus, sterol pools in the Golgi and post-Golgi vesicles are determinants of Osh4p-dependent events that culminate in exocyst complex formation. Polarized exocytic vesicles contain elevated levels of ergosterol and sphingolipids relative to the Golgi membrane from which they came (Klemm et al., 2009). This finding suggests that sterols and sphingolipids are actively segregated from the Golgi membrane and enriched in polarized exocytic vesicles during their biogenesis. It is possible that Osh4p either directly participates or is recruited in response to sterol/sphingolipid sorting at the Golgi. In this scenario, the trigger for Osh4p activities for Sac1p signaling can be traced back to the process of sorting and concentrating sterols into nascent post-Golgi vesicles. These activities are in addition to the *SAC1*-independent Osh4p functions, all of

which contribute to the net outcome of exocyst complex formation and vesicle docking at the PM.

Given the many functions ascribed to various ORPs, it is difficult to define a single conserved mechanism for the entire protein family. For instance, during late endocytic transport, the mammalian ORP1L mediates regulatory interactions between the small GTPase Rab7 and the dynactin complex (Johansson et al., 2007). ORP1L mediates Rab7 exchange between regulatory complexes, which thereby aids dynein recruitment by its βIII spectrin membrane receptor. As a close Rab7 homologue, yeast Sec4p plays a similar role in mediating interactions between myosin (Myo2p) and the exocyst complex. However, despite genetic interactions between *OSH4* and *MYO2* (Figure 4.6.11), we were unable to co-precipitate Osh4p with Myo2p using TAP. Likewise, Osh4p was not detected in complexes with other molecular motors we tested (Smy1p, Kip2p, or Dyn2p). However, from such examples a general model for ORP family function may be taking shape. Depending on their sterol-bound form, Osh4p and other ORPs may simply promote the rearrangement of regulatory protein interactions in coordination with the regulation of PI signaling, potentially by regulating different Sac1p-like lipid phosphatases (Stefan et al., 2011). If this concept is considered in the context of nonvesicular sterol transport, then the role of ORPs during sterol transfer to the PM likely involves the assembly of protein complexes at membrane contact sites partly in response to PI signaling. This explanation is in accord with models proposing that ORPs facilitate sterol transfer via tethering complexes between closely apposed membranes (Schulz et al., 2009). In fact, the yeast ORP Osh1p interacts with a complex that forms a bona fide membrane contact site between the nuclear ER and the vacuole (Kvam and Goldfarb,

2004) and Osh3p mediates similar contact between the ER and the PM, which also involves Sac1p phosphatase activity (Stefan et al., 2011). Because the assembled exocyst complex is in essence a membrane contact site between exocytic vesicles and PM, the role of Osh proteins in polarized exocytosis might simply reflect a general function in promoting contact between adjoining intracellular membranes.

4.4   Materials and Methods

4.4.1 Strains, plasmids, microbial and genetic techniques

Standard methods were used for yeast strain constructions, plasmids, yeast genetic techniques and culture media (Amberg, 2005). Yeast strains and plasmids used in this study are listed in Supplemental Table S1 and S2, respectively. For Erg9p transcriptional repression in *erg9Δ* P*MET3*-*ERG9* cells (CBY745), cells were cultured for 9 hrs in synthetic medium containing 100 mg/L methionine (Beh and Rine, 2004). The method for generating Bgl2p antiserum, and test of antibody specificity, are also provided in Supplemental Materials. Descriptions of plasmid constructions are provided below; all protein fusions described were functional as proven by mutant rescue.

To construct pCB684, *OSH4* and its upstream promoter region was amplified from S288C genomic DNA using primers CBP358 (GGGGGATCCTCACAATCACTCGCGTCTAATCTC) and CBP359 (GGTAACTTAAGAGCGTAATCTGGAACATCGTATGGGTAAAGAGCGTAATCT GGAACATCGTATGGGTACAAAACAATTTCCTTTTCTTCG). The resulting *OSH4*-2xHA product was cloned into pGEM T-Easy (Promega Corp., Madison, WI) from which a *Bam*HI/*Kpn*I *OSH4*-2xHA fragment was isolated and subcloned into the same sites of

pKT10-GAL-HA, generating pCB684. To construct pCB794, *EXO70* was amplified from S288C genomic DNA using primers CBP445 (GGGGTCGACCTATCTCACTAATTGGTTAAGAACAGTAG) and CBP447 (GGGGGATCCATGCCCGCTGAAATTGACAT). The resulting *EXO70* PCR product was cloned into CloneJET (Fermentas UAB, Lithuania) from which the *Bam*HI/*Sal*I *EXO70* fragment was subcloned into the same sites in pAGX2. The resulting plasmid, pCB794, fuses *EXO70* in-frame downstream of the coding sequences of eGFP. *OSH4-*YFP, *OSH4*-RFP, and *KEX2*-CFP fusions were generated as previously described (Longtine et al., 1998). To construct pCB866, a *OSH4-YFP:HIS3* fragment was amplified from CBY4457 genomic DNA using primers CBP516 (GTCGACCGTCTAATCTCAACGGAAGCAT) and CBP517 (GGCTCCTGATTCATTAACGTGAGGATGG). The resulting PCR product was digested with *Sac*I and subcloned into the *Sac*I site in YEplac195, generating pCB866. pCB876 was constructed by re-closing pCB866 after excising a 740 bp *Stu*I/*Zra*I fragment that included part of the *URA3* gene. The missense mutation in *OSH2*(Y963F) was generated by site-direct mutagenesis using the Quick Change Lightning system as described by the manufacturer (Stratagene, La Jolla, CA). The primers used for the designed mutagenesis were CBP514 (CGGCATTTACCGCATCTTCATTCGCATCTACTACA) and CBP515 (TGTAGTAGATGCGAATGAAGATGCGGTAAATGCCG). The *OSH2*(Y963F) missense mutation was confirmed by sequencing. In the final plasmid construct (pCB851), *OSH2*(Y963F) expression was under the control of the *MET3* promoter. To

generate the P^{GAL1}-*SAC1* expression construct pCB366, *SAC1* was amplified with KpnI and SalI sites at its ends and was inserted into the KpnI/XhoI sites of pKT10-GAL-HA.

4.4.2 Fluorescence microscopy and live cell imaging

Wide field fluorescence imaging was performed as described previously (Kozminski et al., 2006). Confocal images were acquired using a Zeiss Axio Observer.Z1 microscope (Carl Zeiss International, Oberkochen, Germany) equipped with a CSU-10 Nipkow spinning disc (Yokogawa Electronic Corp., Tokyo, Japan). Z-stacks were acquired using an Improvision Piezo Focus Drive. Images were acquired using a Zeiss 100 X 1.4 N.A. Plan-Apochromat oil immersion lens and a Hamamatsu EM-CCD C9100-13 camera (Hamamatsu Photonics, Hamamatsu-city, Japan) mounted on a 1.5 X C-mount, using Volocity software (Improvision Inc., Lexington, MA, USA) for digital analysis. GFP and RFP fluorophores were excited with a 491nm and 561nm lasers respectively; emitted light was filtered with GFP ET520/40M or RFP ET593/40M emission filters (Chroma Technology Corp., Rockingham, VT). For each experiment, images were acquired with equivalent exposures and laser power. Bleed-through between fluorescence channels was not detected under the conditions used for image acquisition. To assess *p*-value statistical significance, one-way analysis of variance at a 99.99% confidence limit and subsequent Tukey's multiple comparison tests were used for scatterplot and analysis of Sec4p, Sec5p, and Exo70p polarization data. A two-tail t-test at a 95% confidence limit was used for bud-to-mother ratios of polarization, and a two-tail Fisher's exact test set at a 95% confidence interval was used for Sec5p-3xGFP

aggregation within buds. The statistical significance of all data compiled in histograms was determined at a 95% confidence interval.

4.4.3 Analyses of yeast in vivo protein-protein interactions

To isolate in vivo complexes associated with TAP-tagged proteins, TAP was performed with modifications as previously described (Roberts et al., 2006). Log-phase (1.0 OD_{600} unit/mL) yeast cells were washed in PBS and frozen in liquid nitrogen. Thawed pellets were resuspended in TAP-B1 buffer (Roberts et al., 2006) plus 0.15% NP-40 and extracts were prepared by disruption using acid-washed glass beads. Extracts were incubated for 4 hr with IgG Sepharose (GE Healthcare Bio-Sciences Corp., Piscataway, NJ) at 4˚C, washed once in TAP-B1 buffer plus 0.15% NP-40, and three times in TAP-B2 buffer (Roberts et al., 2006). For the first step in TAP isolation, purified complexes associated with TAP-tagged proteins were released from the IgG Sepharose beads after an overnight incubation in 1 mL TAP-B2 buffer with 0.1 U AcTEV Protease (Invitrogen, Carlsbad, CA) at 4˚C, and beads were pelleted by centrifugation and removed. The supernatant was retained and then incubated with calmodulin-affinity resin (Stratagene, La Jolla, CA) for 4 hr at 4˚C. The resin was washed three times in TAP-B2 buffer, and the TAP purified proteins were separated by SDS-PAGE and detected on immunoblots.

Cdc42p, Sec6p-GFP, and Osh4p-2xHA were expressed in yeast and coIPed from cellular extracts derived from log-phase yeast cells as described by Zajac et al. (Zajac et al., 2005) with modifications; protein complexes were isolated by overnight incubation with antibodies at 4˚C, and protein G- and IgG-coupled beads were incubated at 4˚C for 5

hrs. A rabbit anti-GFP polyclonal antibody (Cell Signaling Technologies, Danvers, MA) was used to precipitate Sec6p-GFP, and a mouse anti-HA monoclonal antibody (Millipore, Billerica, MA) was used to precipitate Osh4p-2xHA. Complexes were isolated using protein G Dynabeads (Invitrogen, Carlsbad, CA). As a control for nonspecific protein precipitation, cell extracts were incubated with species-specific IgG agarose (Santa Cruz Biotechnology, Santa Cruz, CA).

CoIPs with endogenous Rho1p, Sec4p, and Osh4p were conducted as described above, except cell extracts were prepared in bead buffer (50 mM Tris-HCl pH 7.4, 100 mM NaCl, 2 mM EDTA, protease inhibitor cocktail) that was diluted 1:4 with dilution buffer (60 mM Tris-HCl pH 7.4, 190 mM NaCl, 6 mM EDTA, protease inhibitor cocktail). Detergent-treated cell pellets were resuspended in bead buffer containing 1% SDS and diluted 1:4 in dilution buffer containing 1.25% Triton X-100. Rho1p was precipitated using a rabbit anti-Rho1p polyclonal antibody, and Sec4p was precipitated with a goat anti-Sec4p polyclonal antibody. The precipitated proteins in these coIP experiments were detected as described in Zajac et al. (Zajac et al., 2005).

Sec6p-GFP and Osh4p-2xHA were expressed in yeast and coIPed from cellular extracts derived from log-phase yeast cells (1.0 OD_{600} units/mL) cultured in synthetic medium. Cell pellets were washed with cold PBS and frozen in liquid nitrogen. To prepare extracts for coIP, thawed cells were resuspended in lysis buffer and disrupted as described by Zajac et al. (Zajac et al., 2005). Cell extracts were incubated for 5 hrs at 4°C with rabbit IgG agarose (Santa Cruz Biotechnology, Santa Cruz, CA), which was then pelleted by centrifugation. The IgG-conjugated agarose was washed three times in lysis buffer and retained as the control for nonspecific protein precipitation. The extract

supernatant was incubated overnight at 4˚C with a rabbit anti-GFP polyclonal antibody (Cell Signaling Technologies, Danvers, MA) and isolated using Protein G Dynabeads (Invitrogen, Carlsbad, CA). After washing three times in lysis buffer, the beads were resuspended in SDS-loading buffer and released proteins were separated and analyzed on immunoblots. Sec6p-GFP was detected on immunoblots using 1:1000 titre of rabbit anti-GFP polyclonal antibody (Cell Signaling Technologies, Danvers, MA) and a 1:5000 titre HRP-conjugated anti-rabbit light chain-specific secondary antibody (Jackson Immunoresearch Laboratories, West Grove, PA). Osh4p-2xHA was detected on immunoblots using a 1:1000 titre of a mouse anti-HA monoclonal antibody (Millipore, Billerica, MA). Cdc42p and Osh4p-2xHA coIPs were as described above except extracts were pre-incubated with mouse IgG agarose (Santa Cruz Biotechnology, Santa Cruz, CA), and a mouse anti-HA monoclonal antibody (Millipore, Billerica, MA) was used to precipitate Osh4p-2xHA. Endogenous Cdc42p was detected on immunoblots using a 1:1000 titre of an affinity-purified rabbit anti-Cdc42p polyclonal antibody.

Endogenous Rho1p and Osh4p coIPs were also conducted as described above except cell pellets were resuspended in bead buffer (50 mM Tris-HCl pH 7.4, 100 mM NaCl, 2 mM EDTA, protease inhibitor cocktail) and the extract was diluted 1:4 with dilution buffer (60 mM Tris-HCl pH 7.4, 190 mM NaCl, 6 mM EDTA, protease inhibitor cocktail). Detergent-treated cell pellets were resuspended in bead buffer containing 1% SDS and diluted 1:4 in dilution buffer containing 1.25% Triton X-100. All extracts were pre-incubated with rabbit IgG agarose before an overnight incubation at 4˚C with a rabbit anti-Rho1p polyclonal antibody. After coIP, Rho1p was detected on immunoblots using a 1:1000 titre of the rabbit anti-Rho1p polyclonal antibody, whereas Osh4p was detected on

immunoblots using a 1:750 titre of a rabbit anti-Osh4p polyclonal antibody (a gift from Dr. V. Bankaitis, UNC, Chapel Hill, NC) with the HRP-conjugated anti-rabbit light chain-specific secondary antibody. Rho1p and Osh4p-2xHA coIPs from *sec6-4* and wild-type cell extracts were performed as above except the precipitated proteins were detected on immunoblots using Millipore Snap ID (Millipore, Billerica, MA) with a 1:400 titre of Thermo clean blot HRP (Thermo Pierce, Rockford, IL) that was used to eliminate non-specific IgG cross reactivity.

The coIP of endogenous Sec4p and Osh4p was also described as above, in which cell pellets were resuspended in bead buffer containing 1% SDS and cell extracts were diluted 1:4 with dilution buffer containing 1.25% Triton X-100. The extract was incubated for 5 h at 4°C with goat IgG agarose (Santa Cruz Biotechnology, Santa Cruz, CA) and Sec4p was precipitated with a goat anti-Sec4p polyclonal antibody (Santa Cruz Biotechnology, Santa Cruz, CA). Sec4p and anti-Sec4p antibodies were isolated using Protein G Dynabeads (Invitrogen, Carlsbad, CA). The precipitated proteins were separated by SDS-PAGE and detected on immunoblots as previously outlined.

4.5   Figures

Figure 4.5.1: Localization and lifespan of exocyst-associated subunits in cells lacking *OSH* gene function.
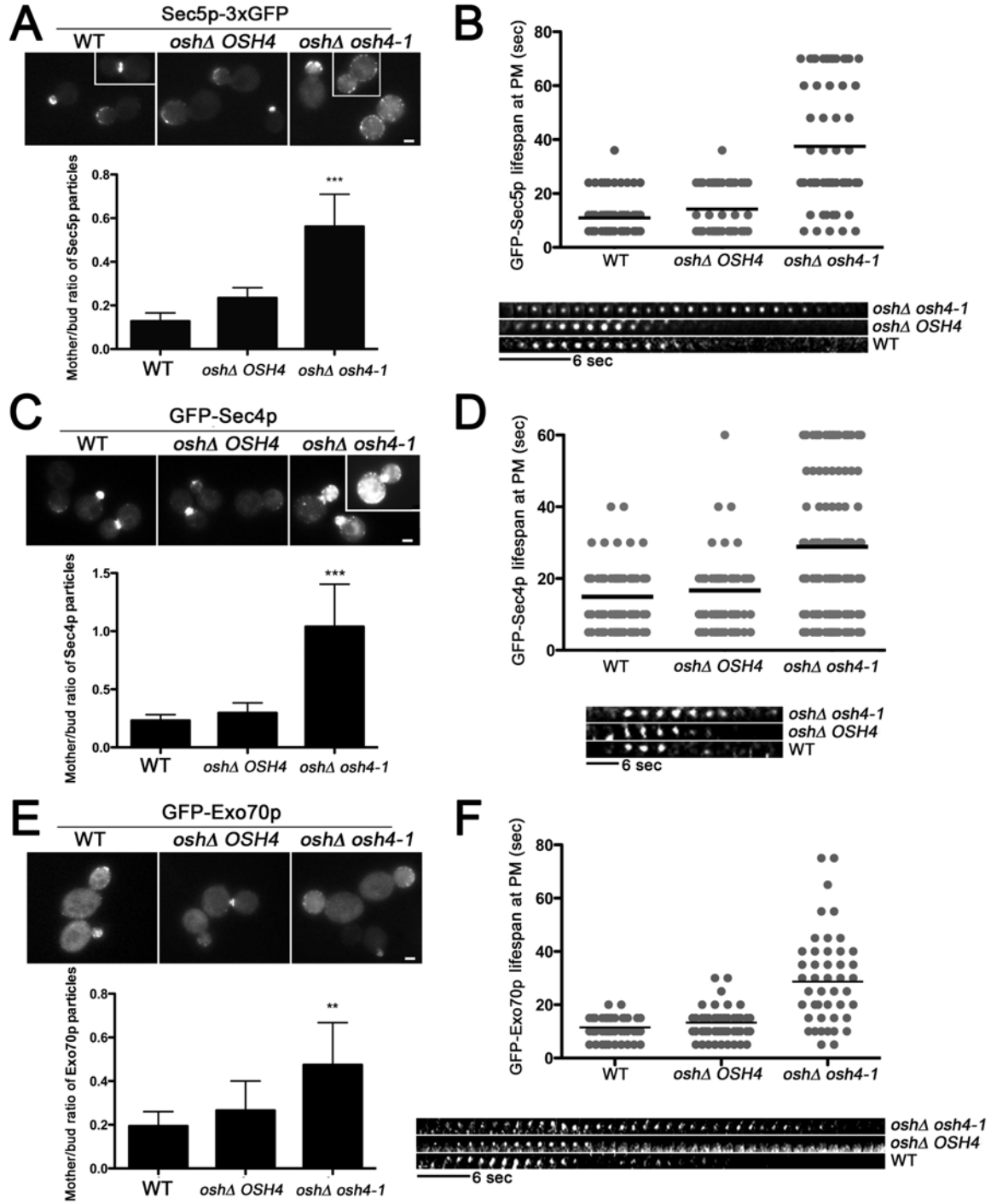
Figure 4.5.1: A and B) Sec5p-3xGFP, (C and D) GFP-Sec4p, and (E and F) GFP-Exo70p particles were tracked in log-phase wild-type (WT; SEY6210), *osh∆ OSH4* (CBY924), and *osh∆ osh4-1* cells (CBY926) cultured at 25˚C and then at 37˚C for 4 h. A and C and E) Representative cell images are shown and polarization defects are quantified in each corresponding histogram. Because discrete particles were difficult to resolve within small buds, only distinct, non-aggregated, particles in medium- and large-budded cells were counted (though this underestimates particle numbers within buds). The fraction of discrete particles in mother cells relative to those in buds is shown (1.0 indicates an even distribution between bud and mother cells, and indicates complete particle depolarization; $n \geq 181$ total particles counted in 20 – 48 cells for each strain). Single asterisk indicates $p < 0.05$, double indicates $p = 0.002$; triple asterisk indicates $p < 0.0001$. Scale bars = 2 μm. B and D and F) Scatterplots showing Sec5p-3xGFP, GFP-Sec4p, and GFP-Exo70p particle lifespans, timed immediately after their appearance at the cell cortex, were plotted per 5 s intervals from 70 s, 60 s, and 80 s time-lapse videos, respectively (n > 50 particles). Below each graph, a time series from movies show representative particle lifespans at the PM. In all experiments, statistically significant differences were evident between either *osh∆ osh4-1* and WT cells, or *osh∆ osh4-1* and *osh∆ OSH4* cells ($p < 0.0001$). ***This work was performed by G.A.**

Figure 4.5.2: Osh4p resides on vesicles targeted to sites of polarized growth
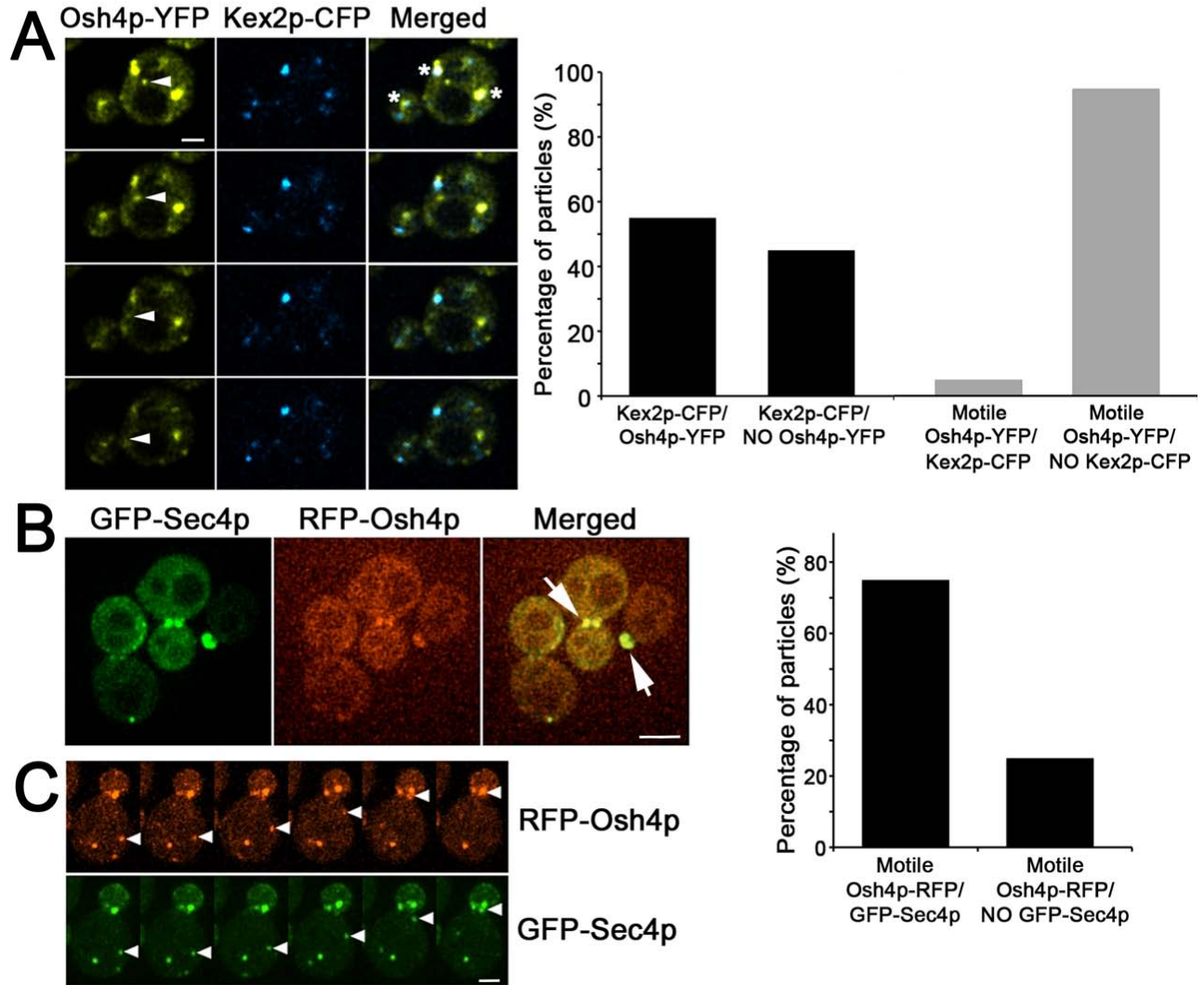
Figure 4.5.2: A) Osh4p-YFP co-localized with Kex2p-CFP Golgi on motile particles that transit into the bud. Wild-type cells (SEY6210) expressing Osh4p-YFP and Kex2p-CFP from integrated constructs were viewed by confocal microscopy. Each panel column (top to the bottom) represents images acquired at a single focal plane (1.6 s/frame). Arrowheads indicate an Osh4p-YFP motile particle moving from the mother cell towards the daughter bud. In merged images, Osh4p-YFP/Kex2p-CFP overlap is

shown in white, and asterisks indicate Osh4p-YFP particles that co-localized with Kex2p-CFP for one or more frames. Scale bar = 2 μm. B) Osh4p-RFP and GFP-Sec4p visualized by confocal microscopy in log-phase wild-type cells (SEY6210) cultured at 30˚C. The merged image shows overlap between Osh4p-RFP and GFP-Sec4p localization at the bud tip and bud neck in small-budded and large-budded cells, respectively (arrows). Scale bar = 4 μm. Co-localization of motile Osh4p-RFP particles with GFP-Sec4p is quantified in the graph. Note that increased *SEC4* dosage enhanced Osh4p-RFP fluorescence at polarized sites over that observed in (A). C) Osh4p-RFP co-localized with GFP-Sec4p post-Golgi vesicles moving from the mother cell into the bud (arrowheads). Each frame was acquired at 2.6 s intervals (0.6 s delay between Osh4p-RFP/GFP-Sec4p image acquisitions), and vesicles were tracked in one focal plane. Scale bar = 2 μm. ***This work was performed by G.A.**

Figure 4.5.3: Osh4p-YFP localization on motile (vesicle) particles was disrupted in *sec6-4*[ts] cells
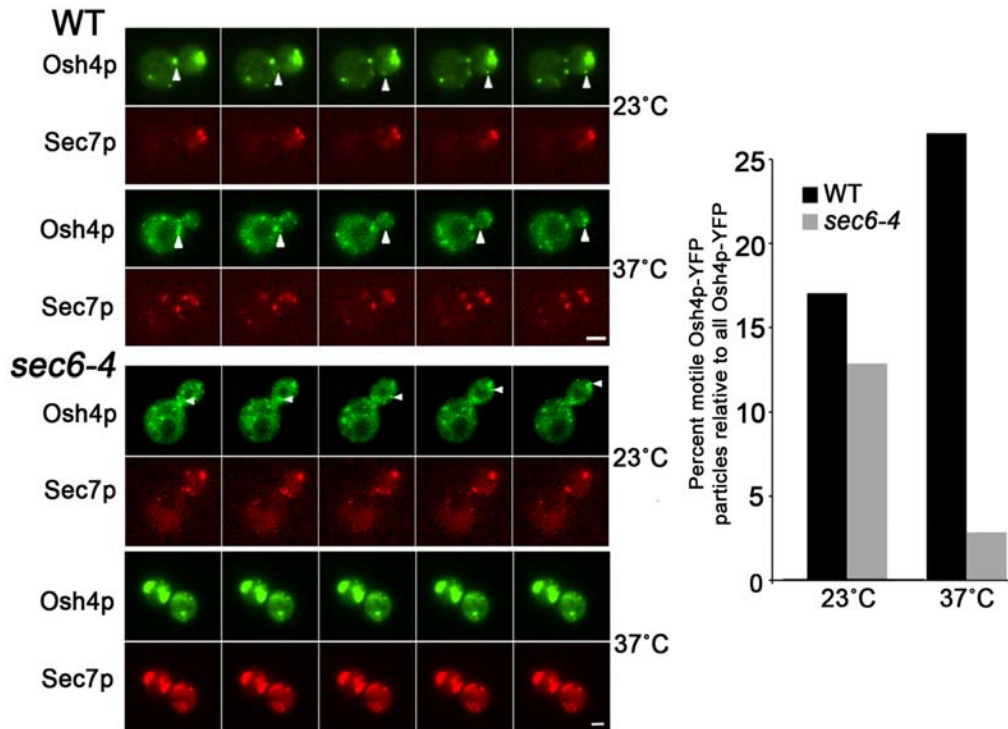
Figure 4.5.3: Images of log-phased wild-type (WT; BY4741) and *sec6-4* cells (CBY4712) transformed with plasmids expressing Osh4p-YFP (pCB876) and Sec7p-dsRED (pLC1329), cultured at 23°C or shifted to 37°C for 2 h. When either strain was cultured at 23°C, Osh4p-YFP was detected on immotile particles that co-localized with the Golgi marker Sec7p-dsRED. Osh4p-YFP was also observed on motile Sec7p-dsRED-independent vesicles (arrowheads) that moved from the mother cell into the bud. Scale bars = 2 μm. In the histogram, the relative proportions of motile Osh4p-YFP vesicles relative to all Osh4p-YFP were quantified; motile Osh4p-YFP particles did not co-localize with Sec7p-dsRED and moved for 3 consecutive frames (3 s each) in a polarized direction toward the bud. For all cells, $n \geq 162$ particles counted. ***This work was performed by G.A**

Figure 4.5.4: Osh4p interacts with exocyst complex-associated proteins.
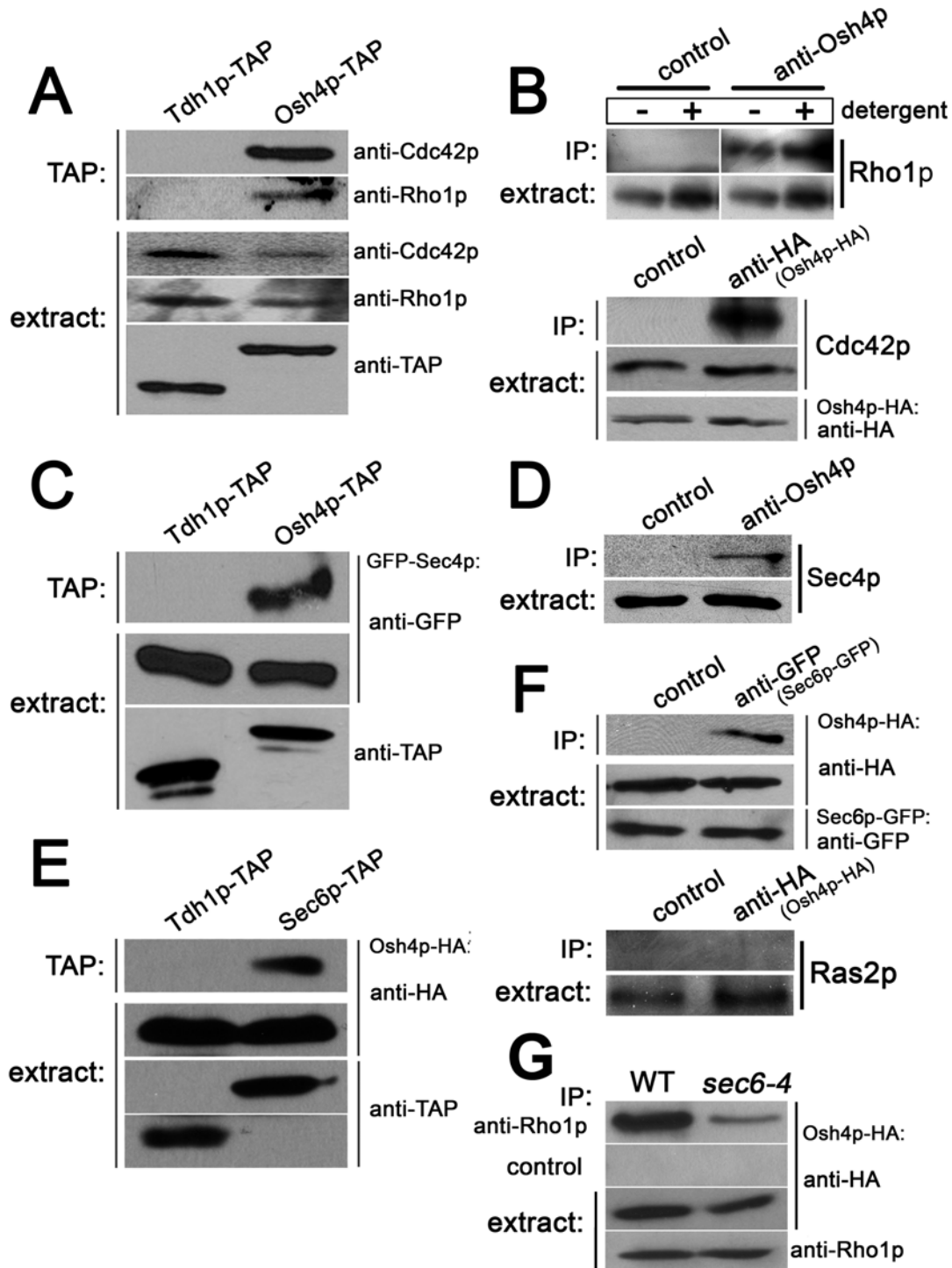
Figure 4.5.4: Immunoblots of (A) Cdc42p and Rho1p, and (C) GFP-Sec4p, before (extract) and after TAP from wild-type cells (BY4741) expressing TAP-tagged Osh4p and Tdh1p. Osh4p-TAP and Tdh1p-TAP were expressed from integrated

constructs from their endogenous promoters, and were detected with an anti-TAP antibody. Anti-Cdc42p and anti-Rho1p antibodies specifically recognized the endogenous wild-type proteins, whereas an anti-GFP antibody detected GFP-Sec4p. Crude extract samples corresponded to 1.5% of input extract used per TAP experiment. B) Immunoblots of co-precipitated Cdc42p after Osh4p-2xHA IP with an anti-HA antibody, and co-precipitated Rho1p after IP of endogenous Osh4p with an anti-Osh4p polyclonal serum. Mouse IgG-agarose and rabbit IgG-agarose were negative controls for Cdc42p and Rho1p precipitation, respectively. Rho1p co-precipitated with native Osh4p after IP in the absence or presence of 1% Triton X-100. D) As detected with an anti-Sec4p polyclonal antibody, native Sec4p co-precipitated with native Osh4p after IP with an anti-Osh4p polyclonal serum and Sec4p did not precipitate with the rabbit IgG-agarose control. E) Osh4p-2xHA co-precipitated with Sec6p-TAP from cell extracts after TAP, but Osh4p-2xHA did not precipitate with the Tdh1p-TAP negative control. F) Osh4p-2xHA co-precipitated with Sec6p-GFP after IP with the anti-GFP antibody, whereas Osh4p-2xHA was not detected upon precipitation with rabbit IgG-agarose (upper panels). From the same cell extracts, Ras2p did not co-precipitate with Osh4p-2xHA after IP with the anti-HA antibody (lower panels). G) Relative to the wild-type control, in extracts prepared from *sec6-4*[ts] cells incubated at 37˚C for 90 min 2.2-fold less Osh4p-2xHA co-precipitated with native Rho1p using an anti-Rho1p antibody (averaged from triplicate independent trials). ***This work was performed by G.A.**

Figure 4.5.5: Osh4(Y97F)p is constitutively active and dominant-lethal.
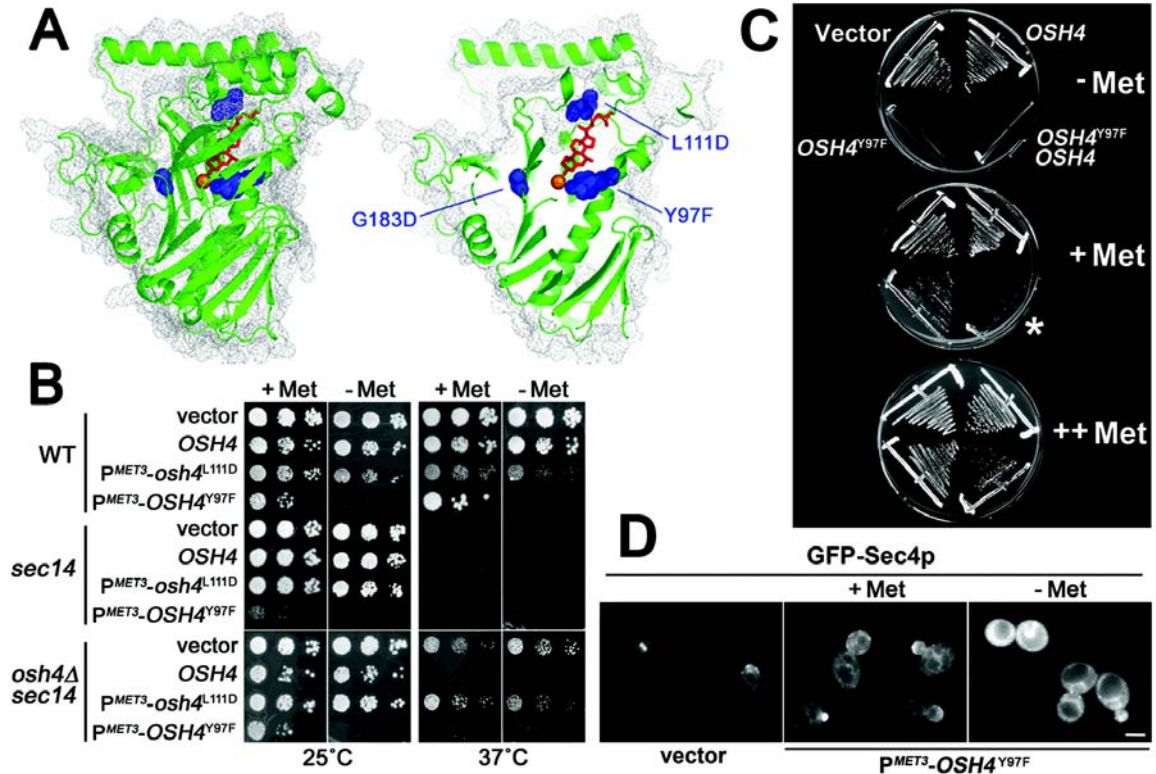
Figure 4.5.5: A) The full-length Osh4p structure (left) and the cut-away view (right) with bound sterol in red, hydrogen-bonded water in orange, and space-filling representations of mutated residues in blue. The G183D substitution corresponds to the temperature-sensitive *osh4-1*[ts] mutation (Beh and Rine, 2004). L111D is a missense mutation at the entrance to the sterol-binding cavity and disrupts membrane association (Im et al., 2005). The Y97F substitution disrupts sterol ligand binding within the protein core (Im et al., 2005). B) Ten-fold serial dilutions of cells grown from equivalent culture densities spotted onto selective media without (- Met) or with 20 mg/L methionine (+ Met), which represses the *MET3* promoter (P*MET3*). Wild-type (WT; SEY6210), *sec14-1*[ts] (CTY1-1A), and *osh4Δ sec14-1*[ts] (CBY844) cells were transformed with the vector control (YEplac195) or *OSH4* (pCB241), P*MET3*-*osh4*[L111D] (p426MET-OSH4L111D), P*MET3*-*OSH4*[Y97F] (p426MET-OSH4Y97F) multicopy plasmids. C) Wild-type cells (WT;

SEY6210) transformed with a P^{MET3}-*OSH4*^{Y97F} high-copy plasmid (p426MET-OSH4Y97F), a low-copy wild-type *OSH4* plasmid (pCB254), or both, were streaked onto solid media containing increasing methionine concentrations at the same positions shown for the top plate. In the absence of methionine (- Met), P^{MET3}-*OSH4*^{Y97F} was expressed and cell growth was inhibited. With 20 mg/L methionine (+ Met), limited P^{MET3}-*OSH4*^{Y97F} repression permitted growth but cells containing both P^{MET3}-*OSH4*^{Y97F} and wild-type *OSH4* plasmid did not grow (asterisk). The latter strain grew poorly even on 100 mg/L methionine medium (++ Met). Cells transformed with the wild-type *OSH4* plasmid grew as well as those with the vector (YEplac195). D) In diploid cells expressing P^{MET3}-*OSH4*^{Y97F} grown at 30˚C, GFP-Sec4p localization was cytoplasmic and absent from motile vesicles. Viable wild-type haploid cells that contained both GFP-*SEC4* and P^{MET3}-*OSH4*^{Y97F} plasmid constructs could not be isolated. Scale bar = 4 μm. ***Panel A performed by C.T.B, Panel B performed by G.D., Panel C and D performed by G.A.**

Figure 4.5.6: *OSH2*^{Y963F} is not dominant-lethal.

Figure 4.5.6: *OSH2*^{Y963F} is not dominant-lethal.

A

```
                          *
OSBP     480  -TVSSYST----TVFRTSKPFNPLLGETFE
Osh1p    861  -TASMYAS----TTNRVSKPFNPLLGETFE
Osh2p    959  -TASSYAS----TTKRVAKPFNPLLGETFE
Osh3p    703  SFLSIYRD----KTRTLRKPFNPLLAETFE
Osh4p     92  TLKSQYCS-RNESLGSEKKPLNPFLGELFV
Osh5p     92  TLRSQYCS-RSESMGSEKKPLNPFLGEVFV
Osh6p    108  YVMKWYLAGWHIAPKAVKKPLNPVLGEYFT
Osh7p    108  KVVAWYLAGWHIGPRAVKKPLNPILGEHFT

Consensus     TT.S.Y.SG.H.TT.RVKKPFNPLLGETFE
                 [F]
```

B

Figure 4.5.6: A) Sequence alignments of Osh1p-7p and human OSBP in regions including and adjacent to conserved tyrosines (asterisk) corresponding to Osh4p tyrosine (Y) 97, substituted for phenylalanine (F) in Osh4(Y97F)p. Solid boxes indicate amino acid identity and shaded boxes denote residue similarities. B) Equivalent culture dilutions were spotted onto solid selective medium without methionine and cultured at the temperatures indicated. P^{MET3}-*OSH2*^{Y963F} (pCB851) expression had no effect on growth in either *oshΔ OSH4* cells (CBY924) or wild-type cells (SEY6210). Compared to the control (pRS426), *OSH2*^{Y963F} rescued *oshΔ osh4-1* cells (CBY926) growth defects. ***Panel A performed by C.T.B and Panel B performed by G.A. but mutant plasmid made by J.J.**

Figure 4.5.7: GFP-Sec4p and Osh4p-YFP mislocalization after sterol depletion.
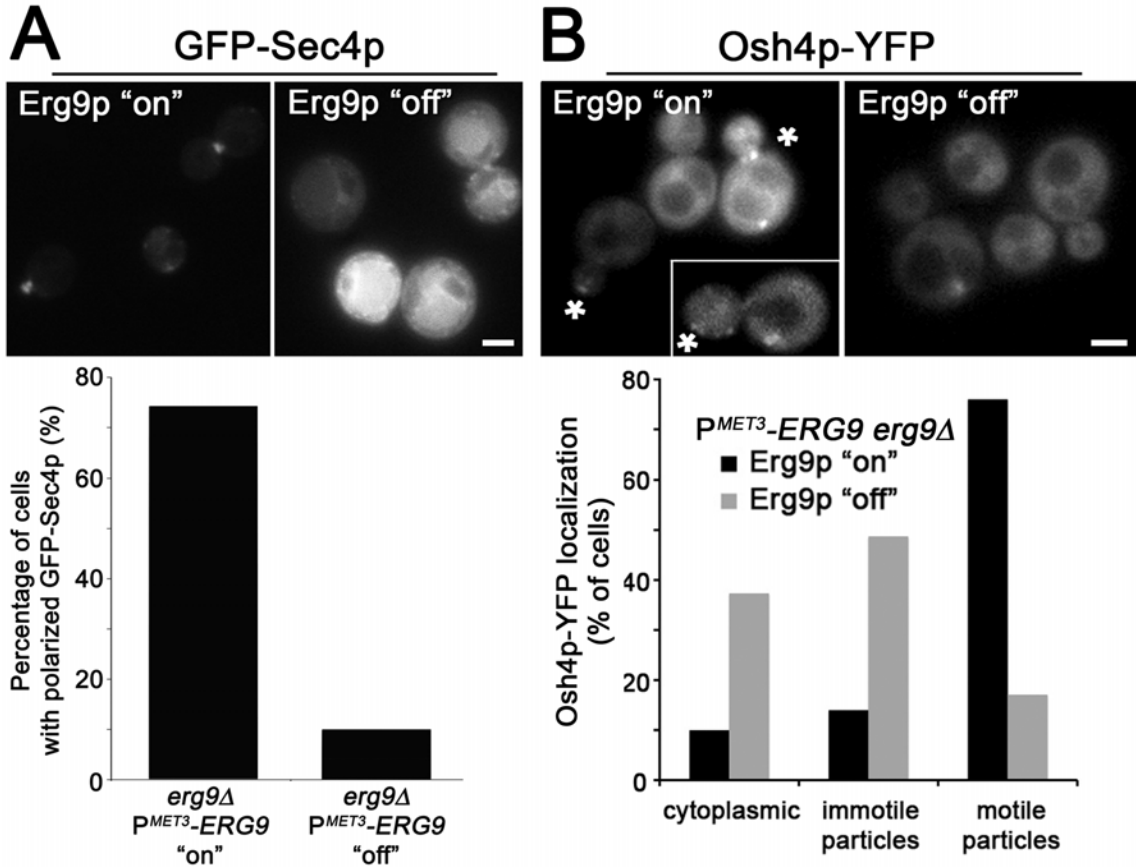
Figure 4.5.7: GFP-Sec4p (A) and Osh4p-YFP (B) localization were visualized in log-phase *erg9Δ* P*MET3*-*ERG9* cells (CBY745) grown at 30˚C. A) In sterol-depleted cells (Erg9p "off") versus sterol producing cells (Erg9p "on"), GFP-Sec4p localization on vesicles and sites of polarization was reduced, as shown in the cell images and quantified in the histogram. B) In sterol-containing cells (Erg9p "on") Osh4p-YFP was observed in the cytoplasm, at sites of polarized growth (indicated by asterisks), and motile and immotile particles. Following sterol depletion (Erg9p "off"), Osh4p-YFP on motile vesicles was reduced and cytoplasmic fluorescence increased, as quantified in the histogram. Images represent equal exposures. Scale bars = 2 μm. ***This work was performed by Gabriel Alfaro.**

Figure 4.5.8: *SAC1* deletion suppresses growth defects caused by increased *OSH4* expression or by the *OSH4*[Y97F] dominant activated allele.
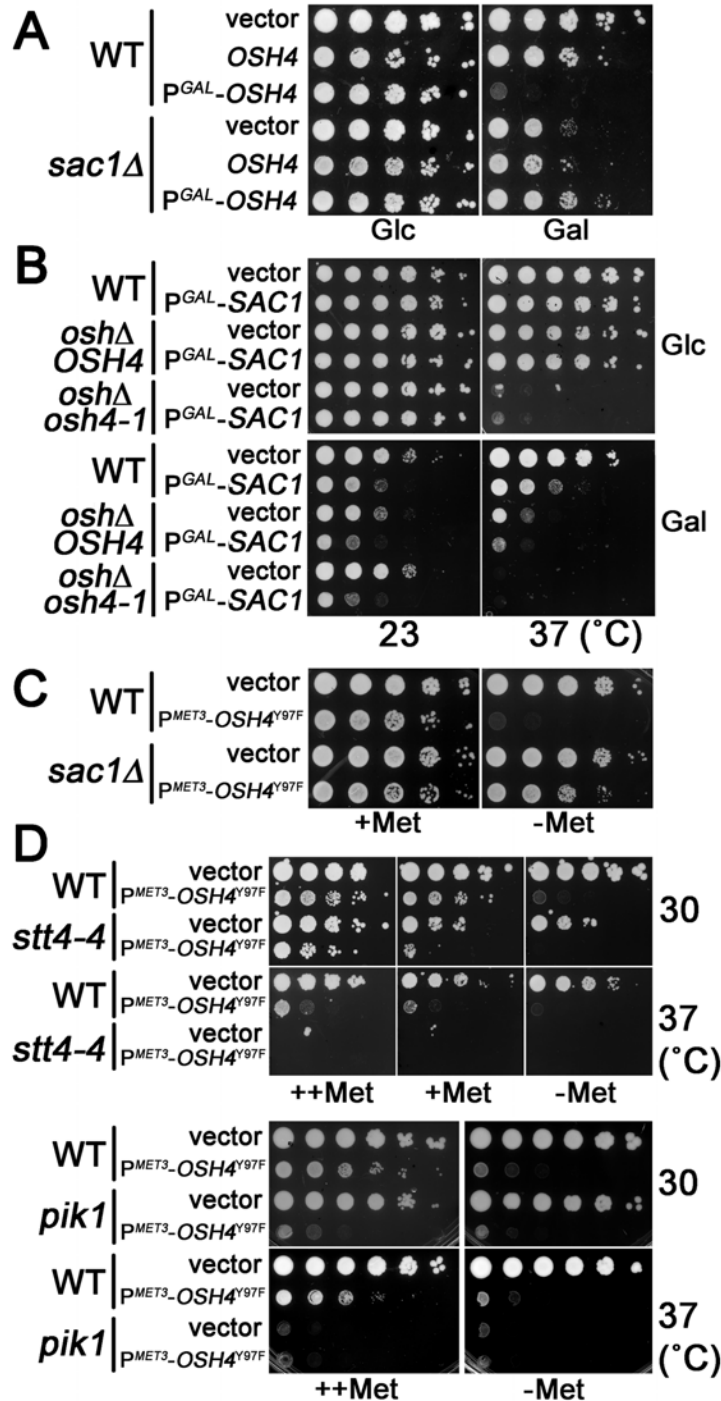
Figure 4.5.8: A) Ten-fold serial dilutions of cells grown from equivalent culture densities spotted onto solid selective media containing glucose (Glc) or galactose (Gal). Wild-type (WT; BY4741) and *sac1Δ* (CBY1730) cells were transformed with the vector

control (YEplac195), a high-copy *OSH4* plasmid (pCB241), or a high-copy P^{GAL}-*OSH4* plasmid (pCB251). When induced in the presence of galactose, P^{GAL}-*OSH4* was deleterious to wild type but not *sac1Δ* cells. B) Ten-fold serial dilutions of WT (SEY6210)*, oshΔ OSH4* (CBY924), and *oshΔ osh4-1* (CBY926) cells containing the vector control (pKT10-GAL-HA) or a plasmid expressing P^{GAL}-*SAC1* (pCB366) spotted on solid media containing either glucose (Glc) or galactose (Gal) and incubated at 23 versus 37˚C. C) Ten-fold serial dilutions of cells spotted onto selective media with 100 mg/L methionine (+ Met) or without methionine (- Met). Wild-type (WT; BY4742) and *sac1Δ* (CBY1730) cells were transformed with the vector control (pCB281) or a P^{MET3}-*OSH4*^{Y97F} high-copy plasmid (p426MET-OSH4Y97F). P^{MET3}-*OSH4*^{Y97F} expression was not lethal in *sac1Δ* cells. D) Serial dilutions of WT (SEY6210) and *stt4-4*^{ts} (AAY102) cells (upper panels), and WT (RSY255) and *pik1-101*^{ts} (NY2189) cells (lower panels), containing the vector or P^{MET3}-*OSH4*^{Y97F} plasmids spotted onto solid media containing 100 mg/L (++ Met), 20 mg/L (+ Met), or no methionine (- Met). Plates were cultured at the temperatures indicated. ***This work was performed by J.J. and C.T.B.**

Figure 4.5.9: Osh4p co-fractionates with markers of polarized exocytic vesicles in
sec6-4 cells.
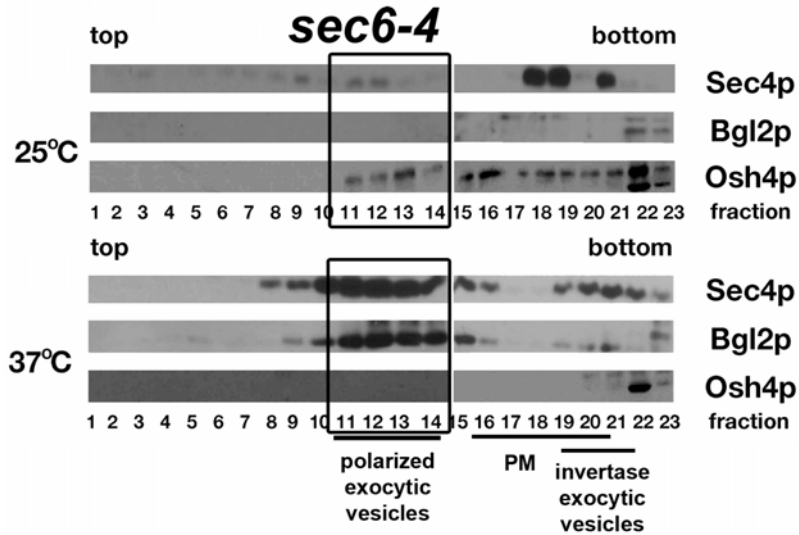
Figure 4.5.9: Immunoblots of 100,000 g pellets of diluted fractions collected from top (fraction 1) to bottom (fraction 23) of an 18-34% Nycodenz-sorbitol buoyant density gradient loaded with extracts prepared from equivalent O.D.$_{600}$ units of _sec6-4^{ts}_ (NY17) cells cultured at 25 or 37°C for 90 min. Equivalent fraction volumes were loaded in each lane for each set of blots and probed with the same antibody titre. Gradient densities corresponding to Bgl2p (polarized exocytic vesicles), invertase activity (invertase vesicles), and PM fractions are indicated. ***This work was performed by S.D. and K.G.K.**

Figure 4.5.10: P^{MET3}-*OSH4*^{Y97F} expression from a low-copy (*CEN*) plasmid produced Osh4(Y97F)p at comparable levels to endogenous Osh4p.
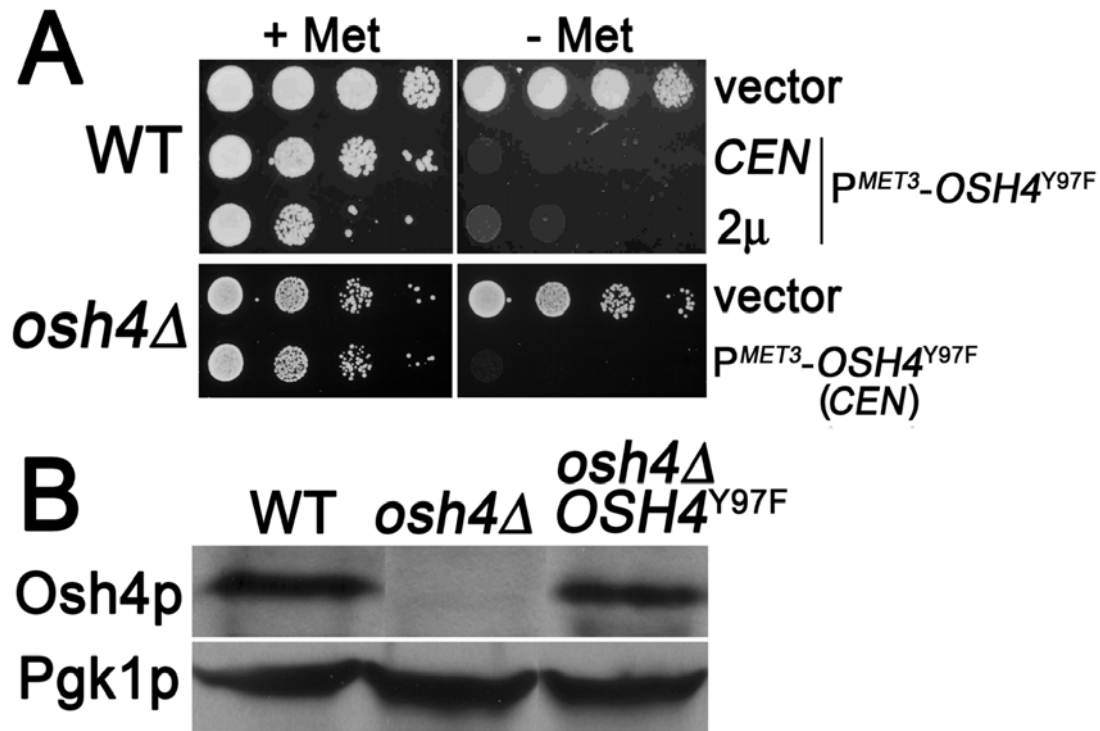
Figure 4.5.10: A) Ten-fold serial culture dilutions (left to right) of wild-type (WT; SEY6210) and *osh4*Δ (HAB821) transformants were spotted onto selective synthetic medium containing either 20 mg/L (+ Met) or no (- Met) methionine, and incubated at 30°C. Wild-type cells transformed with either *CEN*- or multicopy 2μ-based plasmids containing P^{MET3}-*OSH4*^{Y97F} (pCB743 and p426MET-OSH4Y97F, respectively) were inviable when *OSH4*^{Y97F} expression was induced (- Met), as compared to a vector control (pRS426). Expression of P^{MET3}-*OSH4*^{Y97F} on a low-copy *CEN*-based plasmid (pCB743) was also lethal in *osh4*Δ cells as compared to *osh4*Δ cells transformed with the vector control (pRS426). B) After overnight growth in medium lacking methionine,

cellular extracts were isolated from log-phase wild-type cells (WT; SEY6210), *osh4Δ* cells (HAB821), and *osh4Δ* cells that were transformed with the *CEN* plasmid containing P^{MET3}-*OSH4*^{Y97F} (pCB743). Extract proteins were separated by SDS-PAGE, after which Osh4p and Pgk1p (a loading control) were detected on separate immunoblots using anti-Osh4p and anti-Pgk1p antisera. The level of Osh4(Y97F)p was equivalent or slightly less than the endogenous level of Osh4p expressed in wild-type cells. ***This work was performed by G.A.**

Figure 4.5.11: Increased dosage of *OSH4* exacerbated growth defects of conditional *MYO2* mutants.
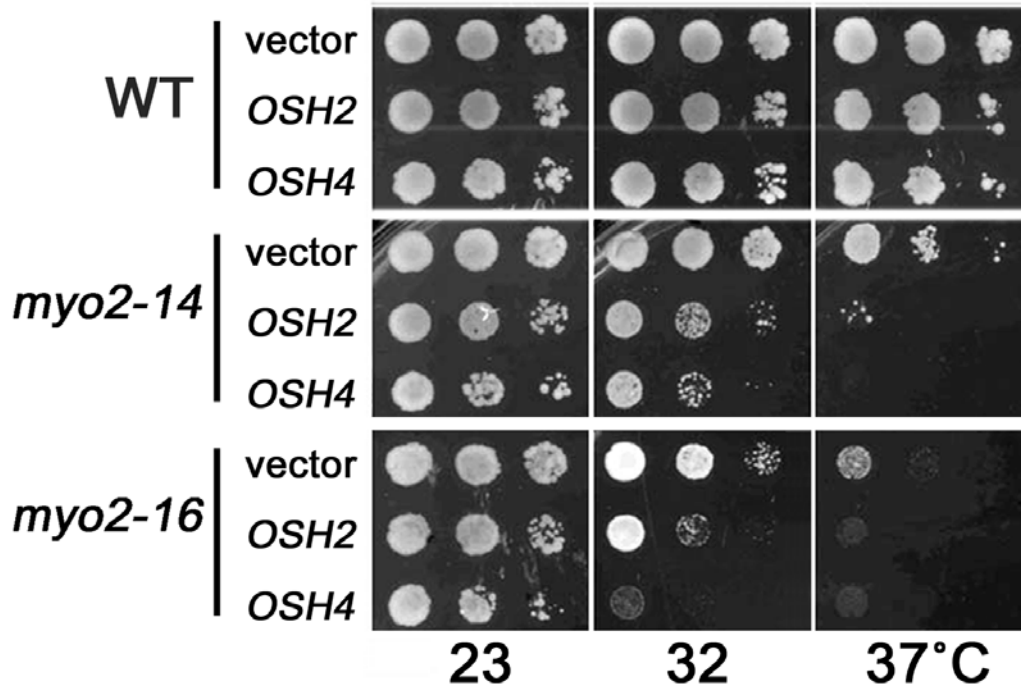
Figure 4.5.11: 10-fold serial culture dilutions were spotted onto selective synthetic medium to compare growth of wild-type (WT; ABY531), *myo2-14*[ts] (ABY534), and *myo2-16*[ts] (ABY536) cells transformed with multicopy plasmids containing *OSH2* (pCB239), *OSH4* (pCB241), or the vector alone control (pRS426). Transformed strains were incubated at 23˚C (permissive growth temperature for *myo2*[ts]), 32°C (semi-permissive growth temperature), and 37˚C (restrictive growth temperature). Multicopy *OSH4* caused growth defects at 32 and 37˚C when expressed in *myo2-14*[ts] and *-16*[ts] cells, whereas multicopy *OSH2* had a significant but lesser effect. ***This work was performed by G.A.**

4.6 Tables

4.6.1 *S. cerevisiae* strains used

Strain	Genotype	Source
AAY102	SEY6210 *stt4Δ::HIS3* [*stt4-4 CEN LEU2*]	(Audhya et al., 2000)
ABY531	*MATα ura3-52 his3Δ200 lys2-801 leu2-3,112 MYO2::HIS3*	(Schott et al., 1999)
ABY534	MATα ura3-52 his3Δ200 lys2-801 leu2-3,112 myo2-14::HIS3	(Schott et al., 1999)
ABY536	MATα ura3-52 his3Δ200 lys2-801 leu2-3,112 myo2-16::HIS3	(Schott et al., 1999)
BY4741	MATa his3Δ1 leu2Δ0 met15Δ0 ura3Δ0	(Winzeler et al., 1999a)
BY4742	MATα his3Δ1 leu2Δ0 lys2Δ0 ura3Δ0	(Winzeler et al., 1999a)
CBY33	*MATα ura3-52 his3Δ200 lys2-801am leu2-3,112 trp1Δ901 suc2Δ9 osh4Δ::HIS3*	
CBY745	*MATα ura3Δ0 leu2Δ0 lys2Δ0 erg9Δ::kan-MX4 HIS3::P^{MET3}-ERG9*	(Beh and Rine, 2004)
CBY844	*MATα ura3-52 his3Δ200 lys2-801 leu2-3,112 sec14-1 osh4Δ::HIS3*	
CBY924	SEY6210 *osh1Δ::kanMX4 osh2Δ::kanMX4 osh3Δ::LYS2 osh4Δ::HIS3 osh5Δ::LEU2 osh6Δ::LEU2 osh7Δ::HIS3* [pCB254]	(Beh and Rine, 2004)
CBY926	SEY6210 *osh1Δ::kanMX4 osh2Δ::kanMX4 osh3Δ::LYS2 osh4Δ::HIS3 osh5Δ::LEU2 osh6Δ::LEU2 osh7Δ::HIS3* [pCB255]	(Beh and Rine, 2004)
CBY1730	BY4742 *sac1Δ::kan-MX4*	(Winzeler et al., 1999a)
CBY3098	*MATa his3Δ1 leu2Δ0 lys2Δ0 ura3Δ0 SEC6-GFP:HIS3*	Invitrogen
CBY3626	*MATa his3Δ1 leu2Δ0 lys2Δ0 ura3Δ0 OSH4-TAP:HIS3*	Open Biosystems
CBY3823	*MATa his3Δ1 leu2Δ0 lys2Δ0 ura3Δ0 TDH1-TAP:HIS3*	Open Biosystems
CBY4007	*MATα ura3-52 his3Δ200 lys2-801am leu2-3,112 trp1Δ901 suc2Δ9 OSH4-mRFP:HIS3*	
CBY4457	*MATα ura3-52 his3Δ200 lys2-801am leu2-3,112 trp1Δ901 suc2Δ9 OSH4-YFP:HIS3*	
CBY4462	CBY4457 *KEX2-CFP:TRP1*	
CBY4491	*MATa his3Δ1 leu2Δ0 lys2Δ0 ura3Δ0 SEC6-*	Open

	TAP:*HIS3*	Biosystems
CBY4712	*MAT*a *his3Δ1 leu2Δ0 lys2Δ0 ura3Δ0 sec6-4:KAN-MX4*	C. Boone, University of Toronto
CTY1-1A	*MATα ura3-52 his3Δ200 lys2-801 leu2-3,112 sec14-1*	(Bankaitis et al., 1989)
DDY1300	*MAT*a *ura3-52 leu2-3,112 his3Δ200 lys2-801 CDC42:LEU2*	(Kozminski et al., 2000)
DDY1304	*MAT*a *ura3-52 leu2-3,112 his3Δ200 lys2-801 cdc42-101:LEU2*	(Kozminski et al., 2000)
DDY1326	*MAT*a *ura3-52 leu2-3,112 his3Δ200 lys2-801 cdc42-118:LEU2*	(Kozminski et al., 2000)
DDY1344	*MAT*a *ura3-52 leu2-3,112 his3Δ200 lys2-801 cdc42-129:LEU2*	(Kozminski et al., 2000)
HAB821	SEY6210 *kes1/osh4Δ::HIS3*	(Jiang et al., 1994)
HAB835	SEY6210 *swh1/osh1Δ::URA3*	(Jiang et al., 1994)
KKY37	*MAT*a *rho1-104^{ts} leu2-3, 112 ura3-52 lys2-801am*	(Kozminski et al., 2003)
NY17	*MAT*a *sec6-4^{ts} ura3-52*	(Novick et al., 1980)
NY2189	*MAT*a *leu2-3,112 ura3-52 pik1-101^{ts}*	(Walch-Solimena and Novick, 1999)
RSY255	*MATα ura3-52 leu2-3,112*	(Novick and Schekman, 1979)
SEY2102	*MATα his4-519 leu2-3,112 ura3-52 bgl2::URA3*	(Klebl and Tanner, 1989)
SEY6210	*MATα ura3-52 his3Δ200 lys2-801am leu2-3,112 trp1Δ901 suc2Δ9*	(Robinson et al., 1988)

Unless otherwise referenced, all strains were created as part of this study.

4.6.2 Plasmids used

Plasmid	Description	Source
p426MET-OSH4L111D	P^{MET3}-$osh4^{L111D}$ 2μ *URA3*	(Im et al., 2005)
p426MET-OSH4Y97F	P^{MET3}-*OSH4*^{Y97F} 2μ *URA3*	(Im et al., 2005)
pAGX2	P^{ACT1}-GFP *CEN URA3*	(Ozaki-Kuroda et al., 2001)
pCB239	*OSH2* 2μ *URA3*	(Kozminski et al., 2006)
pCB241	*OSH4* 2μ *URA3*	(Kozminski et al., 2006)
pCB251	P^{GAL}-OSH4 *2μ* URA3	
pCB254	OSH4 CEN TRP1	(Beh and Rine, 2004)
pCB255	*osh4-1*^{ts} *CEN TRP1*	(Beh and Rine, 2004)
pCB366	P^{GAL}-*SAC1* 2μ *URA3*	
pCB684	*OSH4*-2xHA 2μ *URA3*	
pCB794	P^{ACT1}-GFP-*EXO70 CEN URA3*	
pCB851	P^{MET3}-*OSH2*^{Y936F} 2μ *URA3*	
pCB866	*OSH4*-YFP:*HIS3*-MX 2μ *URA3*	
pCB876	*OSH4*-YFP:*HIS3*-MX 2μ	
pEH138	MBP-*BGL2*	E. Harsay, University of Kansas
pKT10-GAL-HA	P^{GAL}-HA 2μ *URA3*	(Misu et al., 2003)
pLC1329	*SEC7*-dsRED *CEN URA3*	E. Connibear, University of BC
pPG5-SEC5-3xGFP	*SEC5*-3xGFP *URA3*	(Boyd et al., 2004)
pPG5-SEC15-3xGFP	*SEC15*-3xGFP *URA3*	(Boyd et al., 2004)
pRC2098	GFP-*SEC4 CEN URA3*	(Calero et al., 2003)
pRS426	2μ *URA3*	(Sikorski and Hieter, 1989)
YEplac195	2μ *URA3*	(Gietz and Sugino, 1988)

Unless otherwise referenced, all plasmids were created as part of this study.

4.7   Reference List

Amberg, D.C., Burke, D.J, Strathern, J.N (2005). Methods in yeast genetics (Cold Spring Harbor, NY, Cold Spring Harbor Laboratory Press).

Audhya, A., Foti, M., and Emr, S.D. (2000). Distinct roles for the yeast phosphatidylinositol 4-kinases, Stt4p and Pik1p, in secretion, cell growth, and organelle membrane dynamics. Mol Biol Cell *11*, 2673-2689.

Bankaitis, V.A., Malehorn, D.E., Emr, S.D., and Greene, R. (1989). The Saccharomyces cerevisiae SEC14 gene encodes a cytosolic factor that is required for transport of secretory proteins from the yeast Golgi complex. J Cell Biol *108*, 1271-1281.

Baumann, N.A., Sullivan, D.P., Ohvo-Rekila, H., Simonot, C., Pottekat, A., Klaassen, Z., Beh, C.T., and Menon, A.K. (2005). Transport of newly synthesized sterol to the sterol-enriched plasma membrane occurs via nonvesicular equilibration. Biochemistry *44*, 5816-5826.

Beh, C.T., Alfaro, G., Duamel, G., Sullivan, D.P., Kersting, M.C., Dighe, S., Kozminski, K.G., and Menon, A.K. (2009). Yeast oxysterol-binding proteins: sterol transporters or regulators of cell polarization? Mol Cell Biochem *326*, 9-13.

Beh, C.T., Cool, L., Phillips, J., and Rine, J. (2001). Overlapping functions of the yeast oxysterol-binding protein homologues. Genetics *157*, 1117-1140.

Beh, C.T., and Rine, J. (2004). A role for yeast oxysterol-binding protein homologs in endocytosis and in the maintenance of intracellular sterol-lipid distribution. J Cell Sci *117*, 2983-2996.

Beitel, G.J., Clark, S.G., and Horvitz, H.R. (1990). Caenorhabditis elegans ras gene let-60 acts as a switch in the pathway of vulval induction. Nature *348*, 503-509.

Boyd, C., Hughes, T., Pypaert, M., and Novick, P. (2004). Vesicles carry most exocyst subunits to exocytic sites marked by the remaining two subunits, Sec3p and Exo70p. J Cell Biol *167*, 889-901.

Calero, M., Chen, C.Z., Zhu, W., Winand, N., Havas, K.A., Gilbert, P.M., Burd, C.G., and Collins, R.N. (2003). Dual prenylation is required for Rab protein localization and function. Mol Biol Cell *14*, 1852-1867.

Curwin, A.J., Fairn, G.D., and McMaster, C.R. (2009). Phospholipid transfer protein Sec14 is required for trafficking from endosomes and regulates distinct trans-Golgi export pathways. J Biol Chem *284*, 7364-7375.

Dudley, A.M., Janse, D.M., Tanay, A., Shamir, R., and Church, G.M. (2005). A global view of pleiotropy and phenotypically derived gene function in yeast. Mol Syst Biol *1*, 2005 0001.

Fairn, G.D., Curwin, A.J., Stefan, C.J., and McMaster, C.R. (2007). The oxysterol binding protein Kes1p regulates Golgi apparatus phosphatidylinositol-4-phosphate function. Proc Natl Acad Sci U S A *104*, 15352-15357.

Fairn, G.D., and McMaster, C.R. (2008). Emerging roles of the oxysterol-binding protein family in metabolism, transport, and signaling. Cell Mol Life Sci *65*, 228-236.

Fang, M., Kearns, B.G., Gedvilaite, A., Kagiwada, S., Kearns, M., Fung, M.K., and Bankaitis, V.A. (1996). Kes1p shares homology with human oxysterol binding protein and participates in a novel regulatory pathway for yeast Golgi-derived transport vesicle biogenesis. EMBO J *15*, 6447-6459.

Faulhammer, F., Kanjilal-Kolar, S., Knodler, A., Lo, J., Lee, Y., Konrad, G., and Mayinger, P. (2007). Growth control of Golgi phosphoinositides by reciprocal localization of sac1 lipid phosphatase and pik1 4-kinase. Traffic *8*, 1554-1567.

Foti, M., Audhya, A., and Emr, S.D. (2001). Sac1 lipid phosphatase and Stt4 phosphatidylinositol 4-kinase regulate a pool of phosphatidylinositol 4-phosphate that functions in the control of the actin cytoskeleton and vacuole morphology. Mol Biol Cell *12*, 2396-2411.

Gietz, R.D., and Sugino, A. (1988). New yeast-Escherichia coli shuttle vectors constructed with in vitro mutagenized yeast genes lacking six-base pair restriction sites. Gene *74*, 527-534.

He, B., and Guo, W. (2009). The exocyst complex in polarized exocytosis. Curr Opin Cell Biol *21*, 537-542.

He, B., Xi, F., Zhang, X., Zhang, J., and Guo, W. (2007). Exo70 interacts with phospholipids and mediates the targeting of the exocyst to the plasma membrane. EMBO J *26*, 4053-4065.

Im, Y.J., Raychaudhuri, S., Prinz, W.A., and Hurley, J.H. (2005). Structural mechanism for sterol sensing and transport by OSBP-related proteins. Nature *437*, 154-158.

Jiang, B., Brown, J.L., Sheraton, J., Fortin, N., and Bussey, H. (1994). A new family of yeast genes implicated in ergosterol synthesis is related to the human oxysterol binding protein. Yeast *10*, 341-353.

Johansson, M., Rocha, N., Zwart, W., Jordens, I., Janssen, L., Kuijl, C., Olkkonen, V.M., and Neefjes, J. (2007). Activation of endosomal dynein motors by stepwise assembly of Rab7-RILP-p150Glued, ORP1L, and the receptor betalll spectrin. J Cell Biol *176*, 459-471.

Jones, S., Newman, C., Liu, F., and Segev, N. (2000). The TRAPP complex is a nucleotide exchanger for Ypt1 and Ypt31/32. Mol Biol Cell *11*, 4403-4411.

Klebl, F., and Tanner, W. (1989). Molecular cloning of a cell wall exo-beta-1,3-glucanase from Saccharomyces cerevisiae. J Bacteriol *171*, 6259-6264.

Klemm, R.W., Ejsing, C.S., Surma, M.A., Kaiser, H.J., Gerl, M.J., Sampaio, J.L., de Robillard, Q., Ferguson, C., Proszynski, T.J., Shevchenko, A*., et al.* (2009). Segregation of sphingolipids and sterols during formation of secretory vesicles at the trans-Golgi network. J Cell Biol *185*, 601-612.

Kozminski, K.G., Alfaro, G., Dighe, S., and Beh, C.T. (2006). Homologues of oxysterol-binding proteins affect Cdc42p- and Rho1p-mediated cell polarization in Saccharomyces cerevisiae. Traffic *7*, 1224-1242.

Kozminski, K.G., Beven, L., Angerman, E., Tong, A.H., Boone, C., and Park, H.O. (2003). Interaction between a Ras and a Rho GTPase couples selection of a growth site to the development of cell polarity in yeast. Mol Biol Cell *14*, 4958-4970.

Kozminski, K.G., Chen, A.J., Rodal, A.A., and Drubin, D.G. (2000). Functions and functional domains of the GTPase Cdc42p. Mol Biol Cell *11*, 339-354.

Kvam, E., and Goldfarb, D.S. (2004). Nvj1p is the outer-nuclear-membrane receptor for oxysterol-binding protein homolog Osh1p in Saccharomyces cerevisiae. J Cell Sci *117*, 4959-4968.

LeBlanc, M.A., and McMaster, C.R. (2010). Lipid binding requirements for oxysterol-binding protein Kes1 inhibition of autophagy and endosome-trans-Golgi trafficking pathways. J Biol Chem *285*, 33875-33884.

Li, X., Rivas, M.P., Fang, M., Marchena, J., Mehrotra, B., Chaudhary, A., Feng, L., Prestwich, G.D., and Bankaitis, V.A. (2002). Analysis of oxysterol binding protein homologue Kes1p function in regulation of Sec14p-dependent protein transport from the yeast Golgi complex. J Cell Biol *157*, 63-77.

Longtine, M.S., McKenzie, A., 3rd, Demarini, D.J., Shah, N.G., Wach, A., Brachat, A., Philippsen, P., and Pringle, J.R. (1998). Additional modules for versatile and economical PCR-based gene deletion and modification in Saccharomyces cerevisiae. Yeast *14*, 953-961.

Losev, E., Reinke, C.A., Jellen, J., Strongin, D.E., Bevis, B.J., and Glick, B.S. (2006). Golgi maturation visualized in living yeast. Nature *441*, 1002-1006.

Maxfield, F.R., and Menon, A.K. (2006). Intracellular sterol transport and distribution. Curr Opin Cell Biol *18*, 379-385.

Mesmin, B., and Maxfield, F.R. (2009). Intracellular sterol dynamics. Biochim Biophys Acta *1791*, 636-645.

Misu, K., Fujimura-Kamada, K., Ueda, T., Nakano, A., Katoh, H., and Tanaka, K. (2003). Cdc50p, a conserved endosomal membrane protein, controls polarized growth in Saccharomyces cerevisiae. Mol Biol Cell *14*, 730-747.

Mizuno-Yamasaki, E., Medkova, M., Coleman, J., and Novick, P. (2010). Phosphatidylinositol 4-phosphate controls both membrane recruitment and a regulatory switch of the Rab GEF Sec2p. Dev Cell *18*, 828-840.

Muller, H. (1932). Further studies on the nature and causes of gene mutations. roc Sixth Int Congr Genet, 213-255.

Muthusamy, B.P., Raychaudhuri, S., Natarajan, P., Abe, F., Liu, K., Prinz, W.A., and Graham, T.R. (2009). Control of protein and sterol trafficking by antagonistic activities of a type IV P-type ATPase and oxysterol binding protein homologue. Mol Biol Cell *20*, 2920-2931.

Novick, P., Field, C., and Schekman, R. (1980). Identification of 23 complementation groups required for post-translational events in the yeast secretory pathway. Cell *21*, 205-215.

Novick, P., Medkova, M., Dong, G., Hutagalung, A., Reinisch, K., and Grosshans, B. (2006). Interactions between Rabs, tethers, SNAREs and their regulators in exocytosis. Biochem Soc Trans *34*, 683-686.

Novick, P., Osmond, B.C., and Botstein, D. (1989). Suppressors of yeast actin mutations. Genetics *121*, 659-674.

Novick, P., and Schekman, R. (1979). Secretion and cell-surface growth are blocked in a temperature-sensitive mutant of Saccharomyces cerevisiae. Proc Natl Acad Sci U S A *76*, 1858-1862.

Olkkonen, V.M., and Levine, T.P. (2004). Oxysterol binding proteins: in more than one place at one time? Biochem Cell Biol *82*, 87-98.

Ozaki-Kuroda, K., Yamamoto, Y., Nohara, H., Kinoshita, M., Fujiwara, T., Irie, K., and Takai, Y. (2001). Dynamic localization and function of Bni1p at the sites of directed growth in Saccharomyces cerevisiae. Mol Cell Biol *21*, 827-839.

Park, H.O., and Bi, E. (2007). Central roles of small GTPases in the development of cell polarity in yeast and beyond. Microbiol Mol Biol Rev *71*, 48-96.

Pruyne, D., and Bretscher, A. (2000). Polarization of cell growth in yeast. I. Establishment and maintenance of polarity states. J Cell Sci *113 (Pt 3)*, 365-375.

Pruyne, D.W., Schott, D.H., and Bretscher, A. (1998). Tropomyosin-containing actin cables direct the Myo2p-dependent polarized delivery of secretory vesicles in budding yeast. J Cell Biol *143*, 1931-1945.

Raychaudhuri, S., Im, Y.J., Hurley, J.H., and Prinz, W.A. (2006). Nonvesicular sterol movement from plasma membrane to ER requires oxysterol-binding protein-related proteins and phosphoinositides. J Cell Biol *173*, 107-119.

Ridgway, N.D., Dawson, P.A., Ho, Y.K., Brown, M.S., and Goldstein, J.L. (1992). Translocation of oxysterol binding protein to Golgi apparatus triggered by ligand binding. J Cell Biol *116*, 307-319.

Roberts, T.M., Kobor, M.S., Bastin-Shanower, S.A., Ii, M., Horte, S.A., Gin, J.W., Emili, A., Rine, J., Brill, S.J., and Brown, G.W. (2006). Slx4 regulates DNA damage checkpoint-dependent phosphorylation of the BRCT domain protein Rtt107/Esc4. Mol Biol Cell *17*, 539-548.

Robinson, J.S., Klionsky, D.J., Banta, L.M., and Emr, S.D. (1988). Protein sorting in Saccharomyces cerevisiae: isolation of mutants defective in the delivery and processing of multiple vacuolar hydrolases. Mol Cell Biol *8*, 4936-4948.

Schorr, M., Then, A., Tahirovic, S., Hug, N., and Mayinger, P. (2001). The phosphoinositide phosphatase Sac1p controls trafficking of the yeast Chs3p chitin synthase. Curr Biol *11*, 1421-1426.

Schott, D., Ho, J., Pruyne, D., and Bretscher, A. (1999). The COOH-terminal domain of Myo2p, a yeast myosin V, has a direct role in secretory vesicle targeting. J Cell Biol *147*, 791-808.

Schott, D.H., Collins, R.N., and Bretscher, A. (2002). Secretory vesicle transport velocity in living cells depends on the myosin-V lever arm length. J Cell Biol *156*, 35-39.

Schulz, T.A., Choi, M.G., Raychaudhuri, S., Mears, J.A., Ghirlando, R., Hinshaw, J.E., and Prinz, W.A. (2009). Lipid-regulated sterol transfer between closely apposed membranes by oxysterol-binding protein homologues. J Cell Biol *187*, 889-903.

Sikorski, R.S., and Hieter, P. (1989). A system of shuttle vectors and yeast host strains designed for efficient manipulation of DNA in Saccharomyces cerevisiae. Genetics *122*, 19-27.

Songer, J.A., and Munson, M. (2009). Sec6p anchors the assembled exocyst complex at sites of secretion. Mol Biol Cell *20*, 973-982.

Stefan, C.J., Manford, A.G., Baird, D., Yamada-Hanff, J., Mao, Y., and Emr, S.D. (2011). Osh proteins regulate phosphoinositide metabolism at ER-plasma membrane contact sites. Cell *144*, 389-401.

Sturley, S.L. (2000). Conservation of eukaryotic sterol homeostasis: new insights from studies in budding yeast. Biochim Biophys Acta *1529*, 155-163.

Tahirovic, S., Schorr, M., and Mayinger, P. (2005). Regulation of intracellular phosphatidylinositol-4-phosphate by the Sac1 lipid phosphatase. Traffic *6*, 116-130.

TerBush, D.R., and Novick, P. (1995). Sec6, Sec8, and Sec15 are components of a multisubunit complex which localizes to small bud tips in Saccharomyces cerevisiae. J Cell Biol *130*, 299-312.

Urbani, L., and Simoni, R.D. (1990). Cholesterol and vesicular stomatitis virus G protein take separate routes from the endoplasmic reticulum to the plasma membrane. J Biol Chem *265*, 1919-1923.

Wagner, W., Bielli, P., Wacha, S., and Ragnini-Wilson, A. (2002). Mlc1p promotes septum closure during cytokinesis via the IQ motifs of the vesicle motor Myo2p. EMBO J *21*, 6397-6408.

Walch-Solimena, C., Collins, R.N., and Novick, P.J. (1997). Sec2p mediates nucleotide exchange on Sec4p and is involved in polarized delivery of post-Golgi vesicles. J Cell Biol *137*, 1495-1509.

Walch-Solimena, C., and Novick, P. (1999). The yeast phosphatidylinositol-4-OH kinase pik1 regulates secretion at the Golgi. Nat Cell Biol *1*, 523-525.

Wang, P.Y., Weng, J., and Anderson, R.G. (2005). OSBP is a cholesterol-regulated scaffolding protein in control of ERK 1/2 activation. Science *307*, 1472-1476.

Wilkie, A.O. (1994). The molecular basis of genetic dominance. J Med Genet *31*, 89-98.

Winzeler, E.A., Shoemaker, D.D., Astromoff, A., Liang, H., Anderson, K., Andre, B., Bangham, R., Benito, R., Boeke, J.D., Bussey, H.*, et al.* (1999). Functional characterization of the S. cerevisiae genome by gene deletion and parallel analysis. Science *285*, 901-906.

Zajac, A., Sun, X., Zhang, J., and Guo, W. (2005). Cyclical regulation of the exocyst and cell polarity determinants for polarized cell growth. Mol Biol Cell *16*, 1500-1512.

Zhang, X., Orlando, K., He, B., Xi, F., Zhang, J., Zajac, A., and Guo, W. (2008). Membrane association and functional regulation of Sec3 by phospholipids and Cdc42. J Cell Biol *180*, 145-158.

5: **Compensatory Endocytosis Promotes Cortical Actin Polarization in** *Saccharomyces cerevisiae*

Author list: **Gabriel Alfaro***, Jesper Johansen*, and Christopher T. Beh.

5.1   Summary

Cell polarization is maintained by both polarized exocytosis, which transports membrane components to specific locations on the cell cortex, and endocytosis, which counteracts passive diffusion of components from polarized sites[1]. Despite functional links between these processes, they are generally treated as separate events. Here we show that in budding yeast the Rab GTPase Sec4p directly integrates polarized exocytosis with actin patch assembly, which initiates endocytosis[2]. After polarized exocytosis to the plasma membrane (PM) and dissociation from the exocyst complex, Sec4p co-localizes and physically associates during actin patch assembly with the Sla1p, Sla2p, and Las17/Bee1p (yeast WASP) complex of proteins. Mutations that inactivate Sec4p or its GEF, Sec2p, inhibit actin patch formation whereas the activating *sec4-Q79L*

mutation accelerates actin patch assembly. Based on genetic and protein interactions, a pathway for Sec4p involvement in actin patch assembly is defined in which Sec4p transfers at the PM from polarized exocytic vesicles to nascent sites of endocytosis. We propose that the compensatory endocytosis triggered by Sec4p controls surface expansion and kinetically refines polarization.

5.2   Results and Discussion

In specific secretory cells, endocytosis compensates for the expansion of cell surface area caused by vesicular transport to the PM[3]. Following cortical granule exocytosis in Xenopus[4], and after transport to the PM in many other neuronal and non-neuronal cells[5], the mechanistic coupling of endocytosis with exocytosis controls membrane expansion. In *S. cerevisiae*, the first mutants shown to disrupt endocytosis actually corresponded to late secretory (*SEC*) genes, which are implicitly required for exocytosis[6]. Among these late *SEC* genes, *SEC4* encodes a Rab GTPase that moves with vesicles along actomyosin cables from the Golgi to sites of polarized growth at the PM within the daughter bud[7,8]. Sec4p is itself not removed from the PM by endocytosis; instead, Sec4p detachment from the PM is mediated by Gdi1p, a GDP dissociation inhibitor[9]. These results suggest that in addition to its role in polarized exocytosis, Sec4p might also function at the PM during endocytosis. We therefore tested whether Sec4p directly couples these two transport events.

In budding yeast, the polarized sites where exocytic vesicles dock at the PM partially overlap with the more dispersed polarized distribution of cortical actin patches, which are nascent sites of endocytosis[10,11]. As polarized cell growth proceeds during the yeast cell cycle, both exocytic docking sites and actin patches relocate; first from the

incipient bud site in unbudded cells to the bud tip in small-budded cells, then around the entire bud cortex in medium-budded cells, and finally to the mother/bud neck in large-budded cells. During exocytosis, the exocyst complex mediates the docking of vesicles to their targeted sites on the PM. Sec4p anchors a specific subset of exocyst complex subunits, including Sec5p, to the vesicle membrane[12]. Even though Sec4p and Sec5p travel together on post-Golgi vesicles[8], we observe that at any single time the actin patch marker Sla1p-RFP colocalizes at the cortex 4-times more often with GFP-Sec4p particles than with Sec5p-3xGFP particles (N > 340 particles representing > 30 cells/strain). This result suggests a link between Sec4p and actin patches distinct from the exocyst complex.

Because of the fleeting nature of actin patch dynamics, the temporal and spatial colocalization of GFP-Sec4p particles with assembling actin patches is most evident when the entire lifespan of a GFP-Sec4p particle at the cell cortex is analyzed (Figure 5.4.1a, b). The hierarchy of subunit recruitment that defines actin patch assembly first involves a slow coat assembly phase, which occurs over 10-20 s and is marked by the presence of Sla1p, Sla2p, and Las17p[2]. Sla1p and Sla2/End4p (the yeast HIP1r homologue) are conserved endocytic adaptor proteins, and Las17p is the yeast homologue of human Wiskott-Aldrich syndrome protein (N-WASP)[13]. Faster movements are associated with the next phase of actin-meshwork assembly, which is reflected in the motility of Abp1p[2], a mediator of Arp2/3-dependent F-actin branching[13]. To analyze Sec4p localization during the different phases of actin patch subunits assembly, we conducted FRAP (fluorescence recovery after photobleaching) experiments on daughter cells to track each new GFP-Sec4p particle entering the bud and localizing on the PM. After transport to the bud cortex into photobleached zones, GFP-Sec4p particles

colocalize with > 64% of the Abp1p- and Sla1p-and Las17p-RFP foci (N > 90 particles). GFP-Sec4p localization during actin patch assembly also reflects a specific timing; Sec4p associates after Sla1p and Las17p assembly, but leaves as Abp1p is recruited (Figure 5.4.1a). In short, Sec4p exhibits spatial and temporal overlap with endocytosis coat proteins during actin patch assembly.

The functional significance of Sec4p localization with cortical actin is apparent when actin-patch assembly is observed in a *SEC4* conditional mutant. In *sec4-8*[ts] cells cultured at 23˚C, polarized exocytosis is unaffected and comparable to wild type[14]. However, when incubated at 37˚C for 3 hours, the *sec4-8*[ts] mutation disrupts polarized exocytosis[14] and, using the motility and lifetime of actin patch components as a readout, we find that the formation of endocytic sites is also affected (Figure 5.4.1b). In *sec4-8*[ts] cells, Sla1p-RFP- and GFP-Abp1p-marked actin patches persist 265% and 185% longer than in wild type, respectively (Figure 5.4.1b). Under these conditions, GFP-Abp1p assembly is delayed 3-fold following Sla1p-RFP recruitment in *sec4-8*[ts] cells as compared to wild type (Figure 5.4.1b), and the velocity of GFP-Abp1p movement along the PM was 44% slower (Figure 5.4.1c). Because Sec4p GTPase activation requires the Sec2p GEF, we tested whether the *sec2-41*[ts] mutation also affected actin patches. At 37˚C, as was also observed in *sec4-8*[ts] mutant cells, Sla1p-RFP lifetime (Figure 5.4.1b) and GFP-Abp1p motility (Figure 5.4.1c) are defective in *sec2-41*[ts] cells. In addition, at 37˚C, there is a decrease of over 65% in the number of GFP-Abp1p particles and decreases of over 60% in Sla1p-RFP particles observed within *sec2-41*[ts] and *sec4-8*[ts] daughter cell buds relative to wild-type cells (Figure 5.4.1d). These defects are akin to those in early-phase endocytic mutants such as *sla2Δ*, which disrupts regulatory interactions between

endocytic membrane proteins and the actin cytoskeleton[2,13,15]. The morphological defect in actin patch assembly in *sla2Δ* cells is apparent in the localization of GFP-Abp1p, which forms "comet tails" instead of normal punctate actin patches. Comet tails are continuous nucleations of filamentous actin that protrude out into the cytoplasm[15]. After 1 hr at 37˚C, 48% of *sec2-41*[ts] cells, 31% of *sec4-8*[ts] cells, whereas 88% of *sla2Δ* cells exhibited actin comet tails and none were observed in wild-type cells (N > 70 cells) (Figure 5.4.1e). Together these results establish that the formation of endocytic sites, as revealed by actin patch dynamics and Abp1p recruitment, requires Sec4p and its Sec2p GEF.

Because Sec2p and Sec4p promote actin patch assembly and endocytosis, we tested whether other late-acting *SEC* mutants would also affect Sla1p and Abp1p dynamics. Hence, we monitored Sla1p-RFP and GFP-Abp1p motility in *sec6-4*[ts] cells, which contain a conditional mutation in the Sec6p subunit of the exocyst complex that disrupts exocytosis. Compared to wild type, in *sec6-4*[ts] cells incubated at 37˚C there is a modest 165% increase in GFP-Abp1p particle lifetime and a 133% increase in Sla1p-RFP lifetime, relative to wild-type cells (Figure 5.4.1b). These defects are less than those observed in *sec4-8*[ts] and *sec2-41*[ts] cells, but still indicative of some actin patch assembly defects. In contrast, Msb3/4p are functionally redundant Sec4p GTPase-activating proteins (GAPs) that are required for polarized exocytosis and affect actin patch polarization (see below)[16]; however, in *msb3Δ msb4Δ,* cells no defects in GFP-Abp1p motility or in Sla1p-RFP and GFP-Abp1p lifetime are observed (Figure 5.4.1b, d). These findings indicate that different exocytosis mutations impact actin patches in specific ways, suggesting that exocytic dysfunction does not generally impair endocytosis.

The close temporal and spatial relationship between Sec4p and actin patch subunits, Las17p in particular, suggests the possibility of a direct physical interaction. When GST-Sec4p expressed in bacteria is affinity-purified and mixed with either GDP or GTPγS, it binds *in vitro* to radiolabeled Las17p synthesized in a cell-free transcription and translation system (Figure 5.4.2a). To determine whether this interaction is relevant *in vivo*, Sec4p interactions, with actin patch subunits in living cells, were visualized by bimolecular fluorescence complementation (BiFC) (Figure 5.4.2b)[17]. In BiFC, two putative interaction partners are each fused with non-functional halves of a fluorescent protein (i.e. enhanced yellow fluorescent protein [YFP-Venus]). If the interaction partners form a complex in which the amino- (YFP^N) and carboxy- (YFP^C) fragments are within ~50 Å of each other, the fluorescent protein is reconstituted and the interaction is visualized by fluorescence microscopy[17]. Consistent with previous reports, when Las17p-YFP^N and Sla1p-YFP^C are expressed together in yeast, the Las17p/Sla1p interaction generates fluorescence indicative of cortical actin patches; this is also observed when YFP^N-Sec4p is combined with Las17p-YFP^C or Sla1p-YFP^C (Figure 5.4.2b). The BiFC fluorescence between YFP^N-Sec4p and either Las17p- or Sla1p-YFP^C is transient, consistent with the brief duration of Sec4p colocalization with Las17p and Sla1p (data not shown). No fluorescence is detected when YFP^N-Sec4p is expressed with Abp1p-YFP^C, suggesting that Sec4p interactions are specific with respect to actin patch subunits (Figure 5.4.2b). None of the fusion proteins generates fluorescence when expressed alone (data not shown), and the YFP^N-Sec4p BiFC interaction with Las17p-YFP^C is inhibited by competition with increased levels of either wild-type Las17p or Sec4p. An overnight induction of wild-type Las17p from a P^{GAL}-*LAS17* plasmid, or a limited 6 hr induction of

P^{GAL}-*SEC4*, results in a large increase in cells with no detectable YFP^N-Sec4p/Las17p-YFP^C BiFC fluorescent particles, as compared to the same cells without the P^{GAL} plasmids (Figure 5.4.2c). Overall the number of YFP^N-Sec4p/Las17p-YFP^C particles in cells overexpressing Las17p or Sec4p is significantly reduced, comparable to the reduction in particles observed in the Las17p-YFP^N/Sla1p-YFP^C BiFC positive control after *in vivo* competition by P^{GAL}-*LAS17* overexpression (Figure 5.4.2c). These experiments indicate that Sec4p forms a specific complex *in vivo* with Sla1p and Las17p, and Sec4p directly interacts with Las17p both *in vitro* and *in vivo*. We propose that Sec4p is a *bona fide* actin patch component that is recruited to promote a specific transitional event during actin patch assembly; this in turn stimulates subsequent stages in endocytic internalization.

If exo- and endocytosis are coordinated in a coupled cycle, then mutations affecting endocytosis might disrupt polarized exocytosis and vice versa. Having established that *SEC4* mutations affect Sla1p and Abp1p dynamics, we tested whether GFP-Sec4p motility is in turn affected by mutations that disrupt actin patch assembly. In wild-type cells, the vectorial path of GFP-Sec4p changes when it arrives in the bud; before disappearing, GFP-Sec4p makes brief translational movements along the PM[7]. We conducted FRAP experiments on medium- and large-sized daughter cells in which individual GFP-Sec4p particles entering buds were tracked by three-dimensional time-lapse (4D) confocal video microscopy in representative endocytic mutants defective for Bbc1p (a myosin-interacting SH3 domain protein), Las17p, Rvs167p (an amphiphysin homologue), or Sla2/End4p function[13]. Relative to wild type, GFP-Sec4p particle velocity decreases by > 2 fold in *rvs167Δ* cells and *sla2/end4-1*^{ts} cells whereas the velocity of

GFP-Sec4p actually increases 67% in *bbc1Δ* cells (Figure 5.4.3a). Comparable decreases are also evident in *las17-1*[ts] and *-13*[ts] cells, though GFP-Sec4p is not observed on any membrane in *las17Δ* or *las17-14*[ts] cells (Figure 5.4.3b). In these endocytic mutants, the GFP-Sec4p motility defect correlates with increased GFP-Sec4p lifetime. In *las17-1*, *las17-13*, and *sla2/end4-1*[ts] cells, the average lifetime of GFP-Sec4p particles increases by > 50%, whereas it is unchanged in *rvs167Δ* cells and actually decreases by 53% in *bbc1Δ* cells. From this data we conclude that Sec4p motility at the PM is dependent on specific actin patch subunits, which again points to a direct inter-relationship between Sec4p and the endocytic machinery. As an additional assay of polarized exocytosis, the secretion of Bgl2p was analyzed in endocytosis-defective cells (Figure 5.4.3c). Bgl2p is transported in specific exocytic vesicles targeted to sites of polarized growth on the PM where Bgl2p is secreted out of the cell. At 37°C, Bgl2p fails to be exported out of *sec6-4*[ts] exocytosis-defective cells and accumulates internally. Likewise, Bgl2p exocytosis is also blocked in *las17Δ*, *las17-13*, and *sla2Δ* endocytosis mutants. In *rvs167Δ* cells, which affects the last step of internalization, Bgl2p secretion was normal indicating that polarized exocytosis is affected in some but not all endocytosis mutants. These results, however, do support the conclusion that together, polarized exocytosis and endocytosis constitute a coupled transport cycle in budding yeast.

Yeast actin patches are predominantly associated with the PM surrounding sites of polarized growth[18]. The proximity of actin patches to these sites helps maintain the polarized distribution of exocytosed proteins by recycling them before they diffuse to equilibrium[1]. However, the mechanism that controls actin patch polarization is unclear. To determine whether Sec4p and/or Sec2p affects actin patch polarization, we analyzed

the ratio of actin patches polarized within buds relative to those within mother cells in *sec4-8*[ts] and *sec2-41*[ts] mutants. In *sec4-8*[ts] and *sec2-41*[ts] cells incubated at 37°C for 3 hr, the bud-to-mother ratio of Sla1p-RFP and GFP-Abp1p declines by > 400% compared to wild type, indicating a significant loss in actin patch polarization (Figure 5.4.4a). If the polarized exocytosis of Sec4p facilitates the polarized assembly of endocytic sites, then we predict that redistributing Sec4p more uniformly around the PM will in turn cause actin patch depolarization. In *msb3Δ msb4Δ* cells, GFP-Sec4p is more dispersed around the entire surface of the PM and less concentrated at sites of polarized growth as in wild-type cells (Figure 5.4.4b). Consistent with the prediction that Sec4p depolarization leads to actin patch depolarization, Sec4p dispersion in *msb3Δ msb4Δ* cells results in a > 3-fold decrease in the asymmetric localization of Sla1p-RFP and GFP-Abp1p in the bud versus mother cells, relative to wild type (Figure 5.4.4c). This depolarization occurs even though the dynamics of actin patch assembly is unaffected (Figure 5.4.1d). These findings suggest that the polarized distribution of actin patch assembly and endocytic sites is in part dependent on the polarized localization of Sec4p on the PM.

Because loss of Sec4p function perturbed actin patch assembly and polarization, we tested whether constitutive Sec4p activation has a comparable effect. The Sec4p Q79L mutation mimics a Ras oncogenic mutation that lowers intrinsic GTPase activity, locking the protein into the activated GTP-bound form[19]. Although *sec4-Q79L* affects exocytosis, vesicle accumulation is observed only when cells are incubated for prolonged periods (24 hr) at 13°C[19]. To our surprise, *sec4-Q79L* has significant effects on actin patches even at normal or higher growth temperatures. In *sec4-Q79L* cells at 23°C, the lifetime of Sla1p-RFP is 24% less than in wild type, which is comparable to the

reductions in Sla1p-RFP lifetime reported for clathrin and *EDE1* actin-patch mutants[2]. More significantly, in *sec4-Q79L* cells the lifetime of GFP-Abp1p is reduced by 35% (Figure 5.4.4d) and the velocity of GFP-Abp1p movement increases in some strain backgrounds as much as 86% faster than in wild type (Figure 5.4.4d), which is converse to that observed after Sec4p activity is eliminated in *sec4-8*[ts] and *sec2-41*[ts] cells (Figure 5.4.1c, d). These results indicate that reducing Sec4p activity inhibits actin patch assembly, whereas the activated Sec4-Q79L protein stimulates actin patch formation even under conditions that do not impact exocytosis. *SEC4* mutations have the greatest impact on Abp1p recruitment and dynamics as compared to Sla1p. This suggests that Sec4p promotes patch assembly after Las17p- and Sla1p-dependent endocytic coat formation, which is consistent with the timing of Sec4p recruitment during patch assembly. As affirmation of the functional connection between activated Sec4p and actin patch subunits, *sec4-Q79L* causes growth defects in cells expressing increased *SLA1* gene dosage (Figure 5.4.4e). Altogether, these results point to a regulatory role for Sec4p activation in actin patch assembly.

For the polarized formation of actin patches at the bud neck, the EH-domain protein Ede1p plays an important role[20]. Ede1p arrives early during actin patch formation and is recruited to the bud neck. In *ede1Δ* cells, both the density and dynamics of actin patches decrease suggesting Ede1p promotes the creation of incipient endocytic sites[20]. If Sec4p contributes to endocytic site formation by stimulating later events in actin patch development, then we predict Sec4p constitutive activation might suppress earlier *ede1Δ* defects in polarization. In *ede1Δ* cells, *sec4-Q79L* expression partially rescues the reduction in the number of GFP-Abp1p particles, but defects in the number and dynamics

of Sla1p-RFP particles are unchanged (Figure 5.4.4f). These experiments suggest that *SEC4* promotes actin patch assembly downstream of *EDE1* function.

That polarized exocytosis and the reciprocal endocytic event are directly linked pertains not only to budding yeast, but also to other polarized cell types. Membrane traffic to-and-from adherens junctions maintains epithelial apical-basal polarity, which is regulated in part by the endocytic recycling of junctional proteins via the Rho-family GTase Cdc42[21]. In Xenopus eggs, Cdc42 binding to N-WASP facilitates filamentous actin assembly around vesicles docked at the PM and thereby reconfigures exocytosed cortical granules for compensatory endocytic internalization[4]. In budding yeast, however, Las17p lacks the CRIB domain whereby metazoan N-WASP homologues bind Cdc42[22], suggesting that yeast Cdc42p indirectly impacts N-WASP and Arp2/3-dependent actin nucleation at cortical patches. It has also been disputed that Cdc42p trafficking at the yeast PM can account for the polarized coupling of exocytosis and endocytosis[23]. Moreover, classic ultrastructural studies of yeast cells show that exocytic vesicles are in close proximity to cortical actin but not directly associated[10,11].

Based on the above data, the "kiss-and-coat" mode of compensatory endocytosis in Xenopus eggs[24] or "kiss-and-run" recycling of presynaptic exocytic vesicles[5] seem unlikely to apply in yeast. We propose instead that after full fusion of exocytic vesicles with the yeast PM, Sec4p translationally diffuses in the membrane and stimulates endocytic site formation in the vicinity where it was first deposited, adjacent to sites of polarized growth. Sec4p binds Las17p and promotes subsequent events in actin patch assembly required for proper membrane internalization and scission. Although Sec4p was not identified as a requirement for actin patch assembly *in vitro*[25], the biochemical

reconstitution did not include membranes and so membrane-bound regulators like Sec4p would not be applicable. Nonetheless, our results are consistent with findings in *C. elegans* implicating the Sec4p homologue Rab3 in the coordinated exocytosis/endocytosis cycle of synaptic vesicles[26]. Based on these findings and our yeast studies, we suggest that Rab homologues of Sec4p in other polarized cell types induce similar compensatory endocytic events after full fusion of exocytic vesicles.

5.3   Materials and Methods

Strains, plasmids, and genetic techniques.

Yeast strains used are listed in the Supplementary Information (Table S1), along with plasmids (Table S2). Descriptions of translational fusions and plasmid constructions are also provided below. All fusions were functional as tested by complementation of corresponding mutant defects.

Fluorescence microscopy.

Wide field fluorescence microscopy was performed as previously described[26]. Confocal images were captured on a Zeiss Axio Observer.Z1 microscope (Carl Zeiss International, Oberkochen, Germany) equipped with a CSU-10 Nipkow spinning disc (Yokogawa Electronic Corp., Tokyo, Japan), and Z-stacks were acquired using an Improvision Piezo Focus Drive. Z-stacks were separated by 0.5 μm and spanned, at minimum, the entire cell width. Images were acquired using a Zeiss 100 X 1.4 N.A. plan-apochromat oil immersion lens and a Hamamatsu EM-CCD C9100-13 camera (Hamamatsu Photonics, Hamamatsu-city, Japan) mounted on a 1.5 X C-mount and digital analysis and deconvolution was done using Volocity software (Improvision Inc., Lexington, MA). GFP and RFP fluorophores were excited with a 491 nm and 561 nm

lasers respectively; emitted light was filtered with GFP ET520/40M or RFP ET593/40M emission filters (Chroma Technology Corp., Rockingham, VT). Cells were mounted directly onto glass slides in synthetic medium and images were acquired with equivalent exposures and laser power.

To track newly-generated individual GFP-Sec4p particles after entering the daughter bud, the entire bud was first photobleached using a 300 mW solid-state 405 nm laser (Lasiris ColdRay Laser, Stockeryale Inc., Salem, NH). The FRAP laser was used at maximum power for 250 ms when analyzing GFP-Sec4p colocalization with Sla1p-RFP and Abp1p-RFP, and 40 ms for FRAP of GFP-Sec4p/Las17p-RFP-containing cells. The exposure time was 61 ms (71% laser power) and 1.0 sec (67% power) for colocalization experiments involving Sec4p-GFP and Sla1p-RFP, respectively; 51 ms (65% power) and 505 ms (69% power) for Sec4p-GFP and Abp1p-RFP, respectively; and 500 ms (35% power) and 1 sec (40% power) for Las17p-RFP, respectively. For tracking reliability, only new GFP-Sec4p particles transported to the bud cortex, and whose entire lifespan was captured, were analyzed. Only medium and large buds were analyzed, because within smaller buds, particles crossed paths due to high density, which precluded tracking; in all cells, particles that crossed paths were excluded from analysis. Actin comet tails were detected by observing actin patch formation in cells over a 90 sec period by video microscopy. Abp1p-GFP comet tail images were captured with a 400 ms exposure at 17% arc lamp intensity and full gain.

Image analysis.

Particles were manually tracked using the manual tracking function of the visualization and quantification module in Volocity. Manual tracking was also used for

particles tracked by 4D-confocal microscopy. Manual tracking of Sec4p began immediately after FRAP as the Sec4p particle arrived at the bud cortex, and ended after the particle was no longer visible within any focal plane in the cell. Manual tracking of actin patch subunits began when particles first appeared at the PM, and ended when no longer visible within any focal plane. Particle tracings and velocity data were also generated using the Volocity visualization and quantification module. Kymographs were generated using the multiple kymograph module of ImageJ (http://rsb.info.nih.gov/ij/). To mark on kymographs the peak particle fluorescence on the PM, voxel spy from Volocity was used whereby voxel pixel intensities were manually measured during each frame for the entire particle lifetime to choose the frame with highest voxel pixel intensity. If peak voxel intensity remained constant for multiple frames, then the frame with the highest area of peak intensity was chosen. Images of actin comet tails were deconvolved by iterative restoration with a 95% confidence threshold using Volocity 3D deconvolution based on a theoretical PSF calculated from emissions at 509 nm. All images were equivalently processed using Photoshop (Adobe Systems, San Jose, CA). Scatterplots were generated using Graphpad Prism 5 (Graphpad Software, La Jolla, CA). Student t-test statistical analysis comparing mutant with wild-type data sets were used to determine p-values.

In vitro binding assay and Bgl2p polarized exocytosis assay.

GST-Sec4p and GST was expressed in BL21(DE3) Ril cells by induction with 1mM IPTG for 14-16 h at 23°C and lysed by sonication in purification buffer (125 mM Tris pH 8.0 150 mM NaCl) and the protein was immobilized on magnetic glutathione beads (Pierce Protein Research Products, Rockford, IL) via an overnight incubation at

4°C. Protein-bound beads were washed 3 times with purification buffer and 3 times with binding buffer (150 mM Tris pH 7.5 1.5 mM MgCl₂ 50 mM NaCl 0.1% [v/v] Triton X-100). Equivalent amounts of protein-bound beads were resuspended in binding buffer with 1.5 mM GDP or 1.5 mM GTPγS binding buffer and incubated for 30 min at 23˚C. ³⁵[S]-labeled Las17p-Myc, generated in the TNT T7 Coupled Reticulocyte Lysate System (Promega, Madison, WI), was added to each sample and incubated for 1hr at 23˚C. After 6 x 5 min washes with binding buffer containing 1.5 mM GDP or GTPγS, respectively, bound proteins were separated by SDS-PAGE, fixed, and exposed on film. The secretion of Bgl2p was assayed as previously described[27].

BiFC assays of protein interactions.

BiFC was performed as previously described[28] with modifications. For constant expression levels, YFP^N- and YFP^C-fusion constructs were integrated using the modified vectors pHVF1-CT, pUVF2-CT, and pHVF2-NT (a gift from Dr. Christopher Loewen, UBC). Primer combinations for amplifications and integrations are listed in the Supplementary Information (Table S3). Haploid transformants expressing YFP^N- and YFP^C-fusions, respectively, were mated and BiFC assays were conducted by fluorescence microscopy on the resulting diploid cells. For each image, a single optical section was acquired using an YFP filter as previously described[28], and exposure times were 500 ms at full gain. The arc lamp intensity was set at 55% except for YFP^N-Sec4p/Abp1p-YFP^C and Las17p-YFP^N/Sla1p-YFP^C analysis where the intensity was set at 100%. The images were deconvolved using the Volocity 3D deconvolution theoretical point spread function and calculated based on emissions at 520 nm.

Strain and plasmid generation

Carboxyl-terminal GFP and mRFP fusions were integrated into the yeast genome as previously described (Wach et al. 1998). CBY4810 was generated by mating CBY4768 and CBY4775 parent strains; the resulting diploid was sporulated, and after tetrad dissection the haploid CBY4810 was isolated. To generate CBY4846, pCB871 was digested with *Bsr*GI and transformed into CBY4759 and the resulting transformant was grown on 5'-FOA medium to select against cells retaining the *URA3*-marked GFP-*SEC4*, plasmid. The resulting strain (CBY4793) was transformed with pCB768, mated with CBY4810, and after sporulation and tetrad dissection of the resulting diploid, CBY4846 was isolated. To generate pCB591, a *Pvu*I fragment from pRC2098 containing GFP-*SEC4* was ligated into a *Pvu*I digested YCplac22. To generate pCB879 and pCB881, *SLA1*-RFP:*HIS3* from CBY4677 genomic DNA was amplified by PCR and ligated into insT/Aclone (Fermentas), generating pCB878. A *Kpn*I and *Xho*I fragment from pCB878 containing *SLA1*-RFP:*HIS3* was ligated into *Kpn*I and *Sal*I digested YCplac111 and YEplac181, generating pCB879 and pCB881. To generate pCB871, the *sec4*^{Q79L} locus was amplified from JGY73 genomic DNA and ligated into insT/Aclone (Fermentas), generating pCB845. An *Eco*RI and *Xba*I fragment from pCB845 that contained the *sec4*^{Q79L} locus was ligated into pRS303 generating pCB871. To generate pCB768 a *Pvu*I digested fragment from pCB733 that contained P^{ACT1}-GFP-*ABP1* was ligated into YCplac33.
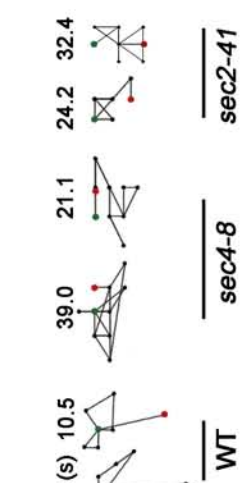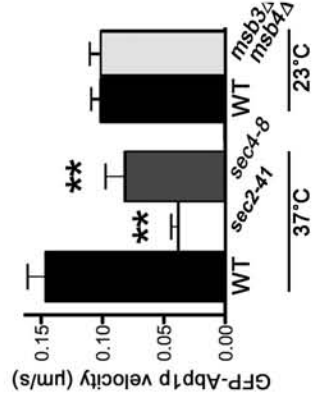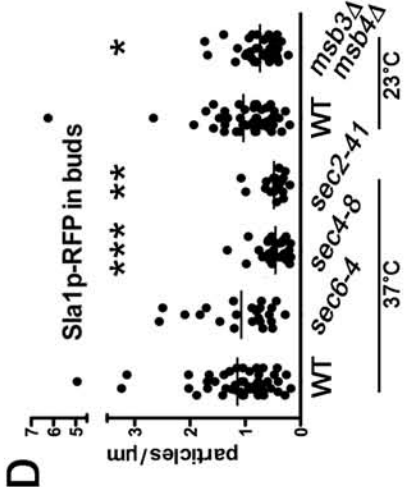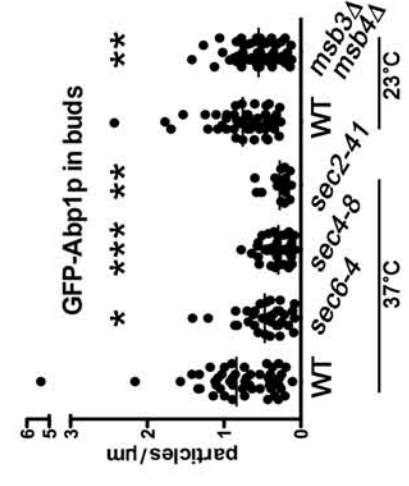
Acknowledgements

5.4 Figures

Figure 5.4.1: Sec4p co-localizes with actin patch subunits and affects actin patch assembly. (Following page)
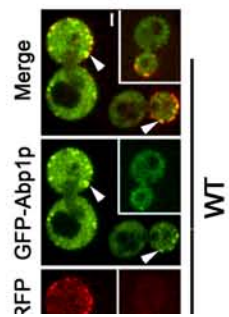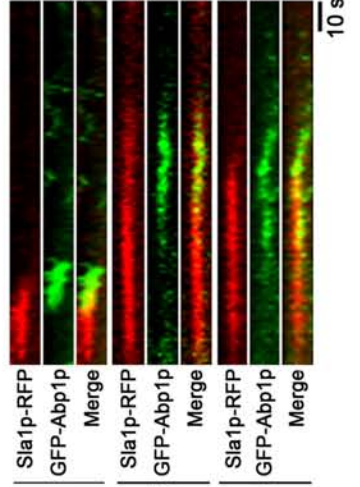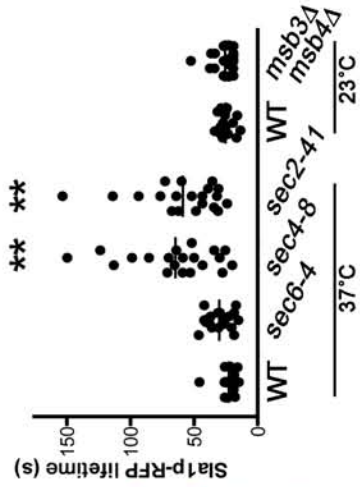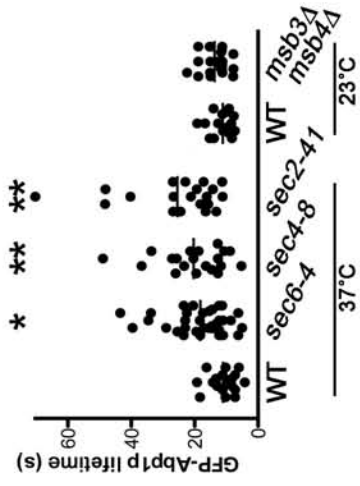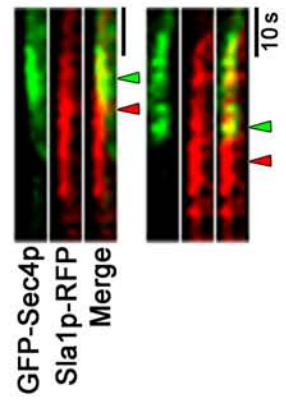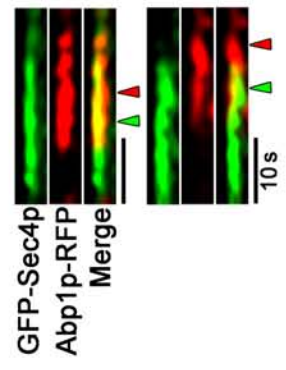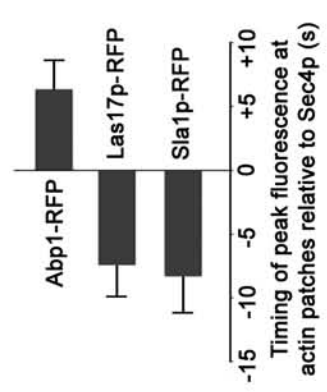
Figure 5.4.1: Sec4p co-localizes with actin patch subunits and affects actin patch assembly. (A) Images of wild-type cells (WT; BY4741) showing the colocalization (arrowheads) of newly transported GFP-Sec4p particles after FRAP with Sla1p-, Las17-, and Abp1-RFP (bar = 2 μm). Corresponding examples of kymographs show relative timings of GFP-Sec4p colocalization with RFP-marked actin patch subunits for two independent events. Maximum voxel fluorescence intensity during the time course is indicated by green (GFP) and red (RFP) arrowheads, and the histogram reports average differences in the maximum fluorescence of each RFP-marked actin patch subunit and GFP-Sec4p (N = 22 particles per strain; 2 particles per each cell analyzed). (B) Left panels show the polarized distribution of Sla1p-RFP and GFP-Abp1p particles (arrowheads) within buds of WT cells. Kymographs show coincident localization of single Sla1p-RFP and GFP-Abp1p particles during actin patch assembly in buds from WT, *sec2-41* (CBY4710) and *sec4-8* (CBY4711) cells incubated at 37°C for 3 hr. As quantified in scatterplots (right), the average lifetime of Sla1p-RFP and GFP-Abp1p particles in *sec6-4* (CBY4712), *sec4-8* and *sec2-41* cells increases relative to WT, whereas no change occurs in *msb3Δ msb4Δ* (CBY1981) relative to its WT parent cultured at 23°C. (C) Two representative tracings of GFP-Abp1p particles moving at the cell cortex in WT, *sec4-8*, and *sec2-41* cells at 37°C, as tracked using confocal video microscopy where the green and red dots mark the first and last positions of the particles, respectively. Tracings are oriented wherein the bud cortex is up and the cell interior is down. Time differences between positions (black dots) are 1 sec and total elapsed times are shown above each tracing. Based on these tracings, average velocities for GFP-Abp1p movement were calculated and plotted in the histogram (N > 30 tracings). (D)

Scatterplots show total numbers of GFP-Abp1p and Sla1p-RFP particles in buds of *sec6-4*, *sec4-8* and *sec2-41* cells relative to WT after incubation at 37˚C, and in buds of *msb3Δ msb4Δ* and WT cells at 23˚C (N > 20 buds; particles counted from 10 μm Z-axis stacks, 0.5 μm apart through each bud). Single, double, and triple asterisks indicate p < 0.05, 0.0015, and 0.0001, respectively. (E) Representative actin patch internalization defects observed in *sec4-8*, *sec2-41*, and *sla2Δ* (CBY4863) cells as shown by Abp1p-GFP "comet tails" (inserts), compared to Abp1p-GFP spots in WT (bar = 2 μm). ***All work in to generate this figure was performed by G.A except the Las17p-RFP colocalization with GFP-Sec4p panel and the comet tails was performed by J.J.**

Figure 5.4.2: Physical interaction of Sec4p with actin patch subunits.
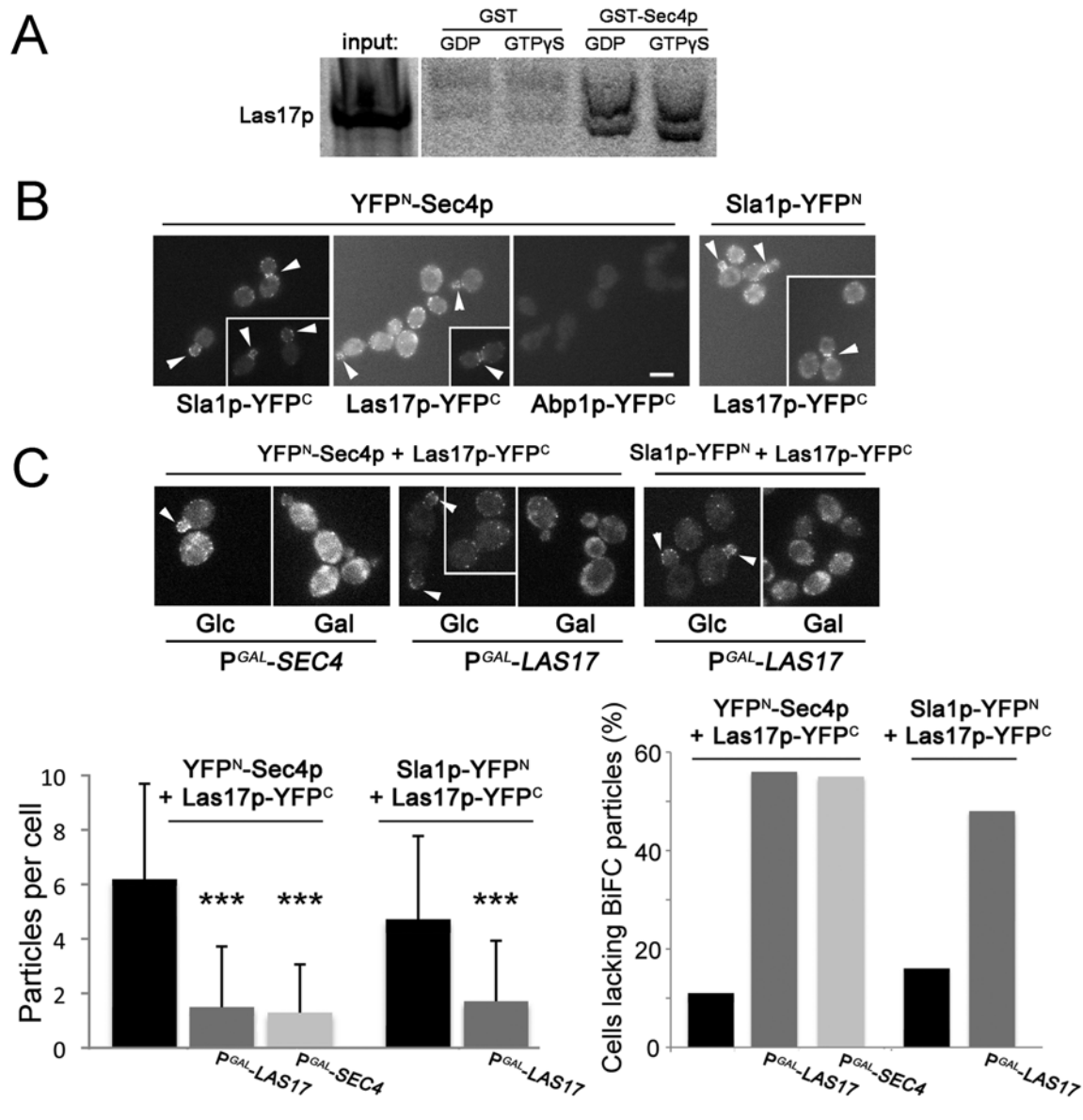
Figure 5.4.2: Physical interaction of Sec4p with actin patch subunits. (A) An *in vitro* binding assay shows ^{35}S-Las17p binding to GST-Sec4p isolated from *E. coli* and immobilized on beads. Equal amounts of GST-Sec4p and the GST negative control were preloaded with GDP or GTPγS prior to the addition of ^{35}S-Las17p. (B) BiFC assays in wild-type cells (SEY6210) expressing Sla2p-YFP^N (CBY4625) or YFP^N-Sec4p

(CBY4629) combined by mating with WT cells (CBY31) expressing Las17p-YFP^C (CBY4660), Sla2p-YFP^C (CBY4661), or Abp1p-YFP^C (CBY4632). Fluorescence at the cell cortex (arrowheads) indicates *in vivo* interactions consistent with actin patch localization (bar = 5 μm). (C) WT cells expressing YFP^N-Sec4p and Las17p-YFP^C (CBY4638) expressing either P^{GAL}-*LAS17* or P^{GAL}-*SEC4* induced by galactose (Gal) or repressed by glucose (Glc). Decreases in BiFC interactions by competition via Las17p or Sec4p overexpression are reported in the histograms (N > 100 cells). *** The *in vitro* binding was performed by J.J. The initial characterization of BiFC interactions was performed by G.A but the final figure was generated by J.J.**

Figure 5.4.3: Reciprocal effects of endocytosis on polarized exocytosis.
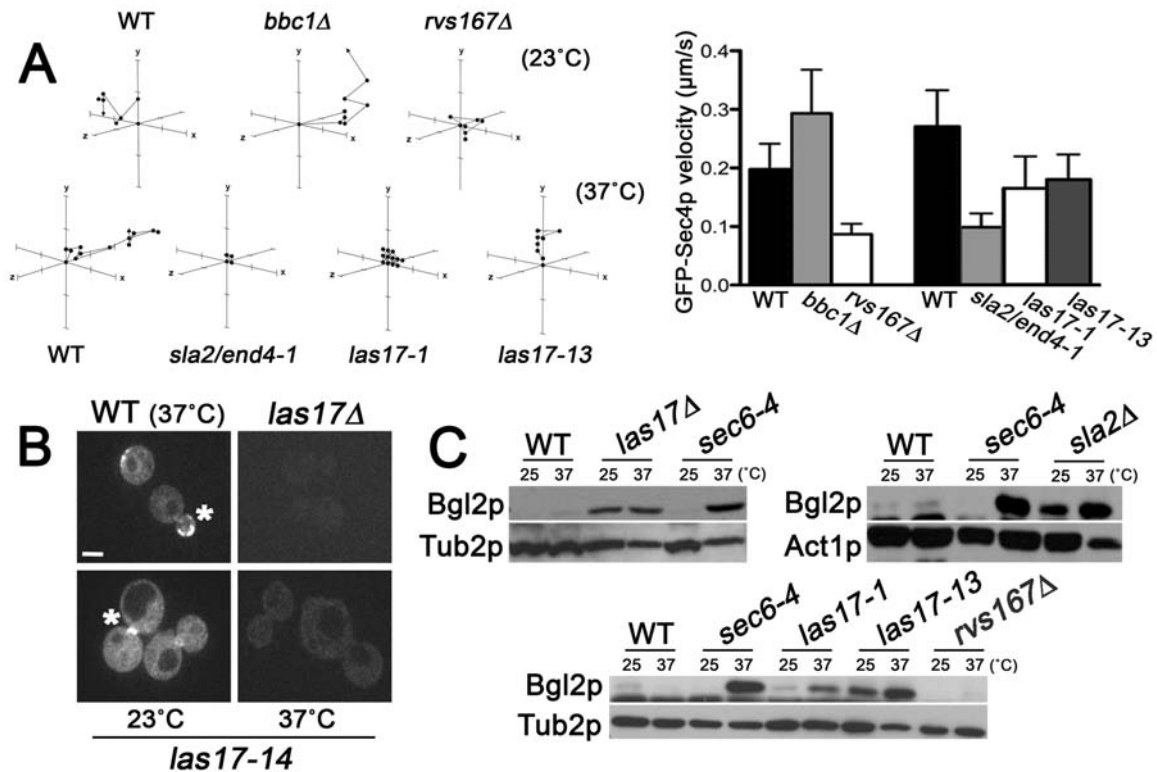
Figure 5.4.3: Reciprocal effects of endocytosis on polarized exocytosis. Sec4p motility is dependent on actin patch assembly. (A) Representative tracings from three-dimensional time-lapse confocal microscopy showing GFP-Sec4p movement after its transport into photobleached zones at the bud cortex in *las17-1^{ts}* (CBY4356)*, las17-13^{ts}* (CBY4357)*, rvs167Δ* (CBY4733)*, bbc1Δ* (CBY4373)*, sla2/end4-1^{ts}* (CBY4452) endocytosis-defective cells, relative to WT (CBY4741). Temperature-conditional mutations were incubated at 37˚C for 2 hrs, whereas motility in deletion mutants was assessed at 23˚C. On each axis, 0.5 μm intervals are indicated. The histogram quantifies the motility for GFP-Sec4p particles at the PM for each strain (N > 30 particles). (B) Images of GFP-Sec4p localization at sites of polarized growth (asterisk) in WT (BY4741), *las17Δ* (CBY1024)*,

and *las17-14* (CBY4358) cells. GFP-Sec4p is not detected on any membrane in *las17Δ* cells, or in *las17-14* cells incubated at 37˚C for 2 hrs (bar = 2 μm). (C) Immunoblots assaying Bgl2p polarized exocytosis showing defective Bgl2p internalization in *sla2Δ* (DDY1980), *las17Δ* (DDY1709), *las17-13* (CBY4357), *las17-1* (CBY4356) endocytosis mutants, compared to the *sec6-4* exocytosis-defective control (NY17) and congenic WT strains (BY4741 and DDY130). Bgl2p exocytosis was not defective in *rvs167Δ* cells (CBY4372). The same blots were probed for tubulin (Tub2p) or actin (Act1p) as internal loading controls. ***This work was performed by G.A. except panel C which was performed by K.G.K and S.D.**

Figure 5.4.4: Actin patch polarization is affected by Sec4p polarization.
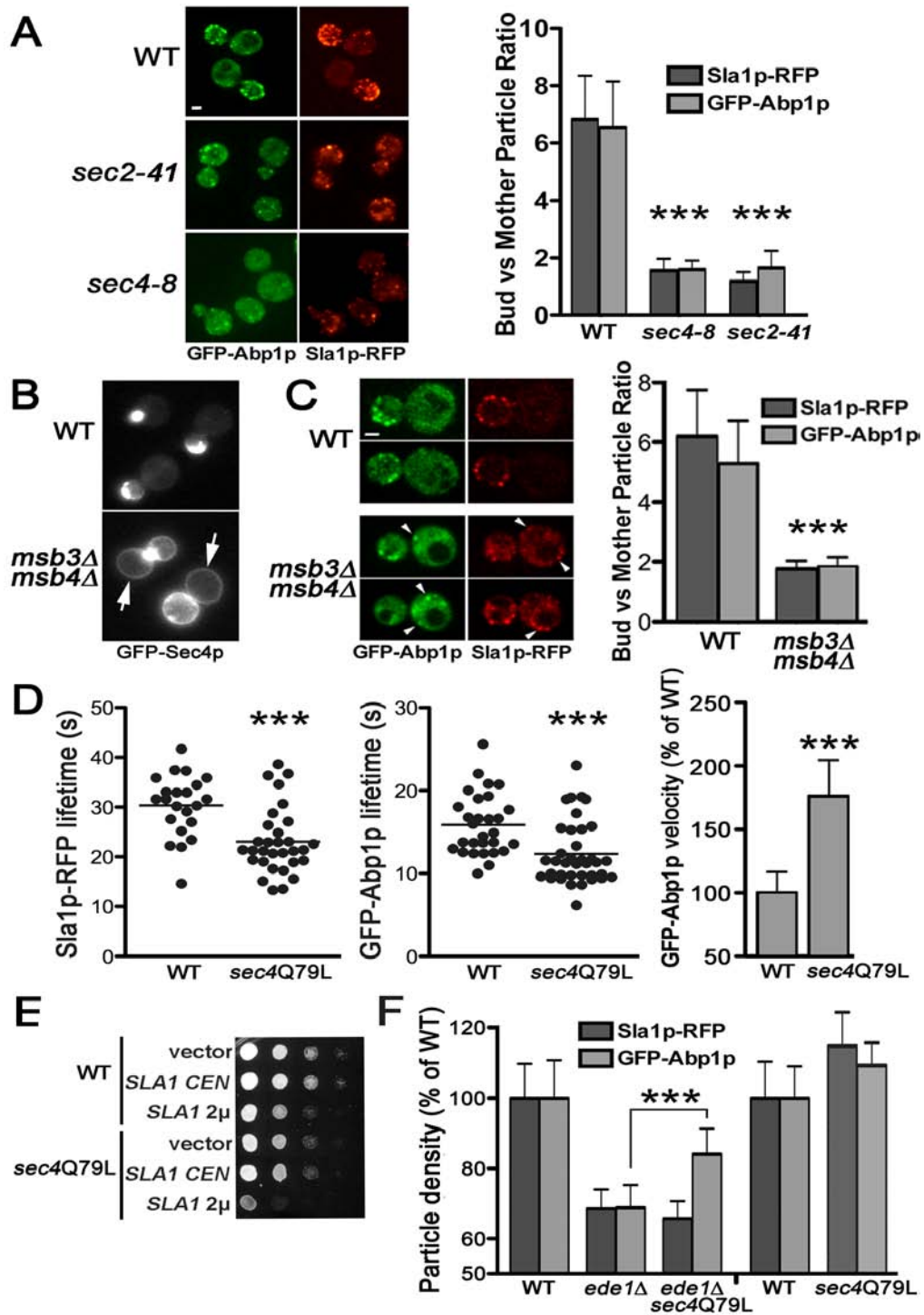
Figure 5.4.4: Actin patch polarization is affected by Sec4p polarization. (A)

Deconvolved flattened image stacks of Sla1p-RFP and GFP-Abp1p in WT (BY4741), *sec4-8*[ts] (CBY4711), and *sec2-41*[s] (CBY4710) cells incubated at 37˚C for 3 hrs acquired by epifluorescence microscopy. The quantification of the Sla1p-RFP and GFP-Abp1p localization in buds versus mother cells ratios for WT, *sec4-8*[ts], and *sec2-41*[ts] cells (N > 20 cells) are in the histogram. (B) Images of GFP-Sec4p fluorescence in WT (BY4741) and the corresponding depolarized GFP-Sec4p in *msb3Δ msb4Δ* (CBY1980) cells. GFP-Sec4p is dispersed around the bud and mother cell cortex (arrows) in 78% of *msb3Δ msb4Δ* cells compared to 0% in WT (N > 100 cells). (C) Images of Sla1p-RFP and GFP-Abp1p expressed in *msb3Δ msb4Δ* cells, showing actin patch depolarization within mother cells (arrowheads), as compared to wild type. The quantification of the Sla1p-RFP and GFP-Abp1p particle localization in buds versus mother cells ratios for WT and *msb3Δ msb4Δ* cells (N > 20 cells) are in the histogram. (D) Scatterplots showing decreases in lifetimes for Sla1p-RFP and GFP-Abp1p particles in WT (BY4741) and *sec4-Q79L* (CBY4793) cells incubated at 23˚C (N > 30 cells). As quantified in the histogram (right), GFP-Abp1p particle velocity increases in *sec4-Q79L* (JGY73) cells relative to its congenic WT control (KEF473A) (N > 70 particles). (E) Tenfold-serial dilutions of WT and *sec4-Q79L* cells containing unicopy (*CEN*) or multicopy (2μ) *SLA1*, and vector plasmids, spotted onto solid medium and incubated at 23˚C. (F) Sla1p-RFP and GFP-Abp1p particle density per μm of cell surface in *ede1Δ* (CBY4775), *ede1Δ sec4-Q79L* (CBY4846), and *sec4-Q79L* (CBY4793) cells cultured at 23˚C as a percentage of the particle density in WT (BY4741) cells (N > 50 medium- and large-budded cells). Asterisks indicate p-values as per Figure 5.4.1d.. ***This work was performed by G.A.**

Tables

Table S1: *S. cerevisiae* strains used

Strain	Genotype	Source
BY4741	*MATa his3Δ1 leu2Δ0 met15Δ0 ura3Δ0*	Winzeler et al. (1999)
BY4742	*MATα his3Δ1 leu2Δ0 lys2Δ0 ura3Δ0*	Winzeler et al. (1999)
CBY31	*MATa leu2-3,122 lys2-801 ura3-52 his3Δ200 trp1Δ901 suc2Δ9*	
CBY1024	*MATa his3Δ1 leu2Δ0 lys2Δ0 ura3Δ0 las17Δ::kan-MX4*	
CBY1980	*MATa his3Δ1 leu2Δ0 met15Δ0 lys2Δ0 ura3Δ0 msb3Δ::kan-MX4 msb4Δ::kan-MX4*	
CBY1981	*MATa his3Δ1 leu2Δ0 ura3Δ0 msb3Δ::kan-MX4 msb4Δ::kan-MX4*	
CBY4356	BY4741 *las17-1:kan-MX4*	P. Hieter, UBC
CBY4357	BY4741 *las17-13:kan-MX4*	P. Hieter, UBC
CBY4358	BY4741 *las17-14:kan-MX4*	P. Hieter, UBC
CBY4372	BY4741 *rvs167Δ::kan-MX4*	Winzeler et al. (1999)
CBY4373	BY4742 *bbc1Δ::kan-MX4*	Winzeler et al. (1999)
CBY4374	BY4741 *sla1Δ::kan-MX4*	Winzeler et al. (1999)
CBY4621	SEY6210 *LAS17*-YFP^{N}*:HIS3*	
CBY4629	SEY6210 *HIS3*:P^{ADH1}-YFP^{N}-*SEC4*	
CBY4632	CBY31 *ABP1*-YFP^{C}*:URA3*	
CBY4635	CBY31 *HIS3*:P^{ADH1}-YFP^{N}-*SEC4*	
CBY4638	*MATα/MATa leu2-3,122/leu2-3,122 lys2-801/lys2-801 ura3-52/ura3-52 his3Δ200/his3Δ200 trp1Δ901/trp1Δ901 suc2Δ9/suc2Δ9 HIS3*:P^{ADH1}-YFP^{N}-*SEC4/SEC4 LAS17*-YFP^{C}*:URA3/LAS17*	
CBY4645	*MATα/MATa leu2-3,122/leu2-3,122 lys2-801/lys2-801 ura3-52/ura3-52 his3Δ200/his3Δ200*	

	*trp1Δ901/trp1Δ901 suc2Δ9/suc2Δ9 HIS3:*P^{ADH1}-YFP^N-*SEC4/SEC4 ABP1*-YFP^C*:URA3/ABP1*	
CBY4657	SEY6210 *LAS17*-YFP^C*:URA3*	
CBY4677	BY4741 *SLA1*-RFP*:HIS3*	
CBY4679	CBY31 *SLA1*-YFP^C*:URA3*	
CBY4681	SEY6210 *SLA1*-YFP^C*:URA3*	
CBY4686	BY4741 *ABP1*-RFP*:HIS3*	
CBY4689	BY4741 *LAS17*-RFP*:HIS3*	
CBY4710	*MAT**a** his3Δ1 leu2Δ0 lys2Δ0 ura3Δ0 sec2-41:kan-MX4*	C. Boone, U. Toronto
CBY4711	*MAT**a** his3Δ1 leu2Δ0 lys2Δ0 ura3Δ0 sec4-8:kan-MX4*	C. Boone, U. Toronto
CBY4712	*MAT**a** his3Δ1 leu2Δ0 lys2Δ0 ura3Δ0 sec6-4:kan-MX4*	C. Boone, U. Toronto
CBY4742	*MATα/MAT**a** leu2-3,122/leu2-3,122 lys2-801/lys2-801 ura3-52/ura3-52 his3Δ200/his3Δ200 trp1Δ901/trp1Δ901 suc2Δ9/suc2Δ9 LAS17-*YFP^N*:HIS3/LAS17 SLA1*-YFP^C*:URA3/SLA1*	
CBY4749	*MATα/MAT**a** leu2-3,122/leu2-3,122 lys2-801/lys2-801 ura3-52/ura3-52 his3Δ200/his3Δ200 trp1Δ901/trp1Δ901 suc2Δ9/suc2Δ9 HIS3:*P^{ADH1}-YFP^N-*SEC4/SEC4 SLA1*-YFP^C*:URA3/SLA1*	
CBY4759	*MAT**a** his3Δ1 leu2Δ0 lys2Δ0 ura3Δ0 sec4Δ::kan-MX4* [GFP-*SEC4 URA3 CEN*]	
CBY4768	*MAT**a** his3Δ1 leu2Δ0 met15Δ0 ura3Δ0 sec2-41:kan-MX4 SLA1*-RFP*:HIS3* [P^{ACT1}-GFP-*ABP1 URA3 CEN*]	
CBY4775	BY4742 *ede1Δ::kan-MX4*	Winzeler et al. (1999)
CBY4787	*MAT**a** his3Δ1 leu2Δ0 lys2Δ0 ura3Δ0 sec4-Q79L:HIS3:sec4Δ::kan-MX4* [P^{ACT1}-GFP-*ABP1 URA3 CEN*]	

CBY4793	*MAT***a** *his3Δ1 leu2Δ0 lys2Δ0 ura3Δ0 sec4-Q79L:HIS3:sec4Δ::kan-MX4*	
CBY4805	BY4742 *SLA1-RFP:HIS3* [P^{ACT1}*-GFP-ABP1 URA3 CEN*]	
CBY4810	*MAT*α *his3Δ1 leu2Δ0 ura3Δ0 ede1Δ::kan-MX4 SLA1-RFP:HIS3* [P^{ACT1}-GFP-*ABP1 URA3 CEN*]	
CBY4846	*MAT*α *his3Δ1 leu2Δ0 ura3Δ0 ede1Δ::kan-MX4 SLA1-RFP:HIS3 sec4-Q79L:HIS3:sec4Δ::kan-MX4* [P^{ACT1}-GFP-*ABP1 URA3 CEN*]	
CBY4863	BY4742 *sla2Δ::kan-MX4*	Winzeler et al. (1999)
DDY130	*MAT***a** *his3Δ200 leu2-3,112 lys2-801 ura3-52*	D. Drubin, UC, Berkeley
DDY904	*MAT*α *his3Δ200 leu2-3,112 lys2-801 ura3-52*	D. Drubin, UC, Berkeley
DDY1438	*MAT*α *his3Δ200 leu2-3,112 lys2-801 ura3-52 las17Δ::URA3*	D. Drubin, UC, Berkeley
DDY1980	*MAT***a** *his3Δ200 leu2-3,112 lys2-801 ura3-52 sla2Δ::URA3*	D. Drubin, UC, Berkeley
JGY73	*MAT***a** *his3Δ200 leu2Δ1 lys2-801 trp1Δ63 ura3-52 sec4-Q79L*	
KEF473A	*MAT***a** *his3Δ200 leu2Δ1 lys2-801 trp1Δ63 ura3-52*	
NY17	*MAT***a** *sec6-4^{ts} ura3-52*	Novick et al. (1980)
RH286-1C	*MAT*a *leu2 ura3 his4 bar1 end4-1(ts)*	Raths et al. (1993)
RSY255	*MAT*α *ura3-52 leu2-3,112*	Novick & Schekman (1979)
SEY2102	*MAT*α *his4-519 leu2-3,112 ura3-52 bgl2::URA3*	Klebl & Tanner (1989)

| SEY6210 | *MATα ura3-52 his3Δ200 lys2-801am leu2-3,112 trp1Δ901 suc2Δ9* | Robinson et al. (1988) |
| W303-1A | *MAT*a *leu2-3,112 ura3-1 his3-11 can1-100 ade2-1* | |

Unless otherwise referenced, all strains were created as part of this study.

Table S2: Plasmids used

Plasmid	Description	Source
pAGX2	P^{ACT1}-GFP *CEN URA3*	Ozaki-Kuroda et al. (2001)
pCB591	GFP-*SEC4 CEN TRP1*	
pCB733	P^{ACT1}-GFP-*ABP1 CEN LYS2*	
pCB768	P^{ACT1}-GFP-*ABP1 CEN URA3*	
pCB871	*sec4^{Q79L} HIS3*	
pCB879	*SLA1*-mRFP:*HIS3-MX6 LEU2 CEN*	
pCB881	*SLA1*-mRFP:*HIS3-MX6 LEU2* 2μ	
pCB941	P^{GAL1}-*SEC4* 2μ *TRP1*	
pCB942	P^{GAL1}-*LAS17* 2μ *TRP1*	
pCB964	GST-*SEC4*	
pDD1737	mRFP:*HIS3-MX6*	D. Drubin, UC, Berkeley
pFA6a-GFP-*HIS3MX6*	GFP:*HIS3-MX6*	Wach et al. (1997)
pGEX-4T-1	GST	GE Healthcare, Little Chalfont, UK
pHVF1-CT	YFP^{F1}:*HIS3-MX6*	C. Loewen, UBC
pHVF1-NT	*HIS3-MX6*:P^{ACT1}-YFP^{F1}	C. Loewen, UBC
pKT10-GAL-HA	P^{GAL}-HA 2μ *URA3*	Misu et al. (2003)

pNB810	*SEC3*-GFP *URA3 CEN*	Finger et al. (1998)
pPG5-SEC5-3xGFP	*SEC5*-3xGFP *URA3*	Boyd et al. (2004)
pPG5-SEC15-3xGFP	*SEC15*-3xGFP *URA3*	Boyd et al. (2004)
pRC2098	GFP-*SEC4 CEN URA3*	Calero et al. (2003)
pRS303	*HIS3*	Sikorski & Hieter (1989)
pRS426	2μ *URA3*	Sikorski & Hieter (1989)
pUVF2-CT	YFP^{F2}:*URA3*	C. Loewen, UBC
YCplac22	*CEN TRP1*	Gietz & Sugino (1988)
YCplac33	*CEN URA3*	Gietz & Sugino (1988)
YCplac111	*CEN LEU2*	Gietz & Sugino (1988)
YEplac181	2μ *LEU2*	Gietz & Sugino (1988)
YEplac195	2μ *URA3*	Gietz & Sugino (1988)

Unless otherwise referenced, all plasmids were created as part of this study.

Table S3: BiFC oligonucleotide primers used

Primer	Sequence	BiFC Construct
CBP520	TATTTCATATAGCTTGTTTTAGTTATTATCCTAT AAAATCTTAAAATACATTAATTCGATGAATTC GAGCTCG	*SLA1*-YFP^C
CBP521	ATCAAGGCAAGCCAACATATTCAATGCTACTG CATCAAATCCGTTTGGATTCTATGTATCATACA CATACGATTTAG	*SLA1*-YFP^C
CBP530	CAACATATTCAATGCTACTGCATCAAATCCGTT TGGATTCTATGTATCATACACATACGATTTAG	*SLA2*-YFP^C
CBP531	TTGTTTTAGTTATTATCCTATAAAATCTTAAAA TACATTAATTCGATGAATTCGAGCTCG	*SLA2*-YFP^C
CBP532	GCTCAAAAGGTCTCTTCCCCAGCAATTATGTGT CTTTGGGCAACTCTATGTATCATACACATACGA TTTAG	*ABP1*-YFP^C
CBP533	TTACGTAAGAATAATATAATAGCATGACGCTG ACGTGTGATTTCGATGAATTCGAGCTCG	*ABP1*-YFP^C
CBP559	AAAAACTAAAGTGGGAGCTCATGACGATATGG ACAATGGTGATGATTGGTATGTATCATACACA TACGATTTAG	*LAS17*-YFP^C
CBP560	AGTGAGTACATAAAATTACATATTTTCTATAAC AGTAGTTTCATCTTTGTTTGCATTCCATCGATG AATTCGAGCTCG	*LAS17*-YFP^C
CBP561	GTATCGTTCACCAGAAAGAATATAAACATAAC AAGATAAACCATACGATTTAGGTGACAC	YFP^N-*SEC4*
CBP562	TAGCTCTTTCCATTACCGGATGAAGCAGAAAC AGTTCTCAAGCCTGACATCGACTCACTATAGG GAGAC	YFP^N-*SEC4*

266

5.5 References

1. Valdez-Taubas, J. & Pelham, H. R. B. Slow diffusion of proteins in the yeast plasma membrane allows polarity to be maintained by endocytic cycling. *Curr. Biol.* **13**, 1636-1640 (2003).

2. Kaksonen, M., Toret, C. P. & Drubin, D. G. A modular design for the clathrin- and actin-mediated endocytosis machinery. *Cell* **123**, 305-320 (2005).

3. Schafer, D. A. Actin puts on the squeeze. *Nature Cell Biol.* **5**, 693-694 (2003).

4. Sokac, A. M., Co, C., Taunton, J. & Bement, W. Cdc42-dependent actin polymerization during compensatory endocytosis in Xenopus eggs. *Nature Cell Biol.* **5**, 727-732 (2003).

5. Gundelfinger, E. D., Kessels, M. M. & Qualmann, B. Temporal and spatial coordination of exocytosis and endocytosis. *Nat. Rev. Mol. Cell Biol.* **4**, 127-139 (2003).

6. Riezman, H. Endocytosis in yeast: several of the yeast secretory mutants are defective in endocytosis. *Cell* **40**, 1001-1009 (1985).

7. Schott, D. H., Collins, R. N. & Bretscher, A. Secretory vesicles transport velocity in living cells depends on the myosin-V lever arm length. *J. Cell Biol.* **156**, 35-39 (2002).

8. Boyd, C., Hughes, T., Pypaert, M. & Novick, P. Vesicles carry most exocyst subunits to exocytic sites marked by the remaining two subunits, Sec3p and Exo70p. *J. Cell Biol.* **167**, 889-901 (2004).

9. Garrett, M. D., Zahner, J. E., Cheney, C. M. & Novick, P. J. *GDI1* encodes a GDP dissociation inhibitor that plays an essential role in the yeast secretory pathway. *EMBO J*. **13**, 1718-1728 (1994).

10. Adams, A.E. & Pringle, J.R. Relationship of actin and tubulin distribution to bud growth in wild-type and morphogenetic-mutant *Saccharomyces cerevisiae*. *J. Cell Biol*. **98**, 934-945 (1984).

11. Kilmartin, J.V. & Adams, A.E. Structural rearrangements of tubulin and actin during the cell cycle of the yeast Saccharomyces. *J. Cell Biol*. **98**, 922-933 (1984).

12. Guo, W., Roth, D., Walch-Solimena, C. & Novick, P. The exocyst is an effector for Sec4p, targeting secretory vesicles to sites of exocytosis. *EMBO J*. **18**, 1071-1080 (1999).

13. Moseley, J.B. & Goode, B.L. The yeast actin cytoskeleton: from cellular function to biochemical mechanism. *Microbiol. Mol. Biol. Rev*. **70**, 605-645 (2006).

14. Harsay, E. & Bretscher, A. Parallel secretory pathways to the cell surface in yeast. *J. Cell Biol.* **131**, 297-310 (1995).

15. Kaksonen, M., Sun, Y., and Drubin, D.G. A pathway for association of receptors, adaptors, and actin during endocytic internalization. *Cell* **115**, 475-487 (2003).

16. Gao, X.-D., Albert, S., Tcheperegine, S.E., Burd, C.G., Gallwitz, D. & Bi, E. The GAP activity of Msb3p and Msb4p for the Rab GTPase Sec4p is required for efficient exocytosis and actin organization. *J. Cell Biol.* **162**, 635-646 (2003).

17. Kerppola, T.K. Bimolecular fluorescence complementation (BiFC) analysis as a probe of protein interactions in living cells. *Annu. Rev. Biophys*. **37**, 465-487 (2008).

18. Pruyne, and Bretscher. Polarization of cell growth in yeast II. The role of the cortical actin cytoskeleton. *J. Cell Sci.* **113**, 571-585 (2000).

19. Walworth, N.C., Brennwald, P., Kabcenell, A.K., Garrett, M. & Novick, P. Hydrolysis of GTP by Sec4 protein plays an important role in vesicular transport and is stimulated by a GTPase-activating protein in *Saccharomyces cerevisiae*. *Mol. Cell. Biol*. **12**, 2017-2028 (1992).

20. Stimpson, H.E.M., Toret, C.P., Cheng, A.T., Pauly, B.S., & Drubin, D.G. Early-arriving Syp1p and Ede1p function in endocytic site placement and formation in budding yeast. *Mol. Cell. Biol.* **20**, 4640-4651 (2009).

21. Duncan, M.C., & Peifer, M. Regulating polarity by directing traffic: Cdc42 prevents adherens junctions from Crumblin' apart. *J. Cell Biol*. **183**, 971-974 (2008).

22. Park, H.-O. & Bi, E. Central roles of small GTPases in the development of cell polarity in yeast and beyond. *Microbiol. Mol. Biol. Rev*. **71**, 48-96 (2007).

23. Layton, A.T., Savage, N.S., Howell, A.S., Carroll, S.Y., Drubin, D.G., & Lew, D.J. Modeling vesicle traffic reveals unexpected consequences for Cdc42p-mediated polarity establishment. *Curr. Biol*. **21**, 184-194 (2011).

24. Sokac, A.M. & Bement, W.M. Kiss-and-coat and compartment mixing: coupling exocytosis to signal generation and local actin assembly. *Mol. Biol. Cell* **17**, 1495-1502 (2006).

25. Michelot, A., Costanzo, M., Sarkeshik, A., Boone, C., Yates, J.R. & Drubin, D.G. Reconstitution and protein composition analysis of endocytic actin patches. *Curr. Biol.* **20**, 1890-1899 (2010).

26. Bai, J., Hu, Z., Dittman, J.S., Pym, E.C.G. & Kaplan, J.M. Endophilin functions as a membrane-bending molecule and is delivered to endocytic zones by exocytosis. *Cell* **143**, 430-441 (2010).

27. Kozminski, K., Alfaro, G., Shuba, S, Beh, C. Homologues of oxysterol-binding proteins affect Cdc42p- and Rho1p-mediated cell polarization in *Saccharomyces cerevisiae*. *Traffic* **7**, 1224-1242 (2006).

28. Manderson, E., Malleshaiah, M., and Michnick, S. A novel genetic screen implicates Elm1 in the inactivation of the yeast transcription factor SBF. *PLoS ONE* **3**, e1500 (2008).

6: **Conclusions:**

The integration of lipid regulation with protein signalling is utilized across Eukarya. The work in this thesis establishes the ORP protein family as conserved lipid dependent regulators of the cell polarization protein machinery. To establish and maintain cell polarization, a balance of protein and lipid transport to and from the plasma membrane is required. The work detailed herein defines a novel mechanism that couples exocytosis with endocytosis, using highly conserved protein and lipid regulators, to maintain cell polarity. Overall, this thesis characterizes novel processes that integrate conserved protein transport pathways with lipid homeostasis to ultimately maintain cell polarization.

6.1   Integrating cell polarity with lipid homeostasis: A conserved mechanism to maintain polarity across Eukarya

The work in this thesis demonstrates that lipid signalling can regulate protein polarization. Recent studies have highlighted that the maintenance of Rho-GTPase Cdc42p polarization is mediated by an asymmetric distribution of lipids between membrane leaflets at the PM (Das et al., 2012). Lipid flippases flip the neutral phosphatylethanolamine lipid from the extracellular to the cytosolic leaflet, which weakens the interaction of Cdc42p with the PM allowing for its extraction by the Rho GDI Rdi1p (Das et al., 2012). Since lipid dependent membrane extraction prevents the diffusion of Cdc42p away from polarized sites, this result demonstrates that lipid homeostasis maintains Cdc42p polarization. In chapter 2, we demonstrated that the

mechanism of *OSH* suppression of specific *CDC42* mutant alleles is linked to the maintenance of Cdc42p polarization. Since Osh4p antagonizes the function of the lipid flippase Drs2p to regulate PM phospholipid composition (Muthusamy et al., 2009), Osh proteins could rescue Cdc42p mutants by controlling the formation of asymmetric lipid domains. The regulation of Rho- and Rab-GTPases by lipid homeostasis is not a yeast specific phenomenon but is conserved across eukaryotes. In Madin-Darby canine kidney cells, the polarization of Cdc42 to apical membranes is dependent on the apical localization of PI(4,5)P (Martin-Belmonte et al., 2007). In addition to the polarized recruitment of Cdc42p by PIPs, Rab-GTPase activity is also affected by PIPs. The yeast Rab Ypt31p is recruited to the TGN by PI(4)P binding (Mizuno-Yamasaki et al., 2010), while both the mammalian Rab11 (de Graaf et al., 2004) and the plant RabA4b (Preuss et al., 2006) are recruited to the TGN by binding a PI(4) kinase. Since Osh4p regulates PI(4)P levels at the Golgi (Li et al., 2002; Chapter 4), ORPs could regulate Golgi PIP levels to control Rab-GTPase recruitment and polarized vesicular transport. Importantly, the human Orp1s can complement the Osh4p Golgi PI(4)P activity (Fairn and McMaster, 2005) demonstrating that Golgi PIP regulation is a conserved ORP activity. Mammalian OSBP utilizes PI(4)P binding at the Golgi to control CERT (Ceramide transport protein) activation (Perry and Ridgway, 2006), emphasizing ORPs conserved role in transducing PIP signals. Overall, GTPase polarization is mediated, in part, through lipid signals and this thesis establishes that ORPs play a conserved role in mediating this polarization.

The importance of these lipid and protein regulatory interactions is highlighted by the broad spectrum of illnesses associated with defects in lipid and protein regulation. Several intracellular pathogens, such as *Chlamydia*, usurp the highly conserved and

essential host PIP and GTPase regulatory machinery. During infection, *Chlamydia* is found in internal vesicles/inclusions where pathogen proteins can recruit the host PI4P regulatory machinery (Moorhead et al., 2010). This newly formed PI4P compartment recruits host Rab-GTPases and vesicles to the "inclusion", which brings host lipids necessary for *Chlamydia* survival (Moorhead et al., 2010). Defects in lipid and GTPase regulation underlie molecular etiology of cancer, highlighted by the tumour suppressor PTEN (Phosphatase and Tensin homologue), which is often mutated in cancer (Salmena et al., 2008). Loss of PTEN increases PI(3,4,5)P levels, which leads to increased activation of the Rho-GTPase Rac through its GEF, Tiam1 (Kovacs et al., 2002). Activated Rac results in polarized actin and protein transport, which is necessary for cell migration and cancer cell metastasis (Sanz-Moreno et al., 2008). In this thesis, we establish that a balance of PIP and sterol signalling is utilized by Osh4p to maintain yeast Rho- and Rab-GTPase dependent cell polarity. Interestingly, human ORPs are a target of a group of anti-cancer compounds called ORPphilins (Burgett et al., 2011), some of which resemble a sterol-PIP fusion compound (Beh et al., 2012). Overall, the work in this thesis, along with recent work in literature, establishes that ORPs regulate protein signalling, such as GTPase-dependent cell polarization, in response to sterol and PIP ligand signals.

6.2 Integrating lipid regulation with GTPase dependent polarized vesicular trafficking: A new model for ORPs in cell polarity

In this thesis, we addressed the model that suggests Osh proteins act solely as non-vesicular lipid transport proteins (Im et al., 2005; Levine and Loewen, 2006; Ngo et al., 2010; Prinz, 2007). Contrary to this model we determined a direct role for the Osh

protein family in *vesicular transport*. The functional connection between *OSH* genes and polarized exocytosis was shown by the mis-localization of small GTPases Rho1p, Sec4p, Cdc42p, and the septin protein complex in *OSH* depleted cells (Chapter 2). These phenotypes are not an indirect consequence of sterol homeostasis defects, since depleting yeast cells of ergosterol did not phenocopy the defects observed in Osh protein depleted cells. Moreover, exocytosis related genes were not identified in a forward screen of the yeast genome for regulators of sterol homeostasis (Chapter 3). To affirm a direct role for Osh proteins in polarized vesicular transport, we examined Osh4p localization in living cells (Chapter 4). We identified Osh4p trafficking on exocytic vesicles that target to sites of polarized growth in addition to its previously reported localization to endosomes and the Golgi (Li et al., 2002). In *SEC6* loss-of-function mutants, Osh4p association with exocytic vesicles decreased, implicating that Osh proteins are recruited to vesicles by interacting with the protein regulators of cell polarity. Through coIP and TAP precipitation experiments, we demonstrated that Osh4p and other Osh proteins physically interact with the exocyst complex and the GTPases Sec4p, Rho1p, and Cdc42p (Chapter 4). Importantly, these proteins are only assembled into one complex when vesicles are docked at the PM, suggesting that Osh proteins interact with the assembled complex and not just with an individual GTPase or exocyst complex subunit. Taken together, these results demonstrate that Osh proteins are directly involved in Rab- and Rho-GTPase mediated vesicular transport and not only in non-vesicular sterol transport.

Structure/function analyses of Osh4p provided the final evidence that Osh proteins are primarily sterol-dependent regulators of intracellular signalling and are not only non-vesicular sterol transport proteins (Chapter 4). We demonstrated that the

Osh4(Y97F)p sterol binding mutation is a gain-of-function mutation that results in dominant lethality. Rather than inactivating the Osh4 protein as expected of a sterol transport protein, the Y97F substitution that blocks sterol binding actually increased Osh4p functional activity. This result indicates that Osh4p utilizes sterol binding as a signalling switch, similar to cholesterol binding by OSBP in the regulation of ERK signalling (Wang et al., 2005b). Importantly, the lethality induced by the activated $OSH4^{Y97F}$ sterol-binding mutation is rescued by the deletion of the PI(4)P lipid phosphatase *SAC1* (Chapter 4). Taken together, these functions are entirely consistent with the activities of a lipid-dependent regulatory protein, which is now our proposed model for primary Osh protein function. This conclusion does not exclude a role for Osh proteins in sterol transport, but instead suggests Osh proteins function primarily as regulators of sterol transport as opposed to lipid carriers.

6.2.2 Model: Yeast ORPs integrate vesicle membrane PIP and sterol homeostasis with polarized vesicular transport

We demonstrated in Chapters 2 and 4 that Osh proteins are primarily lipid dependent regulators of vesicle docking by forming a protein complex between Sec4p, Rho-GTPases, and the assembled exocyst. In Chapter 4, we demonstrated that Osh4(Y97F)p is a gain-of-function mutant that affects Sec4p localization. Moreover, Osh4(Y97F)p dominant lethality can be partially rescued by deletion of the PI(4)P phosphatase *SAC1*. This suggests that Osh proteins utilize a balance between PI(4)P and sterol signalling to regulate Sec4p mediated exocytosis. Recently, a crystal structure for Osh4p was solved with PI(4)P bound within its cholesterol/ergosterol binding pocket (de Saint-Jean et al., 2011). This same study also demonstrated that Osh4p can exchange

sterols and PI(4)P between membranes to establish separate sterol and PI(4)P domains (de Saint-Jean et al., 2011). Importantly, during vesicular transport, sterols are enriched on vesicle membranes (Klemm et al., 2009) while PI(4)P levels are reduced (Mizuno-Yamasaki et al., 2010) relative to the TGN. This change in vesicle membrane composition is important since the decreasing PI(4)P levels is necessary for Sec4p recruitment to the vesicle membrane (Mizuno-Yamasaki et al., 2010). Since Osh4p is localized to both the vesicle and the TGN, it could use its newly defined lipid exchanging function to mediate the PI(4)P and sterol changes on the vesicle. This mechanism is supported by our observation that cells expressing Osh4(Y97F)p, which cannot bind sterols to mediate a sterol for PI(4)P exchange, fail to recruit Sec4p to vesicles. Therefore Osh4p can mediate Sec4p recruitment by establishing the proper vesicle membrane lipid environment.

Taken together, we can propose a new model for Osh4p in polarized vesicular transport (Figure 6.5.1). Osh4p first converts the vesicle membrane environment from PI(4)P rich to poor by exchanging these lipids with sterols from the TGN. As a result of the lower PI(4)P levels at the vesicle, Sec4p can be recruited and activated on the vesicle membrane (Mizuno-Yamasaki et al., 2010). After Sec4p recruitment, Osh4p facilitates the docking of the vesicle to the PM by mediating protein interactions between Sec4p, Rho-GTPases, and the assembled exocyst complex (Figure 6.5.1). Overall, future work using Osh4(Y97F)p and other lipid binding Osh mutants will elucidate the regulatory role that sterol and PI(4)P binding plays on Osh protein dependent regulation of cell polarization.

.

6.3 Maintaining cell polarity by coupling exocytosis and endocytosis through Sec4p: a novel yeast compensatory endocytosis process

In Chapters 2 and 4, we established that the seemingly independent vesicular and non-vesicular lipid transport pathways are coupled to yeast cell polarization through Osh protein activity. In Chapter 5, we addressed another pair of seemingly independent transport pathways that maintain yeast cell polarization, endocytosis and exocytosis. Yeast endocytosis is highly conserved with the mammalian endocytic process (Conibear, 2010). However, in mammalian cells the integration of endocytosis and exocytosis is well defined, while, until this study, a yeast mechanism was unknown. Two models for coupling yeast exocytosis with endocytosis were proposed 27 years ago (Riezman, 1985). The first model is analogous to the metazoan "kiss-and-run" and "kiss-and-coat" models, while the second model is similar to the metazoan "full-fusion" model. We directly tested these models by analysing genetic and protein interactions between actin patch subunits and the exocytosis regulator Sec4p (Chapter 5). We demonstrated by confocal microscopy that Sec4p transits on exocytic vesicles to polarized sites where it co-localizes with cortical actin patches. The functional consequence of this spatial interaction is demonstrated by the loss of actin patch motility and assembly in mutant alleles of *SEC4*, or of its GEF, *SEC2*. Through *in vivo* and *in vitro* binding assays, we established that Sec4p affects actin patch function through direct protein interactions with Las17p and Sla1p but not Abp1p. Overall these results show that a specific exocytosis regulatory protein can affect endocytosis through direct and specific interactions, defining a novel yeast compensatory endocytosis process.

To determine if Sec4p utilizes a process similar to the metazoan "kiss-and-run", "kiss-and-coat", or "full-fusion" models of compensatory endocytosis, we assayed for

interactions between other vesicle proteins with actin patches. None of the vesicle associated exocyst components tested (Sec5p, Sec15p, or Exo70p) co-localized with actin patch markers. Previous studies also showed that exocytic vesicles do not directly co-localize with actin patches in yeast (Adams and Pringle, 1984; Kilmartin and Adams, 1984). Taken together it is unlikely that "kiss-and-run" or "kiss-and-coat" mechanisms occur in yeast suggesting that the yeast compensatory endocytosis mechanism is more likely a "full-fusion" model. The ultimate purpose of coupling exocytosis and endocytosis is to maintain the polarized localization of proteins (Valdez-Taubas and Pelham, 2003). In support of this model, we found that the *in vivo* interactions between Sec4p and actin patch proteins occur preferentially in the daughter bud. Moreover, in *SEC4* and *SEC2* mutant cells, the polarization of the actin patch proteins Sla1p and Abp1p is lost. Taken together, these results define a novel yeast compensatory endocytosis pathway that maintains cell polarity through the direct physical association of Sec4p with specific actin patch proteins. Importantly, the mechanism for exocytic Rab-GTPases in endocytosis in other systems is unclear (Bai et al., 2010), which establishes this study as the first that defines a direct function for an exocytic Rab-GTPase in endocytosis. Therefore, this study not only answers a 27-year-old question by demonstrating how exocytosis and endocytosis are directly coupled in yeast, but it also establishes a novel and possibly conserved role for secretory proteins in endocytosis.

6.3.1 Proposed models for the regulation of Sec4p at actin patches and the mechanism of Sec4p at patches

We identified Sec4p as a regulator of endocytic actin patch formation and a key protein involved in yeast compensatory endocytosis. However, what remains unclear is

the identity of the proteins that regulate Sec4p activity at actin patches and also the ultimate function of Sec4p once recruited to actin patches.

6.3.1.1 Model: PI(4,5)P binding and phosphorylation regulates Sec2p activation of Sec4p at the actin patch

Both *SEC2* and *SEC4* mutant alleles affect actin patch polarization, assembly, and kinetics. Using deletions of *MSB3* and *MSB4*, which are the GAPs of Sec4p, or the constitutively active *SEC4Q79L* mutant in the S288C strain background, we identified that the non-specific accumulation of GTP bound Sec4p does not affect actin patch dynamics. Therefore, the localized activation of the Sec4p GTPase, instead of the recruitment of an already activated GTPase, is necessary to affect actin patch dynamics, similar to Cdc24p activating Cdc42p at the incipient bud site (Nern and Arkowitz, 1998) or Rac activation at the leading edge of motile cells (Nishiya et al., 2005).

Sec2p, the GEF for Sec4p, is an ideal candidate for localized activation of Sec4p at actin patches. In vesicular transport, the activation of Sec4p by Sec2p is dependent on membrane PIP levels (Mizuno-Yamasaki et al., 2010). Interestingly, the active turnover of PIPs, especially PI(4,5)P, is required for multiple stages of actin patch progression and internalization (Di Paolo and De Camilli, 2006; Sun et al., 2007). In fact, many endocytic proteins have PI(4,5)P interaction domains, such as Sla2p (Sun et al., 2005) and Rvs167p (Youn et al., 2010), and PIP regulators physically interact with actin patch proteins (Stefan et al., 2005). Therefore, Sec2p could bind PI(4,5)P at the actin patch to then mediate the localized activation of Sec4p, resulting in subsequent actin patch assembly and progression.

Sec4p has a specific life span at the actin patch, demonstrating that Sec4p dissociation is also regulated. Sec4p is extracted from membranes once in its GDP bound state by Gdi1p, which is the Rab GDP dissociation inhibitor. Two GAPs for Sec4p, Gyp5p and Gyl1p, directly interact with the actin patch protein Rvs167p (Prigent et al., 2011), demonstrating that GAPs could temporally restrict Sec4p activity at actin patches. Moreover, Sec2p is phosphorylated by the kinases Ark1p/Prk1p, which are part of the actin patch (Ptacek et al., 2005). Ark1p and Prk1p are recruited to the actin patch sites slightly after (~1s) Abp1p recruitment (Kaksonen et al., 2005), which corresponds to the timeframe for Sec4p dissociation from the actin patch. Interestingly, in *ark1Δ prk1Δ* cells, both Sla1p and Abp1p accumulate in cytoplasmic punctae, suggesting that the disassembly of the endocytic coat is phosphorylation-dependent (Cope et al., 1999). In both *sec2* and *sec4* conditional mutant yeast, Sla1p and Abp1p also accumulate in cytoplasmic punctae. This demonstrates that the Ark1p and Prk1p dependent coat disassembly could be mediated through the phosphorylation of Sec2p and subsequent regulation of Sec4p activity.

Taken together, we can propose a model for the regulation of Sec4p at the actin patch. Sec2p is first recruited to the actin patch through interactions with PI(4,5)P. This recruitment results in the localized activation of Sec4p at the actin patch. To temporally restrict Sec4p activation, Ark1p or Prk1p is recruited after Abp1p to phosphorylate and inactivate Sec2p. At this time point, the Sec4p GAPs Gyp5p and Gyl1p are recruited through their binding of Rvs167p. This co-ordinated recruitment and regulation of the Sec4p GEF and GAPs will shift the Sec4p population at actin patches to its GDP bound state. This inactivates Sec4p allowing for its membrane extraction by Gdi1p.

6.3.1.2 Models for Sec4p activity at the actin patch: Sec4p recruits Rvs167p to promote vesicle release and/or regulates Las17p

The recruitment of Sec4p promotes actin patch progression, but the mechanism is unclear. Recently, it was shown that *SEC18* was required for actin patch dynamics and progression (Carroll et al., 2012). This *SEC* function is thought to be indirect due to the loss of endocytic recycling. But, the data in Chapter 5 establishes a direct role for Sec4p in actin patch assembly. In *C. elegans,* the Rab GTPase RAB-3, a Sec4p homologue, is essential for the recruitment of endophilin, a BAR domain-containing protein similar to Rvs167p, to sites of clathrin mediated endocytosis (Bai et al., 2010). In *S. cerevisiae,* Prigent and colleagues demonstrated that Rvs167p directly interacts with the Sec4p GAPs, Gyp5p and Gyl1p (Prigent et al., 2011). Our study identified that in *rvs167Δ* cells Sec4p motility decreased and Sec4p lifetime increased at the PM, suggesting that Sec4p function must act, at least in part, through Rvs167p. Thus, one possible role for Sec4p at action patches is to recruit Rvs167p and promote endocytic vesicle release. This is supported by our observation that actin patch internalization is significantly delayed in *sec4* conditional mutants. Future experiments determining the localization and function of Rvs167p in *SEC4* mutants will provide great insight into any putative relationship between Sec4p and Rvs167p.

Another possible function for Sec4p at the actin patch is to control Arp2/3 complex mediated actin nucleation. The activation of the Arp2/3 complex by Las17p is attenuated by the binding of Las17p to Sla1p, Bbc1p (Rodal et al., 2003) or Sla2p (Toshima et al., 2007). In *sla1Δ bbc1Δ* cells, an actin comet tail forms at endocytic sites, due to the uninhibited actin polymerization through Las17p (Kaksonen et al., 2005). Since we demonstrate that both *sec2* and *sec4* conditional alleles form actin comet tails at

endocytic sites, it suggests that Sec4p could be involved at this junction of actin regulation. Moreover, we demonstrated that Sec4p physically interacts with Sla1p and to a lesser extent with Las17p and Sla2p *in vivo,* while constitutively active $SEC4^{Q79L}$ can rescue a loss in Abp1p recruitment but not Sla1p recruitment. These results suggest that Sec4p functions downstream of Sla1p recruitment but upstream of Abp1p/actin polymerization. Therefore, another model for Sec4p function is that it could regulate Las17p activation by binding and releasing Sla1p inhibition of Las17p, allowing for subsequent actin nucleation. Overall, either model for Sec4p activity at the actin patch, namely the regulation of Rvs167p or of Las17p activity, would define a "compensatory endocytosis pathway" since in both mechanisms, the recruitment of Sec4p to the actin patch following an exocytic event will allow for a subsequent compensatory endocytic event to occur.

6.4 Making a case for Osh proteins in the maintenance of cell polarity by coupling lipid signalling with compensatory endocytosis.

The activity of the Osh protein family is linked to both cholesterol homeostasis and polarized vesicular transport. However, previous groups have identified that Osh4p, Osh6p, and Osh7p localize and function at the endosome (Li et al., 2002; Wang et al., 2005a). Moreover, the Osh protein family is required for endocytosis (Beh and Rine, 2004). Although this endocytic activity for Osh proteins could be due to indirect effects caused by changes to the PM lipid environment, a recent study reports that actin patches generated *in vitro* from yeast cell extracts contained Osh proteins (Michelot et al., 2010). In support of this observation, we showed that the mobility of the Arp2/3 complex subunit Arc15p (Figure 6.5.2), but not its polarized localization, is *OSH* dependent.

Specifically, culturing an *oshΔ osh4-1* temperature-sensitive mutant at its non-permissive temperature results in a decrease in motility and a longer life span at the PM of the actin patch marker Arc15p relative to wildtype. Taken together, these results suggest that Osh proteins are members of the actin patch and that they can control the mobility of specific actin patch proteins necessary for endocytosis.

Osh proteins are required for actin patch mobility (Figure 6.5.2); however, the mechanism is unclear. Because a loss of Osh function results in Sec4p accumulation on polarized, but unfused, vesicles in the daughter bud (Chapter 2), defects in actin patch mobility could occur since Sec4p cannot be recruited to the actin patch. However, we demonstrate in Chapter 5 that other exocytic mutants, such as conditional alleles of *sec6* and *sec8*, result in only minor defects in actin patch mobility even though Sec4p targeting to the PM is also blocked. Therefore, although the recruitment of Sec4p could play some part in the Osh requirement at actin patches, it cannot be the sole Osh protein function in endocytosis.

For an Osh protein to affect actin patch assembly and in turn actin patch dynamics, it must interact with specific actin patch proteins in a regulated manner. Both Osh2p and Osh4p were identified as protein components of an *in vitro* generated actin patch (Michelot et al., 2010). In addition, Osh2p interacts in yeast two-hybrid assays with Myo3p and Myo5p, which are actin-patch associated Type I myosins (Tonikian et al., 2009). These Osh2p interactions with the type I myosins were also identified in large proteomic screens for protein-protein interactions (Gavin et al., 2006; Tarassov et al., 2008). Therefore, Osh proteins could promote actin patch mobility by directly interacting

with the myosin motors that restrict actin patch localization to specific membrane domains.

Endocytosis and the internalization at the actin patch is directly affected by PI(4)P and PI(4,5)P levels at sites of endocytosis (Sun et al., 2007; Sun et al., 2005). Although Osh proteins promote Sac1p activity at the PM to modulate PI(4)P levels (Stefan et al., 2011), another group of Sac1-domain containing proteins, Inp51p, Inp52p, and Inp53p, have been shown to control PIP levels at the actin patch (Stefan et al., 2005). Hence, Osh proteins could promote the activity of these Sac1-domain-containing proteins to provide the PIP environment needed for endocytosis to occur. On the other hand, the presence of membranes was not needed to recruit Osh proteins to the *in vitro* assembled actin patch (Michelot et al., 2010), suggesting that the role for Osh proteins is not solely dependent on the modification of endocytic membrane PIP levels.

Osh proteins likely utilize PIP and sterol binding as regulatory events that control their functional association with actin patch proteins. In support of this hypothesis, the poor growth of conditional *INP53* mutants, which affect actin patch PIP homeostasis, is exacerbated by *OSH4* over-expression (Costanzo et al., 2010) and partially suppressed by *OSH7* expression (Parrish et al., 2005). Moreover, the ergosterol synthesis gene *ERG2/END11* is necessary for endocytic vesicle internalization (Munn et al., 1999; Munn and Riezman, 1994), suggesting that the sterol intermediate that accumulates, which is mostly fecosterol, is not permissive for endocytosis (Munn et al., 1999). Interestingly, *OSH4* expression exacerbates the poor growth of *ERG2/END11* mutant cells (Costanzo et al., 2010) demonstrating that the mutant sterol environment in an *ERG2* mutant cell is not permissive for the proper regulation of Osh4p in endocytosis. This relationship between

ORP cholesterol binding, membrane dynamics, and endocytosis is conserved in mammalian cell culture, where over-expression of ORP2 results in an increase in cholesterol transport to the PM and a corresponding enhancement of endocytosis (Hynynen et al., 2005). Altogether, a model can be proposed where Osh proteins, in response to the PIP and sterol environment of the endocytic membrane, will directly interact with actin patch proteins, such as the type I myosin motors, to control actin patch dynamics and assembly. Since Osh proteins also affect Sec4p activity, they could couple PIP and sterol dependent actin patch regulation with the Sec4p-dependent compensatory endocytosis pathway to maintain cell polarization.

In conclusion, the work in this thesis has outlined pathways that integrate lipid homeostasis with the protein machinery that maintains cell polarity. This work also defined a novel ORP and Sec4p-dependent yeast compensatory endocytosis pathway. Since an endocytic role for ORPs in humans (Hynynen et al., 2005) and for Rab-GTPases in *C. elegans* (Bai et al., 2010) has been identified, it implicates both ORPs and Rab-GTPases as direct regulators of endocytosis across eukaryotes. Importantly, the novel cell polarity mechanisms for Osh proteins detailed in this thesis affect processes conserved across eukaryotes (Galletta and Cooper, 2009). Therefore, the experimental results documented herein can open many avenues for future study, especially those focusing on the maintenance of polarized cell growth.

6.5 Figures

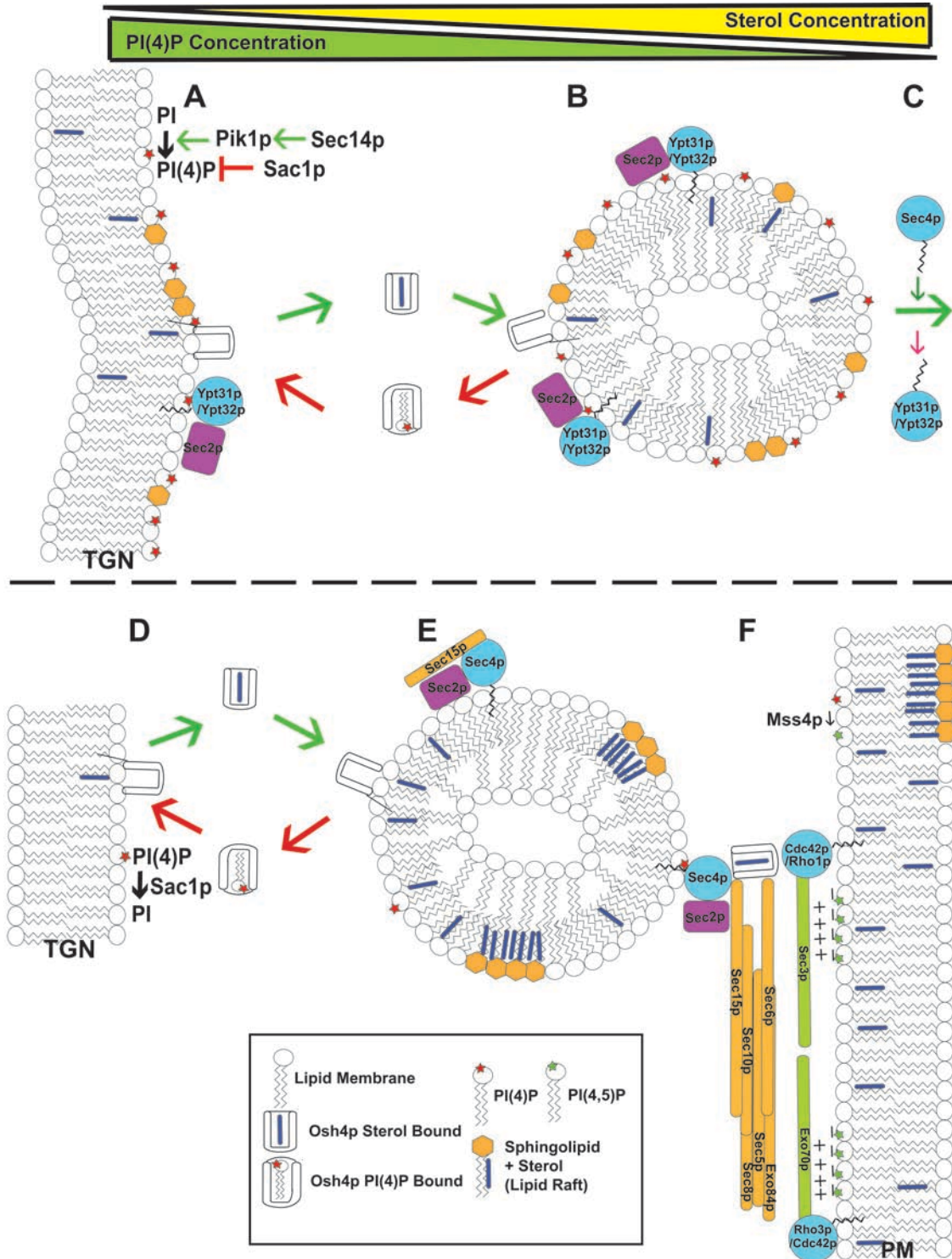**Figure 6.5.1: Model for Osh4p function in polarized exocytosis**

Figure 6.5.1: Model for Osh4p function in polarized exocytosis. Top panel is a recently released vesicle from the TGN, while the bottom panel is a mature vesicle before docking at the PM. As the vesicle matures, PI(4)P levels go down (green triangle) while sterol levels go up (yellow arrow). (A) Increasing PI(4)P levels at the TGN promotes vesicle release and is mediated by Pik1p, which is activated by Sec14p. PI(4)P levels can be attenuated by Sac1p. Increasing PI(4)P levels at the TGN recruits Ypt31p/32p and Sec2p to the developing vesicle. (B) After vesicle release, Osh4p reduces vesicle PI(4)P levels by exchanging it with sterols transported from the TGN. The PI(4)P extracted from the vesicle is transported back to the TGN to continue the PI(4)P/sterol exchange cycle. (C) The reduced PI(4)P levels in vesicle membranes allows for Sec15p to displace Ypt31p/32p from Sec2p, resulting in Sec4p recruitment and activation on the vesicle membrane. (D) Although the initial PI(4)P/sterol concentration gradient allows for early vesicle and TGN PI(4)P/sterol exchange, the depletion of PI(4)P by Sac1p maintains this exchange even with mature vesicles. The sequestering of sterols into ordered domains also supports the continued recruitment of sterol-bound Osh4p to mature vesicles. (E) After the reduction in PI(4)P levels, Sec4p is now able to bind Sec2p and Sec15p. (F) Exocyst assembly docks the vesicle to the PM. The PM-associated exocyst components are recruited by binding Rho-GTPases and also by direct association with PI(4,5)P. The binding of the vesicle-bound exocyst components to the PM associated components is facilitated by sterol bound Osh4p. Osh4p binding to Sec4p and Sec6p allows it to act as a "membrane detector" by promoting exocyst assembly and vesicle docking through eventual association of Osh4p with either the Rho-GTPase or PI(4,5)P at the PM.

Figure 6.5.2: Kinetics of Arc15p on the plasma membrane delayed in *oshΔ osh4-1* cells.
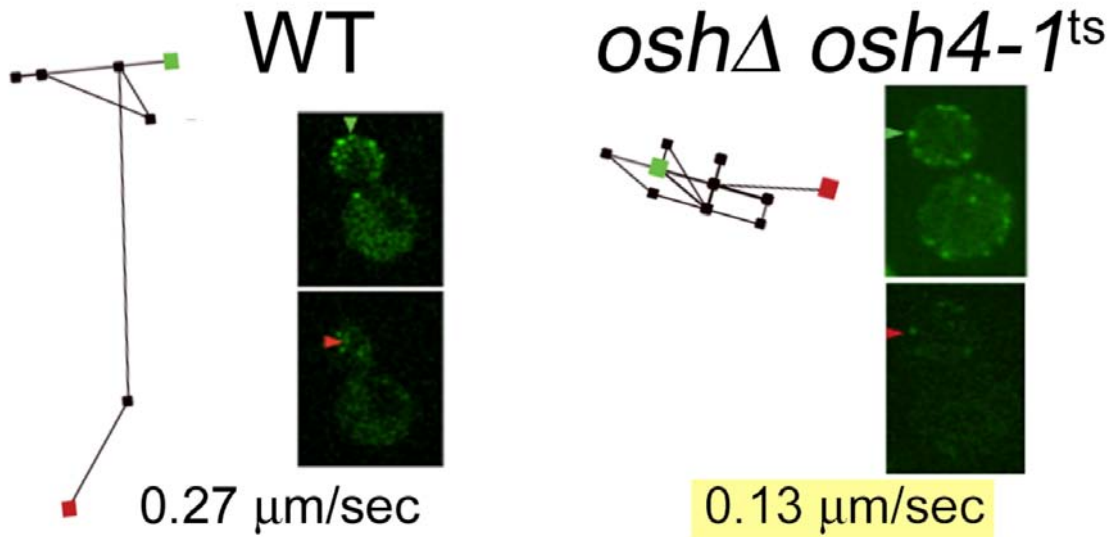

Figure 6.5.2: Particle tracing of GFP-Arc15p particle movement at the cell cortex in WT yeast cells (left) relative to *oshΔ osh4-1* temperature sensitive mutant yeast cells (right) at 37˚C, as visualized using confocal microscopy. The average particle velocity for the entire particle trace (start/green square to end/red square) is below each tracing. Adjacent to the particle tracing are confocal images of the yeast cell detailing the start (green arrow) and end (red arrow) of the GFP-Arc15p particle used to generate the particle trace. These results detail the loss of GFP-Arc15p mobility in *oshΔ osh4-1* cells relative to WT.

6.6 References

Adams, A.E., and Pringle, J.R. (1984). Relationship of actin and tubulin distribution to bud growth in wild-type and morphogenetic-mutant Saccharomyces cerevisiae. J Cell Biol *98*, 934-945.

Alder-Baerens, N., Lisman, Q., Luong, L., Pomorski, T., and Holthuis, J.C. (2006). Loss of P4 ATPases Drs2p and Dnf3p disrupts aminophospholipid transport and asymmetry in yeast post-Golgi secretory vesicles. Mol Biol Cell *17*, 1632-1642.

Bai, J., Hu, Z., Dittman, J.S., Pym, E.C., and Kaplan, J.M. (2010). Endophilin functions as a membrane-bending molecule and is delivered to endocytic zones by exocytosis. Cell *143*, 430-441.

Beh, C.T., and Rine, J. (2004). A role for yeast oxysterol-binding protein homologs in endocytosis and in the maintenance of intracellular sterol-lipid distribution. J Cell Sci *117*, 2983-2996.

Burgett, A.W., Poulsen, T.B., Wangkanont, K., Anderson, D.R., Kikuchi, C., Shimada, K., Okubo, S., Fortner, K.C., Mimaki, Y., Kuroda, M.*, et al.* (2011). Natural products reveal cancer cell dependence on oxysterol-binding proteins. Nat Chem Biol *7*, 639-647.

Carroll, S.Y., Stimpson, H.E., Weinberg, J., Toret, C., Sun, Y., and Drubin., D.G. (2012). Analysis of yeast endocytic site formation and maturation through a regulatory transition point. Mol Biol Cell *23*, 657-668.

Conibear, E. (2010). Converging views of endocytosis in yeast and mammals. Curr Opin Cell Biol *22*, 513-518.

Cope, M.J., Yang, S., Shang, C., and Drubin, D.G. (1999). Novel protein kinases Ark1p and Prk1p associate with and regulate the cortical actin cytoskeleton in budding yeast. J Cell Biol *144*, 1203-1218.

Costanzo, M., Baryshnikova, A., Bellay, J., Kim, Y., Spear, E.D., Sevier, C.S., Ding, H., Koh, J.L., Toufighi, K., Mostafavi, S.*, et al.* (2010). The genetic landscape of a cell. Science *327*, 425-431.

Das, A., Slaughter, B.D., Unruh, J.R., Bradford, W.D., Alexander, R., Rubinstein, B., and Li, R. (2012). Flippase-mediated phospholipid asymmetry promotes fast Cdc42 recycling in dynamic maintenance of cell polarity. Nat Cell Biol *14*, 304-310.

De Craene, J.O., Coleman, J., Estrada de Martin, P., Pypaert, M., Anderson, S., Yates, J.R., 3rd, Ferro-Novick, S., and Novick, P. (2006). Rtn1p is involved in structuring the cortical endoplasmic reticulum. Mol Biol Cell *17*, 3009-3020.

de Graaf, P., Zwart, W.T., van Dijken, R.A., Deneka, M., Schulz, T.K., Geijsen, N., Coffer, P.J., Gadella, B.M., Verkleij, A.J., van der Sluijs, P.*, et al.* (2004). Phosphatidylinositol 4-kinasebeta is critical for functional association of rab11 with the Golgi complex. Mol Biol Cell *15*, 2038-2047.

de Saint-Jean, M., Delfosse, V., Douguet, D., Chicanne, G., Payrastre, B., Bourguet, W., Antonny, B., and Drin, G. (2011). Osh4p exchanges sterols for phosphatidylinositol 4-phosphate between lipid bilayers. J Cell Biol *195*, 965-978.

Di Paolo, G., and De Camilli, P. (2006). Phosphoinositides in cell regulation and membrane dynamics. Nature *443*, 651-657.

Drin, G., Casella, J.F., Gautier, R., Boehmer, T., Schwartz, T.U., and Antonny, B. (2007). A general amphipathic alpha-helical motif for sensing membrane curvature. Nat Struct Mol Biol *14*, 138-146.

Galletta, B.J., and Cooper, J.A. (2009). Actin and endocytosis: mechanisms and phylogeny. Curr Opin Cell Biol *21*, 20-27.

Gavin, A.C., Aloy, P., Grandi, P., Krause, R., Boesche, M., Marzioch, M., Rau, C., Jensen, L.J., Bastuck, S., Dumpelfeld, B.*, et al.* (2006). Proteome survey reveals modularity of the yeast cell machinery. Nature *440*, 631-636.

Ghaemmaghami, S., Huh, W.K., Bower, K., Howson, R.W., Belle, A., Dephoure, N., O'Shea, E.K., and Weissman, J.S. (2003). Global analysis of protein expression in yeast. Nature *425*, 737-741.

Grosshans, B.L., Ortiz, D., and Novick, P. (2006). Rabs and their effectors: achieving specificity in membrane traffic. Proc Natl Acad Sci U S A *103*, 11821-11827.

Guo, S., Stolz, L.E., Lemrow, S.M., and York, J.D. (1999). SAC1-like domains of yeast SAC1, INP52, and INP53 and of human synaptojanin encode polyphosphoinositide phosphatases. J Biol Chem *274*, 12990-12995.

Hua, Z., and Graham, T.R. (2003). Requirement for neo1p in retrograde transport from the Golgi complex to the endoplasmic reticulum. Mol Biol Cell *14*, 4971-4983.

Hynynen, R., Laitinen, S., Kakela, R., Tanhuanpaa, K., Lusa, S., Ehnholm, C., Somerharju, P., Ikonen, E., and Olkkonen, V.M. (2005). Overexpression of OSBP-related protein 2 (ORP2) induces changes in cellular cholesterol metabolism and enhances endocytosis. Biochem J *390*, 273-283.

Im, Y.J., Raychaudhuri, S., Prinz, W.A., and Hurley, J.H. (2005). Structural mechanism for sterol sensing and transport by OSBP-related proteins. Nature *437*, 154-158.

Jarousse, N., and Kelly, R.B. (2001). Endocytotic mechanisms in synapses. Curr Opin Cell Biol *13*, 461-469.

Kaksonen, M., Sun, Y., and Drubin, D.G. (2003). A pathway for association of receptors, adaptors, and actin during endocytic internalization. Cell *115*, 475-487.

Kaksonen, M., Toret, C.P., and Drubin, D.G. (2005). A modular design for the clathrin- and actin-mediated endocytosis machinery. Cell *123*, 305-320.

Kilmartin, J.V., and Adams, A.E. (1984). Structural rearrangements of tubulin and actin during the cell cycle of the yeast Saccharomyces. J Cell Biol *98*, 922-933.

Kovacs, E.M., Ali, R.G., McCormack, A.J., and Yap, A.S. (2002). E-cadherin homophilic ligation directly signals through Rac and phosphatidylinositol 3-kinase to regulate adhesive contacts. J Biol Chem *277*, 6708-6718.

Kvam, E., and Goldfarb, D.S. (2004). Nvj1p is the outer-nuclear-membrane receptor for oxysterol-binding protein homolog Osh1p in Saccharomyces cerevisiae. J Cell Sci *117*, 4959-4968.

Lenoir, G., Williamson, P., Puts, C.F., and Holthuis, J.C. (2009). Cdc50p plays a vital role in the ATPase reaction cycle of the putative aminophospholipid transporter Drs2p. J Biol Chem *284*, 17956-17967.

Levine, T., and Loewen, C. (2006). Inter-organelle membrane contact sites: through a glass, darkly. Curr Opin Cell Biol *18*, 371-378.

Levine, T.P., and Munro, S. (2001). Dual targeting of Osh1p, a yeast homologue of oxysterol-binding protein, to both the Golgi and the nucleus-vacuole junction. Mol Biol Cell *12*, 1633-1644.

Li, X., Rivas, M.P., Fang, M., Marchena, J., Mehrotra, B., Chaudhary, A., Feng, L., Prestwich, G.D., and Bankaitis, V.A. (2002). Analysis of oxysterol binding protein homologue Kes1p function in regulation of Sec14p-dependent protein transport from the yeast Golgi complex. J Cell Biol *157*, 63-77.

Lingwood, D., and Simons, K. (2010). Lipid rafts as a membrane-organizing principle. Science *327*, 46-50.

McCammon, M.T., Hartmann, M.A., Bottema, C.D., and Parks, L.W. (1984). Sterol methylation in Saccharomyces cerevisiae. J Bacteriol *157*, 475-483.

Michelot, A., Costanzo, M., Sarkeshik, A., Boone, C., Yates, J.R., 3rd, and Drubin, D.G. (2010). Reconstitution and protein composition analysis of endocytic actin patches. Curr Biol *20*, 1890-1899.

Mizuno-Yamasaki, E., Medkova, M., Coleman, J., and Novick, P. (2010). Phosphatidylinositol 4-phosphate controls both membrane recruitment and a regulatory switch of the Rab GEF Sec2p. Dev Cell *18*, 828-840.

Moorhead, A.M., Jung, J.Y., Smirnov, A., Kaufer, S., and Scidmore, M.A. (2010). Multiple host proteins that function in phosphatidylinositol-4-phosphate metabolism are recruited to the chlamydial inclusion. Infect Immun *78*, 1990-2007.

Munn, A.L., Heese-Peck, A., Stevenson, B.J., Pichler, H., and Riezman, H. (1999). Specific sterols required for the internalization step of endocytosis in yeast. Mol Biol Cell *10*, 3943-3957.

Munn, A.L., and Riezman, H. (1994). Endocytosis is required for the growth of vacuolar H(+)-ATPase-defective yeast: identification of six new END genes. J Cell Biol *127*, 373-386.

Murphy, D.J., and Vance, J. (1999). Mechanisms of lipid-body formation. Trends Biochem Sci *24*, 109-115.

Nern, A., and Arkowitz, R.A. (1998). A GTP-exchange factor required for cell orientation. Nature *391*, 195-198.

Ngo, M.H., Colbourne, T.R., and Ridgway, N.D. (2010). Functional implications of sterol transport by the oxysterol-binding protein gene family. Biochem J *429*, 13-24.

Nishiya, N., Kiosses, W.B., Han, J., and Ginsberg, M.H. (2005). An alpha4 integrin-paxillin-Arf-GAP complex restricts Rac activation to the leading edge of migrating cells. Nat Cell Biol *7*, 343-352.

Nohturfft, A., Brown, M.S., and Goldstein, J.L. (1998). Topology of SREBP cleavage-activating protein, a polytopic membrane protein with a sterol-sensing domain. J Biol Chem *273*, 17243-17250.

Ortiz, D., Medkova, M., Walch-Solimena, C., and Novick, P. (2002). Ypt32 recruits the Sec4p guanine nucleotide exchange factor, Sec2p, to secretory vesicles; evidence for a Rab cascade in yeast. J Cell Biol *157*, 1005-1015.

Parrish, W.R., Stefan, C.J., and Emr, S.D. (2005). PtdIns(3)P accumulation in triple lipid-phosphatase-deletion mutants triggers lethal hyperactivation of the Rho1p/Pkc1p cell-integrity MAP kinase pathway. J Cell Sci *118*, 5589-5601.

Perry, R.J., and Ridgway, N.D. (2006). Oxysterol-binding protein and vesicle-associated membrane protein-associated protein are required for sterol-dependent activation of the ceramide transport protein. Mol Biol Cell *17*, 2604-2616.

Prigent, M., Boy-Marcotte, E., Chesneau, L., Gibson, K., Dupre-Crochet, S., Tisserand, H., Verbavatz, J.M., and Cuif, M.H. (2011). The RabGAP proteins Gyp5p and Gyl1p recruit the BAR domain protein Rvs167p for polarized exocytosis. Traffic *12*, 1084-1097.

Prinz, W.A. (2007). Non-vesicular sterol transport in cells. Prog Lipid Res *46*, 297-314.

Preuss, M.L., Schmitz, A.J., Thole, J.M., Bonner, H.K., Otegui, M.S., and Nielsen, E. (2006). A role for the RabA4b effector protein PI-4Kbeta1 in polarized expansion of root hair cells in Arabidopsis thaliana. J Cell Biol *172*, 991-998.

Ptacek, J., Devgan, G., Michaud, G., Zhu, H., Zhu, X., Fasolo, J., Guo, H., Jona, G., Breitkreutz, A., Sopko, R.*, et al.* (2005). Global analysis of protein phosphorylation in yeast. Nature *438*, 679-684.

Raychaudhuri, S., Im, Y.J., Hurley, J.H., and Prinz, W.A. (2006). Nonvesicular sterol movement from plasma membrane to ER requires oxysterol-binding protein-related proteins and phosphoinositides. J Cell Biol *173*, 107-119.

Rodal, A.A., Manning, A.L., Goode, B.L., and Drubin, D.G. (2003). Negative regulation of yeast WASp by two SH3 domain-containing proteins. Curr Biol *13*, 1000-1008.

Salmena, L., Carracedo, A., and Pandolfi, P.P. (2008). Tenets of PTEN tumor suppression. Cell *133*, 403-414.

Sanz-Moreno, V., Gadea, G., Ahn, J., Paterson, H., Marra, P., Pinner, S., Sahai, E., and Marshall, C.J. (2008). Rac activation and inactivation control plasticity of tumor cell movement. Cell *135*, 510-523

Sokac, A.M., and Bement, W.M. (2006). Kiss-and-coat and compartment mixing: coupling exocytosis to signal generation and local actin assembly. Mol Biol Cell *17*, 1495-1502.

Sokac, A.M., Co, C., Taunton, J., and Bement, W. (2003). Cdc42-dependent actin polymerization during compensatory endocytosis in Xenopus eggs. Nat Cell Biol *5*, 727-732.

Stefan, C.J., Manford, A.G., Baird, D., Yamada-Hanff, J., Mao, Y., and Emr, S.D. (2011). Osh proteins regulate phosphoinositide metabolism at ER-plasma membrane contact sites. Cell *144*, 389-401.

Stefan, C.J., Padilla, S.M., Audhya, A., and Emr, S.D. (2005). The phosphoinositide phosphatase Sjl2 is recruited to cortical actin patches in the control of vesicle formation and fission during endocytosis. Mol Cell Biol *25*, 2910-2923.

Sullivan, D.P., Ohvo-Rekila, H., Baumann, N.A., Beh, C.T., and Menon, A.K. (2006). Sterol trafficking between the endoplasmic reticulum and plasma membrane in yeast. Biochem Soc Trans *34*, 356-358.

Sun, Y., Carroll, S., Kaksonen, M., Toshima, J.Y., and Drubin, D.G. (2007). PtdIns(4,5)P2 turnover is required for multiple stages during clathrin- and actin-dependent endocytic internalization. J Cell Biol *177*, 355-367.

Sun, Y., Kaksonen, M., Madden, D.T., Schekman, R., and Drubin, D.G. (2005). Interaction of Sla2p's ANTH domain with PtdIns(4,5)P2 is important for actin-dependent endocytic internalization. Mol Biol Cell *16*, 717-730.

Tarassov, K., Messier, V., Landry, C.R., Radinovic, S., Serna Molina, M.M., Shames, I., Malitskaya, Y., Vogel, J., Bussey, H., and Michnick, S.W. (2008). An in vivo map of the yeast protein interactome. Science *320*, 1465-1470.

Tobert, J.A. (2003). Lovastatin and beyond: the history of the HMG-CoA reductase inhibitors. Nat Rev Drug Discov *2*, 517-526.

Tonikian, R., Xin, X., Toret, C.P., Gfeller, D., Landgraf, C., Panni, S., Paoluzi, S., Castagnoli, L., Currell, B., Seshagiri, S*., et al.* (2009). Bayesian modeling of the yeast SH3 domain interactome predicts spatiotemporal dynamics of endocytosis proteins. PLoS Biol *7*, e1000218.

Toshima, J., Toshima, J.Y., Duncan, M.C., Cope, M.J., Sun, Y., Martin, A.C., Anderson, S., Yates, J.R., 3rd, Mizuno, K., and Drubin, D.G. (2007). Negative regulation of yeast Eps15-like Arp2/3 complex activator, Pan1p, by the Hip1R-related protein, Sla2p, during endocytosis. Mol Biol Cell *18*, 658-668.

Valdez-Taubas, J., and Pelham, H.R. (2003). Slow diffusion of proteins in the yeast plasma membrane allows polarity to be maintained by endocytic cycling. Curr Biol *13*, 1636-1640.

Wang, P., Zhang, Y., Li, H., Chieu, H.K., Munn, A.L., and Yang, H. (2005a). AAA ATPases regulate membrane association of yeast oxysterol binding proteins and sterol metabolism. EMBO J *24*, 2989-2999.

Wang, P.Y., Weng, J., and Anderson, R.G. (2005b). OSBP is a cholesterol-regulated scaffolding protein in control of ERK 1/2 activation. Science *307*, 1472-1476.

Youn, J.Y., Friesen, H., Kishimoto, T., Henne, W.M., Kurat, C.F., Ye, W., Ceccarelli, D.F., Sicheri, F., Kohlwein, S.D., McMahon, H.T*., et al.* (2010). Dissecting BAR domain function in the yeast Amphiphysins Rvs161 and Rvs167 during endocytosis. Mol Biol Cell *21*, 3054-3069.

Zeng, G., and Cai, M. (1999). Regulation of the actin cytoskeleton organization in yeast by a novel serine/threonine kinase Prk1p. J Cell Biol *144*, 71-82.